science.sciencemag.org/content/370/6522/1343/suppl/DC1

Supplementary Materials for

The evolution of a tropical biodiversity hotspot

Michael G. Harvey*†, Gustavo A. Bravo†, Santiago Claramunt, Andrés M. Cuervo, Graham E. Derryberry, Jaqueline Battilana, Glenn F. Seeholzer, Jessica Shearer McKay, Brian C. O'Meara, Brant C. Faircloth, Scott V. Edwards, Jorge Pérez-Emán, Robert G. Moyle, Frederick H. Sheldon, Alexandre Aleixo, Brian Tilston Smith, R. Terry Chesser, Luís Fábio Silveira, Joel Cracraft, Robb T. Brumfield‡, Elizabeth P. Derryberry‡

*Corresponding author. Email: mgh272@gmail.com
†These authors contributed equally to this work.
‡These authors contributed equally to this work

Published 11 December 2020, *Science* **370**, 1343 (2020)
DOI: 10.1126/science.aaz6970

This PDF file includes:

Materials and Methods
Supplementary Text
Figs. S1 to S73
Tables S1 to S42
Captions for Tables S43 to S47
References

Other Supplementary Material for this manuscript includes the following:
(available at science.sciencemag.org/content/370/6522/1343/suppl/DC1)

Tables S43 to S47 (Excel)
MDAR Reproducibility Checklist (PDF)

Materials and Methods

1. Data collection

1.1 Sampling

We obtained 1,940 samples from 1,287 of 1,306 currently recognized suboscine species (*32-35*)(see section 3.1) from existing genomic resource collections at natural history museums and during recent field expeditions in Malaysia, Brazil, Bolivia, and Peru (Table S43). Field samples were collected and processed following IACUC protocols A3339-01 (KU), 2012-05 (USNM), and 12-054 (LSU); Comissão de Ética de no Uso de Animais do Instituto de Biociências da Universidade de São Paulo (CEUA) – Protocol 227/2015; and ICMBio/MMA Permanent license for collection of zoological material – 10013-2. We used frozen tissue samples associated with voucher specimens. For species lacking frozen tissue, we cut toe pad fragments from dried study skin specimens. We first selected a sample for genomic data collection from as close to the type locality of each species as possible. In species anticipated to contain cryptic diversity based on expert knowledge (see Acknowledgements), we sampled between 1 and 37 additional individuals that might represent cryptic species or deep subspecific divergences.

1.2 Laboratory methods

We extracted whole genomic DNA from frozen tissues using standard methods and kits (Qiagen, Valencia, CA). Toepads were extracted using a similar strategy, but in an ancient DNA lab where contamination risks were minimized (detailed protocol available at Zenodo repository). We quantified DNA extracts using a Qubit fluorometer (ThermoFisher, Waltham, MA) and sent them to Rapid Genomics (Gainesville, FL) for library preparation and sequence capture following the general protocol of Faircloth et al. (*36*). This protocol involves fragmenting the genomic DNA, ligating barcoded Illumina-compatible adapters, PCR amplification, probe hybridization, and enrichment of hybridized fragments. Samples are then sequenced in multiplex on Illumina HiSeq 2000, 2500, 3000, and X platforms. We conducted sequence capture using a probe set designed to target genomic ultraconserved elements and conserved exons used in prior avian phylogenetic studies (*37*). This probe set contained 4,715 probes targeting 2,321 UCEs and 96 exons.

1.3 Assembly and filtering

We assembled reads into multiple sequence alignments using a pipeline based on the Phyluce assembly pipeline (*38*) with additional code written for this project (*31*). We mapped contigs assembled with Velvet (*39*) and VelvetOptimiser (*40*) to target loci using a modified Phyluce script (extract_UCE_bypass.py) to generate a reference for each sample. We then used BWA (*41*) to map all reads for that individual back to the reference. In cases where the reference assembly was poor (fewer than 1000 loci recovered), we mapped the reads from that sample to reference sequences assembled from one or more samples the same species or a close relative (Table S8). After mapping, we called SNPs and indels and exported consensus sequences for

each locus in each sample using SAMtools (*42*). We hard-masked trailing low-quality bases (<Q20) within resulting consensus sequences using seqtk (see Zenodo repository), trimmed both ends to remove leading or trailing low-depth (<5x) sites, collated sequences by locus using MySQL, and then generated final alignments across samples using MAFFT (*43*). We used as many as 18 dual 10-core 2.8 GHz Intel Xeon E5-2680 v2 CPUs with 64GB RAM on the Cypress cluster (Tulane University, New Orleans, LA). The MySQL database was stored on either a Mac Pro (late 2013) with 32GB RAM and an 8-core processor or ASUS 12-core machine with 16GB RAM.

Visual inspection of MAFFT alignments revealed long ragged ends containing high amounts of missing data and blocks of obvious non-orthologous sequences that were spuriously aligned. Missing data, particularly non-randomly distributed missing data, can be problematic for many phylogenetic methods (*44, 45*). Divergent perspectives exist about the degree to which filtering out missing data is advisable (*46, 47*). Accordingly, we examined both an aggressive and a minimal strategy for filtering alignment columns. First, we used an aggressive filtering strategy in Gblocks 0.91b (*48*). Gblocks is a program for removing poorly aligned positions and divergent regions of an alignment as well as alignment columns with missing data. We used the the "with half" option for gaps, which removes alignment sites that are missing from 50% or more of the sequences and flank depth set to 1,639. This alignment set is referred to as the aggressively filtered dataset in the main text, but is hereafter called the "HGAPF" (for "half gaps filter") dataset in the supplemental. Second, we used a minimal filtering strategy in which we only trimmed the extreme ends of alignments by removing columns with data for fewer than 400 (of 1,962) samples. This alignment set is referred to as the minimally filtered dataset in the main text, but is hereafter referred to as the "T400F" (for "trim 400 missing filter") dataset. Sets of alignments filtered using these divergent strategies allowed us to assess the impact of the inclusion of missing data on downstream analyses.

After filtering by columns to remove missing data, it was evident that some individual sequences contained isolated stretches of non-orthologous sequence information. These were discrete stretches of primarily private or near-private alleles that contrasted sharply with adjacent good stretches of sequence. We removed these spurious sequence stretches using a variable-width sliding window approach in which any sequence stretches with more than 25% private and more than three total private or near-private alleles were removed (ambi_sites_filter.py). Some individual sequences also had stretches of two-way ambiguity codes (M, R, W, S, Y, or K). These stretches of heterozygous sites appeared to represent locations where paralogous reads erroneously mapped to the sequence, resulting in two alternative alleles for many sites. We therefore implemented another variable-width sliding window filter to remove stretches with more than 5% of sites containing a two-way ambiguity code and more than 3 two-way ambiguity codes total. We cleaned up filtered sequences by removing hanging ends containing fewer than 10 nucleotides. Based on visual inspection of the alignments, this strategy effectively removed most obviously non-orthologous sequence segments in the alignments without removing orthologous data, such as divergent regions in outgroup taxa or species expected to occur on long branches in the phylogeny.

1.4 Genome mapping

We established the genomic position of each locus by mapping to an existing genome. Currently, no suboscine has an assembled genome containing high-quality chromosome

assemblies, so we mapped loci to the Zebra Finch (*Taeniopygia guttata*) genome (v.3.2.4), the most complete oscine passerine assembly (*49*). Zebra Finch shares a common ancestor with all suboscines sometime between 27 and 63 Ma (*14, 50, 51*). To obtain a consensus sequence for mapping, we selected the most common allele across ingroup taxa at each variable site, trimming flanking nucleotides with missing data for most samples. We used blastn (*52*) for mapping to the Zebra Finch genome, and used the position of the top-scoring hit. We used the positions of protein-coding genes from Zebra Finch annotation release 103 to identify whether each locus was within a coding region. Loci were considered to fall within a coding region if any portion of their conserved core, as defined above, mapped to an annotated gene. Some subsequent analyses were performed separately on autosomal and sex-linked partitions and partitions containing loci either overlapping or not overlapping annotated coding regions. We also measured the GC content of each locus and the distance between loci on the same chromosome or scaffold.

2. Phylogeny estimation and support

2.1 Heterogeneity in phylogenetic signal across loci

We estimated gene trees for each locus using the maximum likelihood method implemented in RAxML v8.2.8 (*53*). For a random subset of 100 loci, we compared the fit of the GTRGAMMA model to JC69, HKY85, and K80 models using small-sample corrected Akaike Information Criterion (AICc) scores. We calculated AICc scores using final likelihoods, sample sizes based on number of alignment patterns, and the numbers of free parameters including branch lengths output by RAxML. The GTRGAMMA model was the best-fitting model across most loci (see Supplementary Text), and was used for the remainder of the gene tree analyses. We also computed an estimate of topological support for every node in each gene tree using the SH-like approximate likelihood-ratio (aLRT) test (*54*) implemented in RAxML. We used this measure to distinguish between nodes that were supported by a given gene tree and those without statistical support. We examined gene tree heterogeneity by measuring the Robinson-Foulds (RF) distance between each pair of gene trees using the R (*55*) package phangorn (*56*), after trimming them to the set of shared tips between a given pair. To normalize for differences in tree size across pairs, we divided each RF distance measurement by the maximum possible RF distance.

2.2 Species trees using concatenation

We estimated species trees from concatenated datasets using ExaML (*57*) on the Cypress cluster. ExaML is a method for maximum likelihood inference of phylogenies on supercomputers using MPI. First, following ExaML developer recommendations, we generated 100 bootstrap alignments using RAxML and 100 random seed trees. We then found the ML tree for each bootstrap alignment under per-site rate category model (equivalent to CAT in RAxML). We chose 1 in 5 bootstrap trees (n=20) and used those as the seed trees for an ML search under per-site replicate for the original alignment. We conducted branch-length evaluation ("-f E") for each of the 20 rough trees under GAMMA (equivalent to GTRGAMMA in RAxML). We selected the 10 trees with the highest likelihoods, conducted a second ML search under GAMMA for those 10, and identified the tree with the highest likelihood as the final tree. We used RAxML to summarize the 100 bootstrap trees on the final complete alignment tree. We

conducted ExaML analyses on both the T400F and HGAPF alignments, partitioned by locus. We also conducted ExaML analyses on subsets of the T400F alignments representing: (1) only loci mapping to z-linked loci, (2) loci mapping to autosomes, (3) loci mapping to genes, and (4) loci mapping to noncoding regions. The process for these trees was identical to that described above, except we initially generated only 20 bootstrap trees for seeding the full ML search and did not examine bootstrap support for the final ML trees.

As an alternative metric of support for each node, we tallied the proportion of rooted gene trees containing each clade using phyparts (*58*). We used gene trees based on the T400F locus alignments to evaluate the T400F consensus tree, and based on the HGAPF locus alignments to evaluate the HGAPF consensus tree. We first removed from consideration (collapsed) nodes that were poorly supported statistically (SH-like aLRT scores <80; following *54, 59*).

2.3 Gene tree/species tree analyses

We used ASTRAL-III (*60*) to estimate coalescent-based species trees from the individual RAxML gene trees. Astral estimates a species tree from unrooted gene trees by finding the topology with the maximum number of induced quartet trees shared with the gene trees. Following Mirarab and Warnow (*61*), we ran Astral on the maximum likelihood gene tree estimate from each locus, and used RAxML gene trees in which poorly supported nodes (SH-like aLRT scores <80) were collapsed. We evaluated support for each node using the local posterior probabilities assigned by ASTRAL (*62*) and by calculating the proportion of rooted gene trees containing each node after collapsing gene tree nodes with SH-like test scores <80. ASTRAL provides branch lengths in coalescent units, but we also were interested in estimating branch lengths for the ASTRAL tree in units of substitutions, in particular for the purpose of eventual time calibration. We therefore also estimated branch lengths in number of expected substitutions in ExaML with the topology fixed to the Astral topology. We conducted branch length estimation (-f E) as in section 2.2 above using the GAMMA model.

2.4 Time calibration

To obtain a time-scaled tree, we estimated the age of calibration nodes using the fossil record (*63*) and applied the calibrations using a node-based penalized likelihood approach (*64, 65*). We selected calibration nodes that correspond to the most recent common ancestor of clades within which high-quality, old fossils have been found and studied. We then estimated the age of the clade based on the density of its fossil record (*63*). We calculated the unbiased point estimate of clade age as $t_n + t_n/n$ and the confidence interval as $[t_n, t_n/(1-p)^{1/n}]$, in which t_n is the age of the oldest fossil, n is the number of fossils, and p is the confidence level (*66, 67*). The above formulae assume sample independence, which was maximized by using only the first fossil occurrence of the clade in each continent. Using multiple fossils from the same region may confound the time of origin with the time of colonization of the region (*13*). The method also assumes that fossil finds are distributed uniformly along the time interval. We checked for uniformity of the sample of fossil ages of each clade within the interval $[0, t_n + t_n/n]$ using a Kolmogorov-Smirnov test. Finally, the method assumes a precise age for the oldest fossil. Age uncertainty for oldest fossils in our dataset were below 3 million (see below) years so we used the midpoint of the corresponding time interval as the age of the fossil.

We used four calibration nodes. Two of these nodes represent direct ancestors of the Tyranni and two of them are within the oscine outgroup. The first direct ancestor corresponded to the time of origin of Passeriformes, i.e. the most recent common ancestor of Passeriformes and Psittaciformes. The latest phylogenetic analyses of fossils in this group revealed that Pseudasturidae and Halcyornithidae, used in previous calibrations, are outside this clade (*68*) and *Morsoravis sedilis*, from the Fur Formation (54-54.5 Ma; *69*), becomes the oldest fossil of stem-Passeriformes (*68, 70*). First occurrence of birds in the Psittaciformes-Passeriformes clade in each continent is detailed in Table S9, which leads to an estimate of 59.9 Ma for the time of origin of Passeriformes, which we used as a fixed age.

The second direct ancestor calibration corresponded to the most recent ancestor of the clade containing the suborders Tyranni and Passeri (informally named eupasseres), with *Wieslochia weissi* (*71*), from Rauenberg (32-30.5 Ma; *70*) as the oldest fossil. The position of *Wieslochia weissi* as a stem representative of the Tyranni is supported by the presence of a well-developed *processus procoracoideus*, a well-developed *tuberculum ligamenti collateralis ventralis* of the ulna (*13, 71*), and confirmed by a cladistic analysis (*70*). Because using a single fixed age for this node would prevent other calibrations from influencing the age of the Tyranni, we used minimum-maximum bounds based on the confidence interval [31.3Ma, 47.25Ma]. The other two calibration nodes are in the oscine outgroup. One corresponds to the superfamily Certhioidea, with *Certhiops rummeli* from Petersbuch 62, in Germany (18-20.5 Ma; *73*), as the oldest fossil. Because a precise relationship of *Certhiops* within the Certhioidea is not known, we used minimum-maximum bounds [19.25Ma, 52.25 Ma] for calibration. The second calibration corresponds to the clade formed by Passeridae and the nine-primaried oscines (Emberizoidea), with early Miocene fossils in the genera *Passer* and *Loxia* described from Saint-Gérand-le-Puy, France (20-22.4 Ma; *74*). Again, given uncertainty in the precise phylogenetic placement of the oldest fossils, we used minimum-maximum bounds of [21.2Ma, 38.6 Ma] for calibration. A complete list of fossil ages used for estimating age and confidence intervals of calibration nodes is presented in Table S9.

We used these calibrations to rescale the branches of the T400F and HGAPF ExaML trees and the T400F Astral tree (with branch lengths estimated in ExaML) using the penalized likelihood approach (*64*) implemented in TreePL (*65*). We used an optimal smoothing parameter determined by the "random subsample and replicate" cross-validation method. Terminal branch lengths from poor quality samples, such as toe pads, were unreliable because low-grade contamination and errors produced an excess of private alleles (*75*). The resulting inflated terminal branch lengths can bias time calibration deeper in the tree. We therefore conducted TreePL analysis initially on a dataset in which toepads and samples with evidence of low-grade contamination (n = 124; Table S10) were removed. We then added low-quality samples to the initial time-calibrated tree using congruification (*76*) with the TreePL option for time-scaling implemented in geiger-v2 (*77*). We also examined results of a TreePL analysis without the removal and re-addition of poor-quality samples. We further evaluated the impact of the inclusion of each individual sample on time calibration using a jackknifing procedure on the T400F ExaML trees.

To assess the impact of calibration and branch length estimation errors on divergence time estimates we used a resampling procedure as follow. We used the trees derived from the 100 bootstrap alignment to represent variation in branch length estimation. Each tree was then calibrated using TreePL as before but, instead of using the unbiased point estimate for the origin of Passeriformes, we used a random number obtained from the quantile function $t_n/(1-p)^{1/n}$ by

sampling *p* from a uniform distribution between 0 and 1. We summarized the results by computing the 2.5% and 97.5% quantiles of age for each node based on the 100 calibrated trees.

We supplemented this approach with a full Bayesian method that simultaneously estimated the tree topology and divergence times (BEAST2; *78*). Unfortunately, it was impossible to do run BEAST using the full dataset, so we estimated this tree at the family level only. We used the sample with the most complete data in each family (n=24) as well as five outgroup samples. Even then, we needed to subset the data matrix to 50,000 alignment columns (all of which had complete data) to achieve convergence. An initial configuration file was created in BEAUti but was then edited manually to generate the final file. Substitutions were modelled using a GTR model with a gamma mixture for rate heterogeneity. A relaxed log-normal clock was used to model absolute rate heterogeneity across branches (*79*). Calibration densities were set so as to match the main penalized likelihood analysis: a fixed age of 59.9 Ma for the origin of Passeriformes, and uniform distributions with minimum-maximum bounds based on the confidence intervals for each clade as before. We used a birth-death tree prior with incomplete sampling (*80*) that takes into account that the family-level dataset is a small fraction of the species diversity of the group. We used the BDSKY 1.4.5 BEAST add-on (*81*) to implement a 'birth-death skyline contemporary' prior in which we set a uniform prior (0, infinity) for the birth/total death ratio (effective reproduction number R0), a uniform prior (0, infinity) for the "total death" rate ("become uninfectious") prior, and a fixed sampling probability (ρ) of 0.0044, the approximate fraction of species sampled (29 species of ca. 6600 species of Passeriformes plus Psittaciformes). BEAUti defaults were used for other priors. We ran two chains of 50 million generations, discarded the first 10 million generations as burn-in and evaluated stationarity and convergence.

3. Diversification analyses

3.1 Taxonomic classifications

The classification used to determine the set of tips on a phylogeny will impact diversification inferences. We therefore examined a series of alternative classifications and their impact on diversification estimates (Table S43). Our primary classification follows the fourth and most recent edition of the Howard and Moore Complete Checklist of the Birds of the World, published in two volumes (*34, 35*). This list heavily references the literature and includes detailed footnotes, and follows the authoritative taxonomic entities for the New World, the North American Classification Committee (NACC) and South American Classification Committee (SACC) of the American Ornithological Society (AOS). However, the most recent version of the Howard and Moore classification does not include the most recent NACC and SACC changes. We therefore updated the classification to reflect the most recent decisions of the AOS committees (*32, 33*). For analyses and plots examining taxonomic families, we used the family-level classification from the Howard and Moore list (*34, 35*), except we replaced the family name Pipromorphidae with Rhynchocyclidae, following the recommendation of Tello et al. (*82*).

The second classification we examined, the eBird/Clements Checklist (*83*), is almost identical to the Howard and Moore list for the species examined, because it also follows closely the NACC and SACC treatment for New World birds. It does, however, differ somewhat from the Howard and Moore list for the Old World taxa (Table S43). We again updated the eBird/Clements Checklist to reflect decisions from the SACC (there have been no NACC

updates) since the last version (August 2017). The third classification examined was that of the International Union for Conservation of Nature (IUCN) and BirdLife International. This classification does not follow the decisions of society-based taxonomic committees, but instead uses a standard rubric of differentiation in morphological and acoustic characters, scored by experts, to determine species limits. It generally subdivides species ("splits") to a greater degree than the two classifications above. We again used the most recent edition (v2, December 2017; http://datazone.birdlife.org/userfiles/file/Species/Taxonomy/HBW-BirdLife_Checklist_v2%20Dec17.zip), which is based on a two-volume publication (*84, 85*).

We also conducted analyses using sets of tips determined using simple time thresholds rather than the advice of taxonomic authorities. In one tree, we trimmed all nodes <1 Ma, and in another all nodes <2 Ma. Finally, we examined the results of analyses examining our full tree including all intraspecific lineages. Use of these six alternative classifications permits straightforward mapping of suboscine evolutionary diversity to currently recognized taxonomic groups, and also permits evaluation of the impacts of taxonomic uncertainty and the sampling of cryptic diversity on our results.

3.2 Diversification through time

We first examined the dynamics of lineage accumulation through time in suboscines using simple summaries of lineage accumulation and by fitting simple models of diversification to the tree as a whole. We visualized the accumulation of new extant lineages using lineage-through-time (LTT) plots. We also fit pure-birth, birth-death, and diversity dependent models to our tree using maximum likelihood (*86, 87*). We compared LTT plots from the data to LTT plots of 1000 trees simulated using parameter values based on model fit and conditioned on lineage age. We compared the fit of constant-rate and diversity dependent models to our tree using AICc. For subclades, we examined LTT plots for all lineages crossing a threshold set at the median age of currently recognized suboscine families (19.5 Ma). In figures and tables, these clades are generally referred to by the name of the most speciose family included therein for brevity.

We supplemented these analyses with stochastic-branching process models in maximum likelihood and Bayesian frameworks (*88, 89*). We obtained maximum likelihood diversification rate estimated for 5 Ma intervals between 0 and 40 Ma with the bd.shifts.optim function in the R package TreePar (*88*). In addition, we used the TESS library in R to estimate parameters of an episodic birth-death model that assumes that diversification rates are constant but can change at particular points in time across all lineages. The number, timing, and magnitude of shifts in diversification rates are then estimated using reversible-jump MCMC. The hyperpriors for the diversification parameters were determined empirically based on a preliminary analysis as implemented in TESS functions (*90*). The MCMC sampling was run until a minimum of 500 effective samples had accumulated but not for longer than 100,000. Results were summarized by plotting the posterior mean and 95% credible intervals of the speciation rate through time.

Recently, the possibility of identifying unique diversification scenarios from phylogenies of extant species has been challenged (*18*). Simulations suggest that distinct evolutionary histories can lead to quite similar phylogenies, and that commonly used parameters such as speciation, diversification, and extinction rate fail to distinguish between these alternative histories. Louca and Pennell (*18*) do, however, suggest that sets of congruent diversification models can be uniquely identified using certain composite variables of phylogenetic branching patterns, and they identify two such variables that are particularly useful. These are the pulled

diversification rate (r_p) and an initial condition equal to the sampling fraction times the present-day speciation rate (ηo). We used the R package castor (*18, 91*) to estimate these variables using maximum likelihood. We fit both variables both to the tree as a whole, and to a time grid of 25 evenly spaced time points assuming a piecewise linear curve (omitting times prior to 35 Ma to avert estimation error associated with the small number of lineages prior to that time). We ran 100 bootstrap replicates to evaluate uncertainty and ran optimization ten times each for both the real data and the bootstrap samples. For visualization, splines were interpolated using 1000 points within the sampling interval.

3.3 Tip-based estimates of speciation rate and species age

We examined diversification patterns across geographic space and among lineages, first using estimators based on waiting times between speciation events across the tree. Simulation studies have found these estimators are reliable measures of evolutionary processes under many scenarios (*92-94*). Waiting times statistics are particularly useful in a young, diverse clade like the suboscines that is likely experiencing a net increase in diversity. They are also appealing because they can be calculated quickly from large phylogenies.

We examined four statistics based on branching times. First, we estimated speciation rates using the inverse equal splits method (ES; *95, 96*). This is based on the sum of the lengths of the branches subtending each tip on the phylogeny, with the branch's length weighted according to its distance from the tip. With each step toward the root, the branch is down-weighted by ½. This estimator therefore captures speciation dynamics throughout the history of a lineage within the sampled tree, but is heavily weighted toward the present. We refer to these as "recent" speciation rates, but emphasize that recent is a relative term rather than an absolute time interval. We also examined two metrics of species age. One was based on the terminal branch length of each tip (TB), and the other on the median age of each tip's subtending nodes (ND). Both metrics have been used to measure the age of diversity across species or space (e.g., *97-98*). Finally, we calculated evolutionary substitution rate (SR) as the ratio of the total root-to-tip distance from the ExaML tree, which reflects the expected number of substitutions per site, to the total height of the time-calibrated TreePL tree, which reflects time (see, e.g., *99*).

We examined variation in all four estimators across the phylogeny and across geographic space. We calculated the estimators using phylogenies for each of the six alternative classifications described in section 3.1. In addition to obtaining all four statistics for all phylogenetic tips, we calculated ES and SR for each internal branch on the tree. ES for internal branches was calculated using the same formula as for the terminal branches, and SR reflected the ratio of the length of each branch in the non-ultrametric ExaML tree to the same branch in the time-calibrated TreePL tree.

We mapped variation in average values of these estimators across the globe. We used the R packages rgdal (*100*), raster (*101*), maptools (*102*), maps (*103*), rworldmap (*104*), and sp (*105, 106*) to generate a raster with 200km^2 cells for each statistic. Cell values were weighted means calculated by weighting each species's value by the inverse of the number of grid cells in which it occurred. This strategy minimizes the excessive impact of wide-ranging species on perceived geographic patterns (*96*). However, we also examined unweighted maps, and mapped statistics for quartiles of species based on their range sizes following Jetz and Rahbek (*107*). We used species range maps from IUCN/Birdlife International (*108*), cleaned and re-projected using the equal area World Mollweide projection (http://www.greenfirescience.com/data). We pruned each

range map to include only native ranges and only breeding and resident distributions. The taxonomic classification used for range maps was identical to the most recent (December 2017) IUCN/BirdLife international classification for the species examined. For visualizing statistics using the Howard and Moore and eBird/Clements classifications, we combined range maps from IUCN/BirdLife species that were treated as conspecific in either of those classifications. We did not map estimates using the classifications based on 1 Ma or 2 Ma thresholds or treating all samples as tips because it is not clear how the tips from those classifications map to the IUCN/Birdlife species. We also mapped species richness using a similar approach, but did not discount richness values by species range size.

3.4 Model-based analyses of branch-specific speciation and extinction

We supplemented the above analyses of diversification rates with a set of probabilistic modelling approaches. We were interested confirming patterns of variation in speciation rates across the tips of the tree estimated using ES, and also in determining whether there is support for heterogeneity in rates at the level of larger clades. A suite of parametric modeling approaches is available for branch-specific diversification rate estimation, but many have either received criticism (see e.g., *109, 110*) or are very new and have not been independently tested. We therefore examined six different approaches to integrate over potential bias associated with any individual method.

First, we used Bayesian Analysis of Macroevolutionary Mixtures (BAMM; *111, 112*) to identify distinct diversification models across the phylogeny and their respective constant or time-varying speciation and extinction rates. BAMM is a Bayesian method that uses reversible-jump Markov chain Monte Carlo (MCMC) to sample different combinations of models. We conducted BAMM runs using each of the six classifications from section 3.1. We set up BAMM analyses following current best practices and author recommendations *(113, 114*) and examined the results with a series of priors (1, 10, 100) on the expected number of diversification shifts. We conducted a no-data run to examine estimates based only on prior information. Each analysis was run for 200 million generations, sampling every 20,000. We conducted multiple runs to check for convergence, and also checked the traces and effective sample sizes of key parameters and log Likelihood values using coda (*115*) and BAMMtools (*116*). We discarded the first 10% of samples as burn-in. We examined the credible shift set from each run, and identified the shift configuration with the highest maximum a posteriori probability using the getBestShiftConfiguration method.

We also used MEDUSA (*117*) to estimate the best combination of distinct diversification rate models across the tree, each model containing constant speciation and extinction rates through time. MEDUSA uses stepwise AIC to compare the likelihoods of increasing numbers of diversification models fit to a phylogenetic tree. We used turboMEDUSA, now implemented in geiger-v2 (*77*). We ran multiple analyses using each of the six classifications described in section 3.1.

We examined a pair of approaches implemented in RevBayes (*118*). We followed developer recommendations (see Zenodo repository) to evaluate diversification rate under both a conditional birth-death-shift process (CBDS) and finite-rate-category birth-death-shift (FRCBDS) process. The former draws diversification rates from a continuous distribution but assumes rates cannot shift on extinct lineages, whereas the latter does not assume shifts are absent on extinct lineages but draws rates from a discretized distribution with a limited number

of rate categories. For both approaches, we ran RevBayes analyses of 2 chains, each with a 100 thousand-generation burn-in followed by at least 437,500 sampling generations. We evaluated MCMC convergence between and within chains using Tracer v.1.6 (*119*). We examined runs with the prior for expected number of rate shifts set to 1, 10, and 100. For the finite-rate-category analysis, we used a discretized log-normal distribution containing 20 rate categories.

We used a Multi-State Birth-Death (MSBD) model (*120*) to estimate lineage-specific speciation and extinction rates. MSBD allows these rates to vary across the tree independently of any trait by permitting state changes in rates along branches through time. We ran MSBD in the BEAST2 framework (*78*) for 250 million generations (discarding the first 25% as burn-in) using a fixed tree topology (our primary tree) and broad, log-normally distributed priors. We evaluated MCMC convergence using Tracer v.1.6 (*114*). We used a TipRatesLogger to generate a posterior sample of tip speciation rates and used posterior median rates as point estimates following Barido-Sottani et al. (*120*).

Finally, we used the Cladogenetic Diversification Rate Shift (ClaDS) model (*121*). ClaDS is a birth-death model where the rates of a daughter lineage are inherited, or sampled from a distribution parameterized using the parental rates. We attempted to run ClaDS models incorporating constant (ClaDS1) or lineage-specific (ClaDS2) extinction, but they were computationally intractable with a tree of this size. We therefore were limited to examining a pure-birth model (ClaDS0). We ran ClaDS0 in the R package RPANDA (*122*) for 1 million generations (discarding 25% as burn-in). We visualized parameter chains, evaluated convergence, and obtained tip rates using the function MAPS_ClaDS0() to summarize the marginal posterior distributions from the sampler.

3.5 Collection of geographic, species richness, elevation, and climatic data

We obtained data for each study species on a suite of extrinsic variables that might be of evolutionary importance. We used the range data and geographic areas described in sections 3.3 and 3.4 above to obtain geographic variables. Latitude was based on the absolute midpoint latitude of the combined breeding and year-round distribution for each species. Species were assigned to a primary geographic region (Neotropics, Nearctic, or Old World and Australia) using the boundaries from Olson et al. (*123*) based on the region containing the largest fraction of their distribution. For each suboscine species, we calculated the number of other suboscines, passerines (Aves; Passeriformes), or all birds with overlapping ranges. Other species were considered overlapping if their range occupied 5% or more of the focal species' distribution by area. See below (Supplementary Text: Additional Results, section 9.8) for examination of the impact of spatial autocorrelation on range overlap data.

We assigned elevation based on the data from Quintero and Jetz (*8*). We examined elevational minimum, midpoint, and maximum. Species not from mountainous regions were assigned an elevation minimum of 0m, maximum of 150m and midpoint of 75m, following the treatment of "Coastal/Marine" species by Quintero and Jetz. Climatic data were obtained from current data and paleoclimatic simulations available from the PaleoClim portal (*124*). We examined data from five time periods: the present (1973-2013; *124*), the Last Glacial Maximum (ca. 21 ka; *125*), MIS19 (ca. 787 ka; *124*), the mid-Pliocene warm period (3.264-3.025 Ma; *126*), and M2 (ca. 3.3 Ma; *127*). For present-day climate, we examined annual mean temperature (Bio1), temperature seasonality (Bio4), max temperature of the warmest month (Bio5), minimum temperature of the coldest month (Bio6), annual precipitation (Bio12), precipitation seasonality

(Bio15), precipitation of the wettest quarter (Bio16), and precipitation of the driest quarter (Bio17). To address climatic stability through time, we calculated the average difference in both annual mean temperature and annual precipitation between either the last glacial maximum and present (Stability1) or between all successive time periods (Stability2). We obtained climate values for each species by overlaying climatic data and species range maps and calculating mean, median, and variance in values across the distribution of each species for each variable.

Other extrinsic or environmental variables might be important predictors of species richness or diversification dynamics. For example, the age or stability of contemporary habitat or vegetation may be the key determinant of spatial dynamics in avian diversity. Unfortunately, high-resolution paleo habitat and vegetation data are unavailable, thus these metrics are not obtainable currently. Many environmental variables show strong spatial autocorrelation, and distinguishing their relative importance can be challenging (*128*). We used the variables described above as a diverse suite of variables, with available high-resolution paleo and contemporary data, that together capture environmental variation across space.

3.6 Biogeographic analyses

Spatial patterns of branching pattern statistics reflect in part the biogeographic history of a group. We therefore conducted a biogeographic analysis to supplement, and provide historical context for, those results. We used the dispersal-extinction-cladogenesis model (DEC; *129*) as implemented in the R package BioGeoBEARS (*130*) to model the range evolution of suboscine lineages and infer ancestral states. We then used biogeographical stochastic mapping (BSM; *131*) to infer the number and type of bioegeographic events, with a particular focus on the number of transitions between geographic areas. We examined a simple set of three biogeographic areas representing the (1) Neotropics, (2) the Nearctic, and (3) Old World and Australia. Species were assigned to one or more biogeographic areas based on overlap of their IUCN/Birdlife International range maps with these regions, with presence only assigned if greater than 5% of the area of their range fell within a particular biogeographic area (Table S11). The boundary between the Neotropical and Nearctic regions was determined using the biogeographic realms of Olson et al. (*123*). We ran the DEC model without time-stratification and built 100 biogeographic stochastic maps. We then tallied the number of dispersal events in each map. We also ran BioGeoBEARS analysis with a more subdivided set of regions, also based on those of Olson et al. (*123*) combined largely following Morrone (*132*; see Fig. S11). These were intended to capture colonization history among biomes, particularly within the Neotropics.

3.7 Testing associations between speciation dynamics and potential predictors

We used tip rate correlation (TRC) tests and state-dependent speciation and extinction (SSE) models to evaluate associations between suboscine speciation dynamics and potential predictor variables. For binary variables (e.g., comparisons between geographic regions), we used the simulation-based approach (FISSE) presented by Rabosky and Goldberg (*133*). This test involves comparing the observed association between the estimated speciation rate and a variable scored at all phylogenetic tips with a null distribution of associations between the statistic and simulated variables produced by random change (modeled using a Mk model) across the tree (n=1000 simulations). The Mk model is a simplistic approximation of change in geographic

areas across a phylogeny, but involves minimal assumptions (i.e. geographic shifts can occur at any point and in either direction with equal probability). Although Rabosky and Goldberg focused on differences between groups in the inverse equal splits estimator (ES) in FISSE, we apply equivalent tests to measure between-group differences in our other estimates of branching patterns (TB, NH, and SR).

We assessed associations between speciation and age estimates and continuous variables using the related TRC approaches for continuous characters presented by Harvey and Rabosky (*94*). These tests compare the linear association between a trait and tip-specific speciation rates to that between the same estimate and a set of traits simulated using a random model of continuous trait evolution (n=1000 simulations). For our analyses, we used Brownian motion to model random evolution. Brownian motion, like the Mk model for geographic areas, is a simple approximation of the process of geographic range evolution across a latitudinal gradient with few assumptions.

We supplemented these tests with analyses using equivalent SSE models: BiSSE (*134*) for discrete geographic regions and QuaSSE (*86, 135*) for continuous variables (e.g., latitude, species richness). BiSSE and QuaSSE can be used to assess the association between trait states and speciation (or extinction) rates. BiSSE and QuaSSE are more sophisticated than the tests described above in that they simultaneously model speciation, extinction, and trait change across a phylogeny. They are, however, subject to high rates of false inferences of state-dependence (*136*), and have been shown to have higher false inference rates than simulation-based tests using branching pattern statistics (*94, 133*). We used BiSSE and QuaSSE to examine models in which (1) there were no associations between diversification and predictor variables, (2) there was an association between speciation rate and the variable, (3) there was an association between extinction and the variable, or (4) there were associations between both speciation and extinction and the variable of interest.

Due to the issue of high false inference of state-dependence, we also examined key results using an SSE approach that alleviates this issue. The HiSSE approach (*137*) includes a more sophisticated null model of speciation rate variation across the phylogeny, and also can incorporate models in which diversification is linked to a hidden or unknown variable rather than the variable of interest. Unfortunately, HiSSE is only implemented for binary characters, unlike many of our key variables like species richness. To circumvent this, we converted species richness to a binary trait using thresholds to distinguish species occurring in species-rich areas (trait=1) from those in species-poor areas (trait=0). This approach permits the use of HiSSE, but necessarily has less power as much of the variation in the predictor variable is removed. The threshold represents the proportion of species placed in the species-rich category. We explored a suite of thresholds (10-90 percent quantiles, every 10) to evaluate the impact of threshold delineation on results. We compared four models: (1) with an association between species richness and speciation rates, (2) a simple BiSSE null model, (3) a more sophisticated HiSSE null model allowing speciation rates to vary along branches independent of trait change, and (4) a model involving associations between speciation rate and both species richness and an unmeasured hidden trait. These model comparisons were selected to aid in identifying whether observed richness/speciation associations were real or were driven by variation in diversification that was either random or linked to unobserved variables.

We elected to use BiSSE rather than GeoSSE ("Geographic State Speciation and Extinction"; *138*) for three reasons. First, it is more closely analogous to our use of FISSE, which examines a simple binary variable, above. Second, BiSSE and GeoSSE are effectively equivalent

when species do not span both geographic areas. In suboscines, no species are shared between the New World and Old World. Few species are shared between the Nearctic and Neotropical regions, and assigning species to one region, the other, or both is complex because many of the species spanning both regions are long-distance migrants. Finally, when considering both summer and winter distributions, no species are limited to the Nearctic region, and the likelihood model implemented in GeoSSE behaves poorly when a state is missing.

3.8 Sensitivity tests of key associations

We ran a series of sensitivity tests to evaluate whether key associations between diversification dynamics and predictor variables were robust to factors including phylogenetic uncertainty, incomplete sampling, extinction, alternative taxonomic classifications, and the effects of spatial autocorrelation in species richness estimates. Details of the methods used for sensitivity tests are generally brief and are presented alongside the results of those analyses below in the Supplementary Text: Additional Results, section 9.

3.9 Phylogenetic path analysis

We used phylogenetic path analysis (*139*) to evaluate models containing causal relationships between speciation rates and multiple potential predictor variables including direct and indirect effects. In particular, we were interested in whether speciation rates were determined by the environment or instead by standing species richness in a region, which might in turn be environmentally driven. Phylogenetic path analysis integrates phylogenetic generalized least squares (PGLS) with the *d-separation* method for path analysis (*140*) to permit evaluation of complicated causal models while accounting for relatedness among species with shared evolutionary history (*139*). We conducted all phylogenetic path analyses using the R package phylopath (*141*).

We compared a model in which environmental variables directly impacted speciation rate (direct), a model in which environmental variables indirectly impacted speciation rate via their impact on an intermediate variable - standing species richness (indirect), a model in which environmental variables had both direct and indirect effects (both), and a null model with no associations. We compared models using the C-statistic information criterion corrected for small sample sizes (CICc). We then evaluated the importance of each causal path in the best model using the standardized regression coefficient and its standard error.

Supplementary Text: Additional Results

1. Nucleotide sequence data

1.1 Sequence data quality assessment

Statistics summarizing data recovery across loci are presented in Tables S44 (T400F) and S45 (HGAPF), and across samples in Tables S46 (T400F) and S47 (HGAPF). Sequence assembly required 13,465 cpu hours. We recovered data from 1,713 samples on average (SD = 179) across the T400F alignments and 1,765 samples (SD = 40) across the HGAPF alignments. T400F alignments averaged 653 bp in length (SD = 106) with 445 variable sites (SD = 115), whereas HGAPF alignments were 255 bp on average (SD = 58) with 157 variable sites (SD = 46). T400F alignments were missing data from 21% of alignment sites (SD = 3%), whereas HGAPF alignments were missing data from only 2% (SD = 0.7%). The proportion of GC sites averaged 0.39 with a standard deviation of 0.05 in both datasets.

The number of loci recovered across samples averaged 2,087 (SD = 405) for the T400F and 1,891 (SD = 370 for the HGAPF dataset). Sequence read depths for sequences retained in the alignments averaged 262 (SD = 290) for the T400F and 271 (SD = 298) for the HGAPF dataset. Individuals varied widely in missing data (T400F mean = 481.689 sites, SD = 344,026; HGAPF mean = 62,134 sites, SD = 108,249) and in the number of private alleles at variable sites (T400F mean = 220, SD = 309; HGAPF mean = 48, SD = 72).

As anticipated, data recovery was unsuccessful from a larger number of loci in toe pads from dried study skins (T400F: mean = 600, SD = 656; HFAPF: mean = 465, SD = 590), on average, than frozen tissue samples (T400F: mean =286 , SD = 382; HFAPF: mean = 196, SD = 351; Fig. S12a; T400F $t = 4.9$, $p < 0.01$; HGAPF $t = 4.7$, $P < 0.01$). For loci that were recovered, the toe pad sequences contained more missing sites (T400F: mean = 910141, SD = 353932; HFAPF: mean = 142346, SD = 157580) than tissue sequences (T400F: mean = 456976, SD = 326829; HFAPF: mean = 57507, SD = 102867; Fig. S12b; T400F $t = 12.9$, $P < 0.01$; HGAPF $t = 5.5$, $P < 0.01$).

1.2 Data recovery across genomic regions

We recovered data from 2,172 loci that mapped to Zebra Finch autosomes, 165 mapping to the Z chromosome, and 47 that mapped to unmapped scaffolds. 132 mapped to coding regions annotated in the Zebra Finch, whereas the remaining 2,252 loci mapped to areas not annotated as coding (hereafter “non-coding”).

2. Phylogeny

2.1 Selection of nucleotide substitution models

The GTRGAMMA was the best-fitting model across 87 of the subset of 100 alignments examined (Table S12) and was used for subsequent analyses.

2.2 Overview of ExaML species tree analyses

Tree inference using ExaML required 443,559 cpu hours. Five samples were clearly mis-identified or heavily contaminated based on placements across all trees and subsequent inspection of alignments and were removed from further analyses (Table S13).

2.3 Sequence data filtering strategies (HGAPF vs T400F) and impact on tree inference

Average bootstrap support on the T400F complete tree was 94.8 (SD = 15.0, Fig. S13), and the number of RAxML T400F gene trees consistent with each node averaged 164 (SD = 220, Fig. S14). The HGAPF tree had average bootstrap support of 91.1 (SD = 19.3, Fig. S15) and an average of 34 (SD = 57, Fig. S16) RAxML HGAPF gene trees contained each node in the consensus tree. The fact that few gene trees support each node reflects the relative low resolution of gene trees from alignments from conserved regions with relatively few variable sites. The HGAPF and T400F trees had very few topological differences (Fig. S1). The shallow clades visible in the ExaML trees with high concentrations of low bootstrap support (red nodes in Figs. S13 and S15) represent species with dense intraspecific sampling that was pruned for subsequent analyses. Isolated extremely long terminal branches generally represent toepads and poor-quality samples (Table S10) that were omitted for time calibration purposes (see section 3 below). Due to the increased resolution and support of the more data-inclusive T400F tree, we focus primarily on that tree for subsequent analyses, presenting analyses of the HGAPF tree only where they are instructive for confirming or contrasting with the T400F results.

2.4 Variation in trees built from different genomic partitions

The Robinson-Foulds (RF) distance between the T400F ExaML tree of autosomal data and the complete T400F ExaML tree was 172 (Fig. S17), compared to 658 between the sex-linked and complete trees (Fig. S18). The RF distance between the T400F ExaML tree of coding data and the complete T400F ExaML tree was 786 (Fig. S19), compared to 108 between the non-coding and complete trees (Fig. S20). The greater discrepancy between the complete tree and the trees from sex-linked and non-coding partitions may be due to the fact those partitions were both relatively small.

2.5 Comparison of concatenated and coalescent-based species trees

Astral local posterior probabilities, like bootstrap support values for the ExaML trees, were generally high across nodes (mean = 0.92, SD = 0.21; Figs. S21 and S22). Gene tree support averaged 149 across nodes (SD = 219) in the Astral tree (Fig. S23), similar to the T400F ExaML tree and higher than the HGAPF ExaML tree (see section 2.3). The complete Astral tree showed a high degree of topological discordance with the ExaML tree (Fig. S2). However, inspection of the tips that differed in position between the two trees revealed that, in the Astral tree, tips missing from a large number of gene trees were often placed on clearly spurious long branches outside the clade to which they belong based on current taxonomic classification and the results of other analyses. Trimming tips missing from more than 250 gene trees removed most of the spurious long branches and resulted in much higher concordance between the Astral and ExaML trees (Fig. S3). This level of concordance is impressive given that our dataset

comprises poorly resolved gene trees with high potential for estimation error, which can be problematic for Astral (*61*). This concordance suggests that the topologies obtained with ExaML are not substantially biased by not accounting for gene tree heterogeneity.

2.6 Heterogeneity in gene tree support across different genomic regions

Loci from across the genome supported the consensus T400F ExaML, HGAPF ExaML, and T400F Astral topologies (Figs. S24, S25, and S26, respectively). However, there was considerable variation among gene trees both in the number of consensus nodes that they contained and in their topologies and branch lengths. Standard deviations in number of consensus relationships supported across gene trees were 83 for the T400F ExaML tree, 32 for the HGAPF ExaML tree, and 67 for the T400F Astral tree. Average weighted RF distance between gene trees was 0.90 (SD = 0.06) for the T400F alignments and 0.98 (SD = 0.03) for the HGAPF alignments (where the maximum is 1). Sex-linked gene trees supported more nodes in the ExaML trees (T400F ExaML mean = 217, SD = 109) than autosomal gene trees (T400F ExaML mean = 128, SD = 77; Fig. S27a; $t = -10.3$, $P < 0.01$). Gene trees were more heterogeneous at autosomal loci, with an average weighted RF distance of 0.91 (SD = 0.06) versus 0.82 (SD = 0.09) for sex-linked loci ($t = 120.37$, $P < 0.01$). Gene trees from coding and non-coding loci did not differ in the number of consensus tree nodes with which they were concordant (T400F ExaML coding mean = 144, SD = 83; non-coding mean = 134, SD = 82; Fig. S27b; $t = 1.38$, $P = 0.17$). Weighted RF distance averaged 0.89 (SD = 0.06) for the coding loci and 0.90 (SD = 0.06) for non-coding loci.

3. Time calibration

3.1 Comparison of different roots

TreePL time-calibrated trees estimated using either a calibration on the Passeriformes+Psittaciformes node (Psittacopasseres) or on the more inclusive clade formed by Cariamiformes, Falconiformes, Psittaciformes and Passeriformes. Both strategies resulted in highly similar divergence times (Fig. S28), and we therefore focus subsequently on the tree based on the better-supported Psittacopasseres calibration.

3.2 Impact of removal or inclusion of poor quality samples on time calibration

Visual inspection of the ExaML phylogenies (e.g., Figs. S13 and S15) reveals isolated long terminal branches, many of which are toe pad samples or poor quality (e.g., rotten) tissue samples. The inclusion or removal of the tips with long terminal branches had minimal impact on the T400F phylogeny (Fig. S29), but some HGAPF trees with these tips included had inflated divergence time estimates for in some parts of the tree, particularly the Tyrannides clade, relative to the HGAPF trees without these tips and the T400F trees (Fig S30). Because of concerns regarding the impact of these low-quality samples and their long terminal branches on divergence times, we investigated their impact more carefully. We conducted a jackknifing analysis in which we iteratively removed each tip in the ExaML T400F tree, re-estimated a time-calibrated tree in TreePL, and then compared the branch length distribution to the complete tree

using K-F distances, which incorporated branch length differences in distance measurements (*142*). Removal of a subset of tips, 52 in particular, resulted in trees with large differences from the complete tree (Fig. S31), and visual inspection of these trees revealed they often exhibited the inflated crown age for the Tyrannides clade. However, none of the 52 tips that jackknifing indicated had a major impact on the time-calibrated tree were the toepads or poor-qualiity samples with long terminal branches. It seems more likely that the result involving an inflated Tyrannides crown represents a failure of TreePL to appropriately optimize divergence times in those analyses. However, we still considered it safer to remove the poor-quality samples for time-calibration purposes, before replacing them in the tree using congruification (see Materials and Methods). Given that this resulted in a time-calibrated tree without the inflated Tyrannides crown age, and that all time-calibrated trees with the T400F dataset regardless of the inclusion of poor-quality samples recovered similar divergence times, it appears that this tree represents the best estimate of the divergence history of suboscines.

3.3 Uncertainty in species ages resulting from topological and calibration date uncertainty

The combination of bootstrapped alignments and stochastic node ages for Psittacopasseria resulted in relative narrow 95% intervals except for the deepest nodes (Fig. S32). Divergence times within eupasseres were constrained by the maximum bound at 47.25 Ma assumed for the crown age of that clade based on its fossil record.

3.4 Comparison of penalized likelihood and Bayesian approaches to time calibration of family-level tree

The BEAST maximum clade credibility tree was nearly identical in topology to the tree estimated using ExaML (Fig. S33). The two exceptions were the placement of Oxyruncidae (sister to Onychorhynchidae in the primary tree, but sister to Onychorhynchidae+Tityridae in the BEAST tree) and Sapayoidae (sister to Pittidae in the primary tree, but sister to Calyptomenidae in the BEAST tree). However, these arrangements involved adjacent, very short branches and were poorly supported in the BEAST tree. More importantly, the ages of divergence times were highly similar for shared nodes in the two trees (Fig S34). The confidence intervals from one tree generally overlapped the point estimates for the other, and relative timing was highly similar across nodes in the two trees.

3.5 Tree updates

In addition to the trees made available via Zenodo (doi: 10.5281/zenodo.3976115), any future updates to this phylogeny will be made to a living tree at https://suboscine.openwings.org/.

4. Correspondance with existing classifications and prior phylogenetic hypotheses

4.1 Paraphyly and classification comparison

We did not recover paraphyly or polyphyly within currently recognized suboscine suborders or families. Family stem ages averaged 27.7 Ma (SD = 6.1 Ma; Table S2). We did, however, recover 35 cases of paraphyly in suboscine genera (Table S14) and 58 cases of paraphyly within species for which we sampled multiple individuals (Table S15). Most of these cases were consistently recovered across trees and were well supported by tree support values. We also found that many species contained intraspecific divergences that were deeper than many divergences between species. 11.66% of intraspecific divergences were deeper than the median sister species divergence with the Howard and Moore classification, 11.72% with the Clements classification, and 12.10% with the IUCN classification (Fig. S35). This diversity within species was only detectable due to the high level of intraspecific sampling in our dataset.

4.2 Comparison with prior trees

We compared our phylogeny with the prior phylogenetic hypotheses of Jetz and colleagues (*96*). Their tree distributions were assembled for all birds by estimating dated trees for 158 subclades and then joining them to a dated backbone phylogeny. 3,330 species lacking genetic information in their dataset were placed using taxonomic constraints. We compared our results to consensus trees from their study both containing all species and containing only those species with genetic data.

Broadly, our tree appears similar to the Jetz et al. trees for suboscines (for example, in the recovery of three major clades: Eurylaimides, Tyrannides, and Furnariides; Fig. S36), but we found substantial topological differences at and below the family level (Fig. S37). We conducted likelihood ratio testing (*143*), which revealed that the gene trees estimated from our genomic dataset substantially favored the family-level topologies from our study (both concatenated and coalescent-based) over the family-level topology of Jetz et al. (Fig. S38). Moreover, with respect to timing information, the Jetz et al. tree with all tips has some odd rapid divergences at the crowns of some subclades, which are not observed in our tree and perhaps represent artifacts of the strategy for adding the un-sampled tips (Fig. S36).

These differences were consequential for downstream analyses. The inverse equal splits estimator, which is a primary variable used in our diversification analyses (and was also examined by Jetz et al.) are correlated between our tree and the Jetz tree, but the correlations were surprisingly weak (all species tree $R^2 = 0.45$, $P < 0.01$; genetic species only tree $R^2 = 0.60$, $P < 0.01$; Fig. S39). It is noteworthy that the correlation with the all-species tree is weaker than the genetic-species only tree, despite the fact that the latter is missing many tips that are important for calculation of the statistic. This suggests that adding species using taxonomic constraints leads to inferences that are more spurious than leaving those tips out (see also *144*).

Moreover, the key result of our study, that speciation rate is highest in lineages occurring in areas with low species richness, falls apart when the Jetz et al. tree is used. Using their all-tips tree, the slope of the correlation is still negative ($\rho = -0.13$), but it is non-significant ($P = 0.21$), and results using the genetic-species only tree are slightly stronger but similarly non-significant ($\rho = -0.22$, $P = 0.11$). This contrast suggests that a highly resolved and accurate phylogeny of suboscines was necessary to resolve the drivers of diversification dynamics in this group.

5. Diversity-through-time

5.1 Lineage-through-time plots and gamma calculations

Lineage-through-time (LTT) plots show a consistent increase in diversity through time in suboscine birds (Figs. 1, S40). A recent flattening of species accumulation may be due to a combination of factors including un-sampled intraspecific diversity, the lag-time for species recognition of current incipient species, unsorted ancestral polymorphism, or residual sequencing or alignment error. However, it appears to be restricted to the most recent 2 to 2.5 Ma. Gamma (γ) statistics (*145*) were negative regardless of the classification or tree examined (Table S16), consistent with a diversification slowdown. However, the gamma statistic is highly affected by branch lengths near the tips (*146*), and this appeared to drive the negative values in our case. When the most recent 2.5 Ma was removed from gamma calculations, values were positive (Table S16).

5.2 Comparison to simple models of tree-wide diversification

Model comparison using AICc indicated that constant-rate models provide a better fit than diversity-dependent models when fit to the primary suboscine tree (birth-death log Likelihood [LL] = -3626.1, diversity dependent LL = -3658.7, ΔAICc = 67.18). Pure-birth and birth-death models had similar fit (pure-birth LL = -3626.0) with pure-birth slightly favored (ΔAICc = 2.30) and a low estimated extinction rate in the fitted birth-death model (μ = 0.00026). These relative model fits are reinforced in parametric simulations under the maximum likelihood parameter values. The LTT plots of simulated constant-rate trees better-matched the empirical LTT plot than those of diversity-dependent trees (Fig. S41).

5.3 Pulled diversification rate through time

The statistics of Louca and Pennell (*18*) revealed a pulled diversification rate (r_p) that was low and relatively constant over the history of suboscines (Fig. S4). A recent upswing in the last ~2 Ma, and uncertainty is greater prior to ~20 Ma. This latter result is presumably because estimation becomes more challenging when there are fewer nodes present to provide information (*18*). The initial condition equal to the sampling fraction times the present-day speciation rate (ηo) was also quite low (0.00023 [CI = 0.00021 - 0.00158] species/Ma), assuming a sampling fraction of 1). Louca and Pennell indicate that, while changes in pulled diversification rate reflect shifts in speciation and/or extinction, a relatively constant pulled diversification rate suggests diversification dynamics have been relatively stable through time. The relative stability of the pulled diversification rate curve in suboscines, therefore, suggests that the apparent stability of diversification dynamics in the group is detectable using estimators that maximize discrimination of alternative diversification histories.

5.4 Episodic birth-death models

Diversification rates estimated using both TreePar (Figs. S42, S43) and TESS (Figs. 2a, S44-S45) models showed relatively constant speciation rates through time. Both captured an apparent drop in speciation rates in the last 2 Ma that seems to correspond to the halt in lineage accumulation observed in LTT plots. Likelihood ratio tests conducted in TreePar suggest this

recent shift is the only significant shift based on model comparison. The addition of more shifts, earlier in the history of suboscines, did not lead to model improvement (Table S17).

5.5 Diversification through time accounting for branch-specific rate heterogeneity

We identified branch-specific variation in diversification rates corresponding to discrete shifts in rate regimes across the tree using a series of model-based methods (see results in section 7 below). To identify whether trends in diversification-through-time across suboscines resembled those from the above analyses after accounting for branch-specific shifts, we summarized diversification-through-time from the posterior distribution of branch-specific rates from BAMM (Fig. S46). This revealed relatively constant speciation through time (concordant with our results from simpler models), or perhaps a small peak in speciation around 10 Ma, but not an early burst in diversification or a diversity-dependent pattern.

5.6 Family-specific investigation of diversification through time

To determine whether the constant diversification observed through time was an emergent feature of the suboscine tree as a whole or also characterized lineages within suboscines on a more granular scale, we examined lineage-through-time plots, gamma statistics, the fit of simple diversification models, and the pulled diversification rate (*18*) for each family containing at least 20 species (n = 10). These demonstrated some support for heterogeneous diversification curves among families. Family lineage-through time plots showed a mixture of relatively straight (e.g., Furnariidae, see also *147*), variously asymptotic (e.g., Thamnophilidae), and even upturned (Rhinocryptidae) shapes (Fig. S5). Gamma values were negative for most families (Table S3), although this appeared to be again driven by the recent decline in lineage accumulation; removing the last 2.5 Ma of evolution resulted in only Thamnophilidae exhibiting a significant negative gamma. Most families fit a diversity-dependent model better than a birth-death model (Table S4), but this also may have been driven by the recent decline in lineage accumulation. Parametric simulations suggested constant-rate birth-death models could produce lineage accumulation curves quite similar to the real data for most families (Fig. S6). Finally, estimates of the pulled diversification rate (*18*) through time revealed some heterogeneity in diversification histories across families (Fig. S7). Overall, these analyses reveal some evidence for heterogeneity in lineage accumulation across suboscine families, but the degree to which these reflect deterministic versus stochastic processes warrants further scrutiny.

6. Tip-specific branching pattern estimators

6.1 Inverse equal-splits estimator (ES)

The inverse equal splits speciation estimator averaged 0.23 (SD = 0.13) across all tips with the T400F ExaML tree and Howard and Moore classification. The average across all branches (including internal branches) was 0.32 (SD = 0.27). ES was highest in regions of the tree with short internal branches such as within, and especially near the crowns of, some of the diverse subclades of suboscines. ES was, predictably, lower when more lumped classifications were examined, but relative ES values across tips were similar among alternative trees and

classifications (Fig. S47). A few areas in the complete Astral tree with ExaML branch lengths had highly elevated ES values, likely because topological errors in the Astral tree produced very short internal branches in ExaML when it was contrained to the Astral topology. Geographic patterns of ES were similar across trees and classifications (Fig. S48) and (as with other diversification metrics) were similar with and without weighting values based on the inverse of species range size (Fig. S49). There was no significant variation in ES between the Old or New World (Table S18), between the Nearctic and Neotropical regions (Table S19), or across absolute latitudes (Table S20) based on our FISSE-like and ESsim-like tests. However, some tests of differences in ES between the Old World and New World were nearly significant, and visual inspection of the maps of average ES values suggests speciation rates are higher in the New World, and especially North America (Fig. S38). This pattern is robust to maps using different trees and classifications. Moreover, BiSSE found evidence of higher speciation rate in the New World than Old World ($\lambda_0 = 0.168$, $\lambda_1 = 0.080$, $P < 0.01$) and in the Nearctic than Neotropics ($\lambda_0 = 0.553$, $\lambda_1 = 0.123$, $P < 0.01$). QuaSSE also found that a model with a linear association between latitude and speciation rates fit better than a constant association (l.m. = 1.96×10^{-6}, $P < 0.01$). Although they are sensitive to false positives, BiSSE and QuaSSE can also be more powerful than simulation-based tests using summary metrics of branching patterns (*94*), and these positive results may reflect real, subtle geographic differences: speciation rates may be lower in the Old World than the New World, and somewhat higher in temperate North America than the Neotropics. Within the Neotropics, we did detect differences in ES among sub-regions (Table S21), recapitulating patterns evident in the maps. The West Indies, for example, had higher ES than many other Neotropical regions, and the Andes, Patagonia, and "Dry Diagonal" (Caatinga/Cerrado/Chaco/Pampa region) had higher rates than the Atlantic Forest.

6.2 Average node height (NH)

Average node height, which measures the average depth of the diversification events subtending species, averaged 17.7 (SD = 5.57) across all tips with the T400F ExaML tree and Howard and Moore classification. NH was highest in regions of the tree with longer branches toward the present, and lowest in younger clades (Fig. S50). Relative patterns of NH were similar across tips whether mean, median, or log mean NH was examined (Fig. S51). NH was greater in the Neotropics than the Nearctic region based on FISSE analyses with all trees and classifications examined (Tables S22, S23). It did not differ between the New World and Old World (Tables S24, S25), although the maps show perhaps the greatest average NH values in the Old World areas (Figs. S52, S53). Failure to recover differences between the New and Old World may stem from the small sample of suboscine species distributed in the Old World. NH also did not differ significantly with absolute latitude (Tables S26, S27). Among Neotropical regions, there were fewer differences than with ES, but species did average older in the Amazon than the Dry Diagonal, and in the Atlantic Forest than in Central America (Table S28).

6.3 Terminal branch length (TB)

Average node height, which measures the average depth of the diversification events subtending species, averaged 4.11 (SD = 3.24) across all tips with the T400F ExaML tree and Howard and Moore classification. As with NH, TB was highest in regions of the tree with longer branches toward the present, and lowest in younger clades (Fig. S54). TB was greater in the

Neotropics than the Nearctic region based on FISSE analyses with all trees and classifications examined (Table S29). It did not differ between the New World and Old World (Table S30, Fig. S55) or with absolute latitude (Table S31). As with NH, there were few significant differences among Neotropical regions in TB, but species did average older in the Amazon and Atlantic Forest than in Central America (Table S32).

6.4 Substitution rate (SR)

Total root-to-tip substitutions (SR) averaged 0.082 (SD = 0.009) expected changes per site across all tips with the T400F ExaML tree and Howard and Moore classification. Correcting for time, this is an average of 0.0018 (SD = 0.0002) changes per site per Ma. Across branches, including internal branches, SR averaged 0.002 (SD = 0.000; Fig. S56). SR did not vary significantly with region or latitude (Tables S33-S35), although the maps suggest that the average value tends to be higher in the Old World (Fig. S57). There were also no significant differences in SR among sub-regions within the Neotopics (Table S36).

7. Model-based estimates of diversification rate variation

BAMM speciation rates and the inferred best shift configuration for the T400F Howard and Moore tree were nearly identical across different priors (Figs. S58). No shifts were inferred running BAMM with only the prior information. The credible shift set from the BAMM run with a prior of 100 expected shifts (hereafter the focal run) included 1183 distinct shifts, the 9 most probable shown in Fig. S59. BAMM runs on different trees and classifications were qualitatively similar to those from the Howard and Moore T400F tree, although the shifts were positioned on slightly different branches in some cases, some runs had up to 3 additional shifts, and one (the 2 Ma time threshold) was missing the shift leading to the Pipridae radiation (Fig. S60). BAMM speciation rates for the terminal nodes were correlated with the inverse equal-splits estimator based on simple linear regression (Table S37, Fig. S61). Patterns of BAMM speciation rate variation across the globe were also qualitatively similar to those of ES, with higher rates in the New World and especially North America (Fig. S62).

Medusa inferred a qualitatively similar combination of rate shifts to BAMM (Fig. S63). However, the positions of some of the shifts differed slightly, the rate shift subtending Thamnophilidae was missing, and a shift from the ancestral regime to a slower regime was present for the Eurylaimides. Despite these differences and the time-constant speciation rates within regimes for Medusa, variation in speciation rates across the edges leading to each species was correlated with variation in the tip speciation rates from BAMM as well as ES (Table S37, Fig. S61). Medusa speciation rate variation across the globe also mirrored BAMM speciation rates and ES (Fig. S62).

The inferred number of shifts from RevBayes for the finite-rate-category birth-death-shift (FRCBDS) process were 32, 85, and 2,506 (priors of 1, 10, and 100 on expected numbers of shifts), and 69, 932, 1,256 for the same three priors with the conditional birth-death-shift (CBDS) process (Fig. S64). RevBayes does not estimate speciation rates at the tips, but rather at internal nodes. We used the speciation rate at the node subtending each tip and its sister for comparison purposes with other, tip-specific metrics of speciation rate. RevBayes speciation rates using both the finite-rate-category birth-death-shift (FRCBDS) process and conditional birth-death-shift

(CBDS) process were correlated with the BAMM speciation rates, Medusa speciation rates, and ES (Table S37, Fig. S61). Geographic patterns in both sets of RevBayes speciation rates were also qualitatively similar to those from ES, BAMM, and Medusa (Fig. S62).

Results from both MSBD (Fig. S65) and ClaDS (Fig. S66) were generally concordant with those of BAMM, Medusa, and both RevBayes models. Tip speciation rates inferred under both MSBD and CLaDS were significantly correlated with those from the previously implemented models (Table S37, Fig. S61). Like BAMM, Medusa, and RevBayes, inferred diversification dynamics in the MSBD model were generally organized into either very high or very low rates (Fig S65), resulting in low variance in the tip speciation rate metrics. Unlike those models and more similar to ES, ClaDS diversification rates were highly variable across tips (Fig. S66). Geographic patterns in both MSBD and ClaDS speciation rates were similar to those from other methods (Fig. S62).

We treat the results of these models as supplemental to ES for the purposes of this study. ES is an estimator of present-day speciation rates. Unlike all other methods except ClaDS, ES captures fine variation in diversification dynamics across tips (Fig. S67). ES is also useful in that efficient statistical tests for associations with tip variables have been developed and evaluated, and these tests have high power and low false discovery rates (*94*, *133*). We therefore focus on the ES results and treat other speciation rate estimates as supplementary.

8. Historical biogeographic modelling

Area assignments combined with dispersal-extinction-cladogenesis (DEC) modelling indicated that, as expected, the Old World suboscine species comprise a single, deep clade (the Eurylaimides) with a deep history in that region. Based on biogeographic stochastic models, temperate North American species represent just 15-20 (mean = 17.8, SD = 1.3) small and young groups of tropical origin (all <6.3 Ma in age), primarily within the Tyrannidae (Fig. S8). There were even fewer colonizations of Neotropics from the Nearctic (range = 4-9, mean = 6.4, SD = 1.2). Historical biogeographic modeling using more finely partitioned regions (see Fig. S11) failed to optimize, potentially due to the high rate of transitions between areas (e.g. the Amazon and the Dry Diagonal).

9. Evolution-environment associations and sensitivity tests

9.1 Tip rate correlation tests versus species richness and environment

The results of all tests of speciation rate (ES), species age (TB and NH), and species richness versus species richness, geography, and environment are provided in Table S5. Significant and highly significant results are highlighted. The clear pattern that emerges is that species richness is associated with many geographical and environmental variables, but speciation rate is not. The only strong association ($P < 0.01$) recovered involving speciation rate is with suboscine species richness.

9.2 Disentangling environmental stability versus habitat age

Species richness is associated with a suite of environmental variables. In general, lineages with high overlap with other species occur at low latitudes, have large ranges, have short migratory distances, and live in environments with high temperatures, high precipitation, low seasonality, and greater stability in temperature and precipitation through geological time (Table S5). Given the high degree of autocorrelation between these geographic and environmental variables, identifying the primary driver of species overlap is not straightforward. Richness may be determined by multiple variables, or by variables for which appropriate data were unavailable for analysis. In particular, the age of different habitats or environments might vary considerably (e.g., *148*), and this variation might be a critical predictor of species richness (*149*). High-resolution spatial data on habitat age are lacking. However, our climatic stability metrics comparing present-day temperature and precipitation with reconstructions from prior periods may approach a reasonable proxy for the age of the habitats in those areas. It's worth noting that habitat age also interacts with the colonization history of those habitats (see section 7 above), such that richness might be best predicted by the younger of the two quantities: age of habitat in an area and age of colonization.

9.3 In-depth investigation of elevation

Despite the lack of a significant association between ES and elevation, there appears to be moderately elevated ES in the Andes (particularly central and southern Andes) relative to the Amazon Basin and other lowland areas. We investigated this further by restricting the elevation analysis to Neotropical (including South Temperate) species. However, even this analysis produced a non-significant association ($\rho = 0.191$, $P = 0.098$). It appears that, although there may be a tendency for elevated average speciation rates in the mountains and the central and southern Andes in particular, it is not as large an effect as other associations, such as that with species richness.

9.4 Inclusion of New World only versus all suboscines

Old World suboscines are represented by only a small sample size of tips ($n = 49$ species), and exhibit a distinct diversification history that may be associated with their coexistence with large radiations of lineages in the other major subdivision of passerine birds, the oscines or suborder Passeri (*150*). As a result, we focused most comparative analyses on dynamics within the more diverse New World assemblage. Although weaker than in all New World suboscines, the association between speciation rate and suboscine species richness was observed examining only Neotropical suboscines ($\rho = -0.228$, $P = 0.014$), but not all suboscines worldwide ($\rho = -0.147$, $P = 0.098$). However, there was a borderline significant association in all suboscines worldwide when richness was based on all passerines ($\rho = -0.173$, $P = 0.048$) or all birds ($\rho = -0.179$, $P = 0.045$), rather than just suboscines. This suggests that speciation rates in Old World suboscines are similarly tied to species richness, although the assemblage of species most relevant for these dynamics may be broader taxonomically than in the New World.

9.5 Phylogenetic uncertainty

We recovered a significant association between speciation rate and species richness in all 100 bootstrap trees (ρ ranged from -0.278 to -0.258, P value from 0.001 to 0.005). This suggests our result is robust to phylogenetic uncertainty.

9.6 Branch length estimation error

Bias in terminal branch lengths, often due to variation in taxonomic practices among clades or regions, is a perennial concern in studies of diversification dynamics (*151*). It is possible, however, to interrogate to some degree whether branch lengths reflect the biological processes of interest and diversification estimates are robust to these issues. SSE methods, examined below (section 9.11), model the association between a variable of interest and speciation rates throughout the tree (not weighted towards the tips) and should be more robust to errors in terminal branches. In addition, we used sensitivity tests and an analysis of non-ultrametric penultimate branch lengths to evaluate the impact of terminal branch length bias.

We used two strategies for sensitivity testing. In the first, we uniformly shortened or lengthened all terminal branches on the tree the same amount in order to assess the impact of widespread error in terminal branch lengths on results. In the second strategy, we assessed the impact of variation in branch length estimation error across the tree by retaining long terminal branches from toe pad samples (n=124), which were non-randomly distributed across the tree. After time calibrating these trees again with TreePL, we examined their similarity to our primary tree and the impact on our key result (the correlation between the equal splits estimator and species richness). Relative ES values between these treatments and our primary tree are plotted in Fig. S68 and the results of ES-sim tests with these new branch lengths in Table S38. We found that both widespread and isolated adjustment to terminal branch lengths had minimal impact – relative branching rate estimates were highly correlated with those from the original tree, and correlations with species richness were similar across both types of treatments.

We also conducted an analysis of penultimate branch lengths subtending sister species in our non-time-calibrated tree (n=408). These penultimate branches should not be impacted by sequencing errors, sample quality, or polymorphisms sorting within one species. We evaluated whether sister species pairs occurring in species-rich areas (based on the average richness in which the two occur) had longer penultimate branches than those occurring in species-poor areas. If the long terminal branches observed in tropical species are spurious due to the issues mentioned above and there is no biological signal of reduced speciation in these regions, we would expect no relationship. However, we observe a highly significant positive association between species richness and penultimate branch lengths ($R^2 = 0.04$, P = 0.002; Fig. S69). The best explanation for this pattern is lower recent diversification in those regions. Overall these results indicate that the observed speciation rate – species richness association is not driven by terminal branch length bias.

9.7 Alternative taxonomic treatments

We evaluated the impact of taxonomic classification (e.g., the degree to which species were “split” or “lumped”) by comparing results using the three classifications for which it was possible to assemble species distributional data: the primary classification (AOS + Howard and Moore), the AOS + Clements classification, and the IUCN/Birdlife classification. As with the primary (AOS + Howard and Moore) classification, negative associations between species

richness and recent speciation rates were observed using both the AOS + Clements (ρ = -0.247, P = 0.005) and IUCN (ρ = -0.229, P = 0.009) classifications.

9.8 The impact of spatial autocorrelation in species range overlaps

Spatial autocorrelation is a pervasive issue with species distributional data (*152*). Spatial autocorrelation in, for example, species richness might bias downstream analyses, particularly if low resolution of species distributional boundaries prevails in some regions (e.g., less well-studied Neotropical areas) or if the geography of species ranges tends to elevate estimates of range overlap (e.g., narrow elevational ranges in Andean birds). If these areas tend to have higher or lower diversification metrics, associations may reflect artifacts rather than real relationships. To evaluate this possibility, we conducted a permutation test in which we evaluated whether the correlation structure of species overlap values was likely to produce associations with speciation rate (a key result of our study) by chance. We randomly permuted speciation rate values across all suboscine species and assessed whether our statistical test for associations with continuous variables, ESsim (*94*), recovered a significant association with speciation rate. We conducted 1000 permutations. None of the 1000 permutations of speciation rate with range overlap metrics recovered a correlation (ρ) as strong or stronger than that observed in the real data. This indicates that the observed association is robust to the impact of spatial autocorrelation in species richness resulting from spatial biases in the resolution or shape of species distributions.

9.9 Consistent results within subclades and smaller geographic regions

The negative association between species richness and speciation rates was not driven by a single geographic region. Although subsetting the dataset to narrower geographic regions (see Fig. S11) resulted in reduced power to detect associations, most regions still showed negative associations between the two variables, and these were significant in the Amazonian, Neotropical, and Dry Diagonal regions (Table S39, Fig. S70). Similarly, families within suboscines generally exhibited a negative species richness/speciation rate association, which was significant in the large Tyrannidae family (Table S39, Fig. S71).

9.10. Results using alternative speciation rates

Although we focus on speciation rates estimated with ES, we did examine whether a key result, the association between speciation rate and species richness, is evident using alternative branch-specific estimates of speciation rates. We used a simulation-based test similar to ESsim in which trait values (species richness) were randomly simulated across the phylogeny and associations with the estimated speciation rates at tips were examined. Aside from ES, only ClaDS recovered a significant association between speciation rate and species richness (Table S40). As with ES, ClaDS speciation rates were negatively associated with species richness. It is perhaps not surprising that other speciation rate estimates did not exhibit significant associations due to the low variance in tip-specific speciation rates from those methods.

9.11 State-dependent speciation and extinction (SSE) modeling

Based on model comparison using QuaSSE, a model in which speciation rate varied with the species overlap of a lineage fit the suboscine data better than a model with no trait-associated rate variation or a model in which only extinction rate varied with overlap (Table S7). A model in which both speciation and extinction rates varied with species overlap was only slightly less favored than the one with just trait-associated speciation rate variation. Both speciation and extinction were inversely related with species overlap, although MLE extinction rates were low across observed trait values (Fig. S72). This supports the ESsim results that found a negative association between speciation rates and species richness. Although variable extinction rates are notoriously difficult to measure from phylogenies of extant species only (*153*), the QuaSSE results also provide at least preliminary evidence that elevated extinction rates characterize areas with low richness and potentially harsh environments. Several prior studies have indicated that latitudinal gradients exist in extinction rates and may be responsible for reduced species richness at high latitudes (*2, 22, 29, 154-156*).

Despite their limited power, HiSSE models also generally favored models with trait-dependent diversification, depending on the threshold used to delimit species-rich versus species-poor. At thresholds representing the 50, 60, 70, and 80 percent quantiles, the trait-dependent speciation model (HiSSE) was favored over all other models (Fig. S9). When the threshold is set to lower quantiles, the HiSSE model involving an association between speciation rate and both species richness and a hidden variable was generally favored. This result suggests that when the threshold is low such that more than half of the lineages are treated as occurring in species-rich areas (trait=1), speciation rate variation within that group of lineages cannot be explained simply by species richness but requires an additional explanatory variable. This may be because, when the category of species-rich lineages is more inclusive, they represent lineages in distinct areas (e.g., Amazon, Andes, Central America, Caribbean) subject to different evolutionary dynamics.

9.12 Extinction or incomplete sampling

Although our key results are evident using methods that explicitly model both trait-associated and independent extinction (QuaSSE, HiSSE), it might be argued that even SSE methods are insufficient to capture extinction dynamics in trees of extant taxa only. For inadequate modeling of extinction to drive our result, our models would have had to fail to capture very high rates of extinction in areas of high species richness (thereby inferring low speciation rates there). It seems highly unlikely that extinction rates are substantially higher in species-rich regions, both based on existing theory that species are more ephemeral at high latitudes (*2, 22, 29, 154-156*) and on our QuaSSE results indicating extinction rates were lower in species-rich regions.

We conducted further evaluation using a sensitivity analysis to examine the level of extinction that would be required to obscure key results. This also serves as an evaluation of incomplete sampling, as missing species missing due to extinction or lack of sampling produce the same effects. We modeled extinction three different ways. First, we modeled random extinction across the tree by pruning 20%, 40%, 60%, or 80% of the tips. Each extinction treatment was simulated 100 times. Second, we modeled non-random extinction across taxonomic groups. We removed tips from each family based on a proportion sampled from a truncated normal distribution with SD = 0.1 and mean of 0.2, 0.4, 0.6, or 0.8. Each treatment (mean value for the distribution) was sampled 100 times. Third, since small range size might increase extinction probability, we modeled non-random extinction with extinction probability

based on the inverse of relative range size. Again, we removed 20%, 40%, 60%, or 80% of tips and conducted each treatment 100 times. We then tested whether our major result (the negative association between speciation rate and species richness) was still recovered. We found that our major result was robust to the loss of substantial diversity, both randomly and non-randomly across the tree (Table S6). Across all three strategies for modeling extinction, the major result was still evident in all trials at 80% sampling, nearly all trials at 60% and 40% sampling, and still present in roughly half of trials with only 20% of lineages retained (247 of 1,237 species). Our results are robust to simulated extinction, suggesting that severe and extremely geographically biased (toward the tropics) extinction would be needed to yield a spurious result.

9.13 Assumptions about the evolution of species richness

Our SSE tests involving species overlap assume that the species richness experienced by a lineage evolves in a way that is adequately modeled by a Brownian process along branches of the tree. This is an unconventional way to think about species richness. This approximation is intuitively reasonable in that lineages will tend to occur in regions in which their ancestor occurred, which is likely to harbor similar species richness over that interval. However, if cladogenesis is primarily a result of allopatric speciation, it may be that the two daughter lineages sometimes inherit rather different species richness values. Unfortunately, QuaSSE's trait modeling machinery does not permit incorporation of these sorts of jumps. However, we used a parametric bootstrapping test to assess whether Brownian motion is a reasonable approximation of change in species richness across the suboscine phylogeny. We fit Brownian motion to the real data, and then compared this to the fit of 1000 trait datasets simulated across the suboscine tree under Brownian motion. We found the real data were indistinguishable from Brownian motion (P = 0.992). Visualizing a Brownian reconstruction of species richness across the suboscine tree further reveals that lineages with low or high species richness tend to be clustered in particular clades (see Fig. S73), such that inference of ancestral values is more straightforward than it would be were there rapid shifts in richness among close relatives. This suggests that, despite the potential for rapid shifts in species richness at speciation events, change in species richness across suboscine lineages is adequately modeled using a Brownian process.

9.14 Range size and speciation rate

Particularly under geographic speciation scenarios, it is possible that quickly speciation lineages will have more subdivided ranges and that these smaller ranges will in turn lead to less overlap with other species. If this is the case, small range size might drive a negative association between speciation rate and species overlap. However, we do not find elevated speciation rates in small-ranged species (rho = -0.12, P = 0.27). We further conducted a multi-predictor test using range size and species richness. Multi-predictor tests are not possible in the ESsim framework, so we used PGLS. It turns out the association between species richness and speciation rate is only borderline significant (estimate = 1.13×10^{-4}, t = -1.93, P = 0.05). Thus, range size explains part of the effect of species richness. However, a model with species richness as the predictor had a much higher model weight (0.37) than one with range size (0.19; Table S41). Given the much tighter association between species richness and speciation rate, it is clear that species richness is important over-and-above the subdividing impact of speciation on species ranges.

9.15 Sister clade comparisons

Given widespread concerns with diversification modeling (*18, 110, 137*), we also examined our key result using a classic sister group comparison. Sister group comparisons are a largely model-free approach to comparing diversity using phylogenetic trees. To identify sister clades, we examined a comprehensive set of thresholds between low and high species richness. For many of the thresholds, we had dozens of sister group comparisons (Fig. S10a). We used a sign test to evaluate whether clade diversity was associated with species richness. The association was supported at moderate and high threshold values (Fig. S10b). Thus, the relatively model-free sister group comparisons generally support our key result – the negative association between speciation and species richness.

9.16 Phylogenetic path analysis

Phylogenetic path analysis comparing four models of causal relationships among variables favored a model in which environmental variables drove variation in species richness among lineages, and speciation rates were driven both by species richness and environmental variation. However, the only predictor of speciation rates with a standardized regression coefficient with standard errors not overlapping zero was species richness. P-values for the c-statistic were zero in all models (Table S42), which would normally indicate rejection of all of the models. However, an examination of individual p-values for pairwise relationships among variables suggests this result is due to autocorrelation among the parent environmental variables. This lack of conditional independence in the environmental variables is trivial because we are not interested in the unique contributions of individual environmental variables, but rather their overall impact. When the environmental variables were collapsed into a single variable (PC1 of a principal component analysis) in the indirect model, the P value of the c-statistic was not significant (P = 0.208), indicating good model fit.

Figures

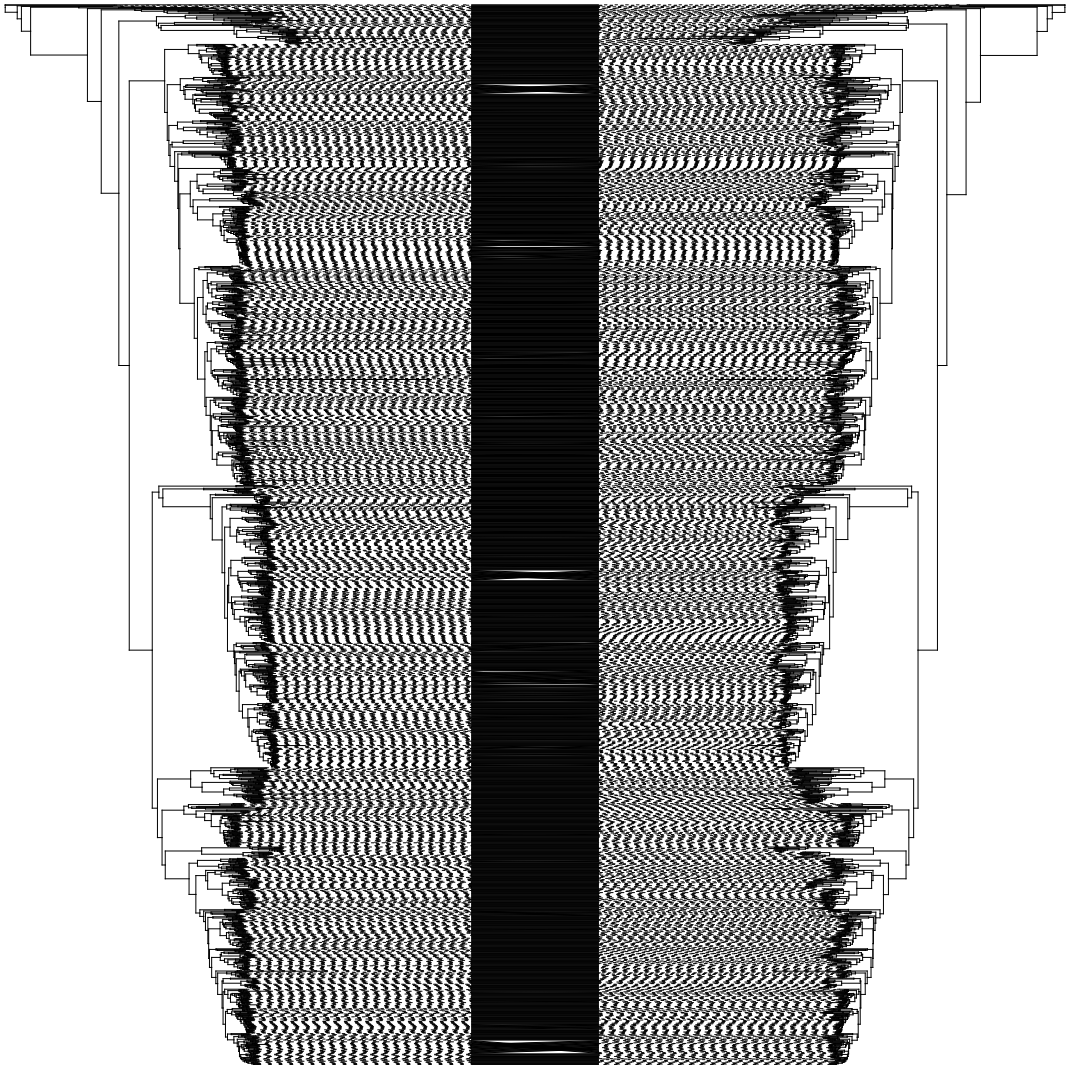

Fig. S1. Cophylogenetic plot of the T400F (left) and HGAPF (right) ExaML topologies showing widespread concordance (the prevalence of horizontal lines) and limited discordance (the isolated crossing lines)

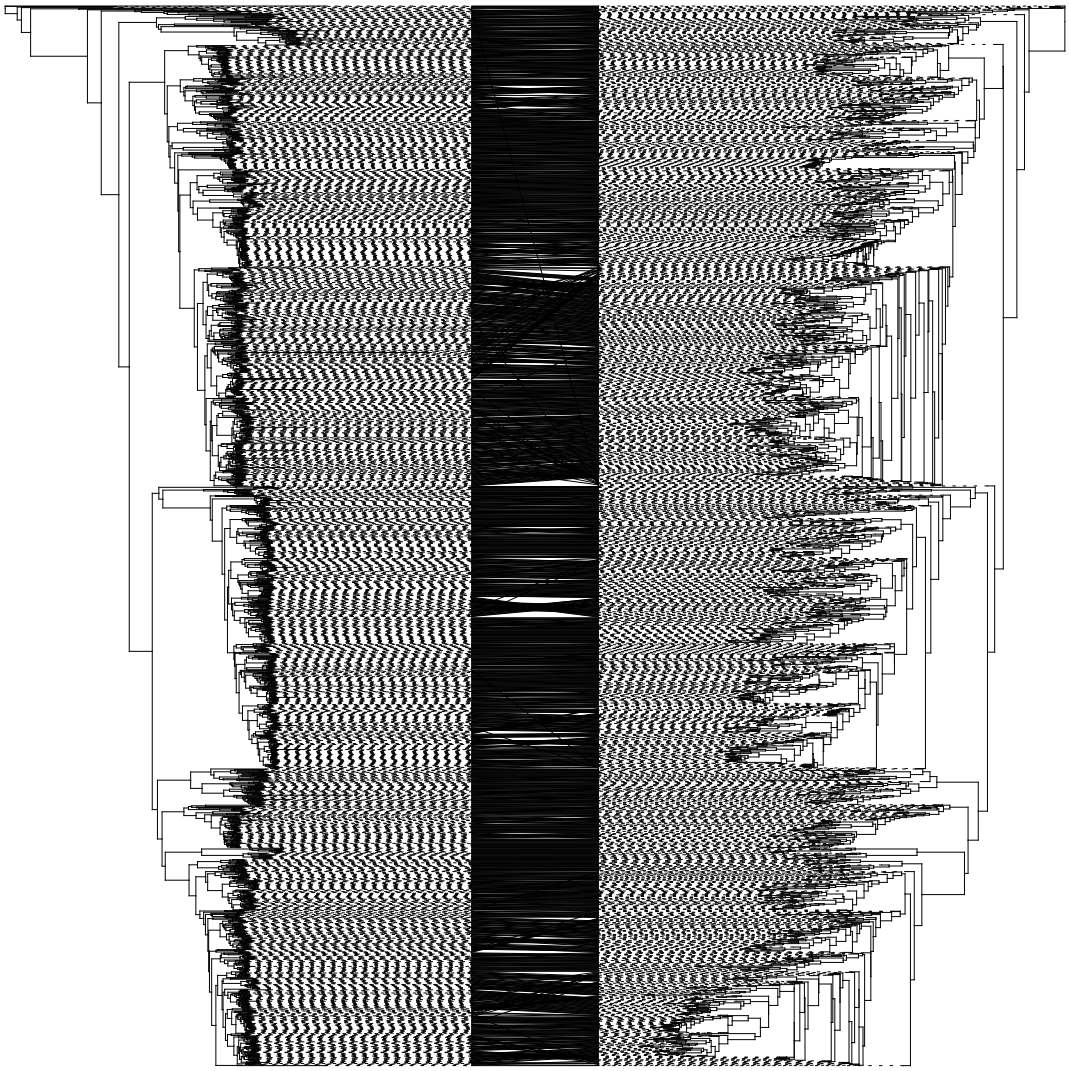

Fig. S2. Cophylogenetic plot of the T400F ExaML (left) and Astral (right) topologies showing concordance

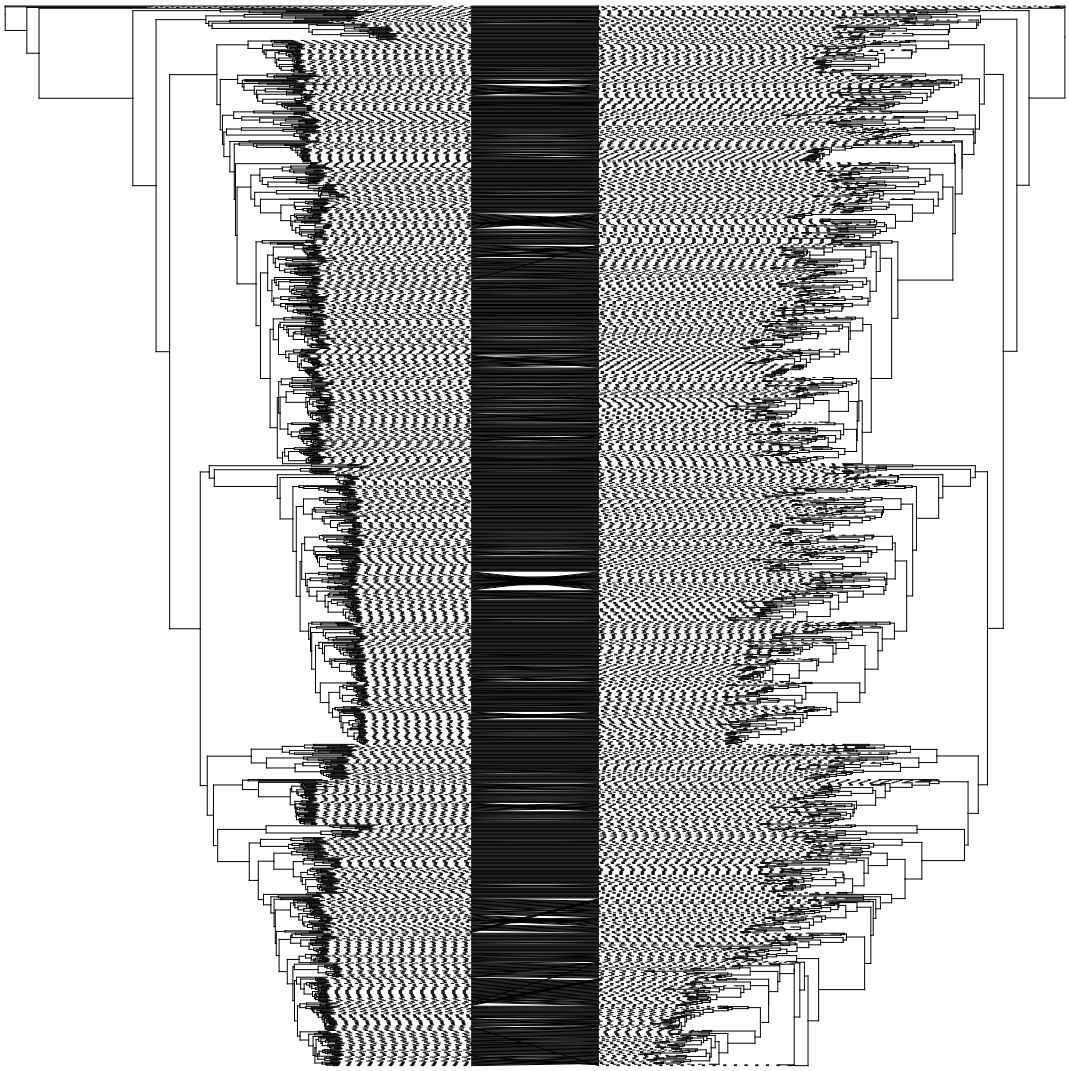

Fig. S3. Cophylogenetic plot of the T400F ExaML (left) and Astral topologies (right) showing concordance after dropping tips missing from >250 gene trees

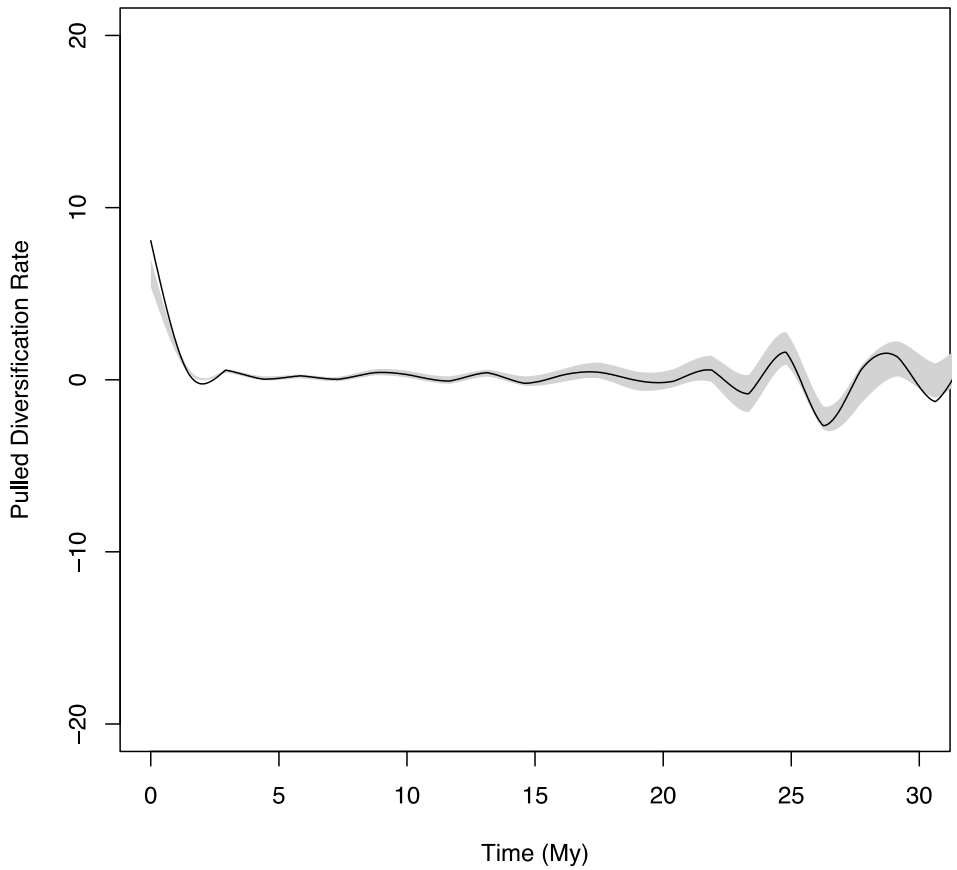

Fig. S4. Best fit (black lines) and confidence intervals based on bootstrap replicates (gray polygons) of pulled diversification rate (r_p) shows relatively constant diversification over the past 30 Ma.

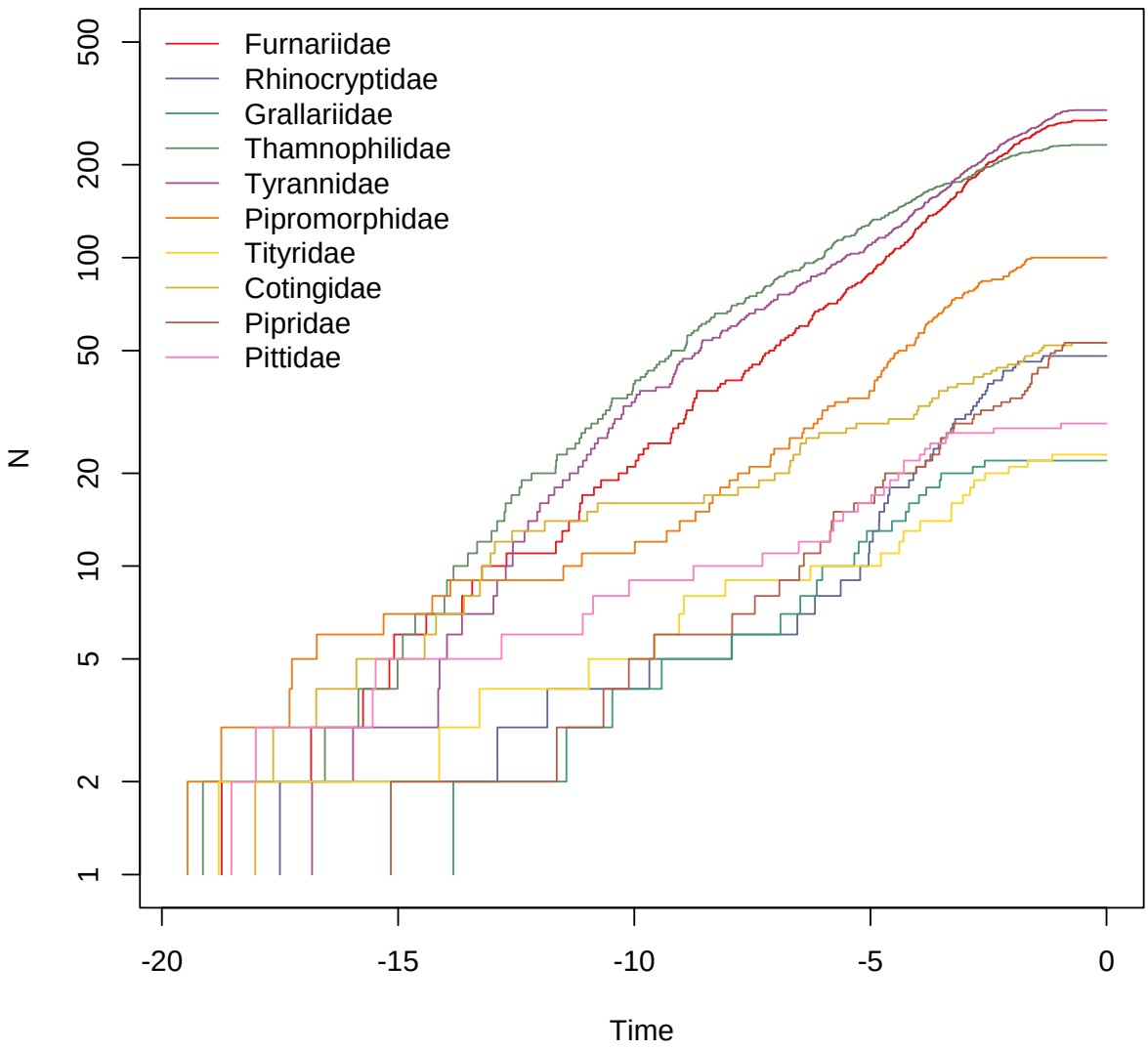

Fig. S5. Lineage through time (LTT) plot of all suboscine family-level clades with more than 20 species

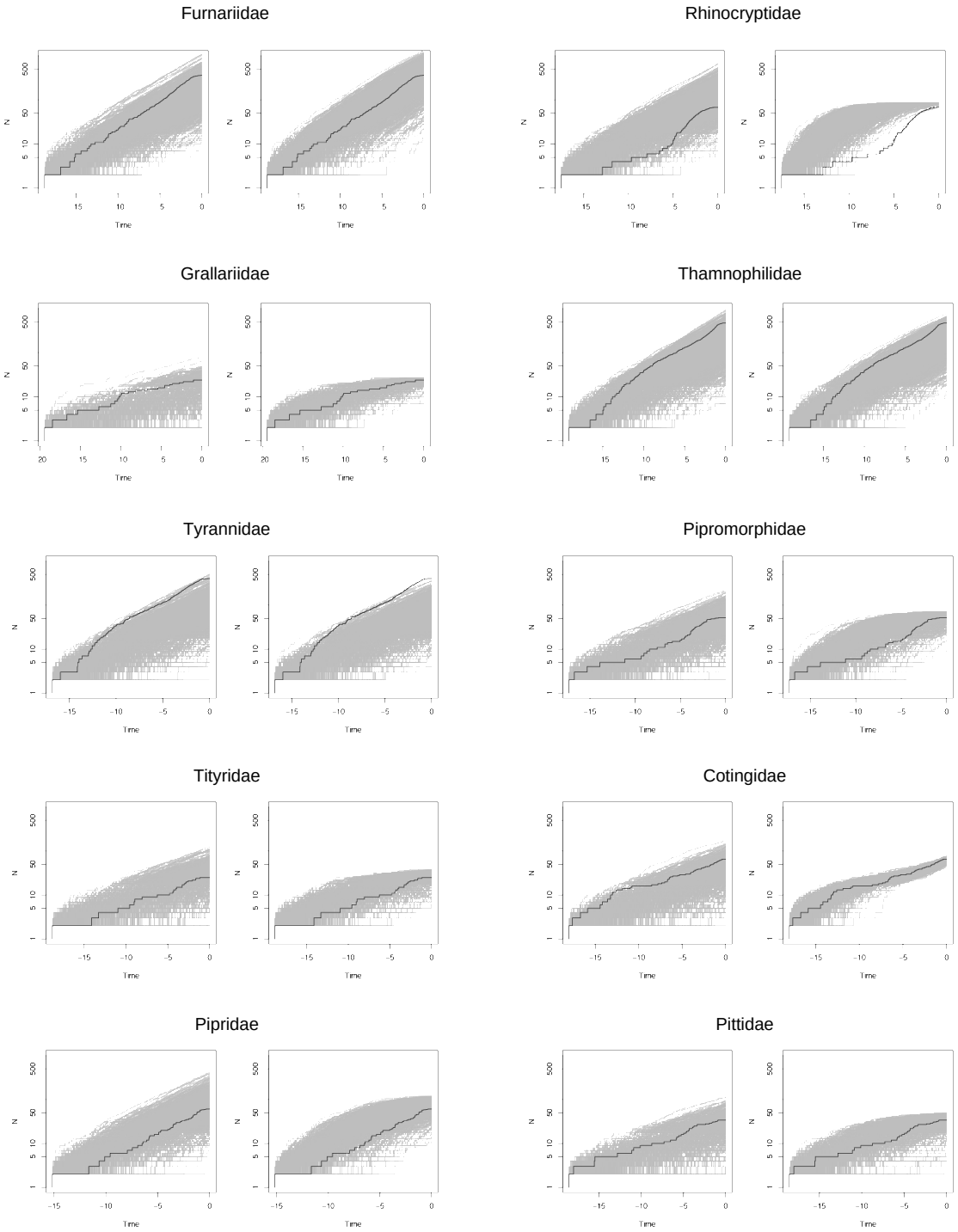

Fig. S6. For each suboscine family-level clade with more than 20 species, the lineage through time (LTT) plot (black lines) compared to 1000 simulations (gray lines) based on maximum likelihood parameter estimates under a birth-death model (left panel) and a diversity-dependent model (right panel)

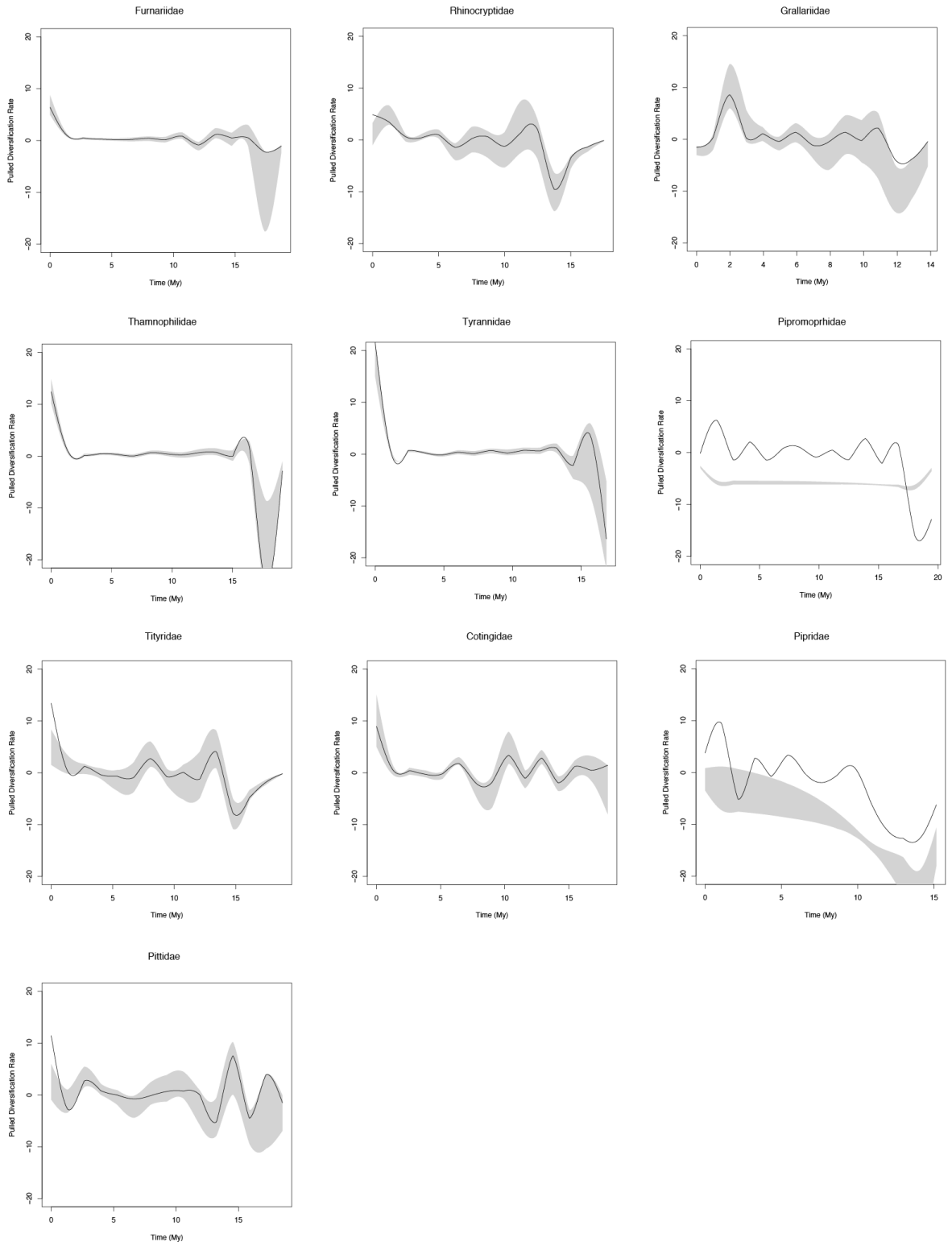

Fig. S7. Best fit (black lines) and confidence intervals based on boostrap replicates (gray polygons) of pulled diversification rate of Louca and Pennell (*18*) shows relatively constant diversification over the past 10 Ma in most suboscine families, with some heterogeneity. Many have a recent upswing in rate, whereas uncertainty becomes greater earlier in each clade when there are few diversification events to provide information

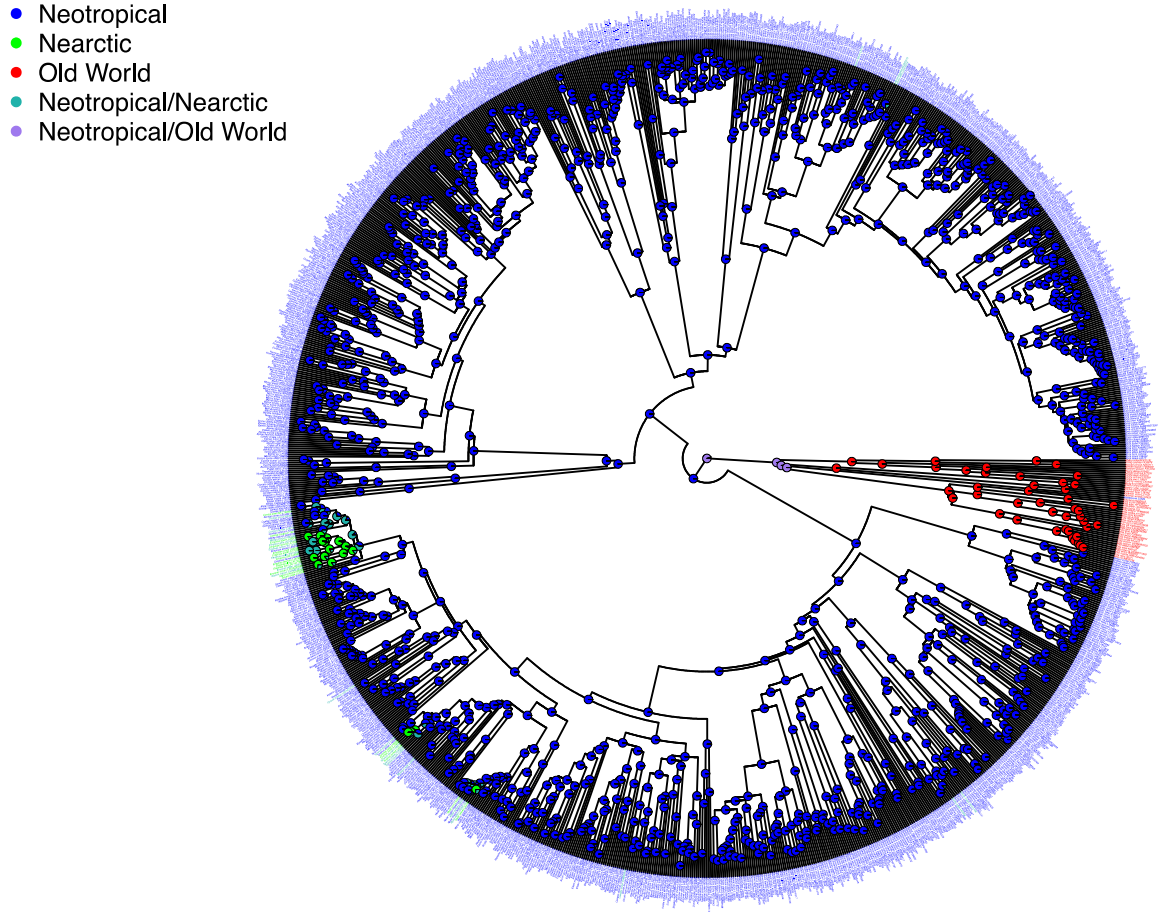

Fig. S8. A map of present (tip label colors) and ancestral (pie charts at nodes) geographic areas based on DEC modelling.

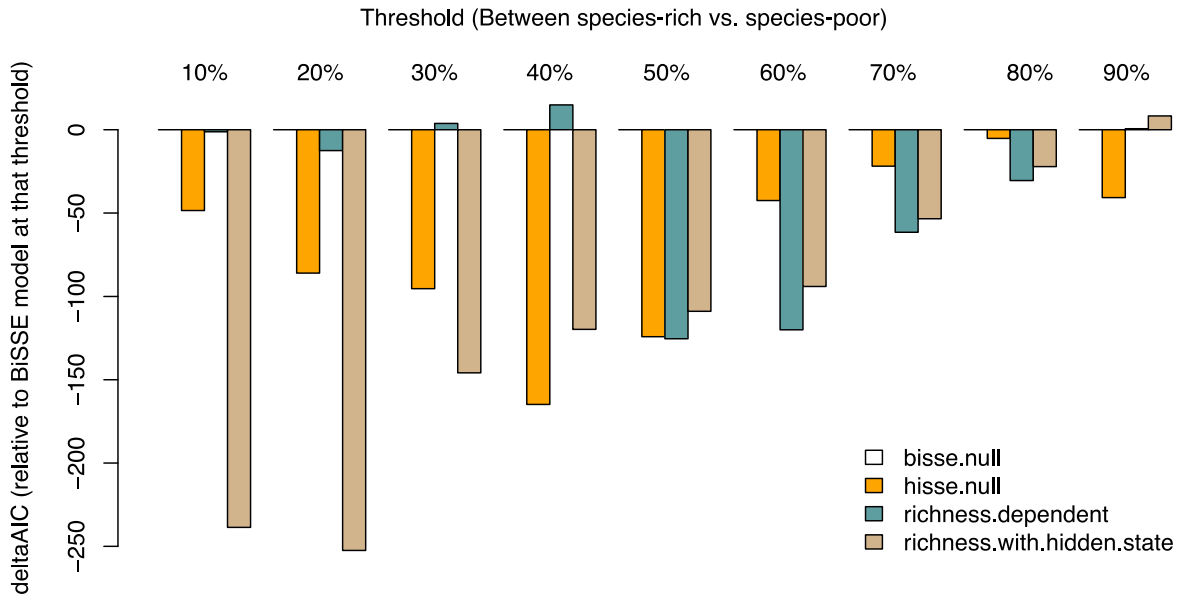

Fig. S9. Plot showing support for alternative models based on analysis with HiSSE (thresholds represent what percentage of tips fall in the species-rich category when converted to a binary trait)

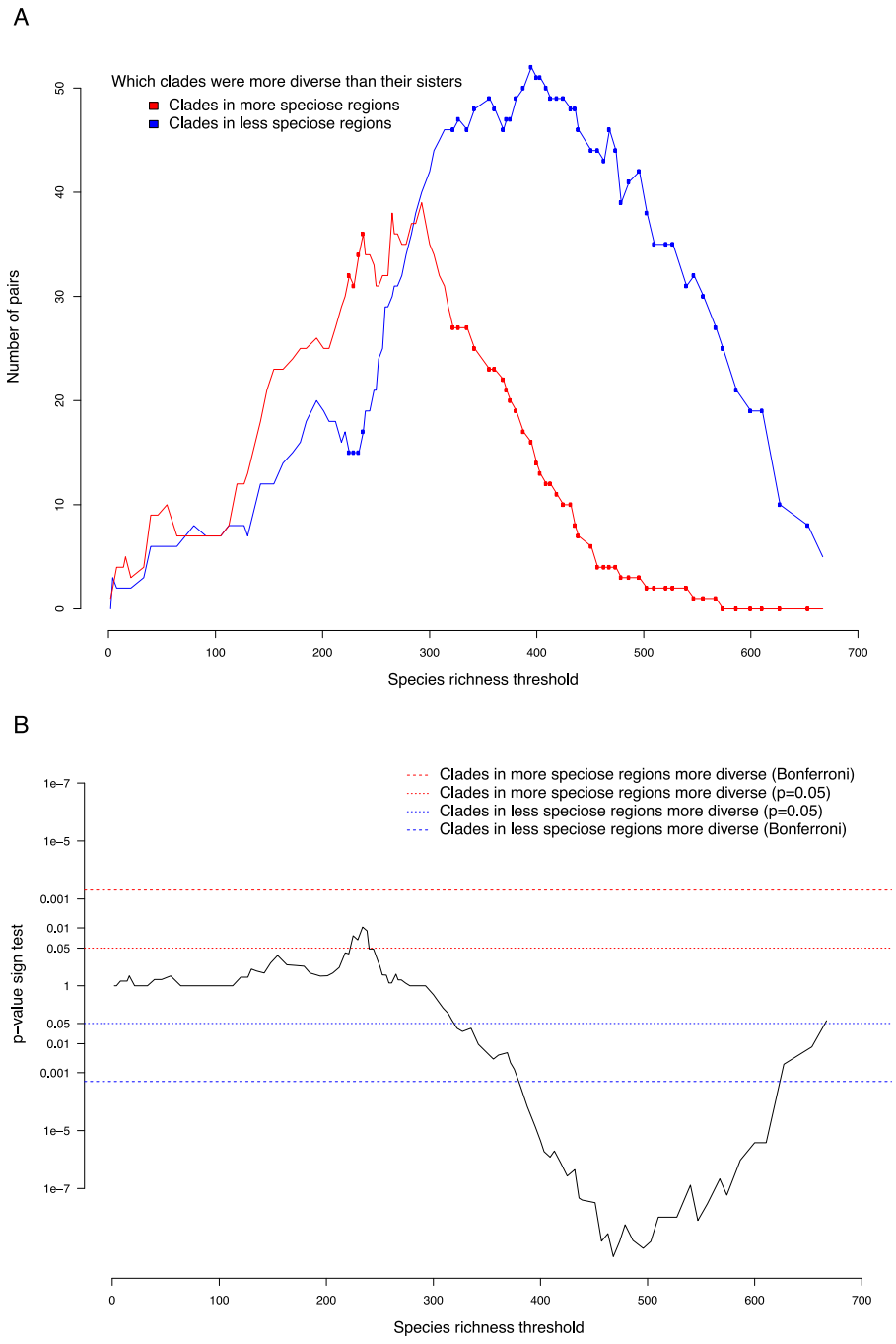

Fig. S10. The results of sister clade comparisons attempting different thresholds to discretize species richness into low versus high diversity. For each threshold, sister groups were identified in which all taxa for one clade had one state and all taxa for the sister clade had the other state. (A) The number of comparisons of each type per threshold. (B) The results of sign tests at each threshold showing the p-value on a log scale, where values above the p-value=1 line show where there was evidence that clades from high diversity regions had more species than their sister groups and values below the p-value=1 line show were there was evidence that clades from low diversity regions had more species than their sister groups. The dotted lines show a p-value of 0.05; the dashed lines show this after a Bonferroni correction for the number of distinct thresholds tried.

Fig. S11. A map showing the extent of the Neotropics as defined for this study. Colored polygons represent the different regions used for the more subdivided BioGeoBEARS analyses and in regional comparisons of diversification statistics. Regions are: West Indies (WI; red), Central America/Chocó (CA; magenta), Andes (AN; green), Amazon (AM; yellow), Dry Triangle (DT; light blue), Atlantic Forest (AF; dark blue), and Patagonia (PA; turquoise).

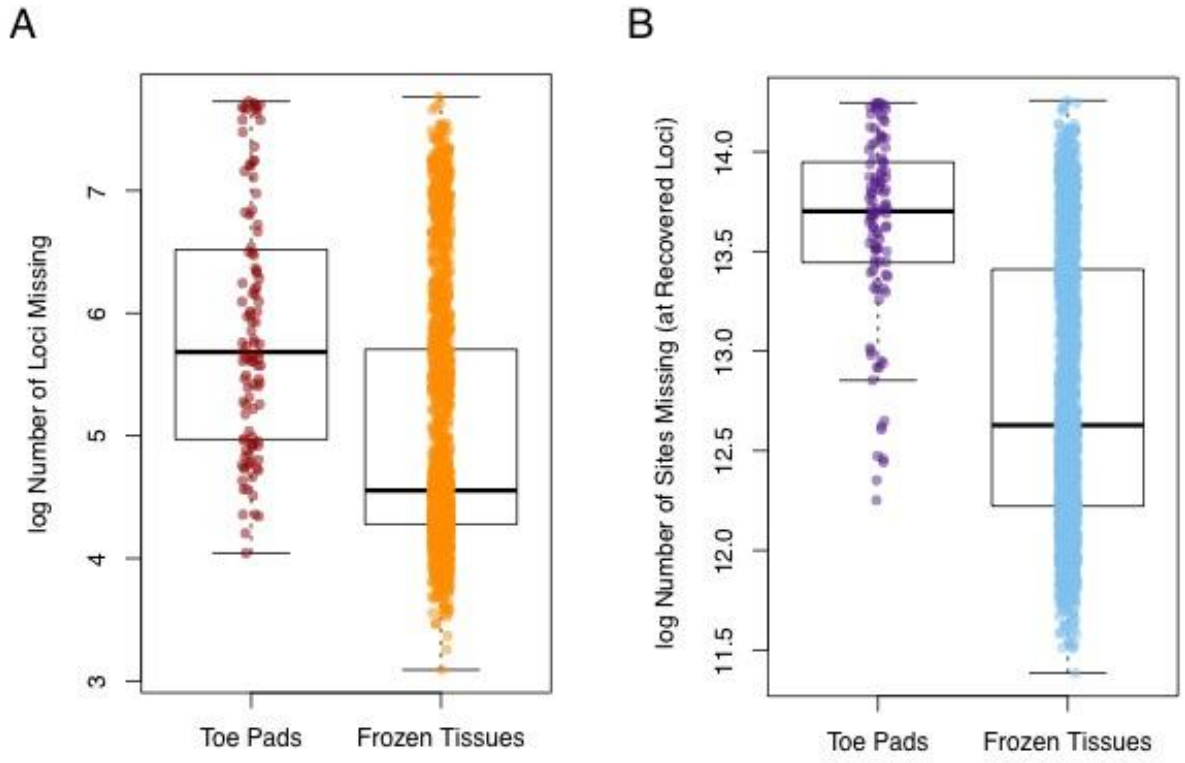

Fig. S12. Comparison of dried toe pad and frozen tissue samples in the number of loci recovered (a) and the average length of sequences across loci for which data were recovered (b).

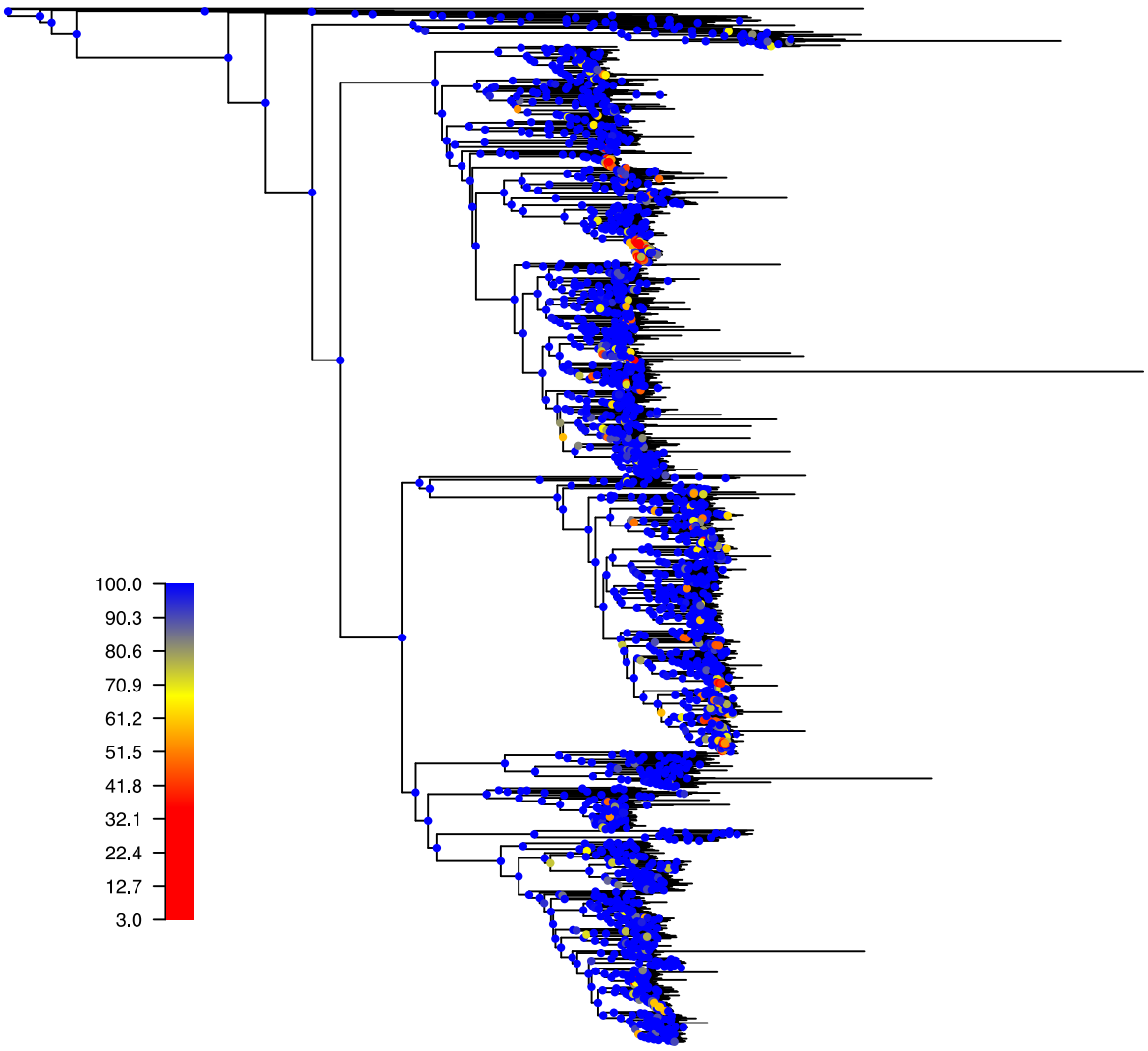

Fig. S13. T400F ExaML tree with nodes colored according to bootstrap support

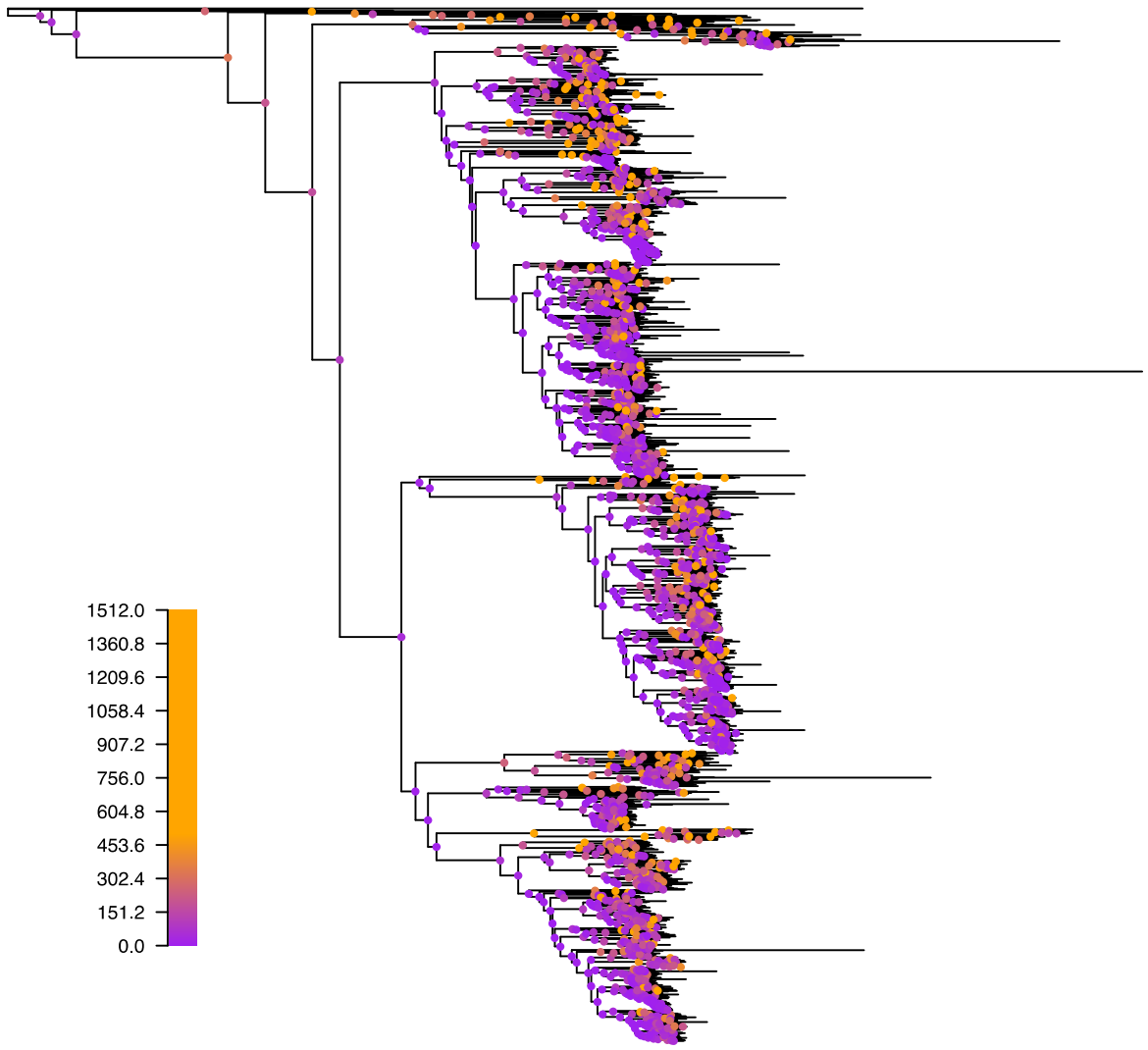

Fig. S14. T400F ExaML tree with nodes colored according to gene tree support

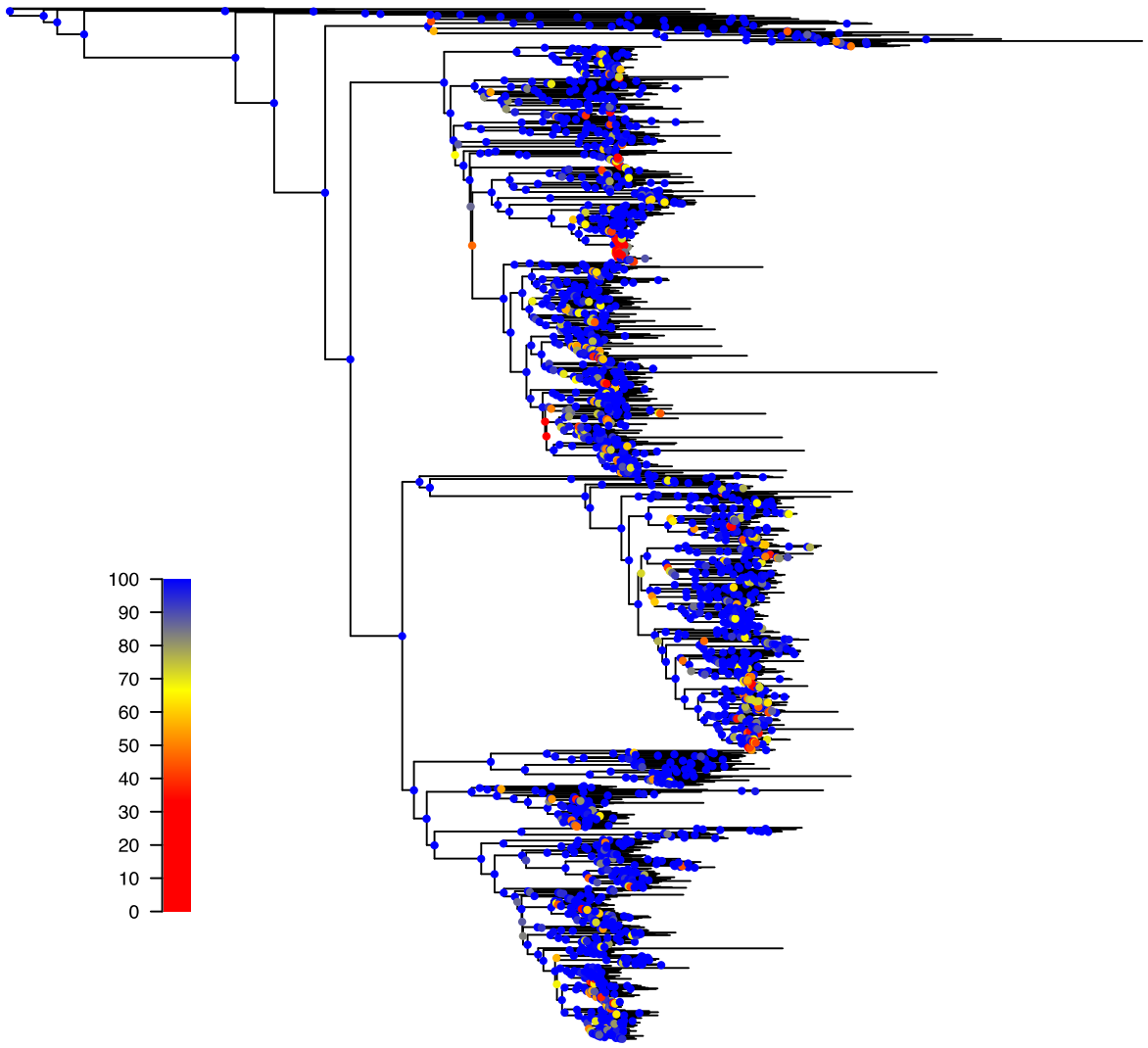

Fig. S15. HGAPF ExaML tree with nodes colored according to bootstrap support

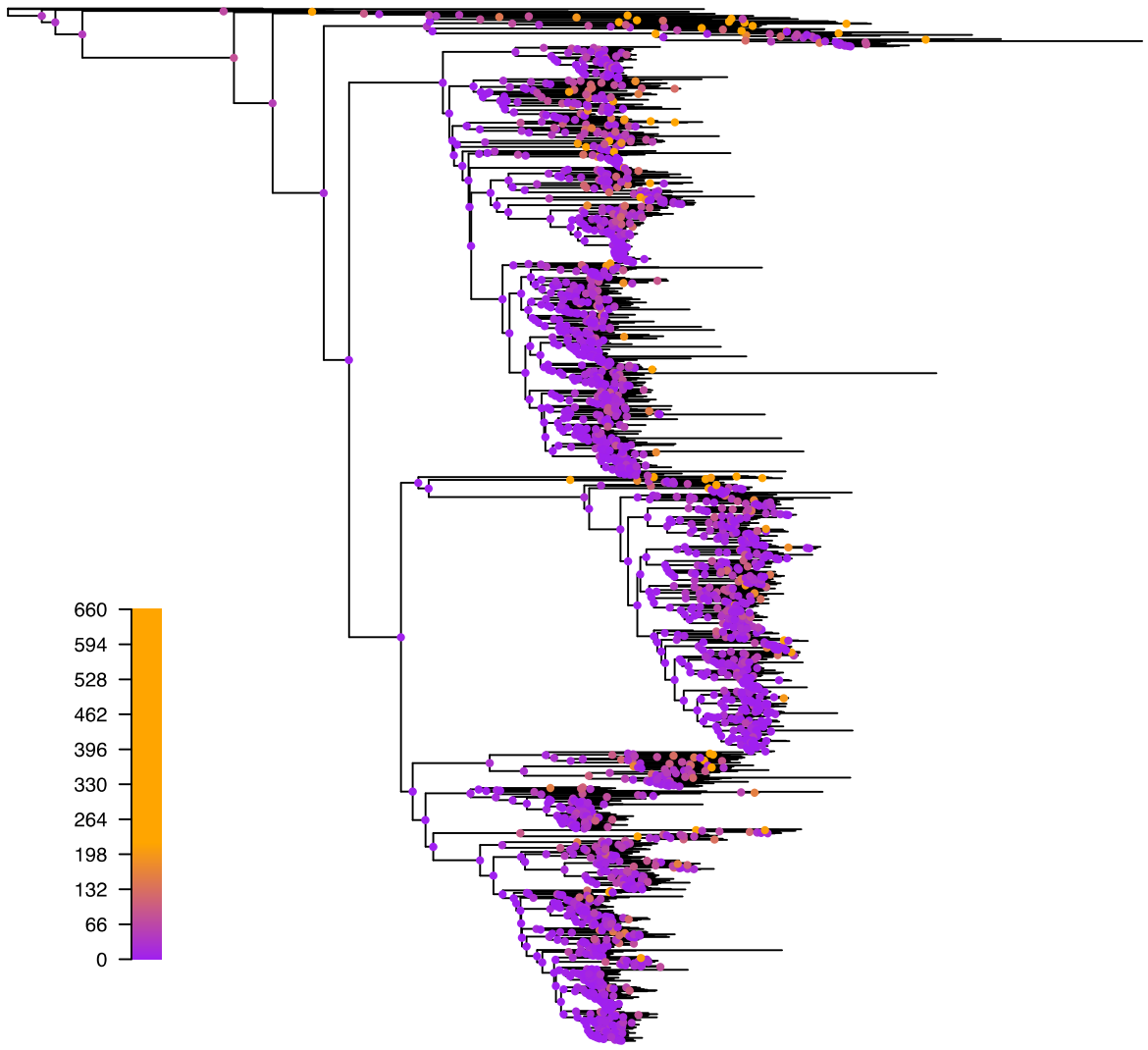

Fig. S16. HGAPF ExaML tree with nodes colored according to gene tree support

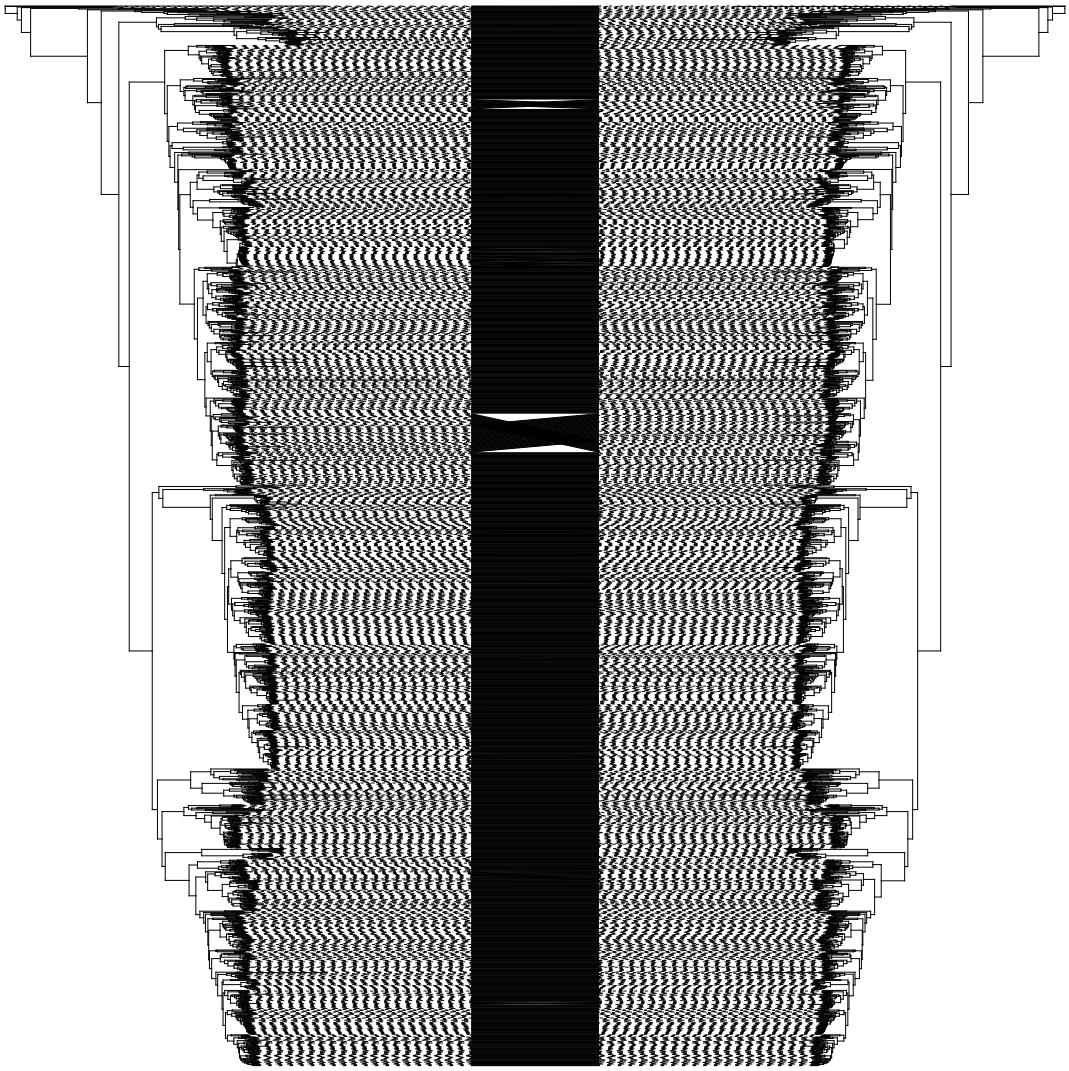

Fig. S17. Cophylogenetic plot of complete (left) versus autosomal (right) T400F ExaML trees showing topological concordance

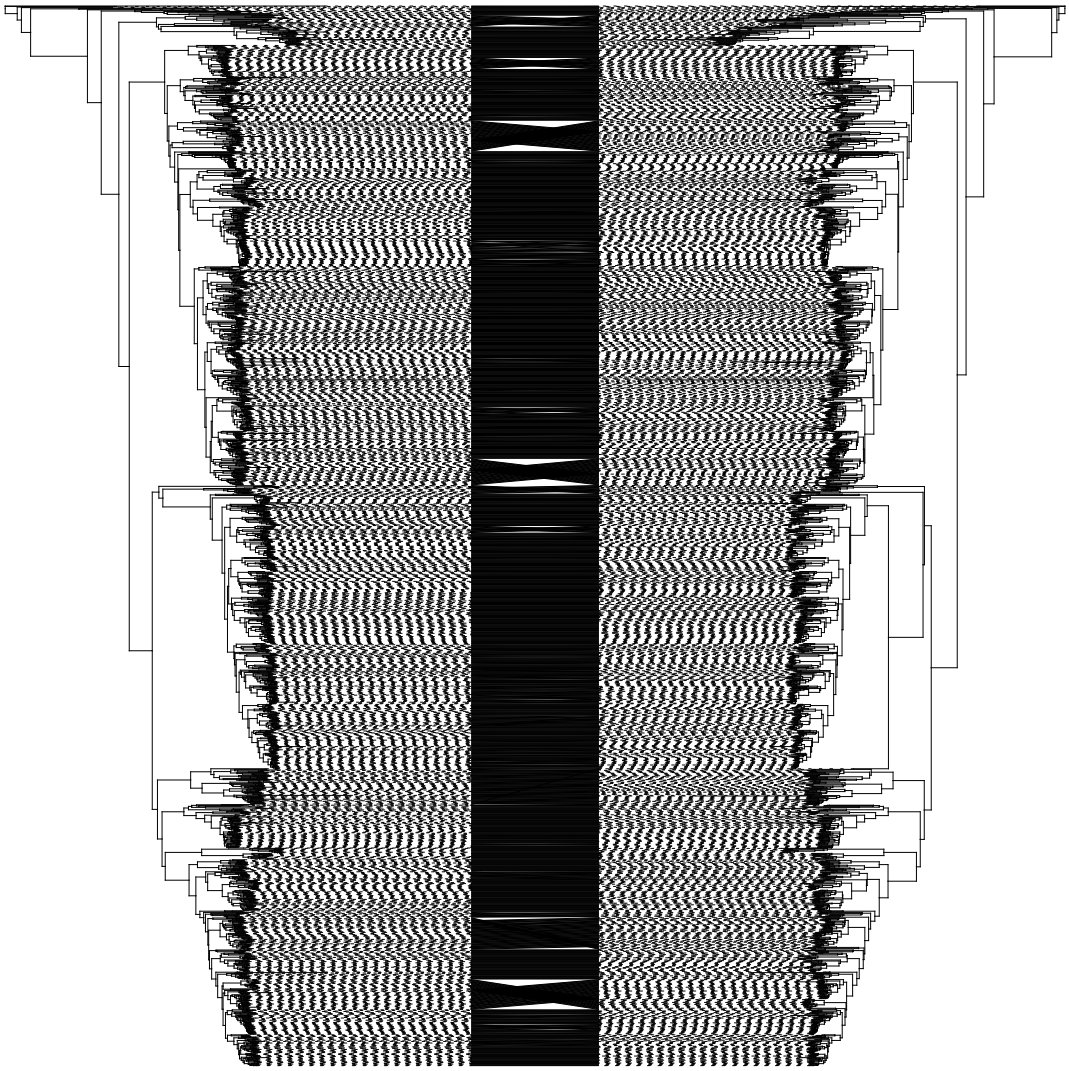

Fig. S18. Cophylogenetic plot of the complete (left) versus sex-linked (right) T400F ExaML trees showing topological concordance

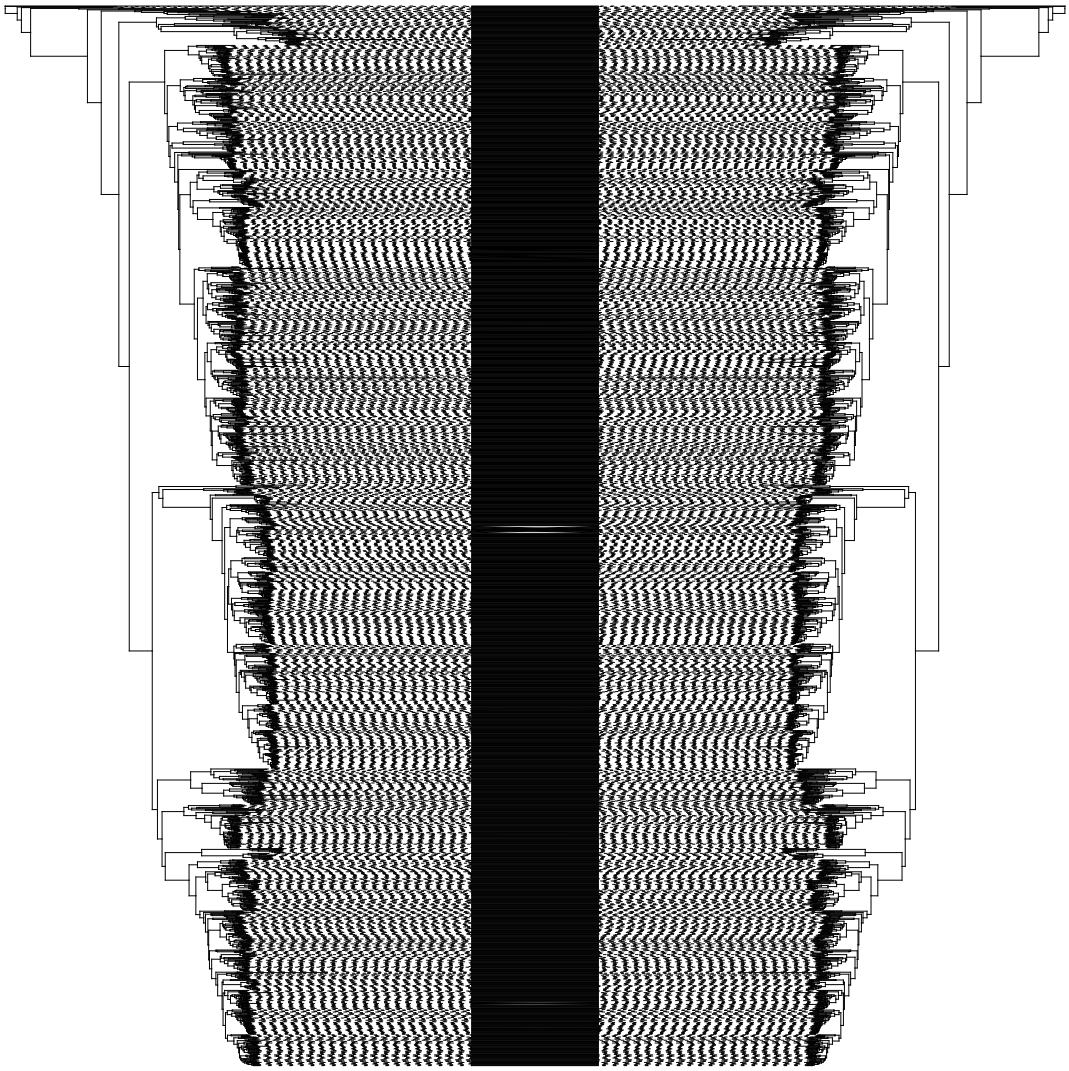

Fig. S19. Cophylogenetic plot of the complete (left) versus non-coding (right) T400F ExaML trees showing topological concordance

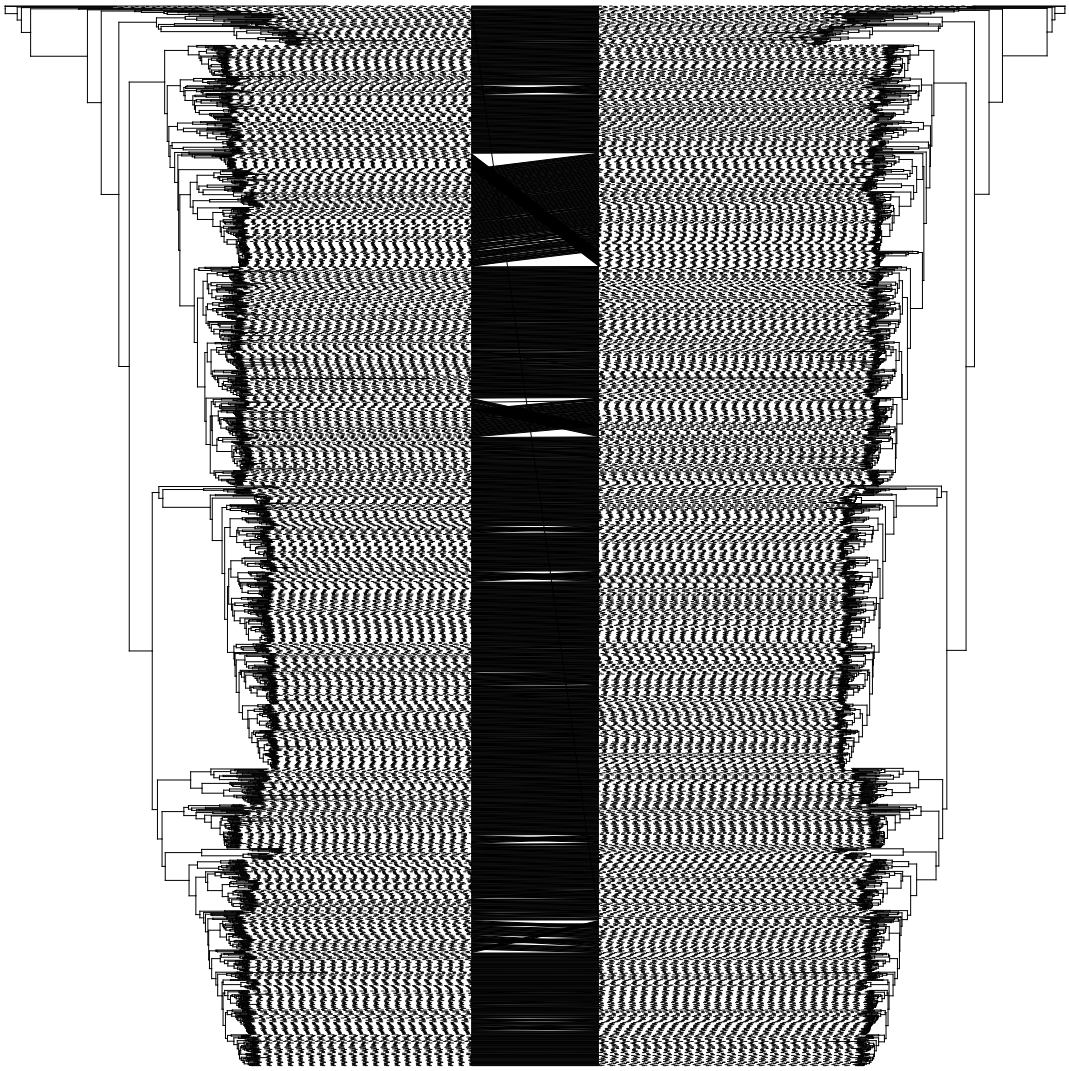

Fig. S20. Cophylogenetic plot of the complete (left) versus coding (right) T400F ExaML trees showing topological concordance

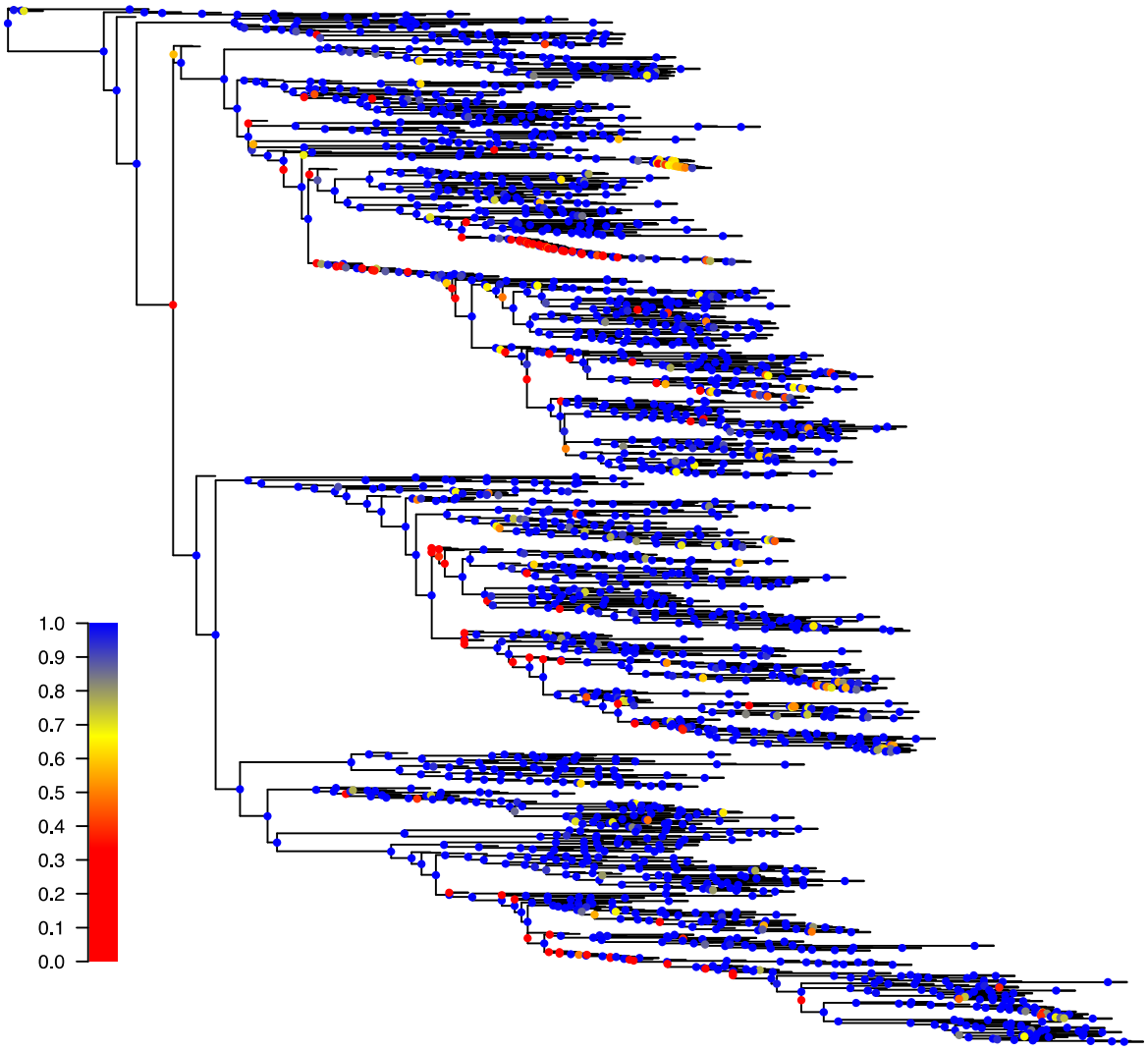

Fig. S21. T400F Astral tree with nodes colored according to local posterior probabilities and branch lengths in coalescent units (terminal branches have zero length in Astral results and are set to the median length of internal branches for visualization)

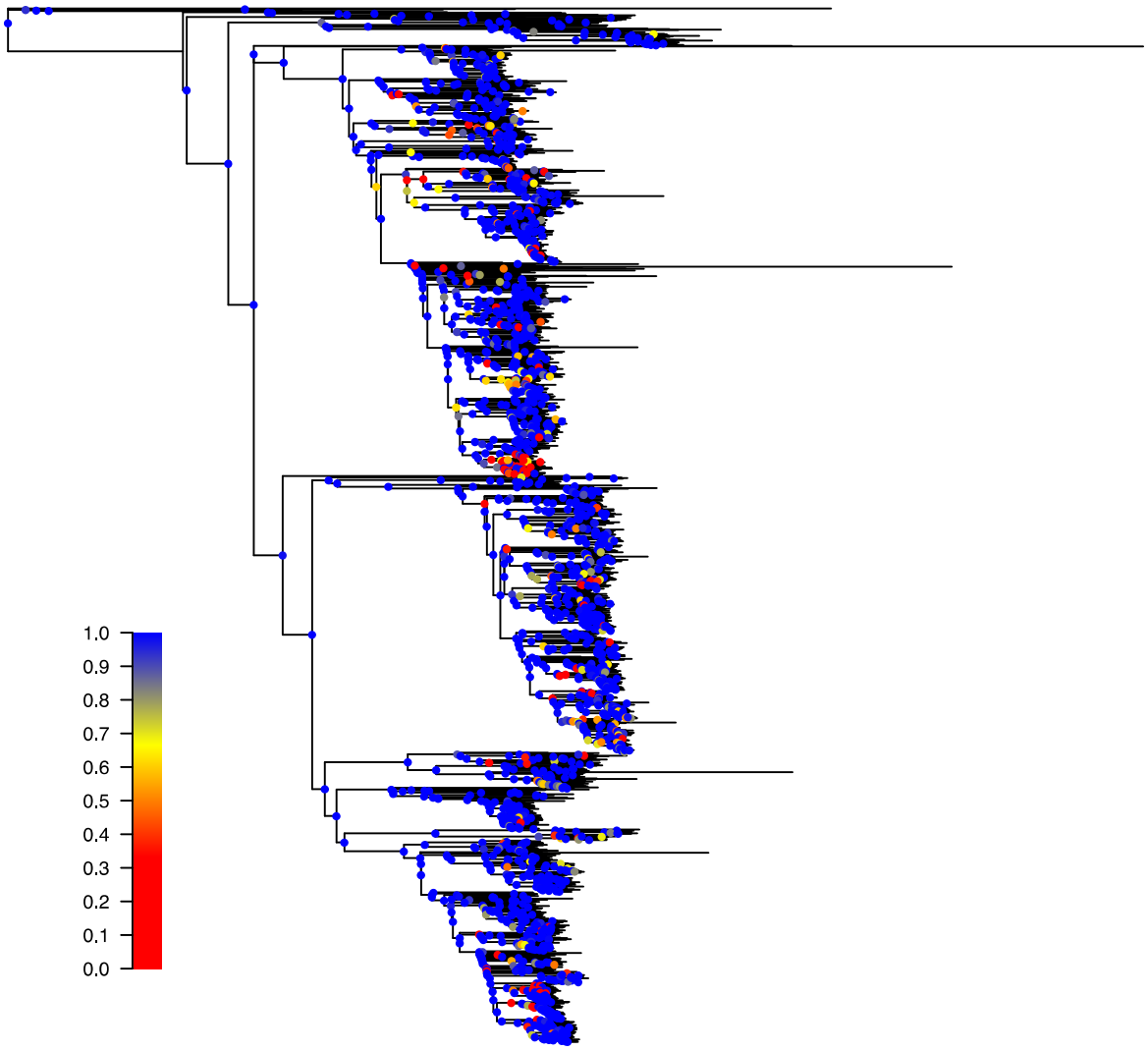

Fig. S22. T400F Astral tree with nodes colored according to local posterior probabilities and branch lengths estimated in ExaML in units of number of expected substitutions

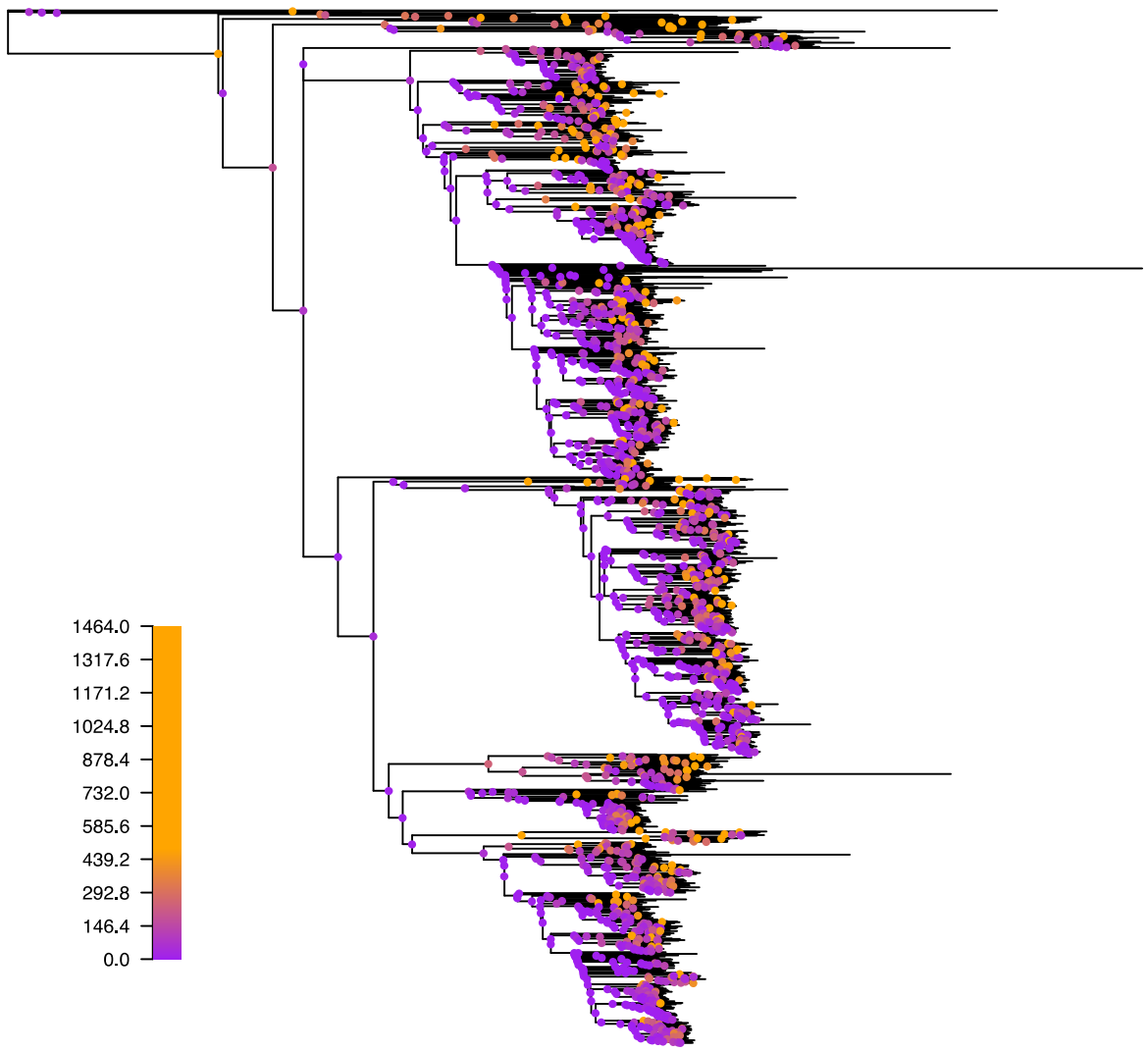

Fig. S23. T400F Astral tree with ExaML branch lengths and nodes colored according to gene tree support

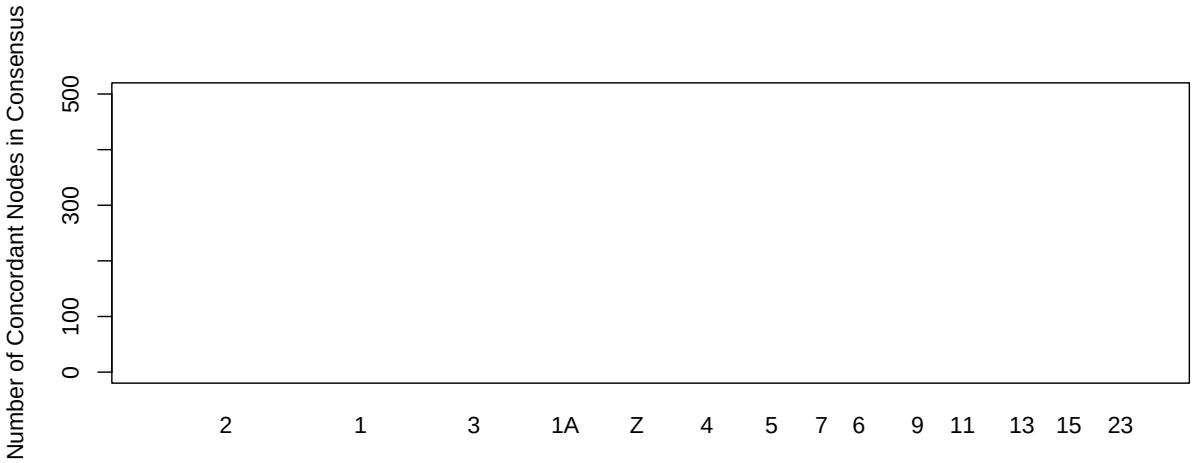

Fig. S24. Manhattan plot of support for T400F ExaML tree across T400F gene trees

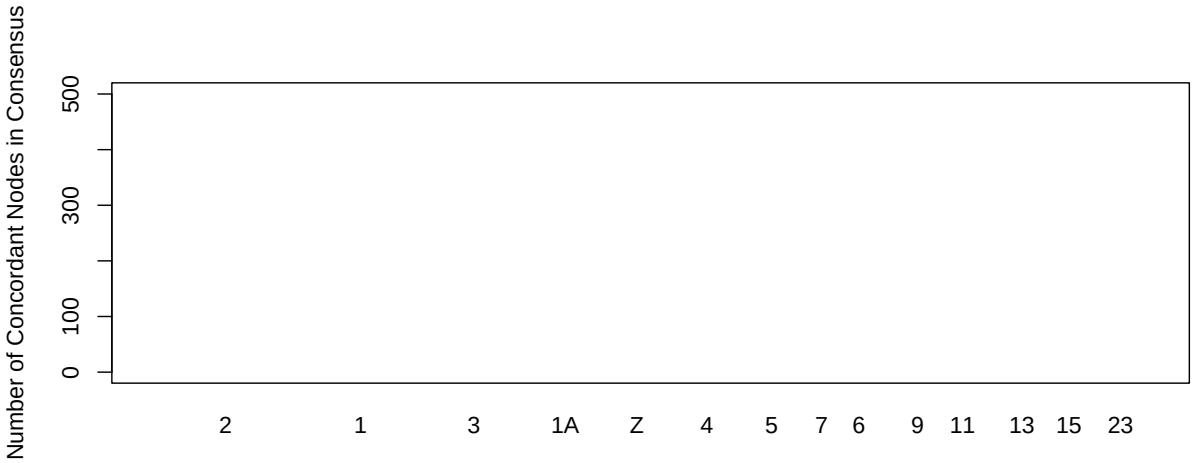

Fig. S25. Manhattan plot of support for HGAPF ExaML tree across HGAPF gene trees

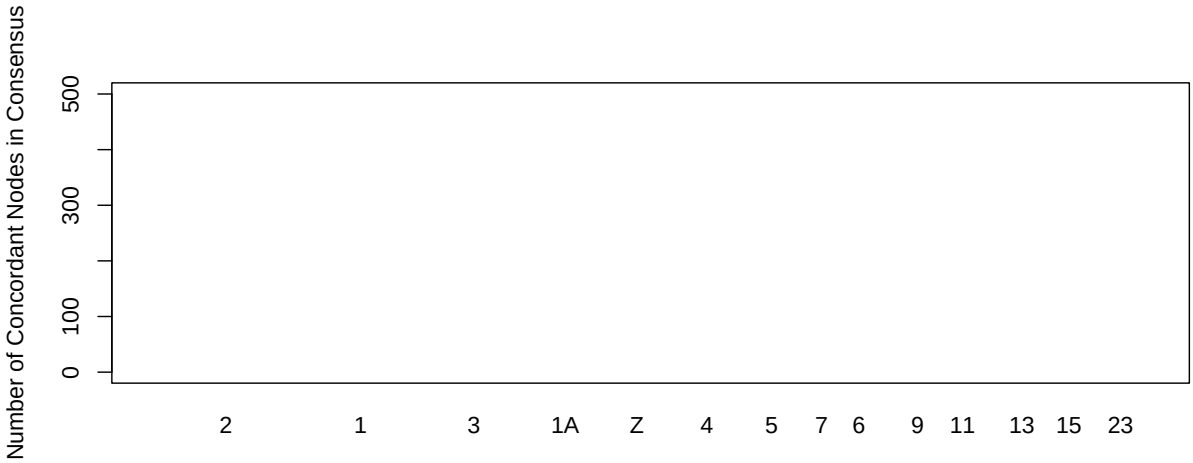

Fig. S26. Manhattan plot of support for T400F Astral tree across T400F gene trees

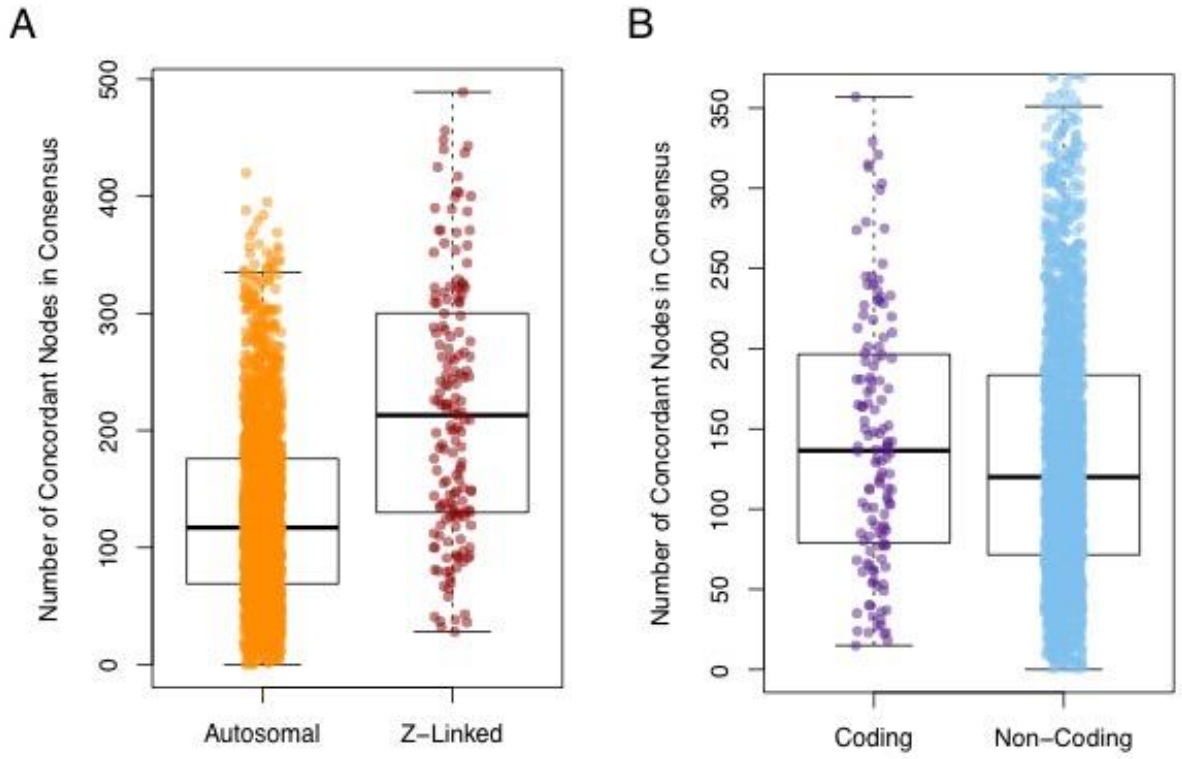

Fig. S27. Plots of the number of nodes in the consensus T400F ExaML tree supported by gene trees from different subsets of the genome

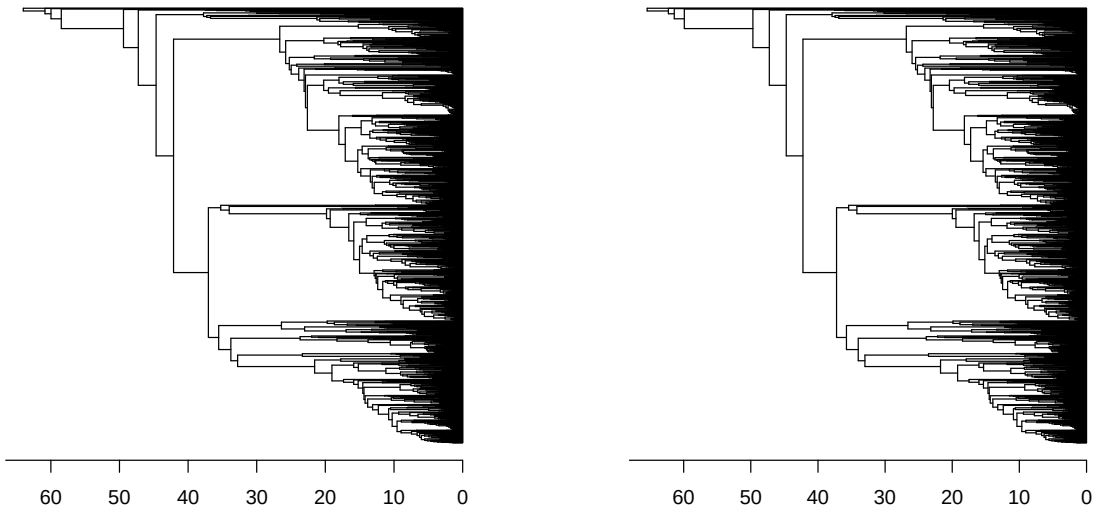

Fig. S28. Comparison of T400F trees using two alternative root calibrations

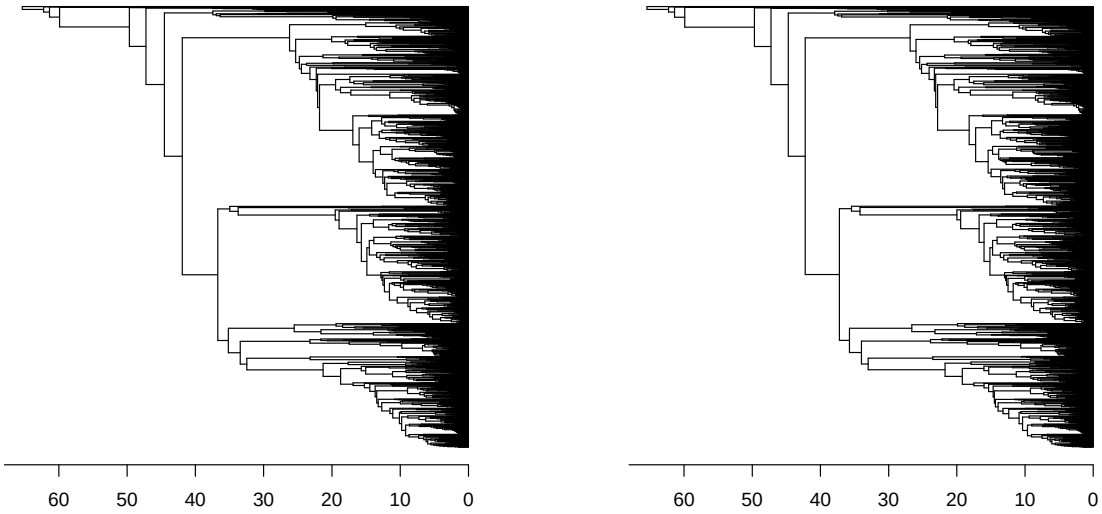

Fig. S29. Comparison of T400F trees with (left) and without (right) poor-quality samples

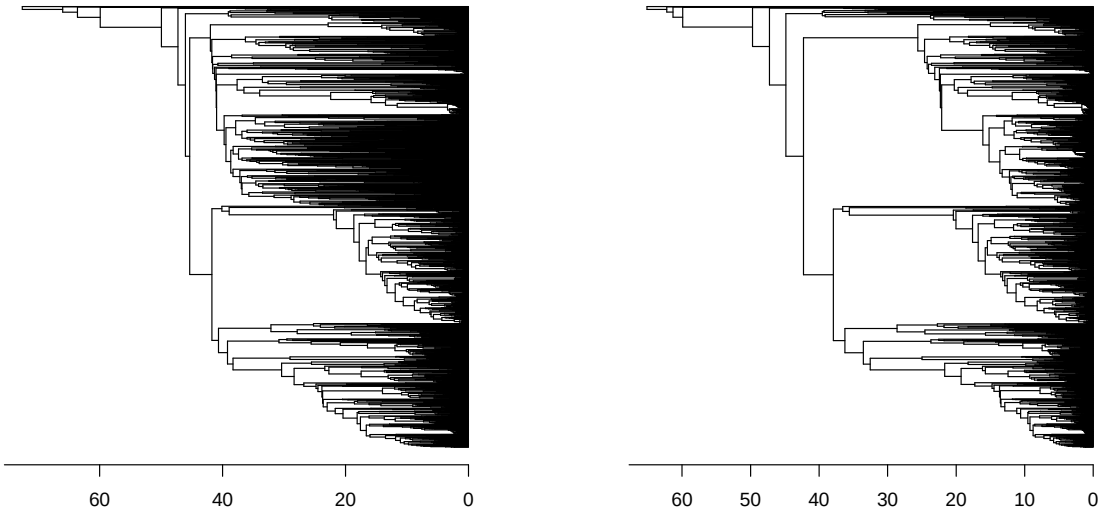

Fig. S30. Comparison of HGAPF trees with (left) and without (right) poor-quality samples

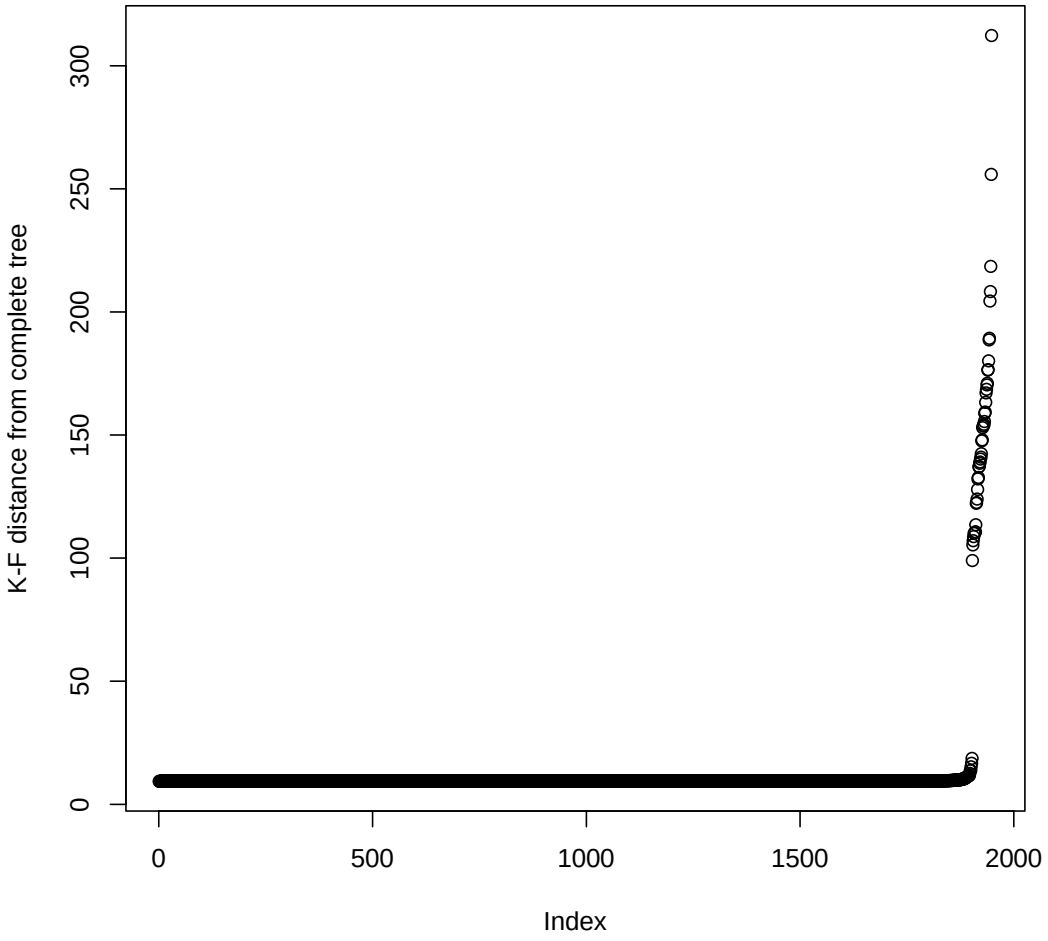

Fig. S31. Plot of K-F distances of each jackknife TreePL tree from the complete TreePL tree. The samples dropped in the 52 trees that are highly dissimilar from the complete tree (>50 K-F distance) have no overlap with the poor-quality samples that exhibit extremely long terminal branch lengths.

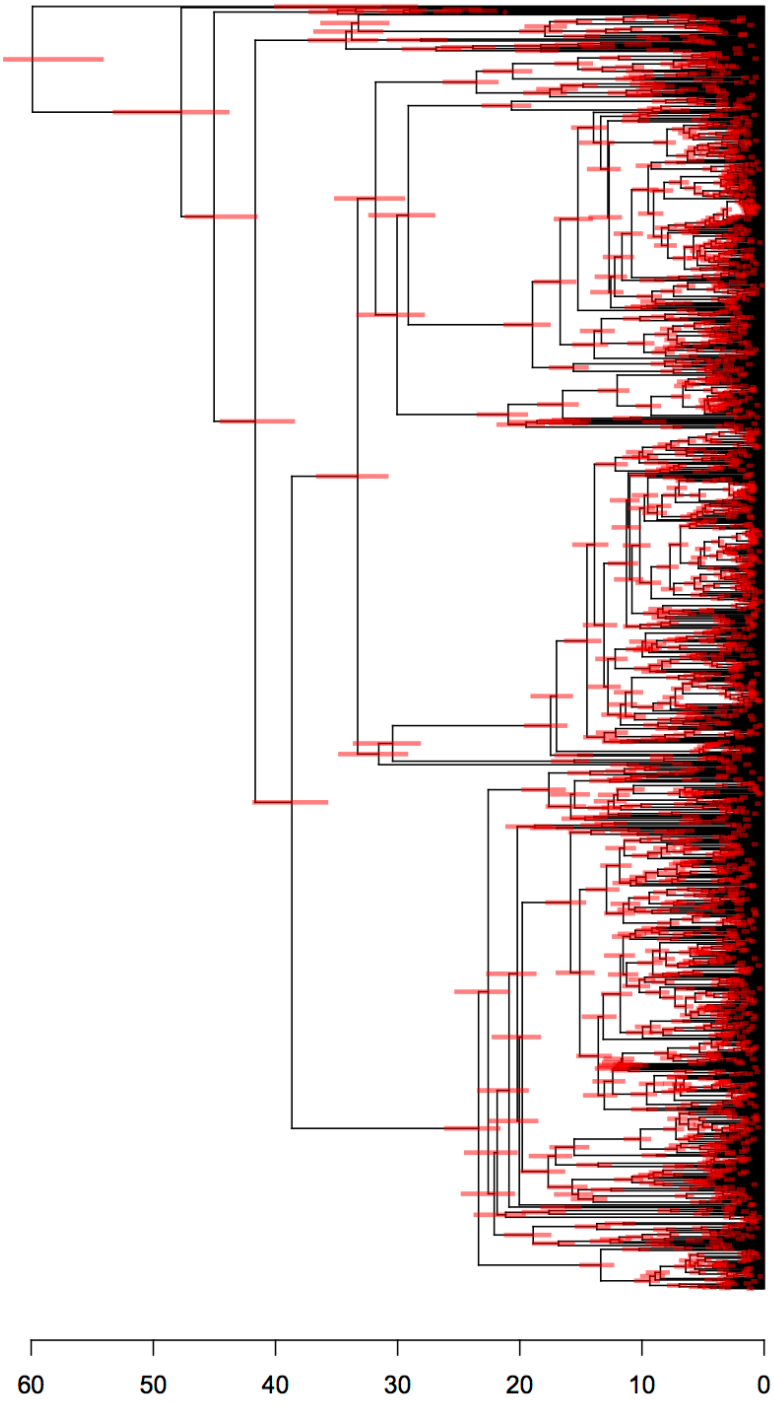

Fig. S32. A phylogeny of suboscine birds showing confidence intervals around node ages.

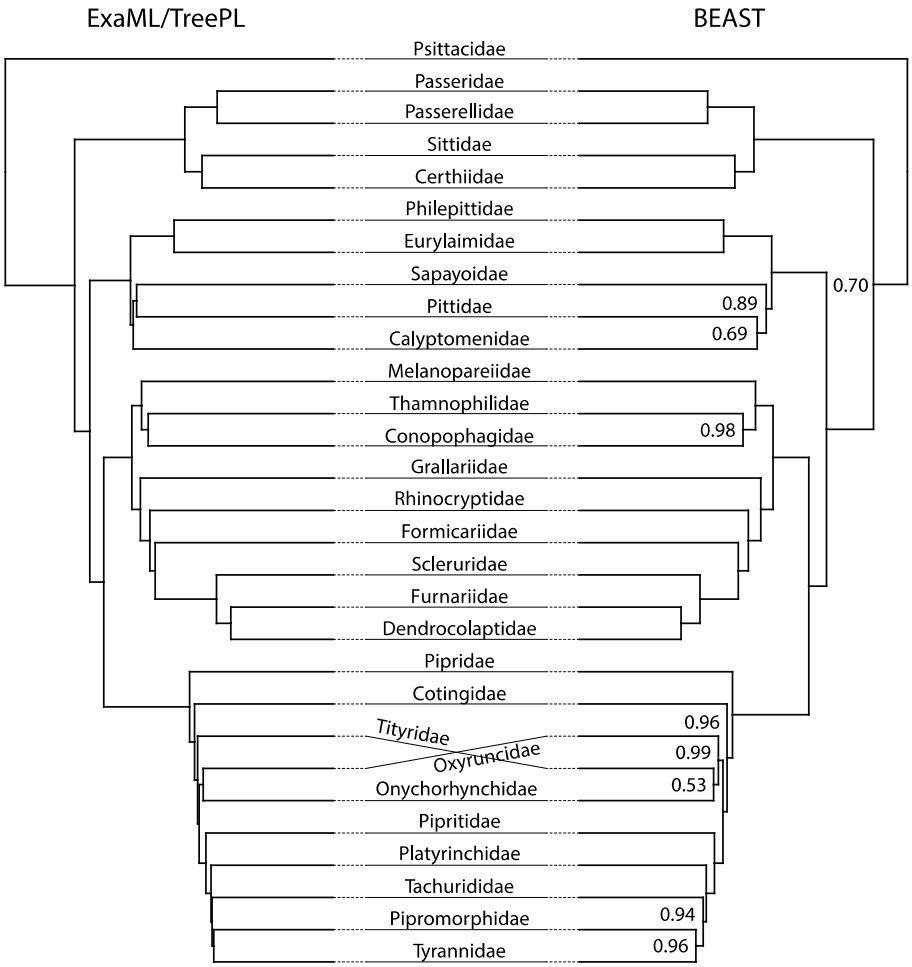

Fig S33. Topologies of our primary tree (left) and the BEAST family-level tree (right). Posterior probability support values are provided for relationships with probability <1.0 in the BEAST analysis.

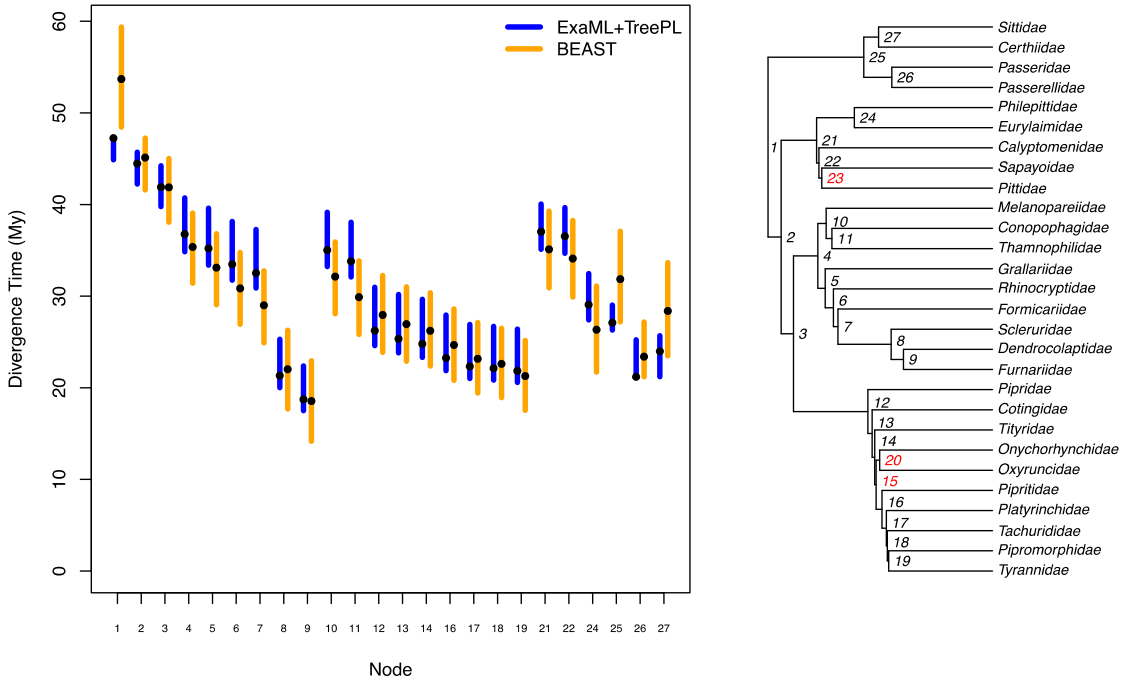

Fig. S34. Relative divergence times of nodes subtending suboscine families in our primary tree versus those estimated using BEAST. The right panel provides a node map. Nodes highlighted in red were not present in the BEAST tree.

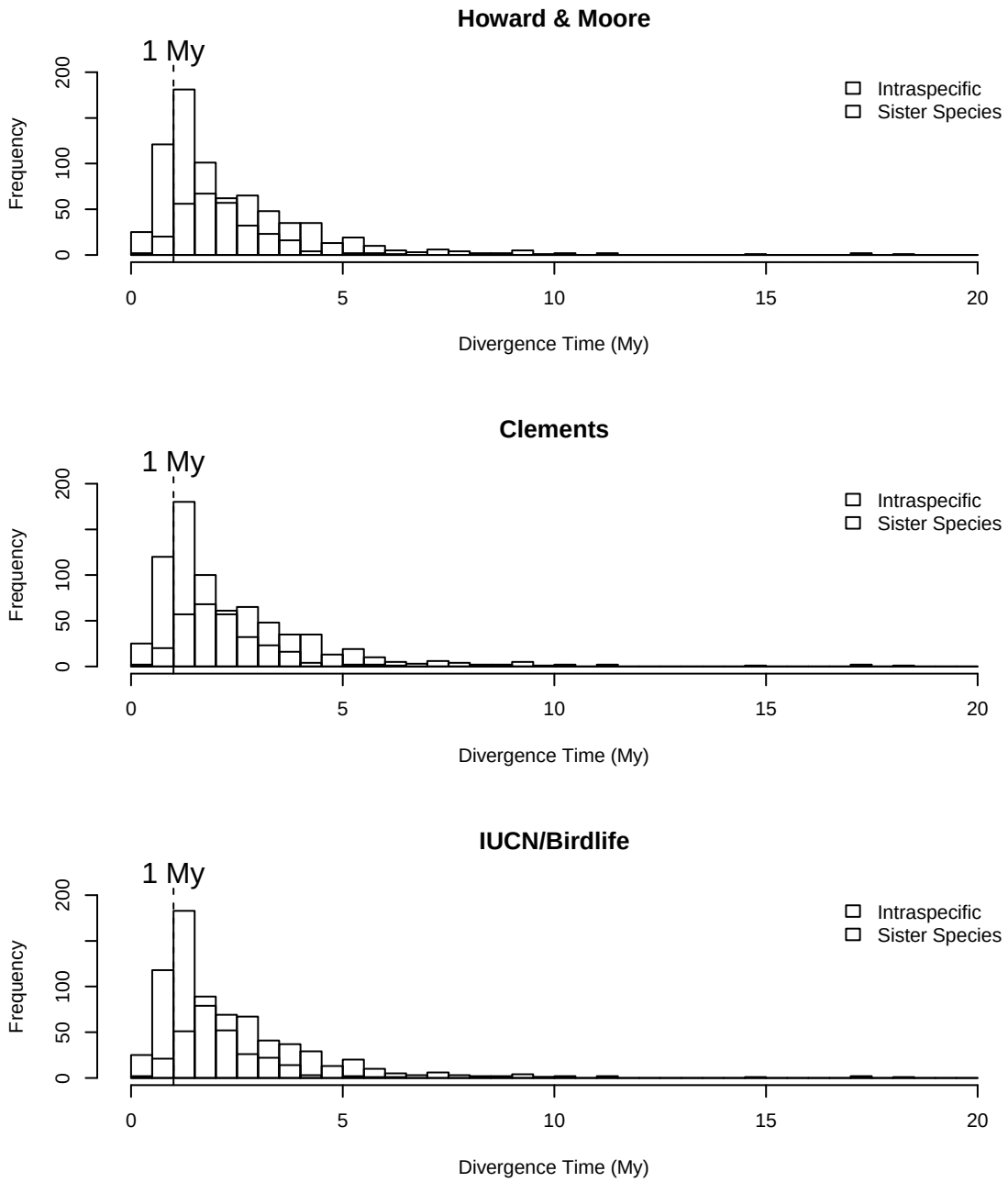

Fig. S35. A comparison of the depth of intraspecific divergence times versus sister species divergence times based on the three classifications from taxonomic authorities considered in our study

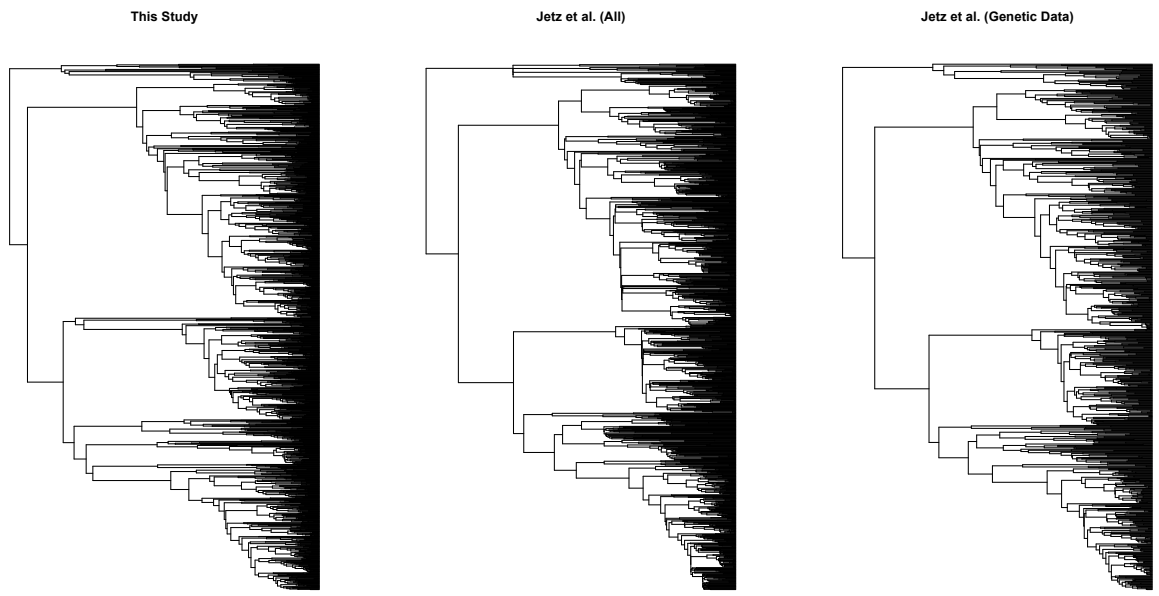

Fig. S36. A comparison of our tree (left), with trees from Jetz et al. (*96*) using all tips including those lacking genetic data (middle) and just tips with genetic data (right)

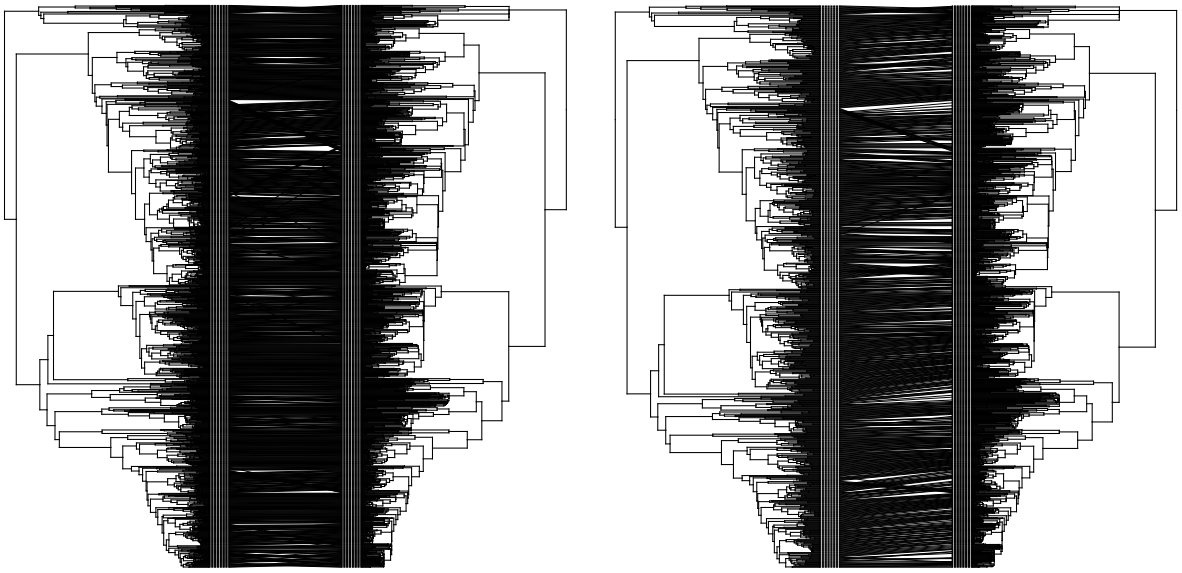

Fig. S37. Plots showing concordance between our tree (left in both plots) and trees from Jetz et al. (*96*) using all tips including those lacking genetic data (right tree in left panel) and just tips with genetic data (right tree in right panel)

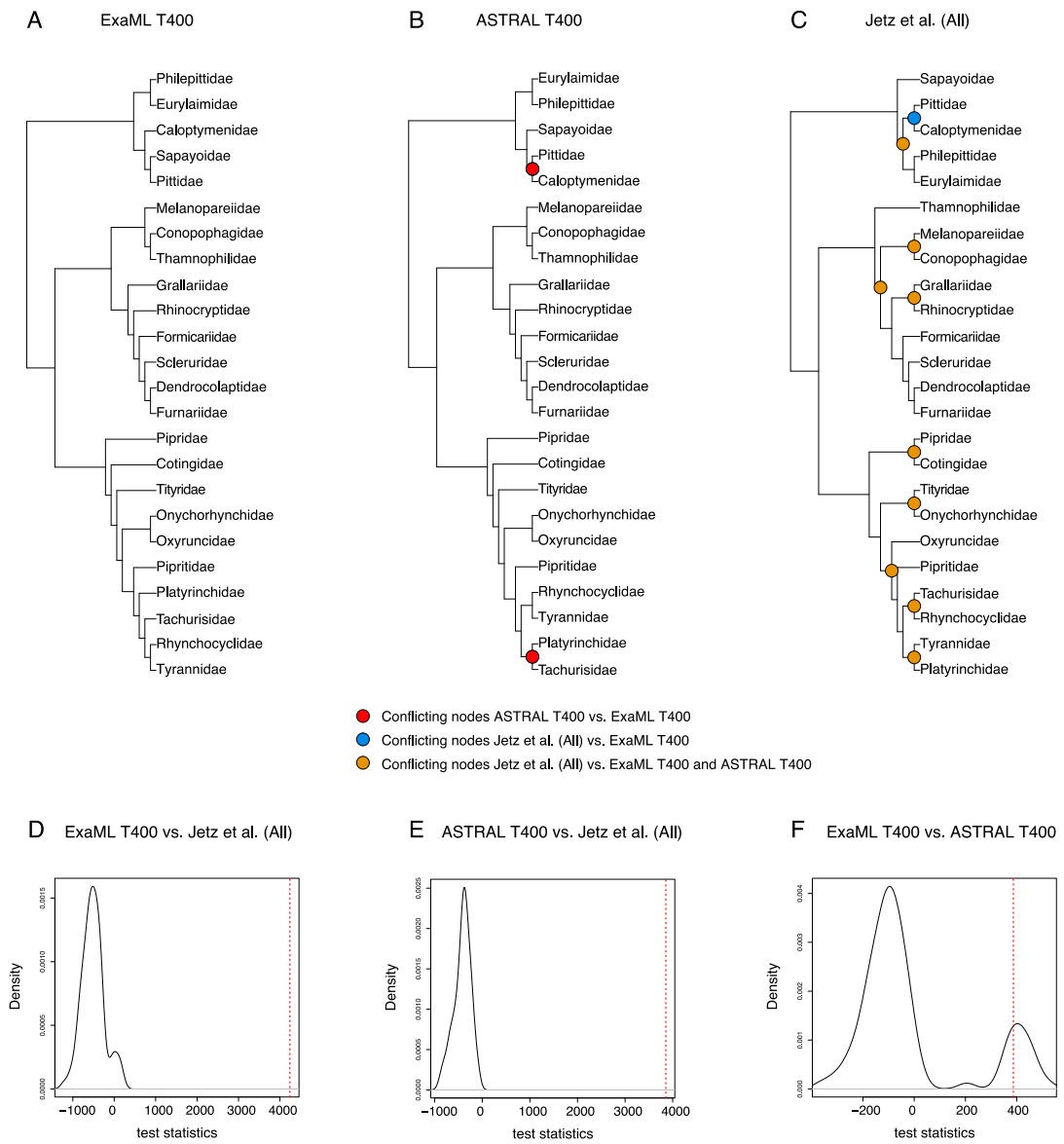

Fig. S38. Family-level phylogeny of the Tyranni based on the ExaML T400 (A), ASTRAL T400 (B), and Jetz et al. (*96*) datasets (C). Circles at nodes denote conflicting clades between different trees. Null distributions and observed t-statistic (dashed red lines) of the likelihood ratio tests (*143*) for the comparisons between ExaML T400 and Jetz et al. (D), ASTRAL T400 and Jetz et al. (E), and ExaML T400 and ASTRAL T400 (F). These analyses were based on the coalescent histories of 1,665 loci that included all 29 families (including outgroups).

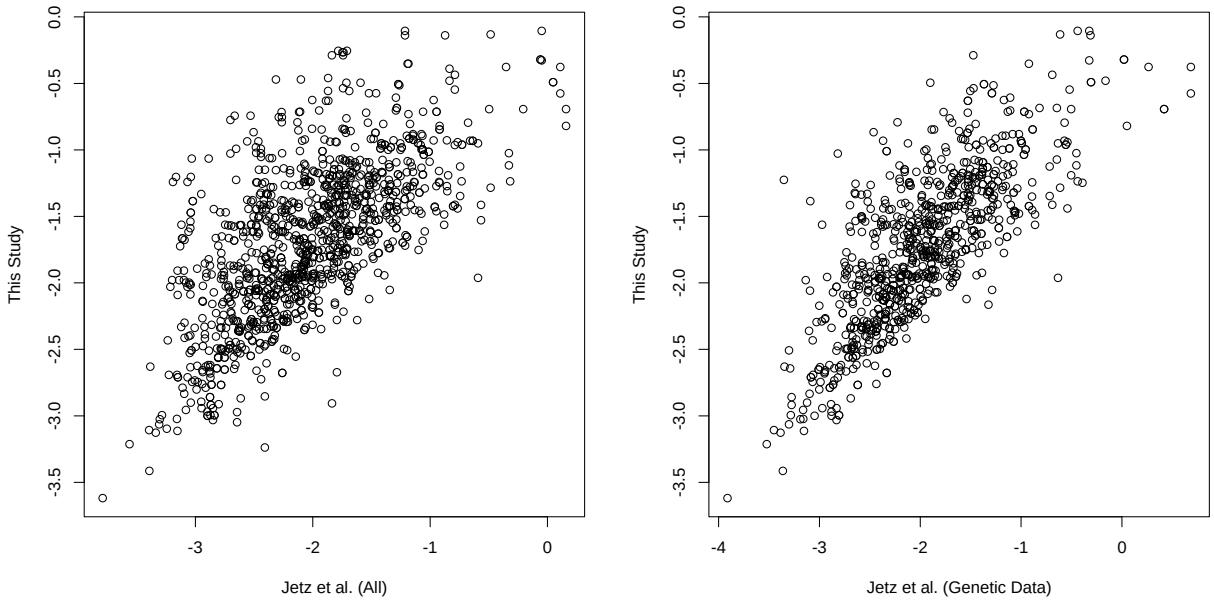

Fig. S39. Plots showing the correlation between speciation rates estimates (ES estimator) in our tree and trees from Jetz et al. (*96*) using all tips including those lacking genetic data (left panel) and just tips with genetic data (right panel)

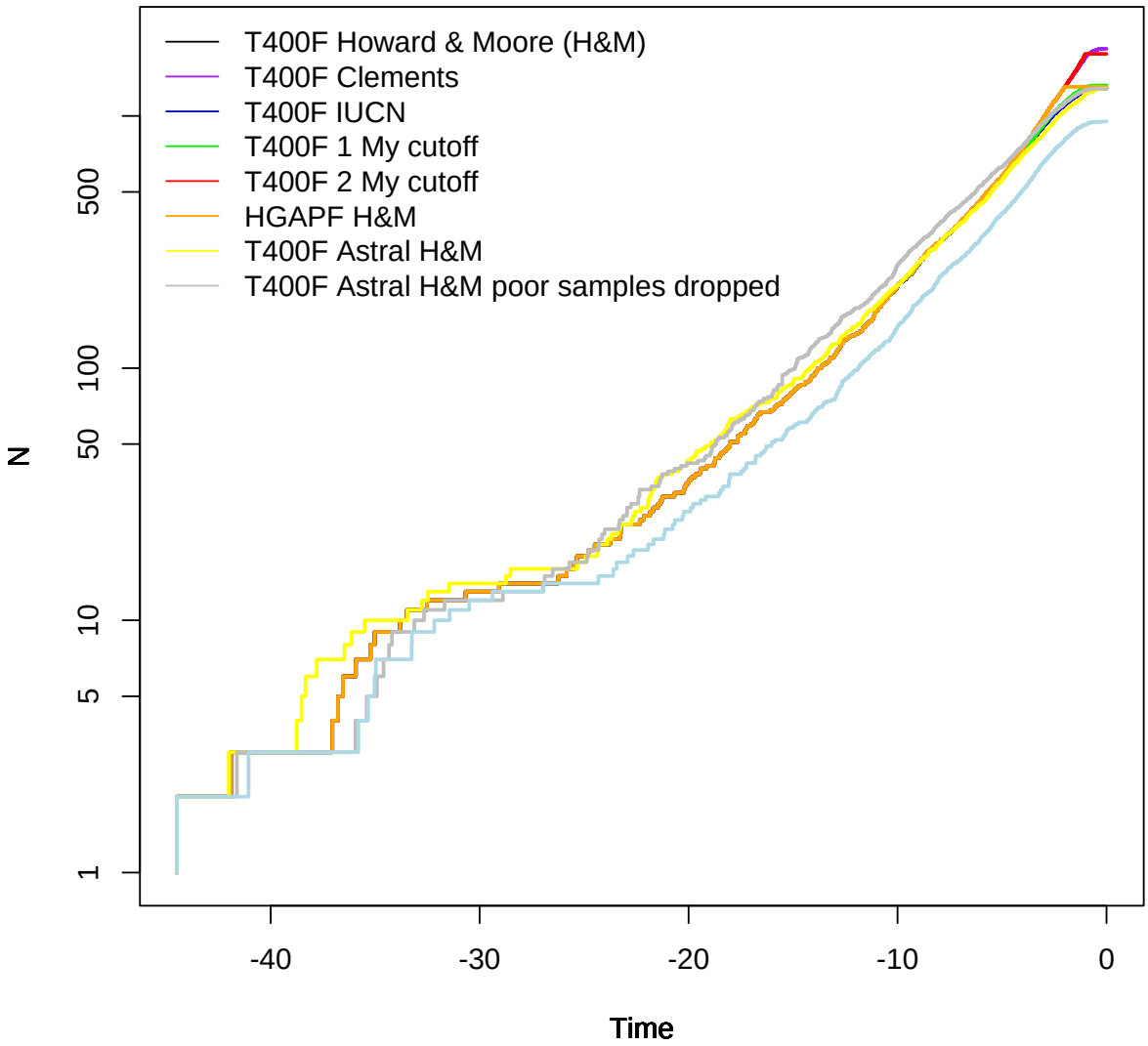

Fig. S40. Lineage through time (LTT) plots of all suboscines for all 6 taxonomies, the HGAPF tree for Howard and Moore classification, and the Astral tree with and without samples missing from >250 gene trees dropped for Howard and Moore classification

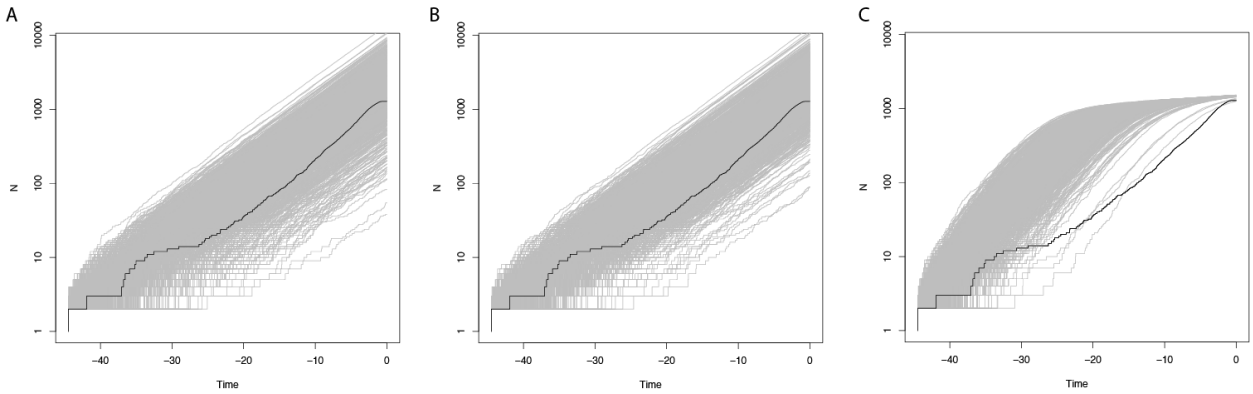

Fig. S41. Lineage through time (LTT) plot of all suboscines (black lines) for the Howard and Moore classification compared to 1000 simulations (gray lines) based on maximum likelihood parameter estimates under: (a) a pure-birth model, (b) a birth-death model, and (c) a diversity-dependent model

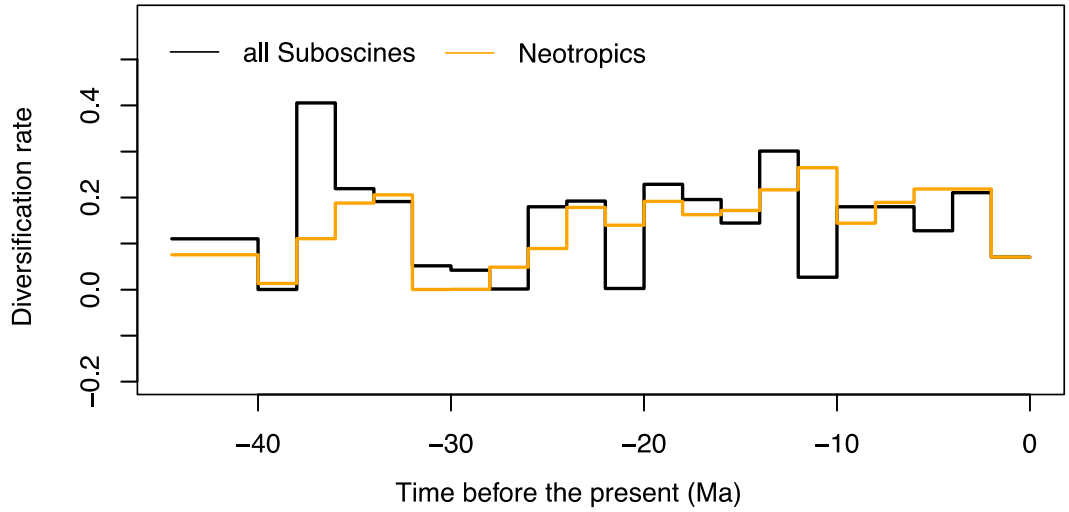

Fig. S42. Diversification rate through time analysis using TreePar with intervals of 2 Ma and a birth-death-shift model as applied to the primary tree of all species and of Neotropical species only

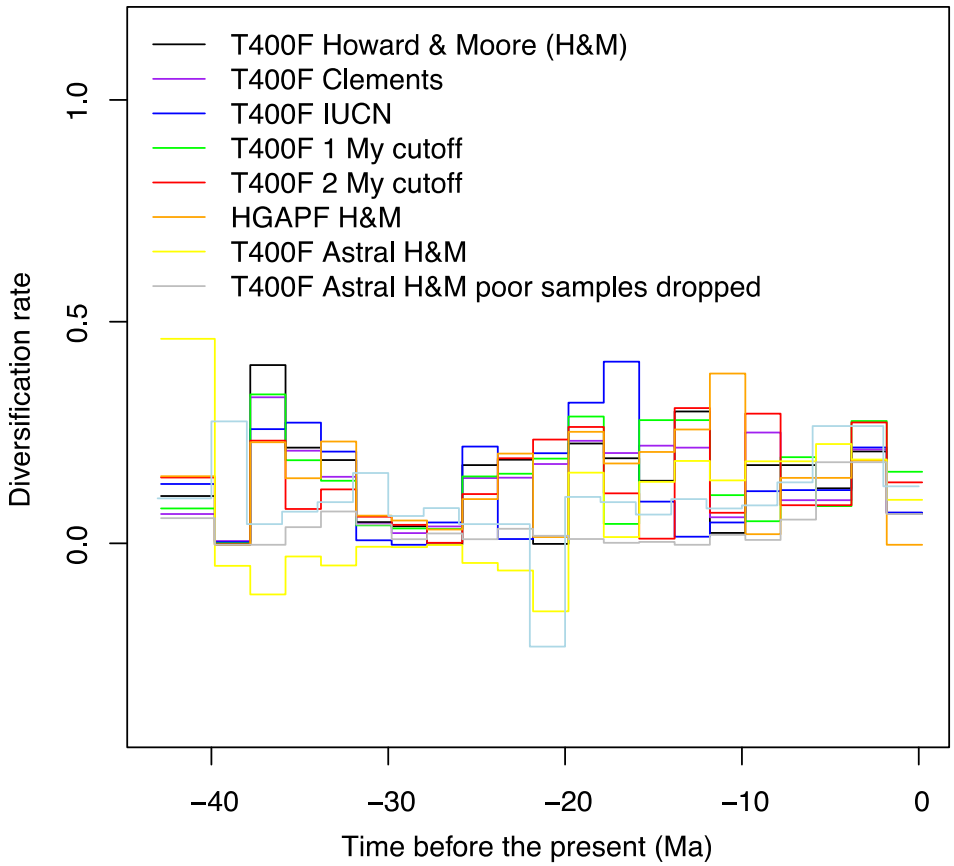

Fig. S43. Diversification rate through time analysis using TreePar with intervals of 2 Ma and a birth-death-shift model as applied to all 6 taxonomies, the HGAPF tree for Howard and Moore classification, and the Astral tree with and without samples missing from >250 gene trees dropped for Howard and Moore classification

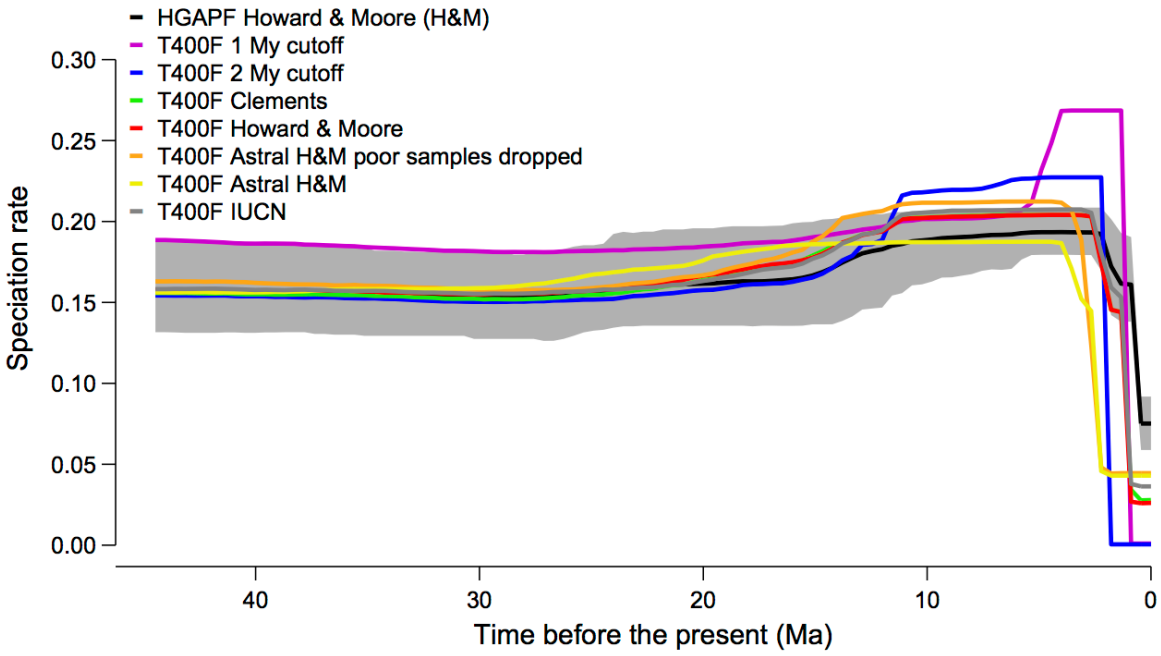

Fig S44. TESS results across different taxonomic classifications

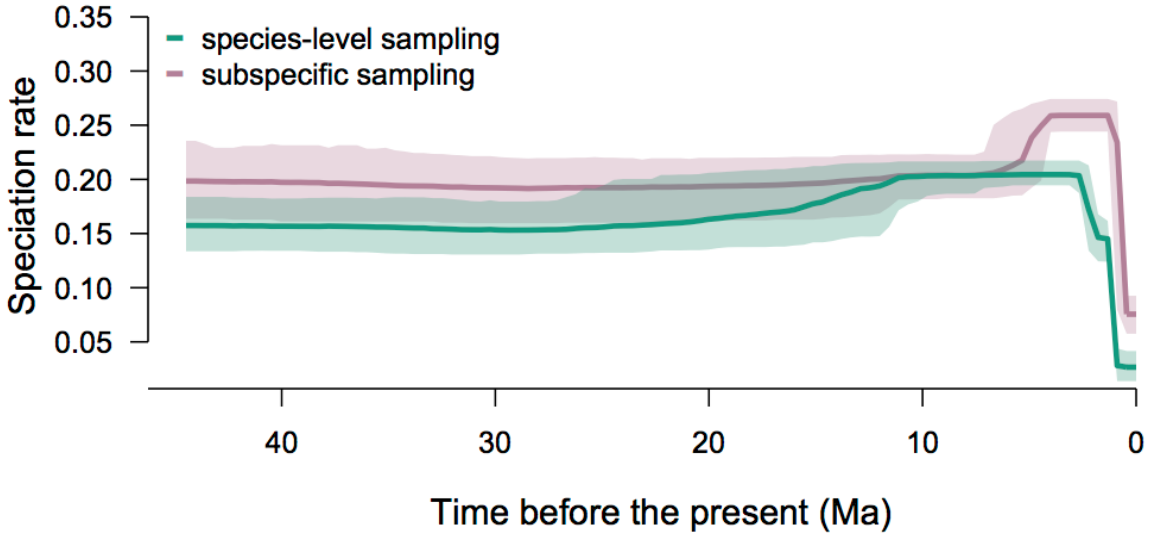

Fig S45. TESS results with vs. without intraspecific diversity

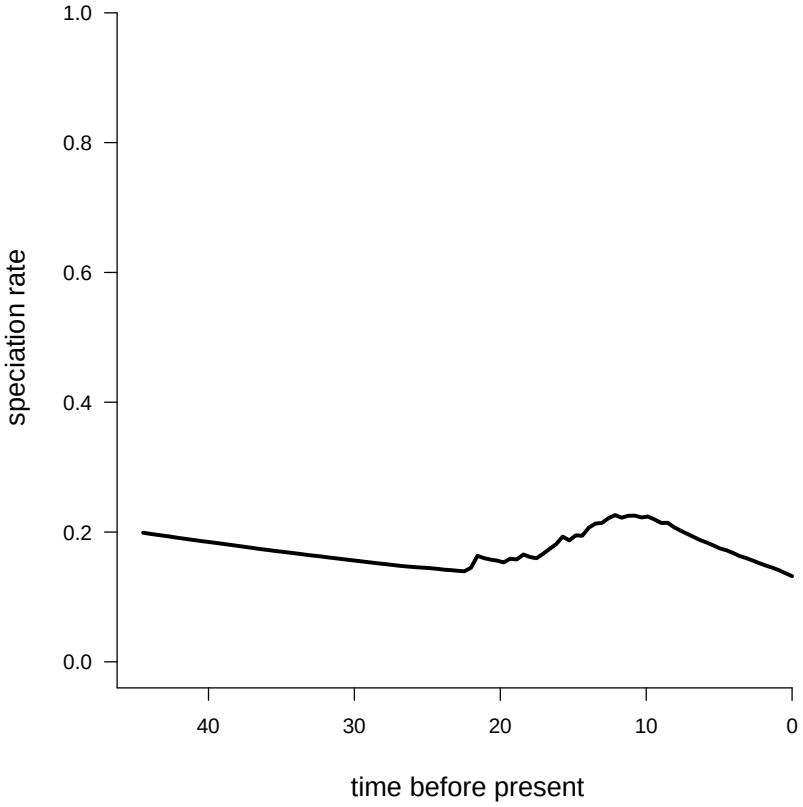

Fig. S46. Plot of speciation rate through time from BAMM after accounting for branch-specific rate heterogeneity shows relatively constant speciation through time or possibly a peak around 10 Ma

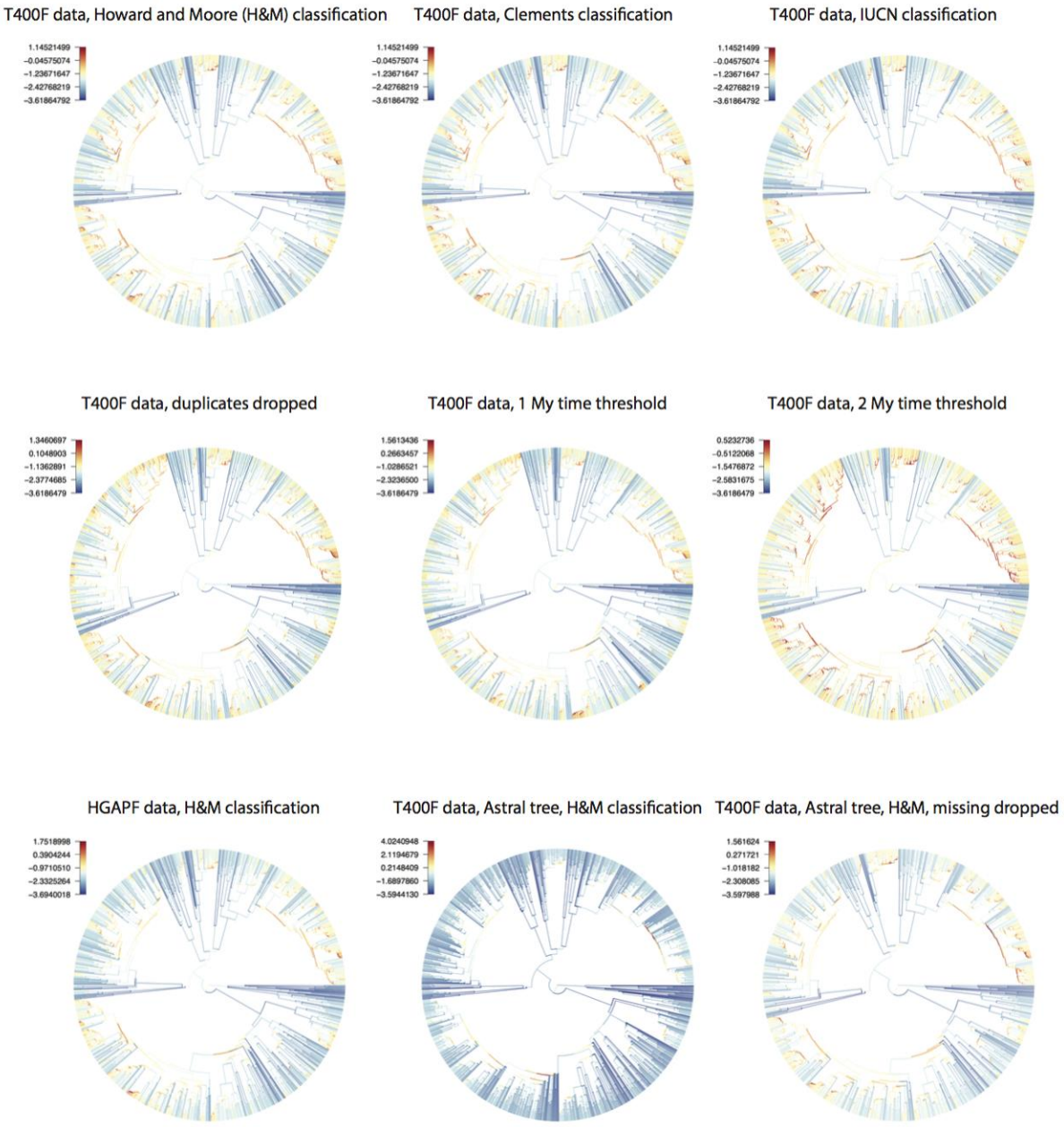

Fig. S47. Log-transformed ES across all branches for all 6 taxonomies, the HGAPF tree for Howard and Moore classification, and the Astral tree with and without samples missing from >250 gene trees dropped for Howard and Moore classification

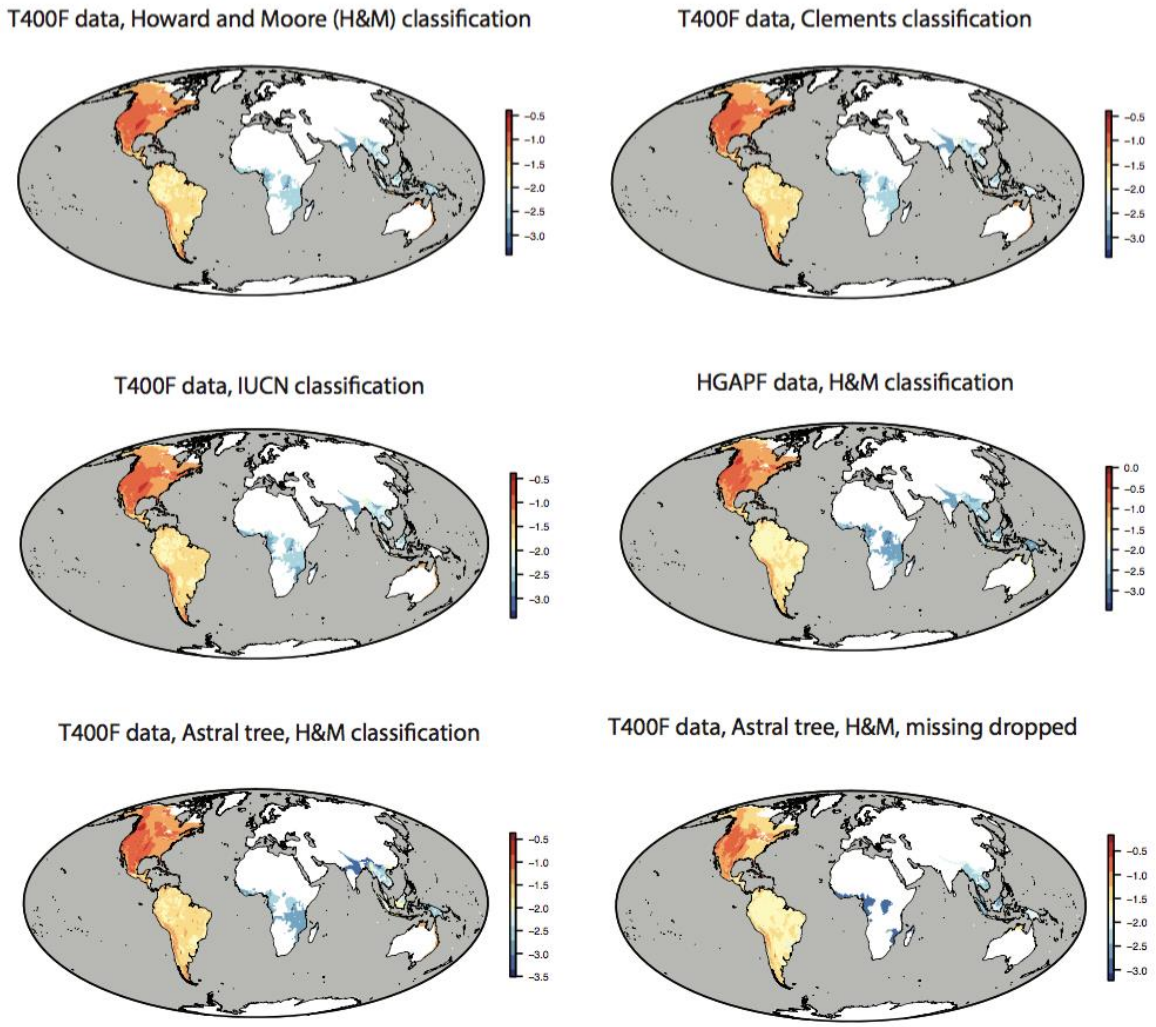

Fig. S48. Log-transformed ES across space for 3 taxonomies, the HGAPF tree for Howard and Moore classification, and the Astral tree with and without samples missing from >250 gene trees dropped for Howard and Moore classification

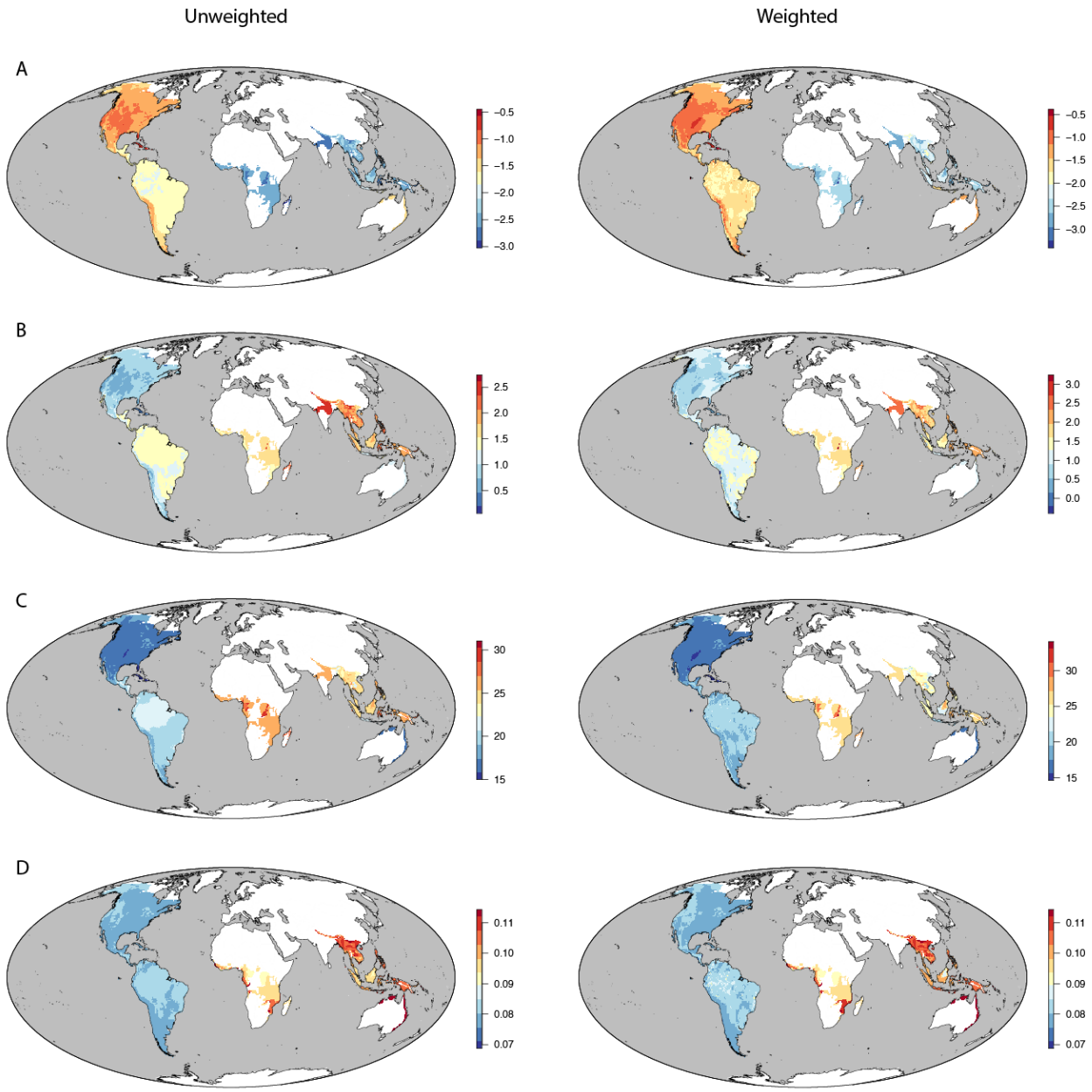

Fig. S49. Unweighted vs weighted maps of (A) the inverse equal-splits speciation rates: ES, (B) the terminal branch length: TB, (C) the node depth: ND, and (D) substitution rate: SR

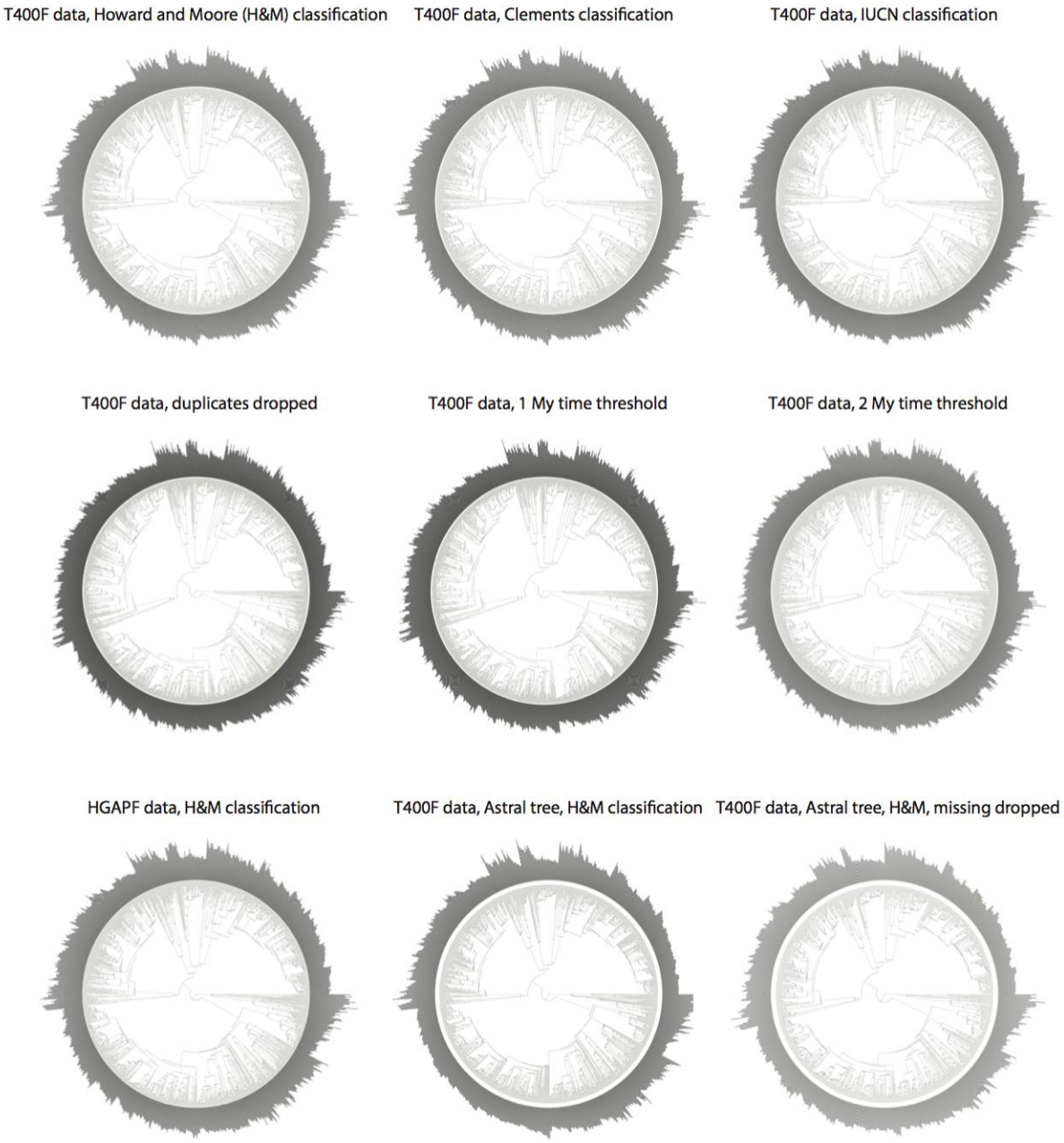

Fig. S50. Mean NH across the tree tips for all 6 taxonomies, the HGAPF tree for Howard and Moore classification, and the Astral tree with and without samples missing from >250 gene trees dropped for Howard and Moore classification

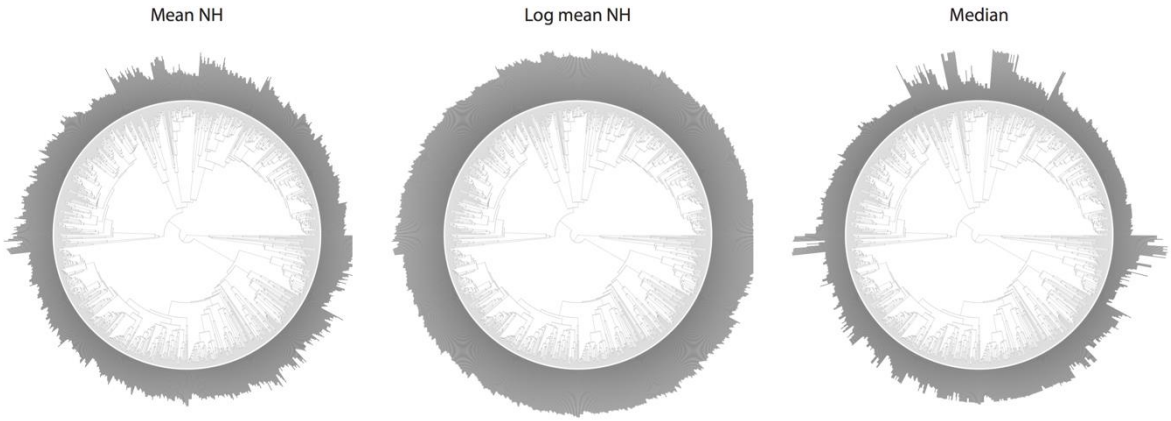

Fig. S51. Comparison of mean NH, log mean NH, and median NH across tree tips

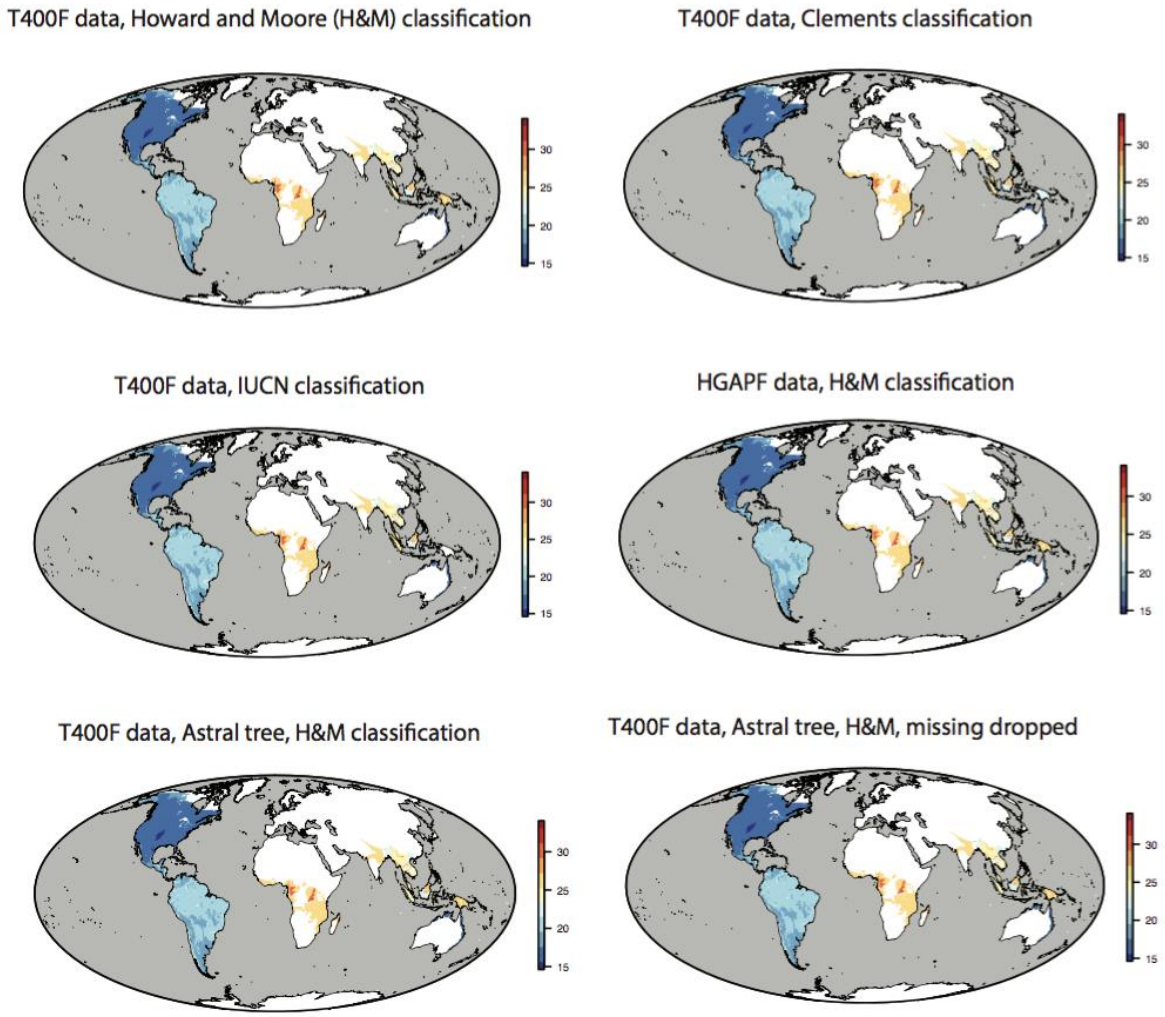

Fig. S52. Mean NH across space for 3 taxonomies, the HGAPF tree for Howard and Moore classification, and the Astral tree with and without samples missing from >250 gene trees dropped for Howard and Moore classification

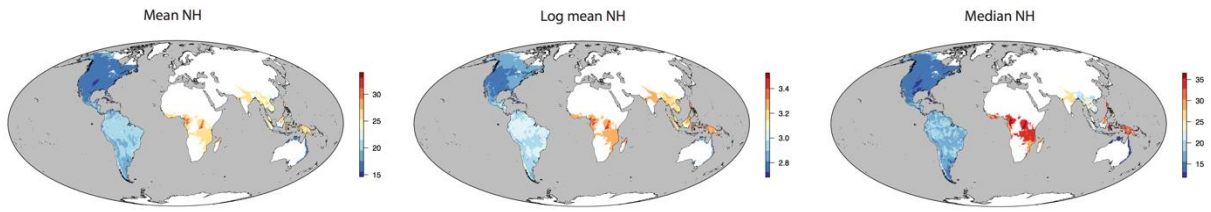

Fig. S53. Comparison of mean NH, log mean NH, and median NH across space

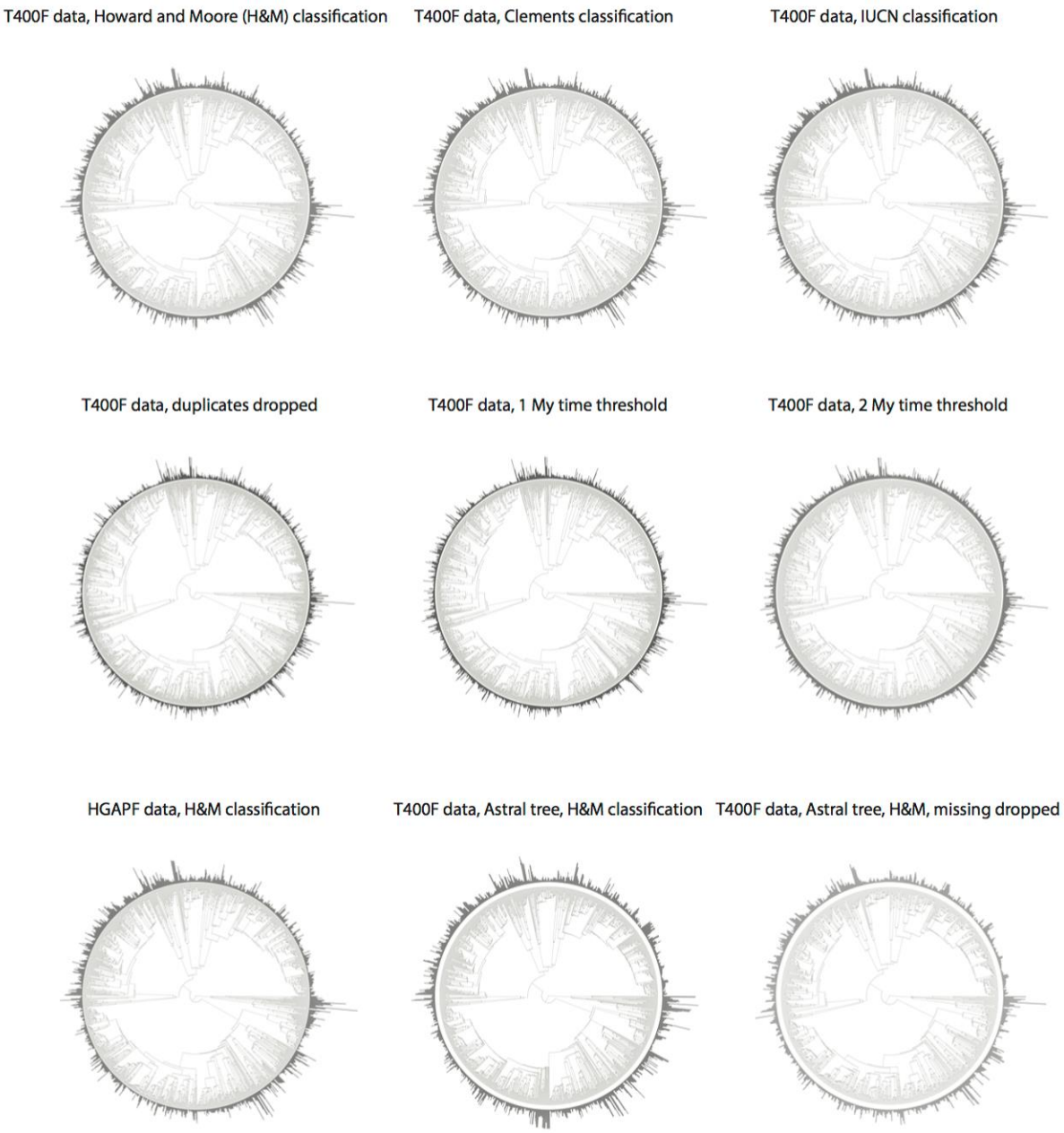

Fig. S54. Log-transformed TB across the tree tips for all 6 taxonomies, the HGAPF tree for Howard and Moore classification, and the Astral tree with and without samples missing from >250 gene trees dropped for Howard and Moore classification

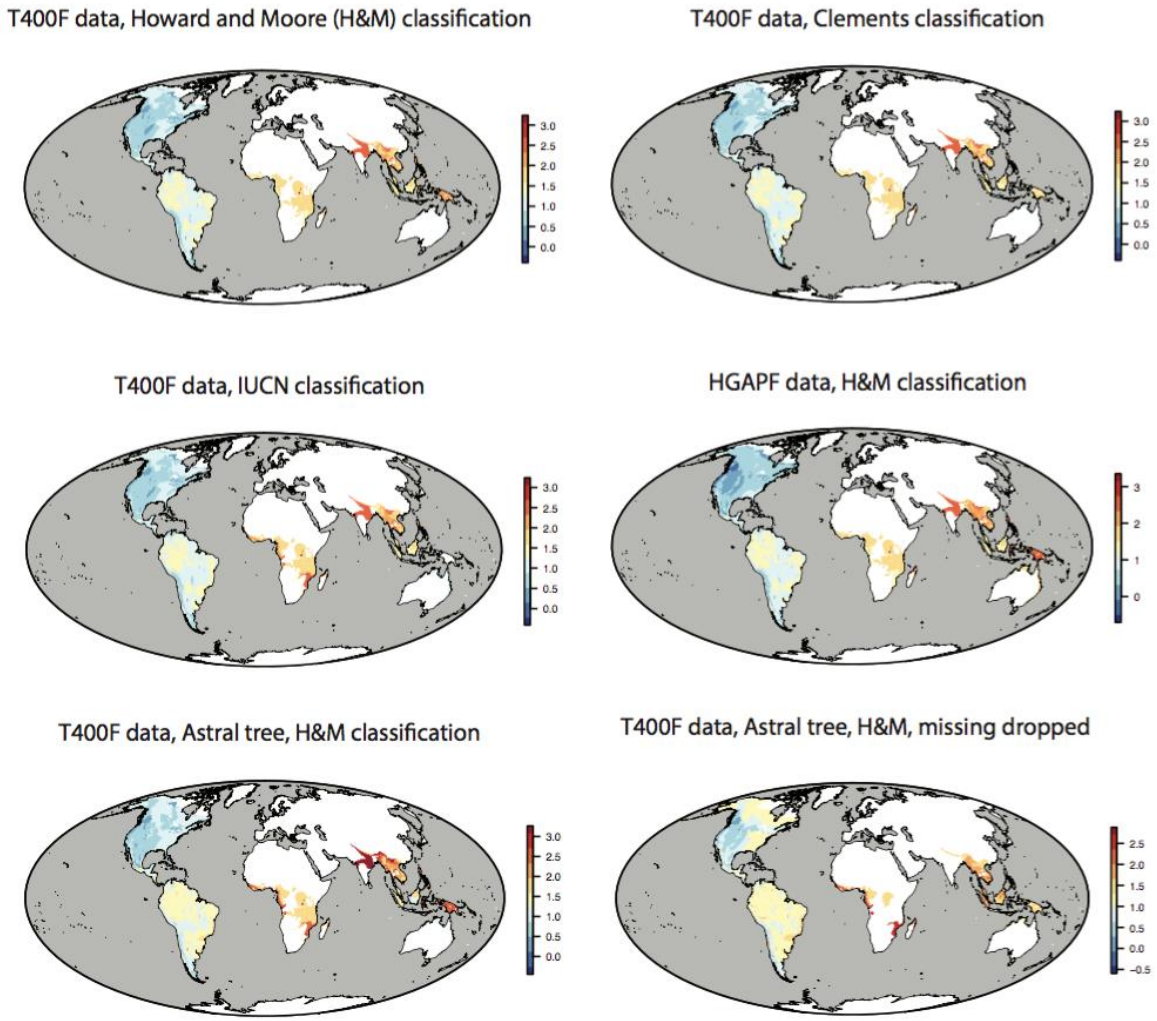

Fig. S55. Log-transformed TB across space for 3 taxonomies, the HGAPF tree for Howard and Moore classification, and the Astral tree with and without samples missing from >250 gene trees dropped for Howard and Moore classification

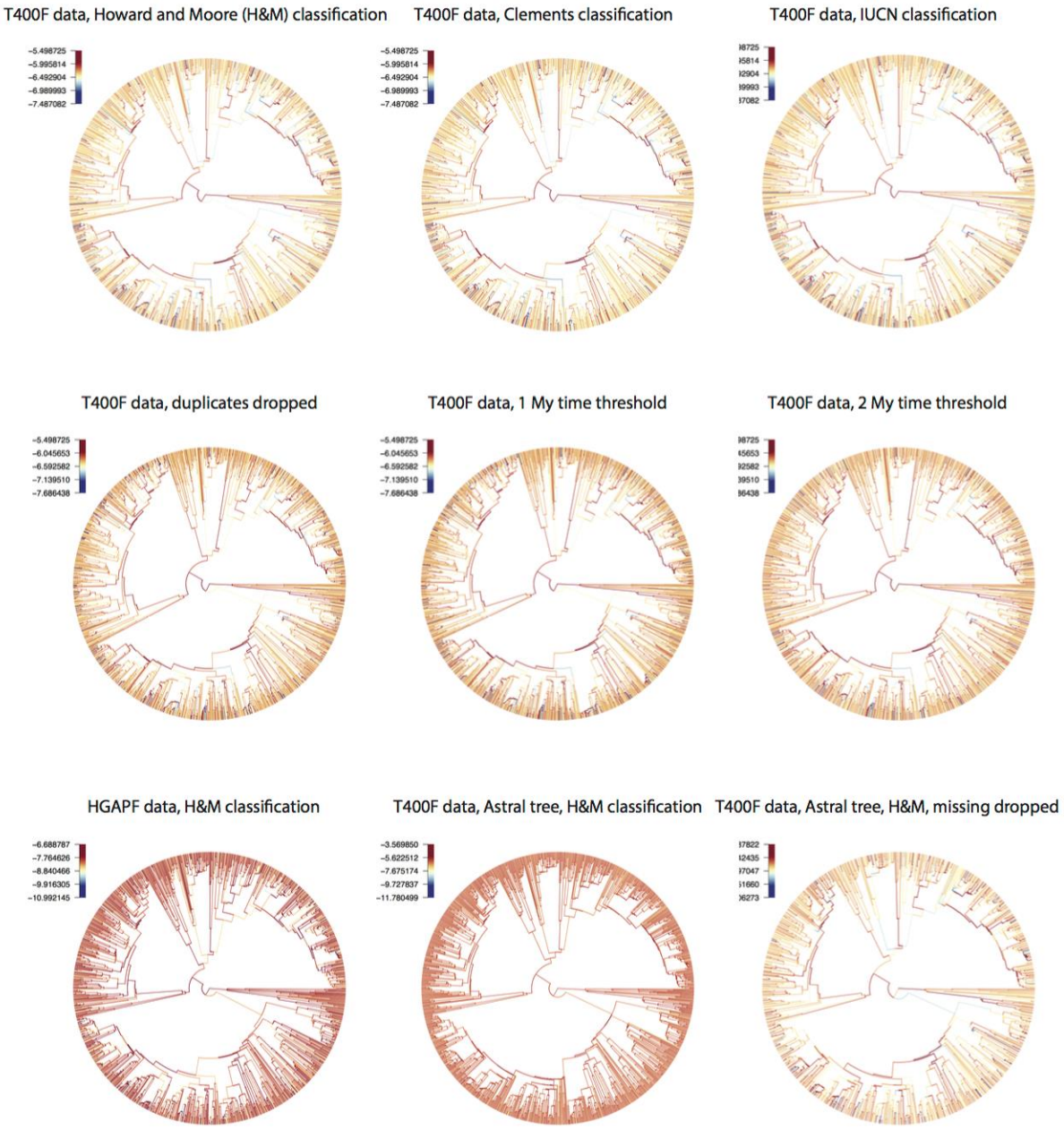

Fig. S56. SR across all branches for all 6 taxonomies, the HGAPF tree for Howard and Moore classification, and the Astral tree with and without samples missing from >250 gene trees dropped for Howard and Moore classification

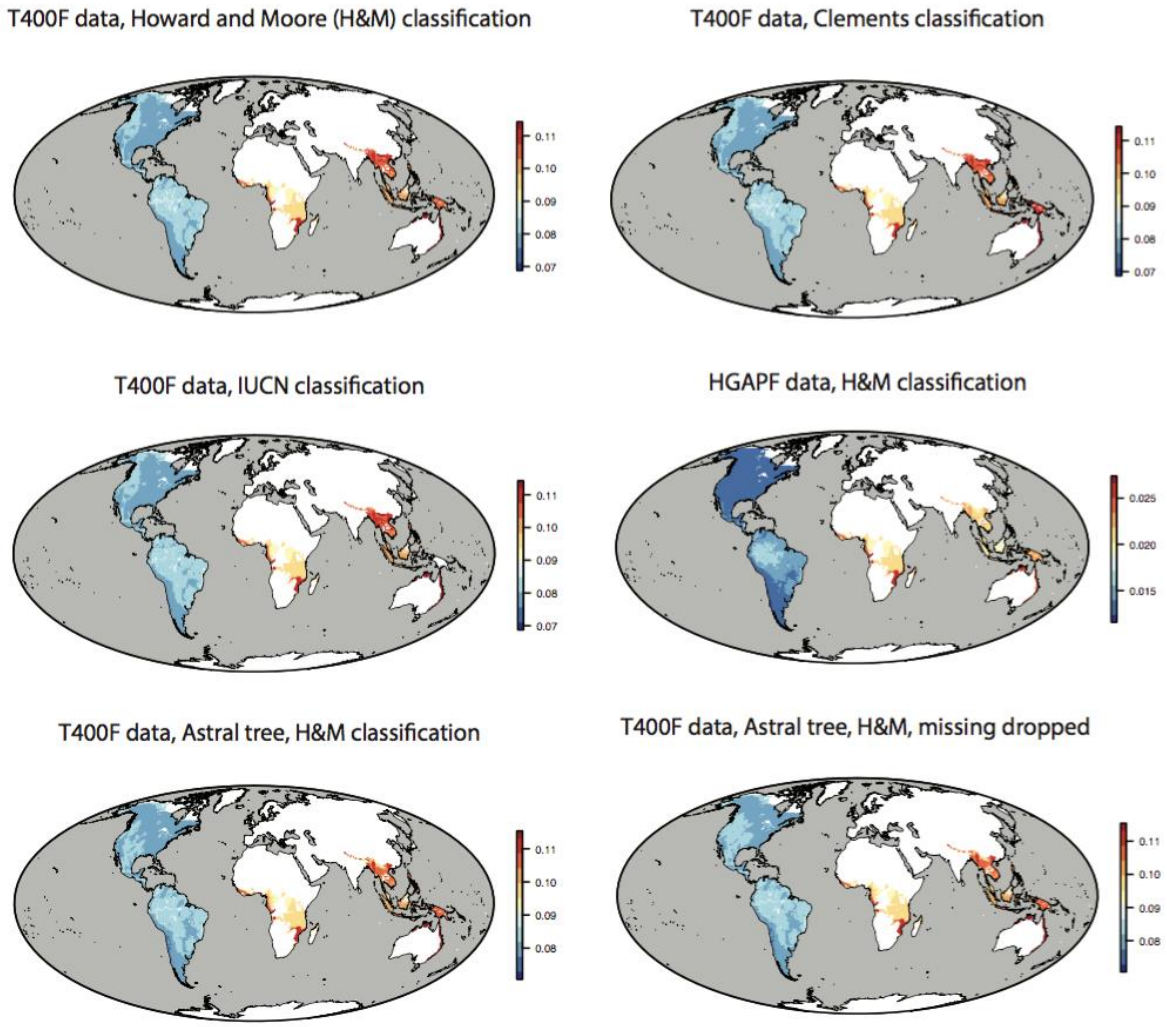

Fig. S57. SR across space for 3 taxonomies, the HGAPF tree for Howard and Moore classification, and the Astral tree with and without samples missing from >250 gene trees dropped for Howard and Moore classification

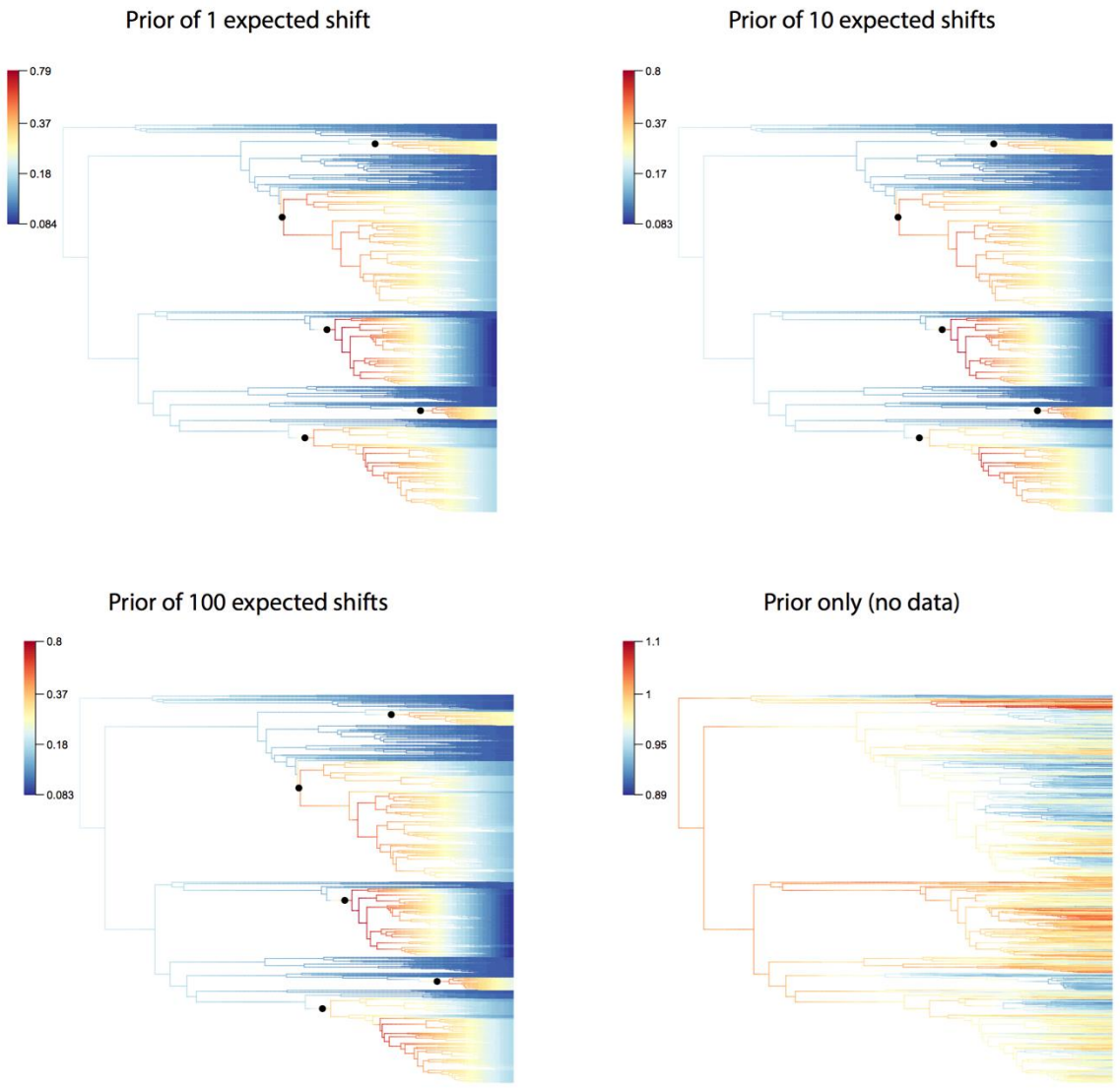

Fig. S58. Plot of BAMM speciation rates across the phylogeny and the best shift configuration with priors for expected number of shifts of 1, 10, and 100 and using only the prior information with no data (no shifts inferred)

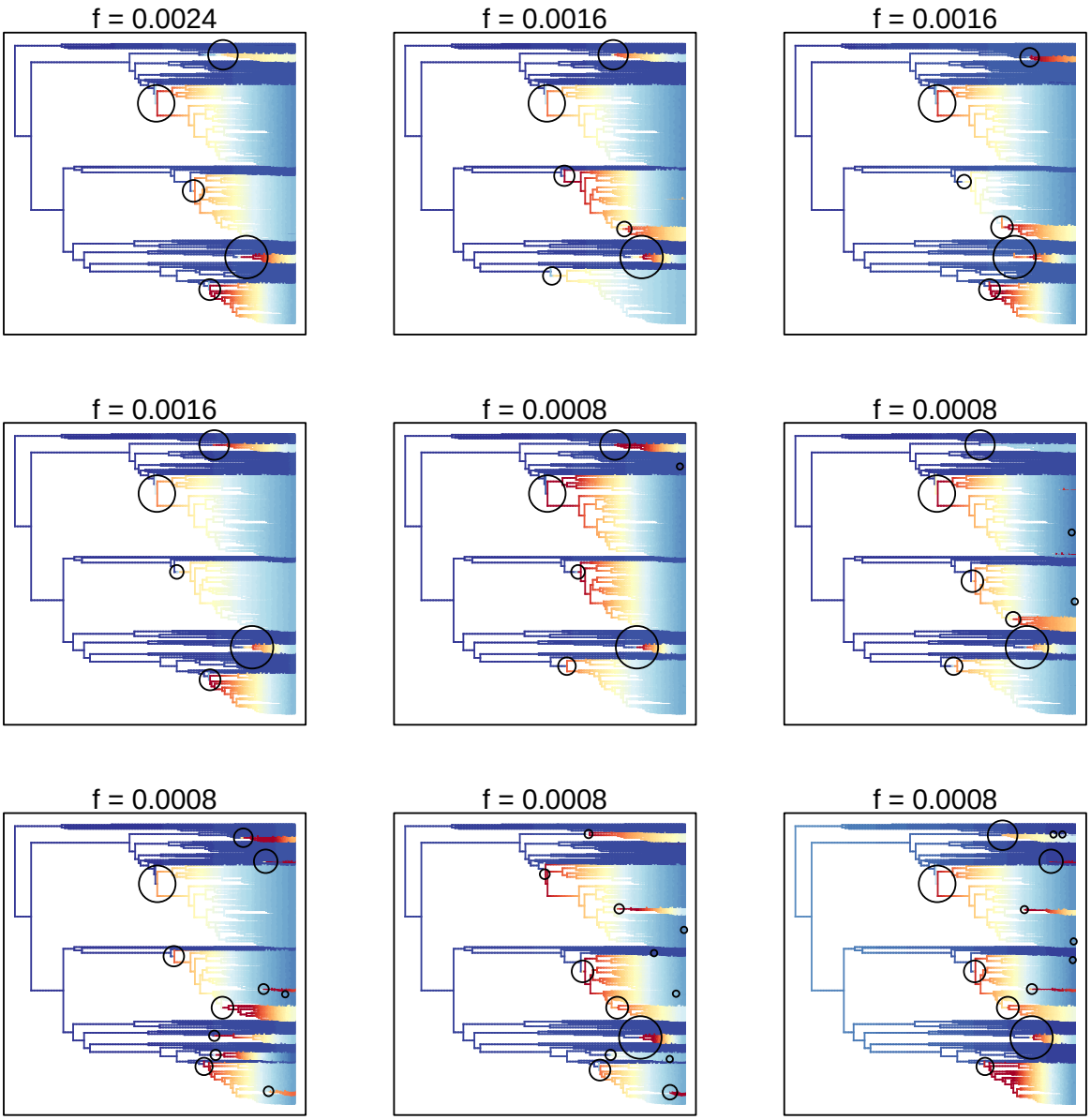

Fig. S59. Plot of the top nine shift conformations and their posterior probabilities (f) from the BAMM credible shift set for the Howard and Moore classification

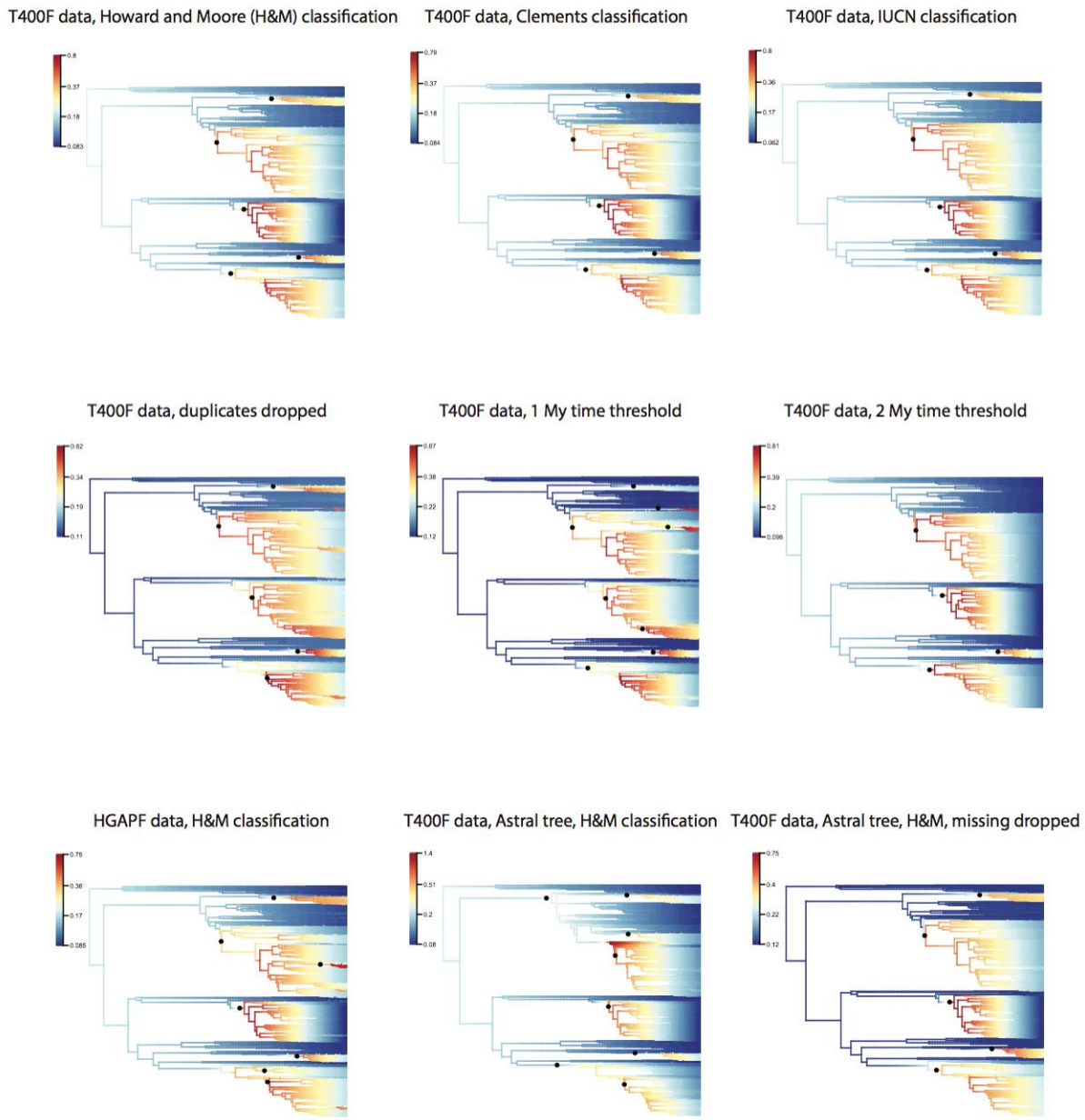

Fig. S60. Plot of BAMM speciation rates across the phylogeny and the best shift configuration for all 6 taxonomies with the T400F tree and Howard and Moore classification, the HGAPF tree for the Howard and Moore classification, and the Astral tree with and without samples missing from >250 gene trees dropped for Howard and Moore classification

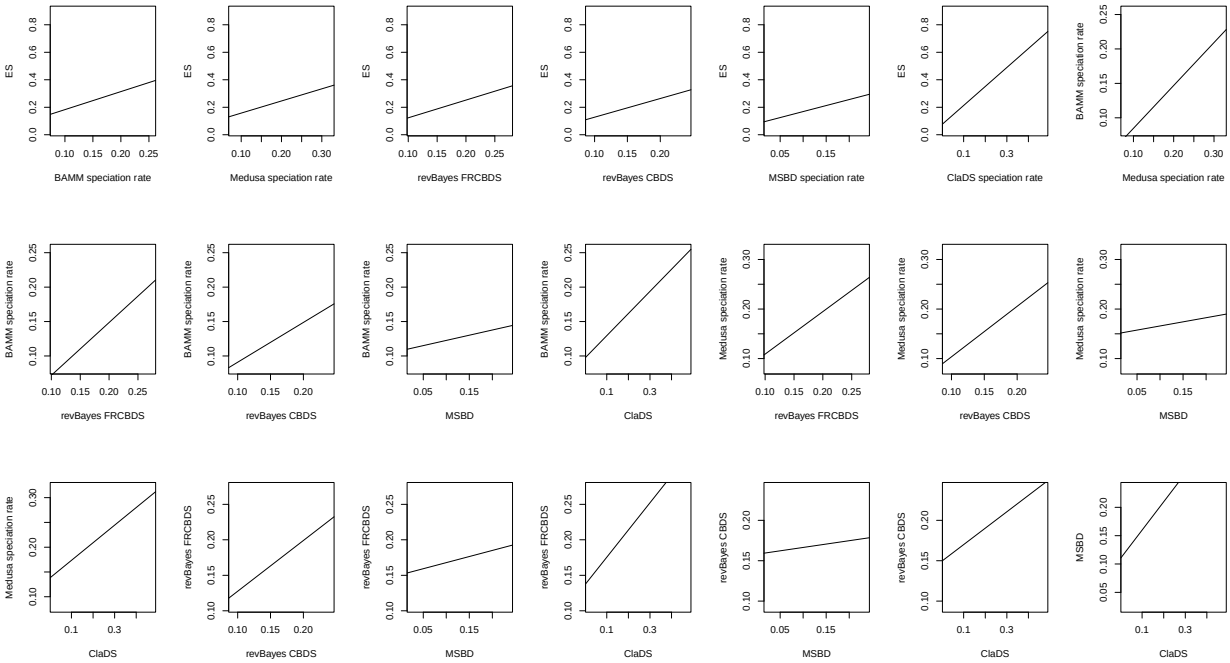

Fig. S61. Regressions comparing speciation rates at tips inferred using ES, BAMM, Medusa, RevBayes with both FRCBDS and CBDS methods (with prior of 10 expected shifts), MSBD, and ClaDS.

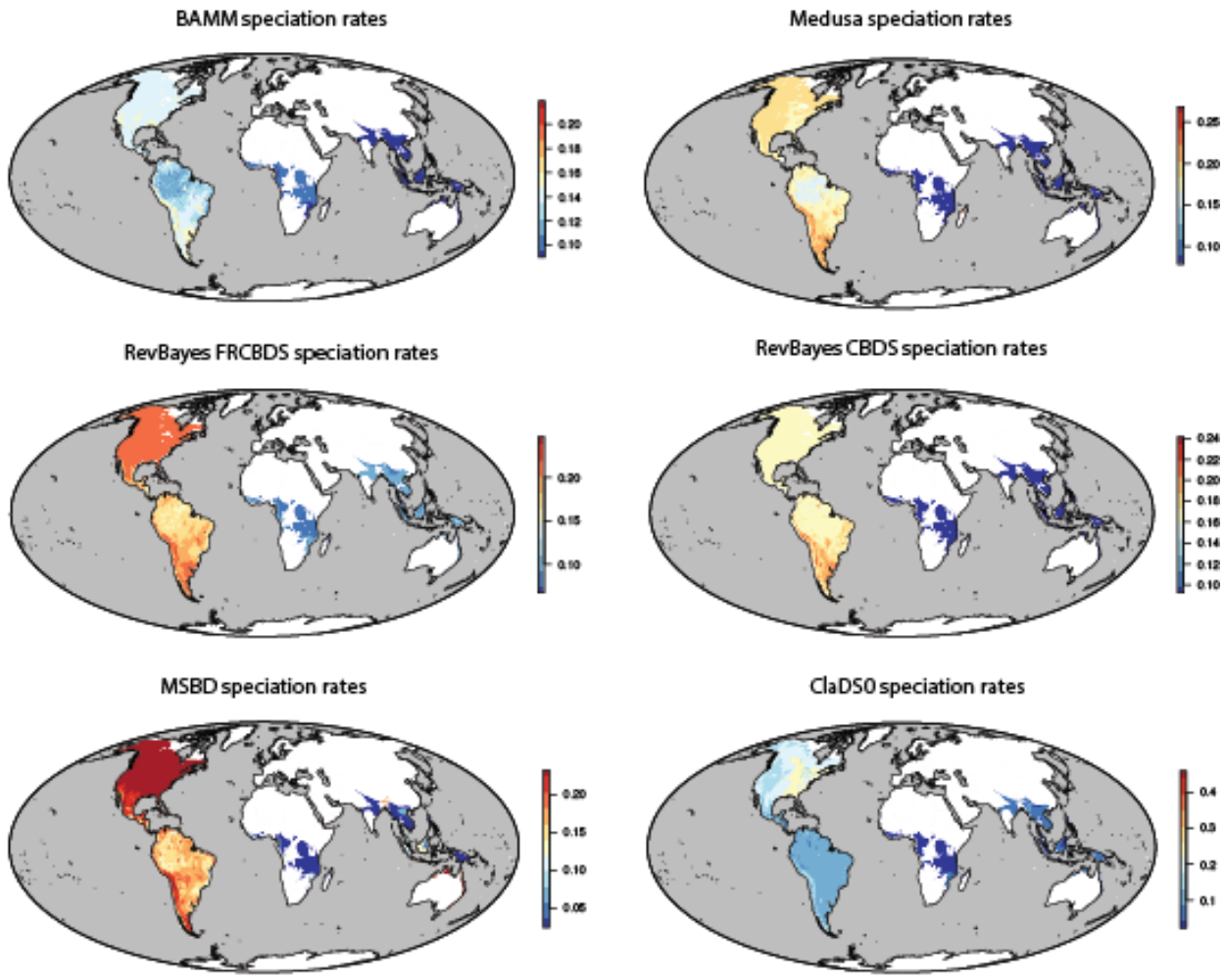

Fig. S62. Maps of BAMM, MEDUSA, RevBayes FRCBDS and CBDS (with prior of 10 expected shifts), MSBD, and ClaDS0 speciation rates across the globe.

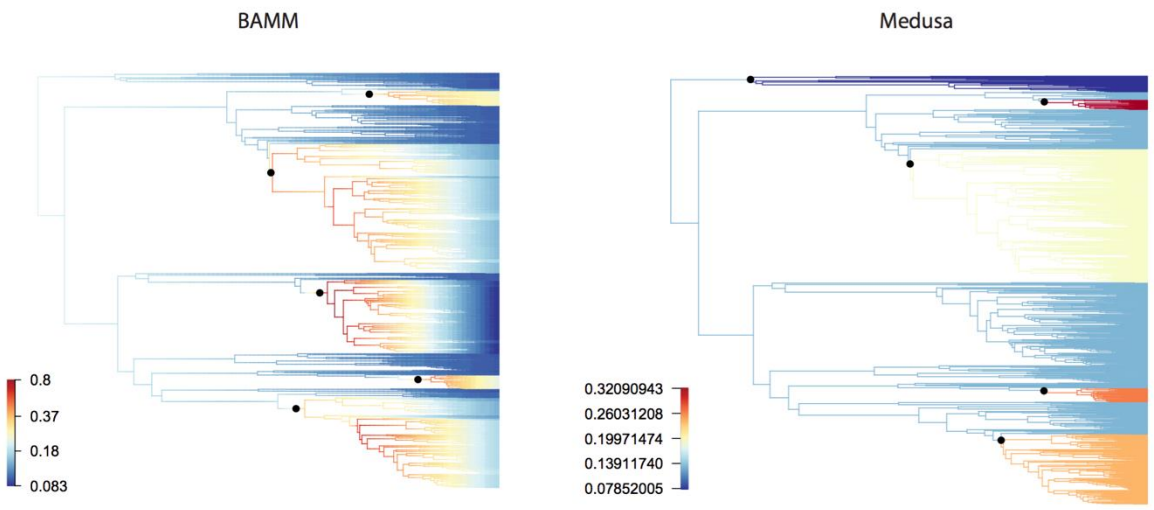

Fig. S63. Comparison of BAMM to MEDUSA speciation rates across the phylogeny and the inferred shift configuration with the T400F tree and Howard and Moore classification

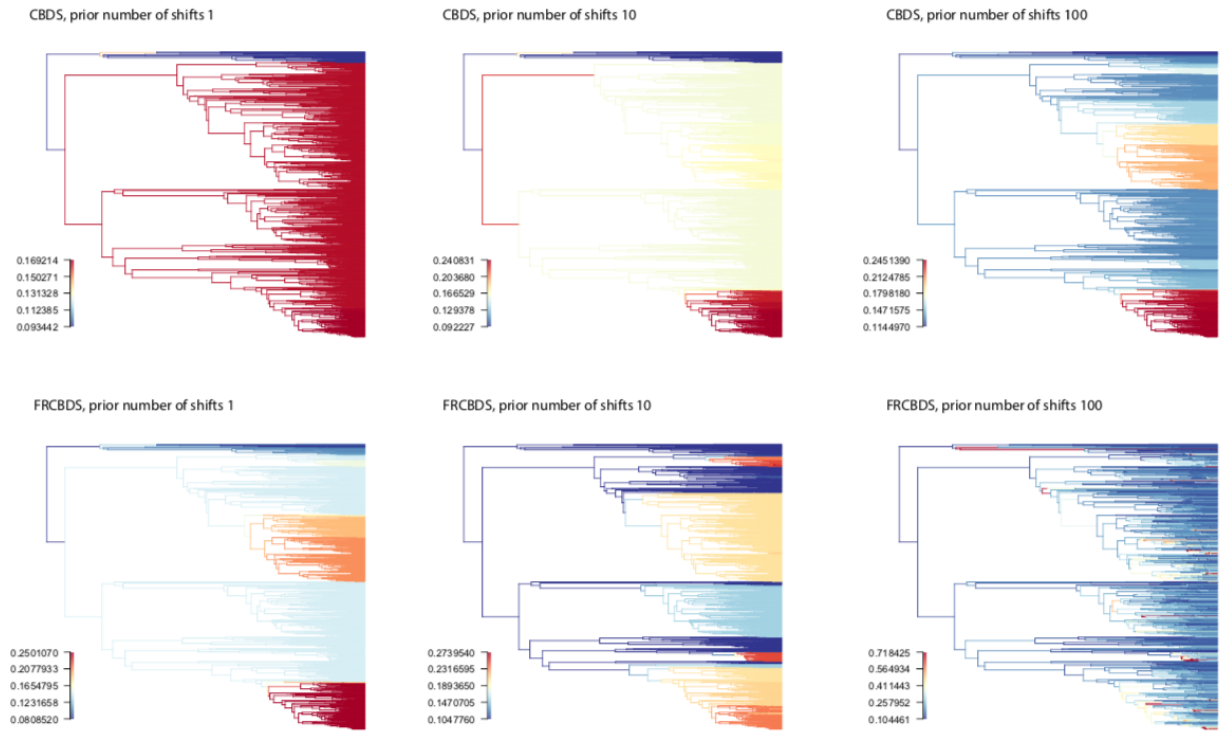

Fig. S64. Plots of RevBayes speciation rates across the phylogeny and the inferred shift configuration using both the finite-rate-category birth-death-shift (FRCBDS) process and conditional birth-death-shift (CBDS) process with prior number of expected shifts set at 1, 10, and 100.

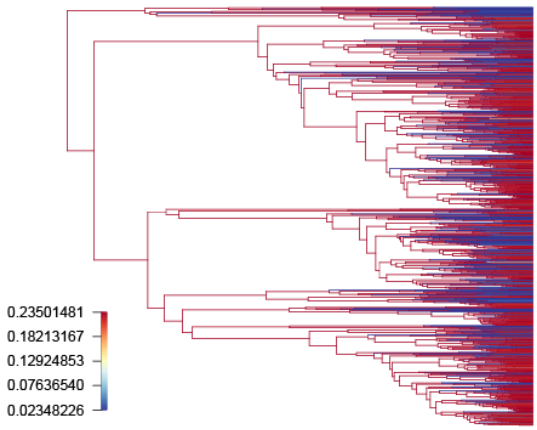

Fig. S65. MSBD speciation rates across the phylogeny with the T400F tree and Howard and Moore classification

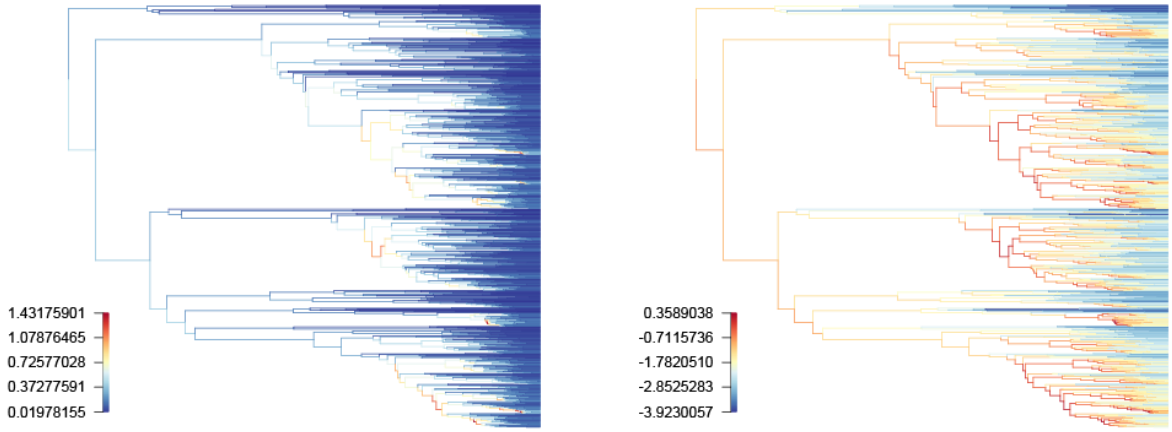

Fig. S66. ClaDS0 speciation rates across the phylogeny with the T400F tree and Howard and Moore classification. A few branches have very high rates, thus variation is more evident when log-transformed (right panel)

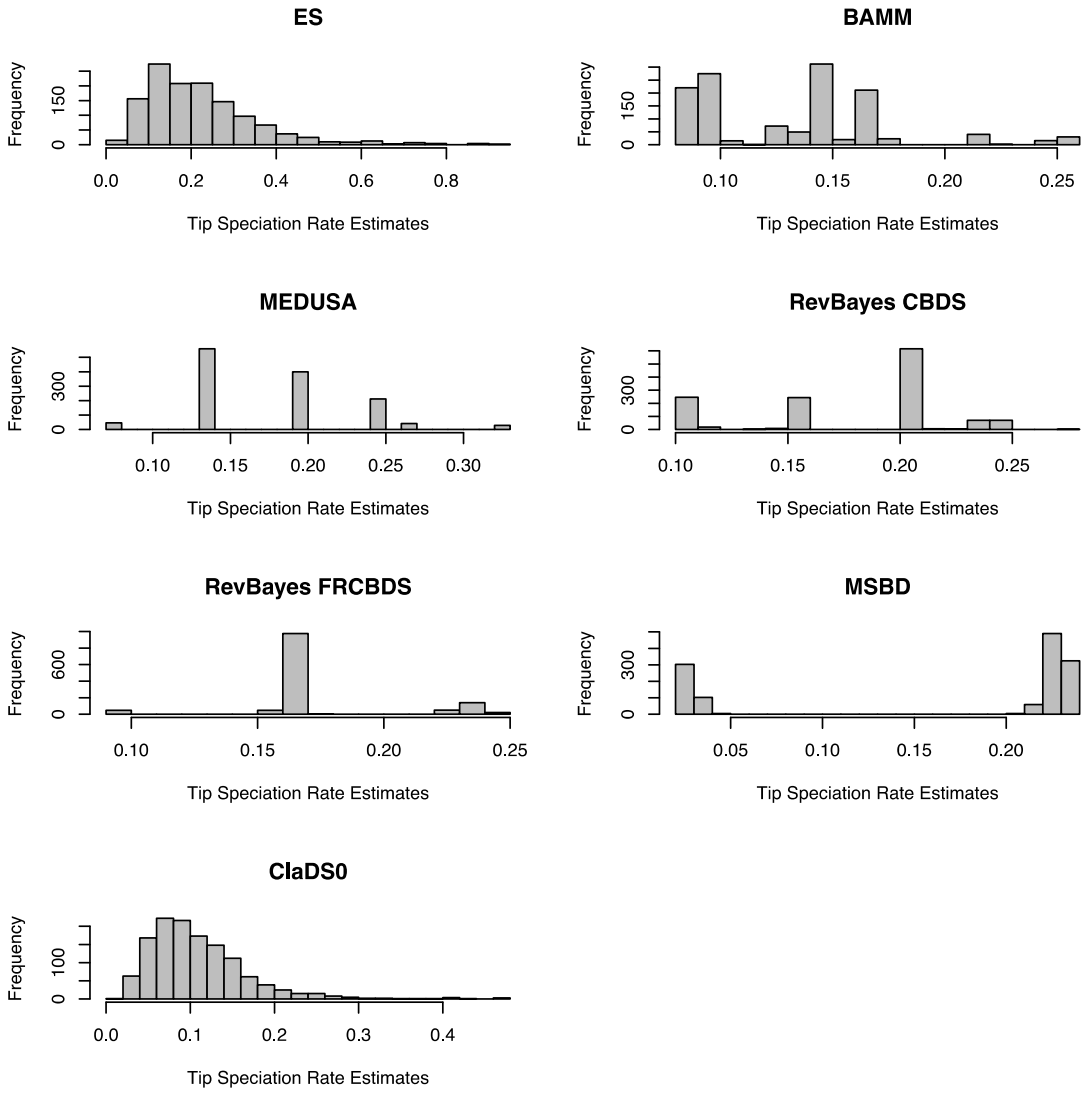

Fig. S67. Histograms of tip speciation rate estimates across all methods examined, showing greater variation in estimates from ES and ClaDS than other methods

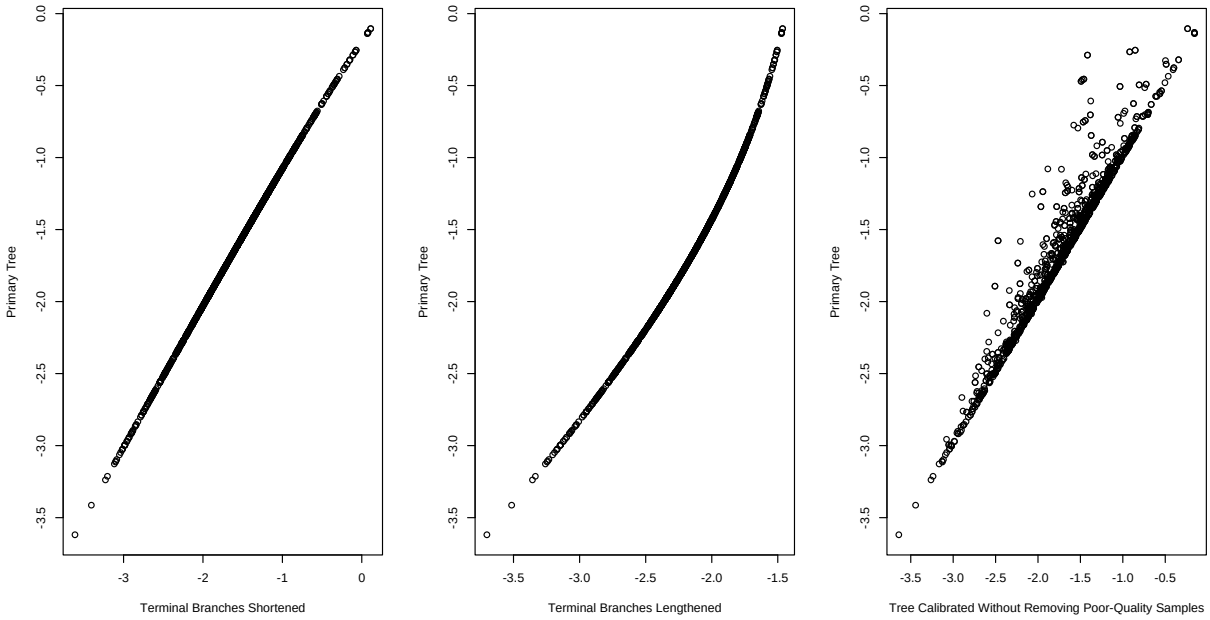

Fig. S68. The correlation between ES from the primary tree and trees with terminal branches uniformly shortened (left) or uniformly lengthened (middle), between the primary tree and a tree estimated using TreePL without removal of the poor-quality samples with long terminal branches (right)

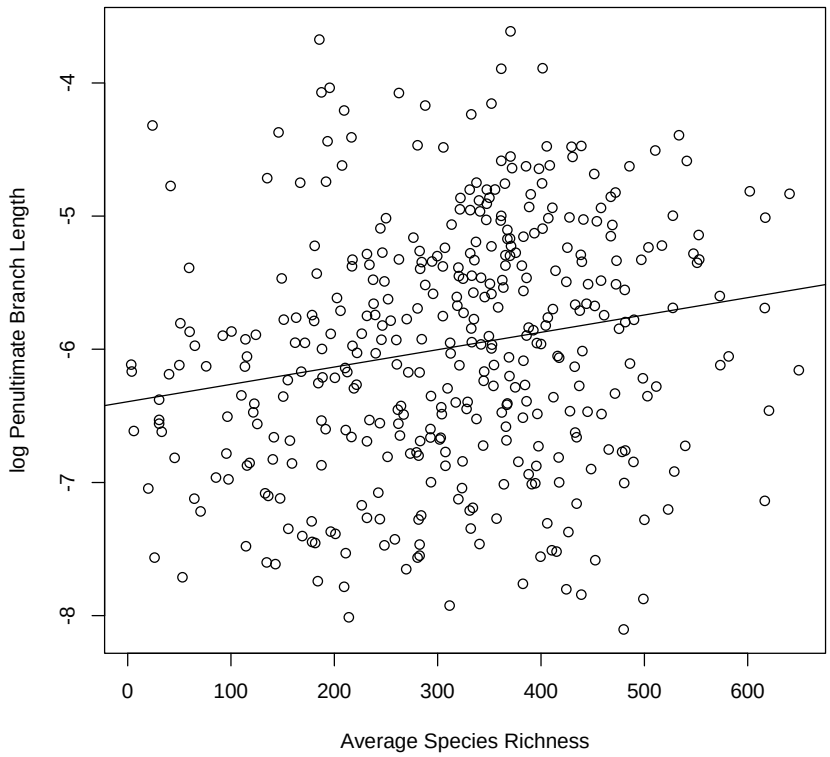

Fig. S69. The association between log penultimate branch lengths and average species richness in suboscine species pairs.

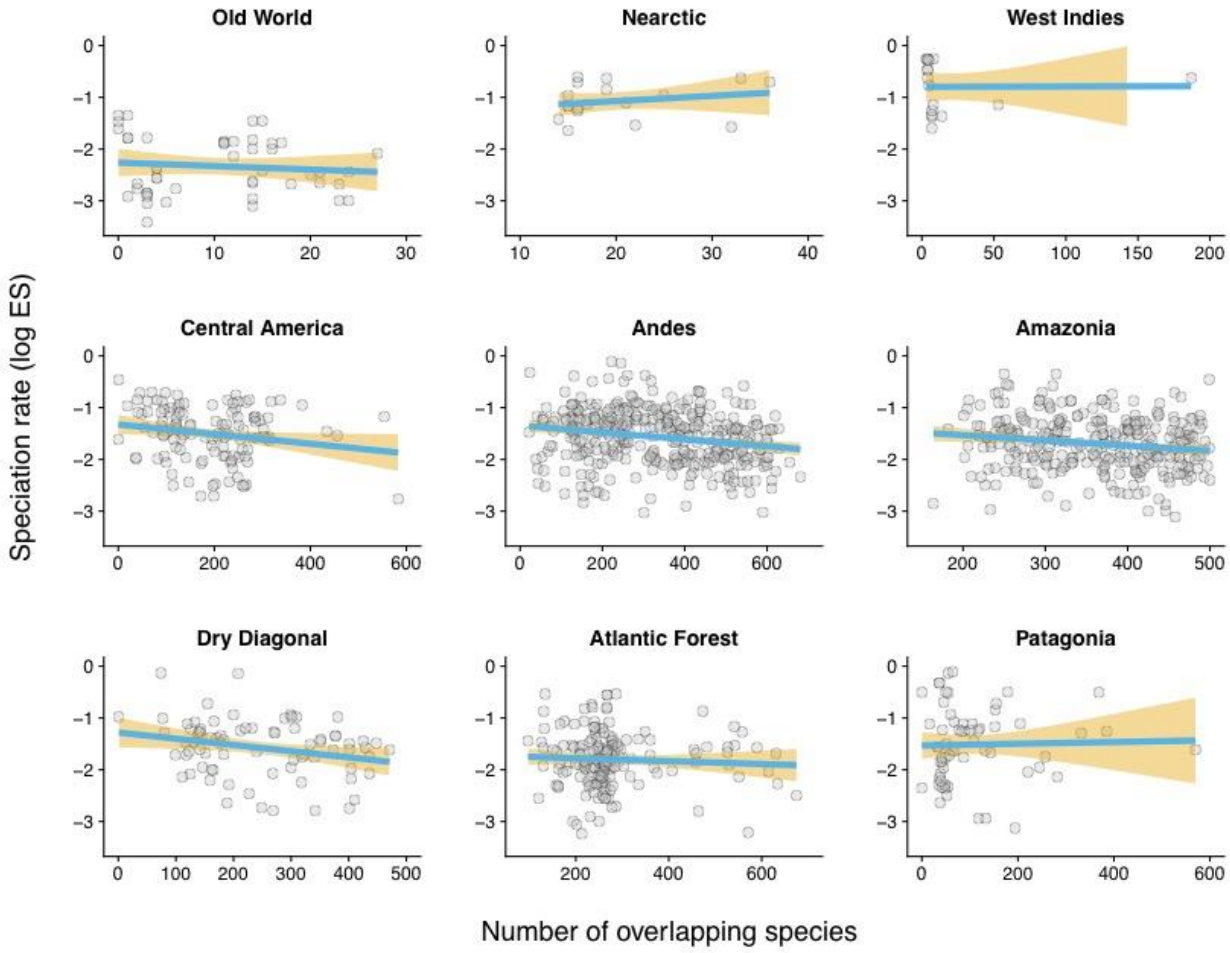

Fig. S70. Plots of the association between species richness and speciation rates for different regions (statistics are reported in Table S39)

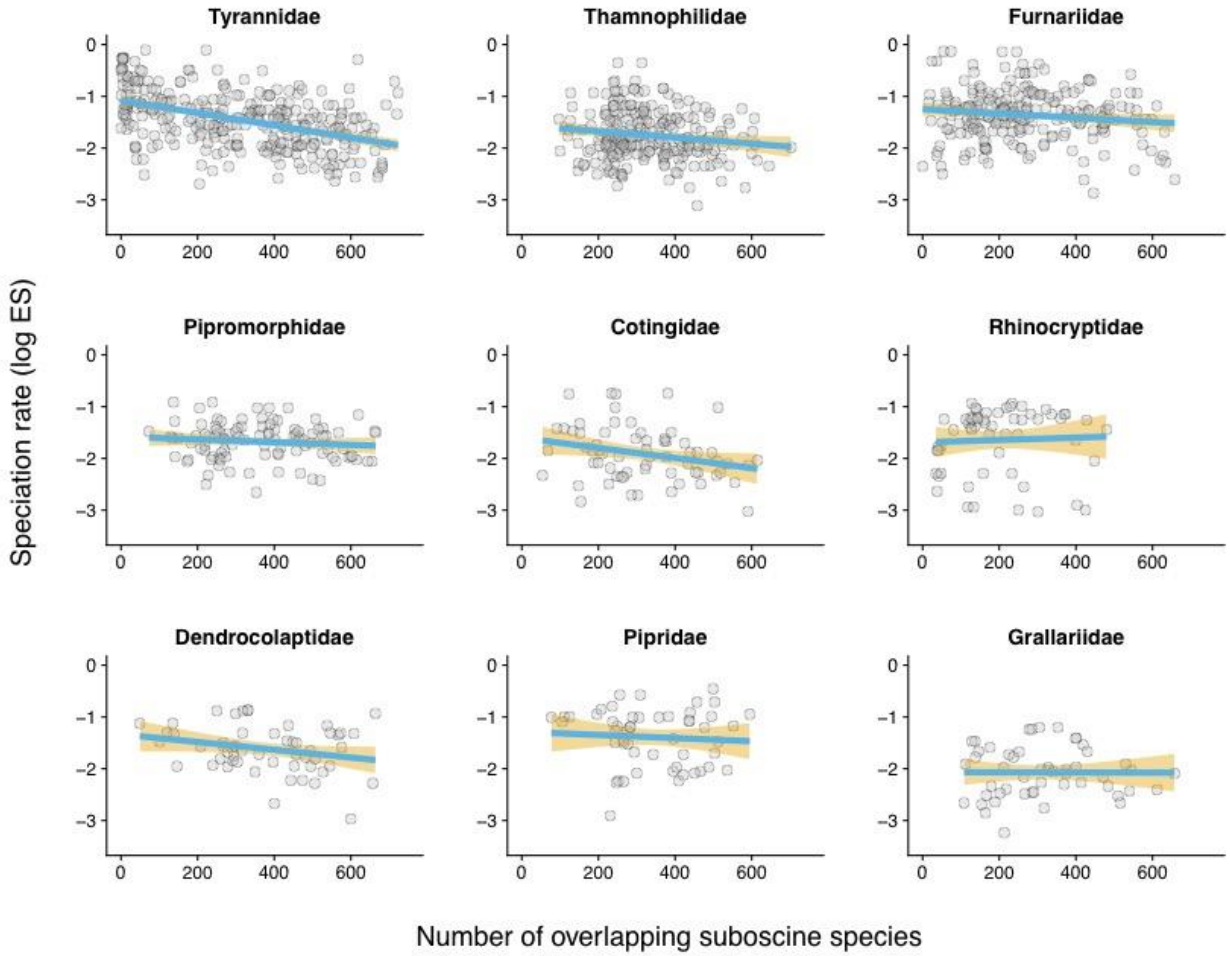

Fig. S71. Plots of the association between species richness and speciation rates for those families containing > 50 species (statistics are reported in Table S39)

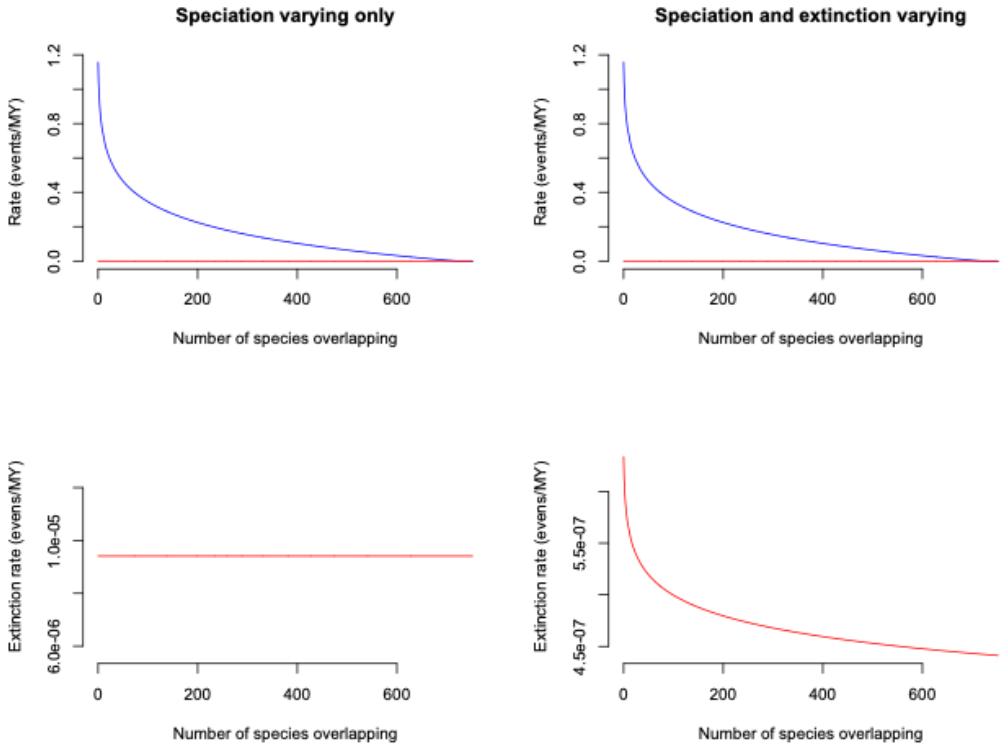

Fig. S72. Curves of MLE speciation and extinction rates from two QuaSSE models (L: speciation varying, R: both speciation and extinction varying)

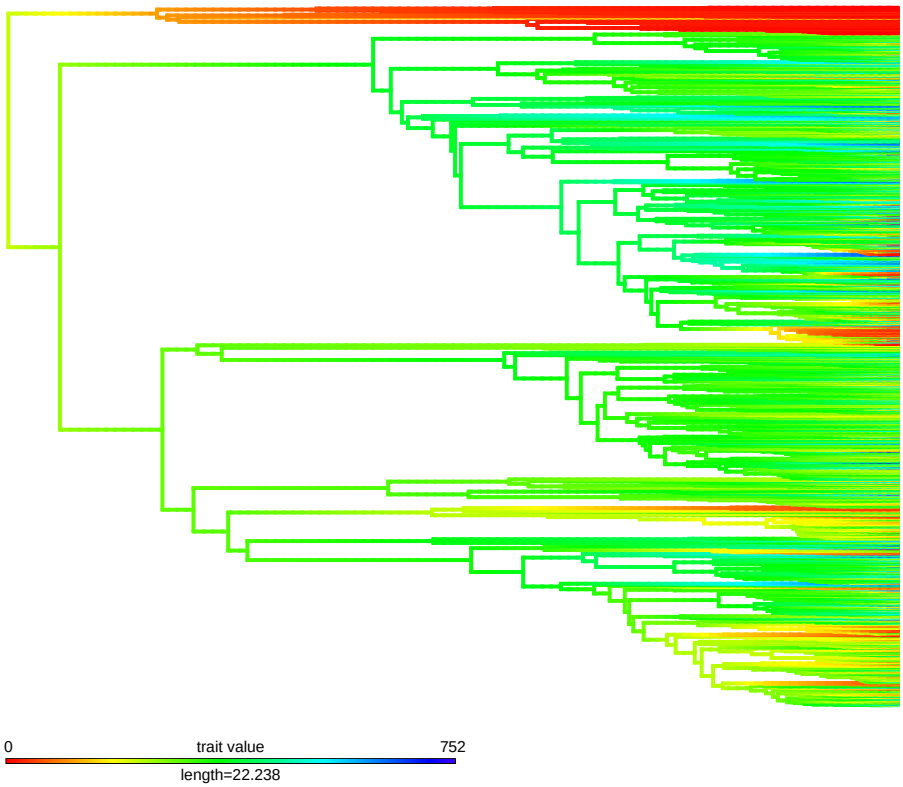

Fig. S73. Brownian reconstruction of species richness across the suboscine tree showing ancestral estimates

Tables

Table S1. Comparison with prior datasets

	Length	Tips	Total Size
Jarvis et al. (*49*)	322,150,876	48	15,463,242,048
Current study	1,559,815	1,940	3,026,041,100
Smith and Brown (*157*)			2,805,378,526
Irissari et al. (*158*)	1,964,339	100	196,433,900
Simion et al. (*159*)	401,632	97	116,874,912
Prum et al. (*14*)	394,457	198	78,102,486

Table S2. Suboscine family ages in the T400F time-calibrated tree

Family	Stem age (Ma)	Crown age (Ma)
Furnariidae	18.7	16.8
Rhinocryptidae	33.5	23.3
Tyrannidae	21.8	16.8
Thamnophilidae	33.8	19.7
Cotingidae	25.3	20.0
Pipridae	26.2	15.2
Pipromorphidae	21.8	19.5
Calyptomenidae	36.5	30.7
Platyrinchidae	22.3	20.2
Dendrocolaptidae	18.7	15.7
Formicariidae	32.5	23.2
Conopophagidae	33.8	17.7
Eurylaimidae	29.1	25.8
Pittidae	35.9	18.5
Scleruridae	21.3	17.7
Grallariidae	35.2	25.5
Tityridae	24.8	21.2
Melanopareiidae	35.0	12.7
Onychorhynchidae	23.7	19.9
Philepittidae	29.1	20.2
Oxyruncidae	23.7	3.1
Pipritidae	23.3	18.2
Sapayoidae	35.9	NA
Tachurisidae	22.1	NA

Table S3. Gamma (γ) test statistics without and with trimming of the most recent 2.5 Ma for all suboscine family-level clades with more than 20 species

Family	γ	P Value	Trimmed γ	Trimmed P Value
Furnariidae	-7.49	6.83×10^{-14}	1.20	0.23
Rhinocryptidae	-3.33	8.83×10^{-4}	2.46	0.01
Grallariidae	-3.08	2.06×10^{-3}	-0.11	0.91
Thamnophilidae	-8.94	3.85×10^{-19}	-3.75	1.76×10^{-4}
Tyrannidae	-7.17	7.35×10^{-13}	-0.61	0.54
Pipromorphidae	-4.57	4.86×10^{-6}	1.10	0.27
Tityridae	-0.96	0.33	1.31	0.19
Cotingidae	-2.14	0.03	-0.71	0.48
Pipridae	-1.74	0.08	0.10	0.92
Pittidae	-2.24	0.03	0.01	0.99

Table S4. The results of diversity-dependent (dd) versus constant-rate birth-death (bd) model comparisons indicate support for diversity dependence in some lineages (highly negative ΔAICc values) across family-level clades with more than 20 species

Family	Diversity dependent log Likelihood	Constant-rate birth-death log Likelihood	ΔAICc
Furnariidae	-671.70	-703.15	-60.85
Rhinocryptidae	-114.59	-119.04	-6.61
Grallariidae	-52.64	-59.11	-10.20
Thamnophilidae	-616.72	-654.08	-72.67
Tyrannidae	-724.94	-777.52	-103.13
Pipromorphidae	-242.56	-270.34	-53.44
Tityridae	-62.47	-63.39	0.86
Cotingidae	-150.26	-153.28	-3.78
Pipridae	-125.18	-127.16	-1.69
Pittidae	-80.85	-84.24	-4.26

Table S5 Associations between evolutionary dynamics and various predictor variables.

	Variable Name	Speciation Rate (ES)		Age (TB)		Age (NH)		Diversity	
		ρ	P	ρ	P	ρ	P	ρ	P
Richn.	richness suboscines	**-0.247**	**0.006****	**0.194**	**0.014***	0.177	0.084	NA	NA
	richness passerines	**-0.216**	**0.017***	**0.171**	**0.020***	0.149	0.126	NA	NA
	richness all birds	**-0.223**	**0.021***	**0.176**	**0.022***	0.155	0.105	NA	NA
Lat/Elevation	elev.mid	0.187	0.100	-0.122	0.254	-0.122	0.414	-0.077	0.410
	elev.max	0.203	0.064	-0.138	0.174	-0.133	0.342	-0.045	0.657
	elev.min	0.133	0.264	-0.079	0.454	-0.086	0.547	-0.108	0.164
	elev.range	0.152	0.212	-0.116	0.286	-0.101	0.428	0.048	0.625
	lat.mid	0.162	0.100	-0.114	0.214	-0.111	0.376	**-0.582**	**0.002****
	lat.max	0.115	0.296	-0.063	0.488	-0.087	0.537	**-0.399**	**0.002****
	lat.min	0.061	0.597	-0.030	0.765	-0.035	0.773	**-0.288**	**0.002****
	range.area	-0.119	0.270	0.107	0.288	0.064	0.645	**0.428**	**0.002****
	mig.dist	0.135	0.180	-0.084	0.406	-0.143	0.236	**-0.254**	**0.002****
Climate	temp.mean	-0.175	0.057	0.102	0.142	0.117	0.222	**0.318**	**0.001****
	temp.median	**-0.173**	**0.049***	0.101	0.152	0.114	0.177	**0.321**	**0.001****
	temp.var	0.164	0.063	-0.115	0.088	-0.150	0.122	-0.109	0.055
	temp.instab1.mean	**0.171**	**0.047***	-0.105	0.150	-0.162	0.106	**-0.207**	**0.002****
	temp.instab1.median	**0.169**	**0.035***	-0.103	0.146	-0.162	0.117	**-0.201**	**0.001****
	temp.instab2.mean	0.152	0.079	-0.097	0.155	-0.138	0.150	**-0.142**	**0.019***
	temp.instab2.median	0.143	0.093	-0.088	0.191	-0.131	0.149	**-0.134**	**0.025***
	temp.seasonality.mean	0.129	0.122	-0.081	0.195	-0.112	0.191	**-0.391**	**0.001****
	temp.seasonality.median	0.132	0.118	-0.084	0.193	-0.111	0.200	**-0.418**	**0.001****
	temp.seasonality.var	0.116	0.135	-0.084	0.180	-0.136	0.139	-0.051	0.253
	temp.season.instab1.mean	0.117	0.140	-0.066	0.239	-0.121	0.171	**-0.317**	**0.001****
	temp.season.instab1.median	0.099	0.162	-0.052	0.293	-0.100	0.246	**-0.327**	**0.001****
	temp.season.instab2.mean	0.079	0.235	-0.046	0.328	-0.084	0.275	**-0.233**	**0.001****
	temp.season.instab2.median	0.066	0.283	-0.033	0.375	-0.078	0.319	**-0.228**	**0.001****
	max.temp.mean	-0.133	0.108	0.074	0.214	0.074	0.291	**0.189**	**0.002****
	max.temp.median	-0.130	0.109	0.072	0.246	0.070	0.342	**0.187**	**0.002****
	max.temp.var	0.158	0.066	-0.117	0.114	-0.130	0.181	-0.104	0.069
	max.temp.instab1.mean	**0.191**	**0.043***	-0.129	0.072	-0.167	0.093	**-0.247**	**0.001****
	max.temp.instab1.median	**0.190**	**0.030***	-0.128	0.070	-0.169	0.101	**-0.243**	**0.001****
	min.temp.mean	**-0.176**	**0.048***	0.101	0.161	0.128	0.174	**0.347**	**0.001****
	min.temp.median	-0.174	0.057	0.100	0.139	0.125	0.172	**0.357**	**0.001****
	min.temp.var	0.123	0.128	-0.081	0.213	-0.139	0.171	0.000	0.483
	min.temp.instab1.mean	0.083	0.219	-0.032	0.403	-0.093	0.224	-0.011	0.427
	min.temp.instab1.median	0.085	0.238	-0.033	0.383	-0.093	0.228	-0.009	0.443
	precip.mean	-0.155	0.080	0.096	0.148	0.131	0.140	**0.335**	**0.001****
	precip.median	-0.151	0.084	0.091	0.168	0.129	0.158	**0.314**	**0.001****
	precip.var	-0.075	0.274	0.040	0.363	0.074	0.300	**0.199**	**0.001****
	precip.instab1.mean	-0.033	0.399	0.006	0.494	0.038	0.397	-0.031	0.331
	precip.instab1.median	-0.016	0.436	-0.007	0.489	0.022	0.465	-0.108	0.052
	precip.instab2.mean	-0.039	0.364	0.005	0.494	0.037	0.370	0.017	0.441
	precip.instab2.median	-0.036	0.383	0.003	0.493	0.033	0.399	-0.026	0.396
	precip.seasonality.mean	0.109	0.144	-0.102	0.148	-0.069	0.321	**-0.219**	**0.001****

precip.seasonality.median	0.098	0.161	-0.095	0.155	-0.062	0.323	-0.176	**0.005****
precip.seasonality.variance	-0.006	0.496	-0.012	0.452	0.036	0.411	0.063	0.201
precip.season.instab1.mean	0.023	0.424	-0.008	0.462	-0.042	0.388	-0.014	0.458
precip.season.instab1.median	0.057	0.321	-0.029	0.376	-0.077	0.261	-0.082	0.141
precip.season.instab2.mean	0.048	0.352	-0.043	0.316	-0.020	0.441	-0.102	0.092
precip.season.instab2.median	0.046	0.347	-0.032	0.373	-0.033	0.419	**-0.125**	**0.037***
precip.wettest.q.mean	-0.135	0.106	0.075	0.214	0.109	0.210	**0.343**	**0.001****
precip.wettest.q.median	-0.133	0.103	0.072	0.214	0.109	0.217	**0.319**	**0.001****
precip.wettest.q.var	-0.060	0.284	0.029	0.369	0.045	0.367	**0.298**	**0.001****
precip.wettest.q.instab1.mean	-0.052	0.306	0.022	0.412	0.040	0.407	-0.037	0.319
precip.wettest.q.instab1.median	-0.033	0.377	0.010	0.445	0.022	0.433	-0.114	0.055
precip.wettest.q.instab2.mean	-0.083	0.225	0.043	0.352	0.048	0.361	**0.126**	**0.033***
precip.wettest.q.instab2.median	-0.080	0.261	0.041	0.323	0.048	0.363	0.068	0.175
precip.driest.q.mean	**-0.168**	**0.046***	0.121	0.097	0.149	0.109	**0.241**	**0.001****
precip.driest.q.median	-0.141	0.082	0.104	0.140	0.124	0.155	**0.152**	**0.009****
precip.driest.q.var	-0.125	0.142	0.081	0.186	0.126	0.173	**0.193**	**0.001****
precip.driest.q.instab1.mean	-0.075	0.243	0.050	0.312	0.061	0.334	**0.234**	**0.001****
precip.driest.q.instab1.median	-0.037	0.355	0.019	0.420	0.030	0.431	**0.120**	**0.050***
precip.driest.q.instab2.mean	-0.112	0.156	0.087	0.193	0.090	0.226	**0.229**	**0.002****
precip.driest.q.instab2.median	-0.090	0.220	0.075	0.203	0.069	0.301	**0.144**	**0.015***

***** $P < 0.05$
****** $P < 0.01$

Table S6. The results of extinction sensitivity tests.

Model conditions	20% removed	40% removed	60% removed	80% removed
Random extinction				
Average ρ	-0.27	-0.27	-0.26	-0.22
Proportion significant	1.00	1.00	0.93	0.47
Extinction variable across families				
Average ρ	-0.27	-0.26	-0.25	-0.23
Proportion significant	1.00	0.99	0.83	0.52
Extinction variable according to inverse of range size				
Average ρ	-0.27	-0.29	-0.31	-0.34
Proportion significant	1.00	1.00	1.00	0.97

Table S7. QuaSSE model comparison results showing support for models with associations between species overlap and speciation and extinction rates as well as parameter values

	Minimal	**Speciation-dependence**	**Extinction-dependence**	**Speciation- and extinction-dependence**
log Likelihood	-5016.2	- 4979.0	- 5016.2	- 4979.0
AIC	10038	9966	10040	9968
Chi-Squared	-	74.44	0.02	74.45
Pr(>|Chi|)	-	$< 2.20 \times 10^{-16}$	0.90	$< 2.20 \times 10^{-16}$
λ	0.17	1.16	0.17	1.16
μ	0.00	9.41×10^{-6}	-0.03	$-6.34 \times 10^{=7}$
λ slope	-	-0.18	-	-0.18
μ slope	-	-	0.00	$-2.91 \times 10^{=8}$

Table S8. Alternate references used for mapping data from low quality samples

Sample	Samples used to produce reference
Acropt_ortnyx_L30027	Acropt_ortnyx_PhAMC1246
Acropt_ortnyx_PhAMC1246	Acropt_ortnyx_L30027
Akleto_goeld_LSU21212	Akleto_goeld_LSU9293
Akleto_goeld_LSU9293	Akleto_goeld_LSU21212
Anaire_alpin_NM34088	Anaire_parlus_A12192, Anaire_flaviro_CU52375, Anaire_nigrosta_F391921, Anaire_regide_LSU72421, Anaire_ferna_CM120730
Anaire_ferna_CM120730	Anaire_parlus_A12192, Anaire_flaviro_CU52375, Anaire_alpin_NM34088, Anaire_nigrosta_F391921, Anaire_regide_LSU72421, Anaire_parlus_A12192
Anaire_flaviro_CU52375	Anaire_parlus_A12192, Anaire_alpin_NM34088, Anaire_nigrosta_F391921, Anaire_regide_LSU72421, Anaire_ferna_CM120730
Anaire_nigrosta_F391921	Anaire_parlus_A12192, Anaire_flaviro_CU52375, Anaire_alpin_NM34088, Anaire_regide_LSU72421, Anaire_ferna_CM120730
Anaire_parlus_A12192	Anaire_flaviro_CU52375, Anaire_alpin_NM34088, Anaire_nigrosta_F391921, Anaire_regide_LSU72421, Anaire_ferna_CM120730, Anaire_ferna_CM120730
Anaire_regide_LSU72421	Anaire_parlus_A12192, Anaire_flaviro_CU52375, Anaire_alpin_NM34088, Anaire_nigrosta_F391921, Anaire_ferna_CM120730
Attila_cinmeus_K1236	Attila_cinmeus_SB11685
Attila_cinmeus_SB11685	Attila_cinmeus_K1236
Batara_cinrea_LSU18607	Batara_cinrea_SPML159
Batara_cinrea_SPML159	Batara_cinrea_LSU18607
Calytur_criata_A494721	Calytur_criata_A494720, Neopip_cinmom_L42825, Calytur_criata_A4379, Calytur_criata_A494720, Calytur_criata_A4379
Carpod_hopkei_L29961	Carpod_nitdus_A247754
Carpod_nitdus_A247754	Carpod_nitdus_A247754, Carpod_hopkei_L29961, Carpod_hopkei_L29961, Carpod_nitdus_A247754
Cliba_erylus_L61296	Cliba_erylus_SB28253
Cliba_erylus_SB28253	Cliba_erylus_L61296
Clytoc_ali_A133422	Clytoc_ali_A133422, Neocta_niger_L2749, Neocta_niger_L2749, Clytoc_ali_A133422
Coniop_mcilh_K1416	Coniop_mcilh_L78827
Coniop_mcilh_L78827	Coniop_mcilh_K1416
Contop_coope_A17527	Contop_viren_L37174
Contop_viren_L37174	Contop_coope_A17527
Corapi_alter_LSU28374	Corapi_alter_L28407

Corvus_coride_A17778	Passer_L52749
Corydo_sumnus_L77291	Pseutom_graueri_F311050, Pseutom_graueri_A764296, Psaris_dalsia_K25407
Coryph_ala_L18894	Coryph_ala_S636126
Coryph_ala_S636126	Coryph_ala_L18894
Cymlai_lintus_GBR163161	Cymlai_lintus_IN1551, Cymlai_lintus_LSU28690, Cymlai_lintus_MZU92809
Cymlai_lintus_IN1551	Cymlai_lintus_GBR163161, Cymlai_lintus_LSU28690, Cymlai_lintus_MZU92809
Cymlai_lintus_LSU28690	Cymlai_lintus_GBR163161, Cymlai_lintus_IN1551, Cymlai_lintus_MZU92809
Cymlai_lintus_MZU92809	Cymlai_lintus_GBR163161, Cymlai_lintus_IN1551, Cymlai_lintus_LSU28690
Dendre_rufula_F389815	Dendre_rufula_L4562
Dendre_rufula_L4562	Dendre_rufula_F389815
Dichro_cincta_L10517	Dichro_cincta_LSU6919, Dichro_cincta_MZU86486
Dichro_cincta_LSU6919	Dichro_cincta_L10517, Dichro_cincta_MZU86486
Dichro_cincta_MZU86486	Dichro_cincta_L10517, Dichro_cincta_LSU6919
Dryphi_devil_LSU9683	Dryphi_devil_MPEG69273
Dryphi_devil_MPEG69273	Dryphi_devil_LSU9683
Dysith_leuctus_COP07N0158	Dysith_leuctus_LSU6111, Dysith_leuctus_YPM139344
Dysith_leuctus_LSU6111	Dysith_leuctus_COP07N0158, Dysith_leuctus_YPM139344
Dysith_leuctus_YPM139344	Dysith_leuctus_COP07N0158, Dysith_leuctus_LSU6111
Dysith_mental_L33085	Dysith_mental_MZUSP85740, Dysith_mental_LSU2003, Dysith_mental_LSU22639, Dysith_mental_LSU66338, Dysith_mental_LSU26463, Dysith_mental_LSU69439, Dysith_mental_LSU69289, Dysith_mental_LSU48490, Dysith_mental_MZU94637, Dysith_mental_MZU87834
Dysith_mental_LSU2003	Dysith_mental_MZUSP85740, Dysith_mental_LSU22639, Dysith_mental_LSU66338, Dysith_mental_LSU26463, Dysith_mental_LSU69439, Dysith_mental_LSU69289, Dysith_mental_LSU48490, Dysith_mental_L33085, Dysith_mental_MZU94637, Dysith_mental_MZU87834
Dysith_mental_LSU22639	Dysith_mental_MZUSP85740, Dysith_mental_LSU2003, Dysith_mental_LSU66338, Dysith_mental_LSU26463, Dysith_mental_LSU69439, Dysith_mental_LSU69289, Dysith_mental_LSU48490, Dysith_mental_L33085, Dysith_mental_MZU94637, Dysith_mental_MZU87834
Dysith_mental_LSU26463	Dysith_mental_MZUSP85740, Dysith_mental_LSU2003, Dysith_mental_LSU22639, Dysith_mental_LSU66338, Dysith_mental_LSU69439, Dysith_mental_LSU69289, Dysith_mental_LSU48490, Dysith_mental_L33085, Dysith_mental_MZU94637, Dysith_mental_MZU87834

Dysith_mental_LSU48490	Dysith_mental_MZUSP85740, Dysith_mental_LSU2003, Dysith_mental_LSU22639, Dysith_mental_LSU66338, Dysith_mental_LSU26463, Dysith_mental_LSU69439, Dysith_mental_LSU69289, Dysith_mental_L33085, Dysith_mental_MZU94637, Dysith_mental_MZU87834
Dysith_mental_LSU66338	Dysith_mental_MZUSP85740, Dysith_mental_LSU2003, Dysith_mental_LSU22639, Dysith_mental_LSU26463, Dysith_mental_LSU69439, Dysith_mental_LSU69289, Dysith_mental_LSU48490, Dysith_mental_L33085, Dysith_mental_MZU94637, Dysith_mental_MZU87834
Dysith_mental_LSU69289	Dysith_mental_MZUSP85740, Dysith_mental_LSU2003, Dysith_mental_LSU22639, Dysith_mental_LSU66338, Dysith_mental_LSU26463, Dysith_mental_LSU69439, Dysith_mental_LSU48490, Dysith_mental_L33085, Dysith_mental_MZU94637, Dysith_mental_MZU87834
Dysith_mental_LSU69439	Dysith_mental_MZUSP85740, Dysith_mental_LSU2003, Dysith_mental_LSU22639, Dysith_mental_LSU66338, Dysith_mental_LSU26463, Dysith_mental_LSU69289, Dysith_mental_LSU48490, Dysith_mental_L33085, Dysith_mental_MZU94637, Dysith_mental_MZU87834
Dysith_mental_MZU87834	Dysith_mental_MZUSP85740, Dysith_mental_LSU2003, Dysith_mental_LSU22639, Dysith_mental_LSU66338, Dysith_mental_LSU26463, Dysith_mental_LSU69439, Dysith_mental_LSU69289, Dysith_mental_LSU48490, Dysith_mental_L33085, Dysith_mental_MZU94637
Dysith_mental_MZU94637	Dysith_mental_MZUSP85740, Dysith_mental_LSU2003, Dysith_mental_LSU22639, Dysith_mental_LSU66338, Dysith_mental_LSU26463, Dysith_mental_LSU69439, Dysith_mental_LSU69289, Dysith_mental_LSU48490, Dysith_mental_L33085, Dysith_mental_MZU87834
Dysith_mental_MZUSP85740	Dysith_mental_LSU2003, Dysith_mental_LSU22639, Dysith_mental_LSU66338, Dysith_mental_LSU26463, Dysith_mental_LSU69439, Dysith_mental_LSU69289, Dysith_mental_LSU48490, Dysith_mental_L33085, Dysith_mental_MZU94637, Dysith_mental_MZU87834
Dysith_occlis_H4028	Dysith_occlis_LSU33931, Dysith_occlis_LSU44189
Dysith_occlis_LSU33931	Dysith_occlis_LSU44189, Dysith_occlis_H4028
Dysith_occlis_LSU44189	Dysith_occlis_LSU33931, Dysith_occlis_H4028
Elaen_dayi_A4751	Elaen_flavter_L6792
Elaen_flavter_L6792	Elaen_dayi_A4751
Elaen_paltan_K3955	Elaen_paltan_A4855
Empinax_atrcep_L28310	Empinax_diffi_A15581
Empinax_diffi_A15581	Empinax_atrcep_L28310
Empinax_hammo_L47262	Empinax_hammo_LSU19434

Empinax_hammo_LSU19434	Empinax_hammo_L47262
Empinax_trail_LSU141724	Empinax_trail_MCZ337725
Epinec_leulma_LSUMZ18242	Epinec_eryura_ANSP16560
Epinec_ornata_LSU74213	Epinec_ornata_LSU78113
Epinec_ornata_LSU78113	Epinec_ornata_LSU74213
Euryla_steer_K19050	Euryla_steer_K19186
Formvor_grisea_COPIC1436	Formvor_grisea_K1215ok, Formvor_grisea_FMNH394490, Formvor_grisea_COPML771, Formvor_grisea_LSU46513, Formvor_grisea_COPML659, Formvor_grisea_COPYPL49, Formvor_grisea_L15217, Formvor_grisea_ICN36199, Formvor_grisea_ICN38217, Formvor_grisea_MCP3156, Formvor_grisea_ICN37055, Formvor_grisea_ICNAMC1366
Formvor_grisea_COPML659	Formvor_grisea_K1215ok, Formvor_grisea_FMNH394490, Formvor_grisea_COPML771, Formvor_grisea_LSU46513, Formvor_grisea_COPIC1436, Formvor_grisea_COPYPL49, Formvor_grisea_L15217, Formvor_grisea_ICN36199, Formvor_grisea_ICN38217, Formvor_grisea_MCP3156, Formvor_grisea_ICN37055, Formvor_grisea_ICNAMC1366
Formvor_grisea_COPML771	Formvor_grisea_K1215ok, Formvor_grisea_FMNH394490, Formvor_grisea_LSU46513, Formvor_grisea_COPML659, Formvor_grisea_COPIC1436, Formvor_grisea_COPYPL49, Formvor_grisea_L15217, Formvor_grisea_ICN36199, Formvor_grisea_ICN38217, Formvor_grisea_MCP3156, Formvor_grisea_ICN37055, Formvor_grisea_ICNAMC1366
Formvor_grisea_COPYPL49	Formvor_grisea_K1215ok, Formvor_grisea_FMNH394490, Formvor_grisea_COPML771, Formvor_grisea_LSU46513, Formvor_grisea_COPML659, Formvor_grisea_COPIC1436, Formvor_grisea_L15217, Formvor_grisea_ICN36199, Formvor_grisea_ICN38217, Formvor_grisea_MCP3156, Formvor_grisea_ICN37055, Formvor_grisea_ICNAMC1366
Formvor_grisea_FMNH394490	Formvor_grisea_K1215ok, Formvor_grisea_COPML771, Formvor_grisea_LSU46513, Formvor_grisea_COPML659, Formvor_grisea_COPIC1436, Formvor_grisea_COPYPL49, Formvor_grisea_L15217, Formvor_grisea_ICN36199, Formvor_grisea_ICN38217, Formvor_grisea_MCP3156, Formvor_grisea_ICN37055, Formvor_grisea_ICNAMC1366

Formvor_grisea_ICN36199	Formvor_grisea_K1215ok, Formvor_grisea_FMNH394490, Formvor_grisea_COPML771, Formvor_grisea_LSU46513, Formvor_grisea_COPML659, Formvor_grisea_COPIC1436, Formvor_grisea_COPYPL49, Formvor_grisea_L15217, Formvor_grisea_ICN38217, Formvor_grisea_MCP3156, Formvor_grisea_ICN37055, Formvor_grisea_ICNAMC1366
Formvor_grisea_ICN37055	Formvor_grisea_K1215ok, Formvor_grisea_FMNH394490, Formvor_grisea_COPML771, Formvor_grisea_LSU46513, Formvor_grisea_COPML659, Formvor_grisea_COPIC1436, Formvor_grisea_COPYPL49, Formvor_grisea_L15217, Formvor_grisea_ICN36199, Formvor_grisea_ICN38217, Formvor_grisea_MCP3156, Formvor_grisea_ICNAMC1366
Formvor_grisea_ICN38217	Formvor_grisea_K1215ok, Formvor_grisea_FMNH394490, Formvor_grisea_COPML771, Formvor_grisea_LSU46513, Formvor_grisea_COPML659, Formvor_grisea_COPIC1436, Formvor_grisea_COPYPL49, Formvor_grisea_L15217, Formvor_grisea_ICN36199, Formvor_grisea_MCP3156, Formvor_grisea_ICN37055, Formvor_grisea_ICNAMC1366
Formvor_grisea_ICNAMC1366	Formvor_grisea_K1215ok, Formvor_grisea_FMNH394490, Formvor_grisea_COPML771, Formvor_grisea_LSU46513, Formvor_grisea_COPML659, Formvor_grisea_COPIC1436, Formvor_grisea_COPYPL49, Formvor_grisea_L15217, Formvor_grisea_ICN36199, Formvor_grisea_ICN38217, Formvor_grisea_MCP3156, Formvor_grisea_ICN37055
Formvor_grisea_L15217	Formvor_grisea_K1215ok, Formvor_grisea_FMNH394490, Formvor_grisea_COPML771, Formvor_grisea_LSU46513, Formvor_grisea_COPML659, Formvor_grisea_COPIC1436, Formvor_grisea_COPYPL49, Formvor_grisea_ICN36199, Formvor_grisea_ICN38217, Formvor_grisea_MCP3156, Formvor_grisea_ICN37055, Formvor_grisea_ICNAMC1366

Formvor_grisea_LSU46513	Formvor_grisea_K1215ok, Formvor_grisea_FMNH394490, Formvor_grisea_COPML771, Formvor_grisea_COPML659, Formvor_grisea_COPIC1436, Formvor_grisea_COPYPL49, Formvor_grisea_L15217, Formvor_grisea_ICN36199, Formvor_grisea_ICN38217, Formvor_grisea_MCP3156, Formvor_grisea_ICN37055, Formvor_grisea_ICNAMC1366
Formvor_grisea_MCP3156	Formvor_grisea_K1215ok, Formvor_grisea_FMNH394490, Formvor_grisea_COPML771, Formvor_grisea_LSU46513, Formvor_grisea_COPML659, Formvor_grisea_COPIC1436, Formvor_grisea_COPYPL49, Formvor_grisea_L15217, Formvor_grisea_ICN36199, Formvor_grisea_ICN38217, Formvor_grisea_ICN37055, Formvor_grisea_ICNAMC1366
Formvor_litto_MCPRBL141	Formvor_litto_NC43
Formvor_litto_NC43	Formvor_litto_MCPRBL141
Formvor_melgas_FMNH392854	Formvor_melgas_LSU6675
Formvor_melgas_LSU6675	Formvor_melgas_FMNH392854
Formvor_rufa_FMNH392619	Formvor_rufa_K3561, Formvor_rufa_KU18778
Formvor_rufa_K3561	Formvor_rufa_KU18778, Formvor_rufa_FMNH392619
Formvor_rufa_KU18778	Formvor_rufa_K3561, Formvor_rufa_FMNH392619
Formvor_serra_MCPRBL184	Formvor_serra_MZUSP85432
Formvor_serra_MZUSP85432	Formvor_serra_MCPRBL184
Freder_undul_LSU4826	Freder_undul_MZUSPJ282
Freder_undul_MZUSPJ282	Freder_undul_LSU4826
Gralria_quit_H2523	Gralria_quit_LSUMZ104492
Gralula_ferpec_LSUMZ8056	Gralula_linfro_IC33814
Gralula_linfro_IC33814	Gralula_ferpec_LSUMZ8056
Haffer_immlata_Ph208	Haffer_immlata_H92
Heliob_conta_F389197	Heliob_conta_MZU82580
Heliob_conta_MZU82580	Heliob_conta_F389197
Hellma_gular_L32238	Hellma_gular_L3515
Hemit_graden_L32603	Hemit_graden_LSUMZ109001
Hemit_inotus_L3847	Hemit_inotus_YPM101772
Hemit_inotus_YPM101772	Hemit_inotus_L3847
Herpsi_axill_LSU33661	Herpsi_axill_LSU58398
Herpsi_axill_LSU58398	Herpsi_axill_LSU33661
Herpsi_ruftus_KU3776	Herpsi_ruftus_LSU78137, Herpsi_ruftus_LSU2200, Herpsi_ruftus_MZU94326

Herpsi_ruftus_LSU2200	Herpsi_ruftus_LSU78137, Herpsi_ruftus_KU3776, Herpsi_ruftus_MZU94326
Herpsi_ruftus_LSU78137	Herpsi_ruftus_KU3776, Herpsi_ruftus_LSU2200, Herpsi_ruftus_MZU94326
Herpsi_ruftus_MZU94326	Herpsi_ruftus_LSU78137, Herpsi_ruftus_KU3776, Herpsi_ruftus_LSU2200
Herpsi_selowi_CP3140	Herpsi_selowi_SP83298, Herpsi_selowi_UFP4917
Herpsi_selowi_UFP4917	Herpsi_selowi_SP83298, Herpsi_selowi_CP3140
Heteroc_autiivert_L42512	Heteroc_autiivert_LAlvarez
Heteroc_autiivert_LAlvarez	Heteroc_autiivert_L42512
Hirund_fernea_SB10509	Hirund_fernea_Y101003
Hirund_fernea_Y101003	Hirund_fernea_SB10509
Hypleu_gutus_MCP3130	Hypleu_gutus_WDHB1805
Hypleu_gutus_WDHB1805	Hypleu_gutus_MCP3130
Hypmis_hypxan_LSU10573	Hypmis_hypxan_LSU42673, Hypmis_hypxan_MZUSP92826, Hypmis_hypxan_LSU7074, Hypmis_hypxan_LSU35402, Hypmis_hypxan_MZUSP92436
Hypmis_hypxan_LSU35402	Hypmis_hypxan_LSU42673, Hypmis_hypxan_MZUSP92826, Hypmis_hypxan_LSU7074, Hypmis_hypxan_LSU10573, Hypmis_hypxan_MZUSP92436
Hypmis_hypxan_LSU42673	Hypmis_hypxan_MZUSP92826, Hypmis_hypxan_LSU7074, Hypmis_hypxan_LSU10573, Hypmis_hypxan_LSU35402, Hypmis_hypxan_MZUSP92436
Hypmis_hypxan_LSU7074	Hypmis_hypxan_LSU42673, Hypmis_hypxan_MZUSP92826, Hypmis_hypxan_LSU10573, Hypmis_hypxan_LSU35402, Hypmis_hypxan_MZUSP92436
Hypmis_hypxan_MZUSP92436	Hypmis_hypxan_LSU42673, Hypmis_hypxan_MZUSP92826, Hypmis_hypxan_LSU7074, Hypmis_hypxan_LSU10573, Hypmis_hypxan_LSU35402
Hypmis_hypxan_MZUSP92826	Hypmis_hypxan_LSU42673, Hypmis_hypxan_LSU7074, Hypmis_hypxan_LSU10573, Hypmis_hypxan_LSU35402, Hypmis_hypxan_MZUSP92436
Inezia_inoata_L37759	Inezia_tentri_IC26451
Inezia_tentri_IC26451	Inezia_inoata_L37759
Iodop_fusca_S626253	Iodop_pipra_SP50046, Iodop_pipra_SP70511, Iodop_isalae_L9597
Iodop_isalae_L9597	Iodop_pipra_SP50046, Iodop_pipra_SP70511, Iodop_fusca_S626253
Iodop_pipra_SP50046	Iodop_pipra_SP70511, Iodop_fusca_S626253, Iodop_isalae_L9597, Iodop_pipra_SP70511

Isleri_hauxw_LSU4270	Isleri_hauxw_MZU83855, Isleri_hauxw_MZU86503, Isleri_hauxw_MZU92884
Isleri_hauxw_MZU83855	Isleri_hauxw_LSU4270, Isleri_hauxw_MZU86503, Isleri_hauxw_MZU92884
Isleri_hauxw_MZU86503	Isleri_hauxw_LSU4270, Isleri_hauxw_MZU83855, Isleri_hauxw_MZU92884
Isleri_hauxw_MZU92884	Isleri_hauxw_LSU4270, Isleri_hauxw_MZU83855, Isleri_hauxw_MZU86503
Knipo_hudso_L18865	Knipo_hudso_L19103
Knipo_hudso_L19103	Knipo_hudso_L18865
Lepthr_coeru_L1985	Lepthr_isirei_IC35523
Lepthr_isirei_IC35523	Lepthr_coeru_L1985
Lepthr_vilasi_G59269	Lepthr_vilasi_G59270
Lepthr_vilasi_G59270	Lepthr_vilasi_G59269
Lipau_fuscin_H5187	Lipau_fuscin_IC33464
Lipau_fuscin_IC33464	Lipau_fuscin_H5187
Lipau_unifus_L11747	Lipau_unifus_L72146
Lipau_unifus_L72146	Lipau_unifus_L11747
Lipau_urolis_L58450	Lipau_urolis_SM24135
Lipau_urolis_SM24135	Lipau_urolis_L58450
Lipau_vocran_L3149	Lipau_vocran_GUNA27
Lipau_weberi_H2080	Lipau_weberi_H4853
Lipau_weberi_H4853	Lipau_weberi_H2080
Lophot_piltus_H1935	Lophot_piltus_L44510
Lophot_piltus_L44510	Lophot_piltus_H1935
Lophot_vitsus_A18368	Oncost_cingul_K1962
Melan_maxlia_K3240	Melan_maxlia_L68147
Melan_maxlia_L68147	Melan_elega_P18505, Melan_maxlia_K3240
Merula_ater_MZUBOR1401	Merula_ater_MZUBOR1439
Merula_ater_MZUBOR1439	Merula_ater_MZUBOR1401
Mionec_macco_A4812	Mionec_oleag_L71895
Mionec_oleag_L71895	Mionec_macco_A4812
Musaxi_albfro_LSU22576	Musaxi_albfro_L61400
Muspip_vetula_A315092	Muspip_vetula_MZUBOR1433, Muspip_vetula_MZUBOR1434
Muspip_vetula_MZUBOR1433	Muspip_vetula_MZUBOR1434, Muspip_vetula_A315092, Muspip_vetula_MZUBOR1434
Muspip_vetula_MZUBOR1434	Muspip_vetula_A315092, Muspip_vetula_MZUBOR1433, Muspip_vetula_MZUBOR1433
Myiar_phalus_SB28498	Myiar_swaoni_A6077
Myiar_swaoni_A6077	Myiar_phalus_SB28498
Myiar_tuber_LSUMZ15135	Myiar_tuber_MPEGBR163112

Myiar_tuber_MPEGBR163112	Myiar_tuber_LSUMZ15135
Myiopag_cotta_LSUMZ143820	Myiopag_virata_K1914, Myiopag_virata_LSU18455, Myiopag_virata_K1914, Myiopag_virata_LSU18455
Myiopho_flavns_L33885	Myiopho_rormae_A12334
Myiopho_rormae_A12334	Myiopho_flavns_L33885
Myiorn_albtri_L58401	Myiorn_albtri_LSU40633
Myiorn_albtri_LSU40633	Myiorn_albtri_L58401
Myiorn_spnov_MZUCAX01	Myiorn_spnov_MZUMAPI19
Myiorn_spnov_MZUMAPI19	Myiorn_spnov_MZUCAX01
Myiotri_orntus_H4556	Myiotri_orntus_L43994
Myiotri_orntus_L43994	Myiotri_orntus_H4556
Myioze_caysis_GCN983	Myioze_caysis_L9221
Myioze_caysis_L9221	Myioze_caysis_GCN983
Myrbor_myorin_A8837	Myrbor_myorin_LSU907, Myrbor_myorin_MPEG9511, Myrbor_myorin_MPEG390
Myrbor_myorin_LSU907	Myrbor_myorin_MPEG9511, Myrbor_myorin_A8837, Myrbor_myorin_MPEG390
Myrbor_myorin_MPEG390	Myrbor_myorin_LSU907, Myrbor_myorin_MPEG9511, Myrbor_myorin_A8837
Myrbor_myorin_MPEG9511	Myrbor_myorin_LSU907, Myrbor_myorin_A8837, Myrbor_myorin_MPEG390
Myrrul_axill_KU629	Myrrul_axill_L55209, Myrrul_axill_USNM1824, Myrrul_axill_KU772
Myrrul_axill_KU772	Myrrul_axill_L55209, Myrrul_axill_KU629, Myrrul_axill_USNM1824
Myrrul_axill_L55209	Myrrul_axill_KU629, Myrrul_axill_USNM1824, Myrrul_axill_KU772
Myrrul_axill_USNM1824	Myrrul_axill_L55209, Myrrul_axill_KU629, Myrrul_axill_KU772
Myrrul_ignota_LSU4098	Myrrul_ignota_LSU46586
Myrrul_ignota_LSU46586	Myrrul_ignota_LSU4098
Myrrul_iheri_LSU21213	Myrrul_iheri_MZU96715, Myrrul_iheri_MZU96271
Myrrul_iheri_MZU96271	Myrrul_iheri_LSU21213, Myrrul_iheri_MZU96715
Myrrul_iheri_MZU96715	Myrrul_iheri_LSU21213, Myrrul_iheri_MZU96271
Neocta_niger_L2749	Clytoc_ali_A133422
Neopip_cinmom_L42825	Calytur_criata_A494720, Calytur_criata_A4379, Calytur_criata_A494721
Neoxol_ruftri_L70016	Neoxol_ruftri_LSU14025, Neoxol_ruftri_LSU14025
Neoxol_ruftri_LSU14025	Neoxol_ruftri_L70016
Nesotr_ridway_F299961	Phaeo_murina_L90440, Phaeo_murina_L48589
Ochoec_diade_H1821	Ochoec_pullla_A7059
Ochoec_pullla_A7059	Ochoec_diade_H1821
Ochrhy_rufdus_L103908	Ochrhy_rufdus_LSU61481

Ochrhy_rufdus_LSU61481	Ochrhy_rufdus_L103908
Oncost_cingul_K1962	Lophot_vitsus_A18368
Oncost_olieum_L2222	Oncost_olieum_L26945
Oncost_olieum_L26945	Oncost_olieum_L2222
Oxyrun_critus_H4846	Oxyrun_critus_L40549, Oxyrun_critus_Y139814, Oxyrun_critus_L5568, Oxyrun_critus_SP88522, Oxyrun_critus_L2080, Oxyrun_critus_Y139410
Oxyrun_critus_L2080	Oxyrun_critus_L40549, Oxyrun_critus_Y139814, Oxyrun_critus_H4846, Oxyrun_critus_L5568, Oxyrun_critus_SP88522, Oxyrun_critus_Y139410
Oxyrun_critus_L40549	Oxyrun_critus_Y139814, Oxyrun_critus_H4846, Oxyrun_critus_L5568, Oxyrun_critus_SP88522, Oxyrun_critus_L2080, Oxyrun_critus_Y139410
Oxyrun_critus_L5568	Oxyrun_critus_L40549, Oxyrun_critus_Y139814, Oxyrun_critus_H4846, Oxyrun_critus_SP88522, Oxyrun_critus_L2080, Oxyrun_critus_Y139410
Oxyrun_critus_SP88522	Oxyrun_critus_L40549, Oxyrun_critus_Y139814, Oxyrun_critus_H4846, Oxyrun_critus_L5568, Oxyrun_critus_L2080, Oxyrun_critus_Y139410
Oxyrun_critus_Y139410	Oxyrun_critus_L40549, Oxyrun_critus_Y139814, Oxyrun_critus_H4846, Oxyrun_critus_L5568, Oxyrun_critus_SP88522, Oxyrun_critus_L2080
Oxyrun_critus_Y139814	Oxyrun_critus_L40549, Oxyrun_critus_H4846, Oxyrun_critus_L5568, Oxyrun_critus_SP88522, Oxyrun_critus_L2080, Oxyrun_critus_Y139410
Passer_L52749	Corvus_coride_A17778
Percno_arena_LSU42797	Percno_arena_LSUK162
Percno_arena_LSUK162	Percno_arena_LSU42797
Percno_rufons_L55295	Percno_rufons_MPEGJAP144, Percno_rufons_LSU7011
Percno_rufons_LSU7011	Percno_rufons_L55295, Percno_rufons_MPEGJAP144
Percno_rufons_MPEGJAP144	Percno_rufons_L55295, Percno_rufons_LSU7011
Phace_macpec_K9737	Phace_macpec_L84423
Phace_macpec_L84423	Phace_macpec_K9737
Phaeo_murina_L48589	Phaeo_murina_L90440, Nesotr_ridway_F299961, Phaeo_murina_L90440
Phaeo_murina_L90440	Phaeo_murina_L48589, Nesotr_ridway_F299961, Phaeo_murina_L48589
Physca_exius_K3613	Physca_lanoni_IC31805, Physca_lanoni_IC32557
Physca_flavren_USNM525978	Physca_vircen_SB11750, Physca_venlis_SB20729
Physca_lanoni_IC31805	Physca_lanoni_IC32557, Physca_lanoni_IC32557, Physca_exius_K3613
Physca_lanoni_IC32557	Physca_lanoni_IC31805, Physca_exius_K3613, Physca_lanoni_IC31805
Physca_venlis_SB20729	Physca_vircen_SB11750, Physca_flavren_USNM525978

Physca_vircen_SB11750	Physca_venlis_SB20729, Physca_flavren_USNM525978
Phytot_raidii_L451	Phytot_raidii_LSU448
Phytot_raidii_LSU448	Phytot_raidii_L451
Pitta_angol_F396328	Pitta_reiowi_AMNH296892
Pitta_bracura_A778678	Pitta_molcen_K23289, Pitta_nympha_AMNH447700, Pitta_sorida_K14471
Pitta_caelea_A11090	Pitta_cyane_K31228, Pitta_schder_USNM264502, Pitta_niplen_A463316, Pitta_caelea_WFVZ38385
Pitta_caelea_WFVZ38385	Pitta_niplen_A463316, Pitta_caelea_A11090
Pitta_cyane_K31228	Pitta_caelea_A11090, Pitta_schder_USNM264502
Pitta_molcen_DOT17176	Pitta_molcen_K23289
Pitta_molcen_K23289	Pitta_versi_A2371, Pitta_molcen_DOT17176
Pitta_niplen_A463316	Pitta_caelea_A11090, Pitta_caelea_WFVZ38385
Pitta_oat_A2636	Pitta_soror_K23304
Pitta_reiowi_AMNH296892	Pitta_angol_F396328
Pitta_sorida_K14471	Pitta_bracura_A778678
Pitta_soror_K23304	Pitta_oat_A2636
Pitta_versi_A2371	Pitta_molcen_K23289
Poeci_senex_L1987B	Poeci_senex_L86191
Poeci_senex_L86191	Poeci_senex_L1987B
Polioc_exsul_L41655	Polioc_exsul_L72003
Polioc_exsul_L72003	Polioc_exsul_L41655
Polyst_peclis_L38120	Polyst_peclis_YPM137548
Polyst_peclis_YPM137548	Polyst_peclis_L38120
Psaris_dalsia_K25407	Pseutom_graueri_F311050, Pseutom_graueri_A764296, Corydo_sumnus_L77291
Pseucol_dinel_A270377	Pseucol_scleri_L38161
Pseucol_scleri_L38161	Pseucol_dinel_A270377
Pseutom_graueri_A764296	Pseutom_graueri_F311050, Corydo_sumnus_L77291, Psaris_dalsia_K25407, Pseutom_graueri_F311050
Pseutom_graueri_F311050	Pseutom_graueri_A764296, Pseutom_graueri_A764296, Corydo_sumnus_L77291, Psaris_dalsia_K25407
Psilor_gutus_A796861	Psilor_gutus_LGE2403, Psilor_gutus_LGE2991
Psilor_gutus_LGE2403	Psilor_gutus_LGE2991, Psilor_gutus_A796861, Psilor_gutus_LGE2991
Psilor_gutus_LGE2991	Psilor_gutus_A796861, Psilor_gutus_LGE2403, Psilor_gutus_LGE2403
Pyrigl_leunot_ANSP18393	Pyrigl_leunot_LSU66339, Pyrigl_leunot_LSU66203, Pyrigl_leunot_LSU31392
Pyrigl_leunot_LSU31392	Pyrigl_leunot_ANSP18393, Pyrigl_leunot_LSU66339, Pyrigl_leunot_LSU66203
Pyrigl_leunot_LSU66203	Pyrigl_leunot_ANSP18393, Pyrigl_leunot_LSU66339, Pyrigl_leunot_LSU31392

Pyrigl_leunot_LSU66339	Pyrigl_leunot_ANSP18393, Pyrigl_leunot_LSU66203, Pyrigl_leunot_LSU31392
Pyrode_scutus_L44166	Pyrode_scutus_SP93046
Pyrode_scutus_SP93046	Pyrode_scutus_L44166
Pyrrho_cinmeus_AMNH388114	Pyrrho_cinmeus_L8072
Pyrrho_cinmeus_L8072	Pyrrho_cinmeus_AMNH388114
Sakerus_canad_K5831	Sakerus_canad_MZU93732, Sakerus_canad_MZU77973
Sakerus_canad_MZU77973	Sakerus_canad_K5831, Sakerus_canad_MZU93732
Sakerus_canad_MZU93732	Sakerus_canad_K5831, Sakerus_canad_MZU77973
Sakerus_luctu_MZU90015	Sakerus_luctu_MZU92813
Sakerus_luctu_MZU92813	Sakerus_luctu_MZU90015
Schiff_turdi_GBR16313	Schiff_turdi_SP91512
Schiff_turdi_SP91512	Schiff_turdi_GBR16313
Scler_mexic_L35770	Scler_mexic_UWB105935
Scler_mexic_UWB105935	Scler_mexic_L35770
Scyta_altir_L43814	Scyta_altir_L7677
Scyta_altir_L7677	Scyta_altir_L43814
Scyta_partri_L1281	Scyta_partri_L8184
Scyta_partri_L8184	Scyta_partri_L1281
Sipia_berle_LSU12026	Sipia_berle_LSU29981
Sipia_berle_LSU29981	Sipia_berle_LSU12026
Siptor_strcol_H7493	Siptor_strcol_L6202
Siptor_strcol_L6202	Siptor_strcol_H7493
Stigma_bud_FMN392923	Stigma_bud_L31591
Stigma_bud_L31591	Stigma_bud_FMN392923
Syna_albes_K3064	Syna_zimme_L44781
Syna_scuata_L58410	Syna_scuata_MZU94627
Syna_scuata_MZU94627	Syna_scuata_L58410
Syna_uniufa_H23	Syna_uniufa_H8472, Syna_uniufa_L8403
Syna_uniufa_H8472	Syna_uniufa_H23, Syna_uniufa_L8403
Syna_uniufa_L8403	Syna_uniufa_H8472, Syna_uniufa_H23
Syna_zimme_L44781	Syna_albes_K3064
Taraba_major_L12814	Taraba_major_LSU60855, Taraba_major_LSU10797, Taraba_major_LSU52941, Taraba_major_LSU66728, Taraba_major_MZU94636, Taraba_major_MZUJ1128
Taraba_major_LSU10797	Taraba_major_L12814, Taraba_major_LSU60855, Taraba_major_LSU52941, Taraba_major_LSU66728, Taraba_major_MZU94636, Taraba_major_MZUJ1128
Taraba_major_LSU52941	Taraba_major_L12814, Taraba_major_LSU60855, Taraba_major_LSU10797, Taraba_major_LSU66728, Taraba_major_MZU94636, Taraba_major_MZUJ1128

Taraba_major_LSU60855	Taraba_major_L12814, Taraba_major_LSU10797, Taraba_major_LSU52941, Taraba_major_LSU66728, Taraba_major_MZU94636, Taraba_major_MZUJ1128
Taraba_major_LSU66728	Taraba_major_L12814, Taraba_major_LSU60855, Taraba_major_LSU10797, Taraba_major_LSU52941, Taraba_major_MZU94636, Taraba_major_MZUJ1128
Taraba_major_MZU94636	Taraba_major_L12814, Taraba_major_LSU60855, Taraba_major_LSU10797, Taraba_major_LSU52941, Taraba_major_LSU66728, Taraba_major_MZUJ1128
Taraba_major_MZUJ1128	Taraba_major_L12814, Taraba_major_LSU60855, Taraba_major_LSU10797, Taraba_major_LSU52941, Taraba_major_LSU66728, Taraba_major_MZU94636
Tereno_eryrus_SB09133	Tereno_eryrus_W105709
Tereno_eryrus_W105709	Tereno_eryrus_SB09133
Thamman_ardcus_L6896	Thamman_ardcus_MZU92005
Thamman_ardcus_MZU92005	Thamman_ardcus_L6896
Thamman_caesi_MZU92757	Thamman_caesi_SP91353, Thamman_caesi_MZU93855, Thamman_caesi_MZUJ867
Thamman_caesi_MZU93855	Thamman_caesi_SP91353, Thamman_caesi_MZU92757, Thamman_caesi_MZUJ867
Thamman_caesi_MZUJ867	Thamman_caesi_SP91353, Thamman_caesi_MZU93855, Thamman_caesi_MZU92757
Thamman_caesi_SP91353	Thamman_caesi_MZU93855, Thamman_caesi_MZU92757, Thamman_caesi_MZUJ867
Thamman_satnus_LSU4600	Thamman_satnus_MZU92763
Thamman_satnus_MZU92763	Thamman_satnus_LSU4600
Thamman_schnus_LSU76233	Thamman_schnus_LSU992
Thamman_schnus_LSU992	Thamman_schnus_LSU76233
Thamphil_aethi_MZU81269	Thamphil_aethi_MZUJ1799, Thamphil_aethi_MZU95391, Thamphil_aethi_MZU93741, Thamphil_aethi_MZU85797
Thamphil_aethi_MZU85797	Thamphil_aethi_MZUJ1799, Thamphil_aethi_MZU95391, Thamphil_aethi_MZU93741, Thamphil_aethi_MZU81269
Thamphil_aethi_MZU93741	Thamphil_aethi_MZUJ1799, Thamphil_aethi_MZU95391, Thamphil_aethi_MZU85797, Thamphil_aethi_MZU81269
Thamphil_aethi_MZU95391	Thamphil_aethi_MZUJ1799, Thamphil_aethi_MZU93741, Thamphil_aethi_MZU85797, Thamphil_aethi_MZU81269
Thamphil_aethi_MZUJ1799	Thamphil_aethi_MZU95391, Thamphil_aethi_MZU93741, Thamphil_aethi_MZU85797, Thamphil_aethi_MZU81269
Thamphil_amacus_MZU81272	Thamphil_amacus_MZU90063, Thamphil_amacus_MZU93755, Thamphil_amacus_MZU88911
Thamphil_amacus_MZU88911	Thamphil_amacus_MZU90063, Thamphil_amacus_MZU93755, Thamphil_amacus_MZU81272

Thamphil_amacus_MZU90063	Thamphil_amacus_MZU93755, Thamphil_amacus_MZU88911, Thamphil_amacus_MZU81272
Thamphil_amacus_MZU93755	Thamphil_amacus_MZU90063, Thamphil_amacus_MZU88911, Thamphil_amacus_MZU81272
Thamphil_ambus_MZU86040	Thamphil_ambus_MZU91378
Thamphil_ambus_MZU91378	Thamphil_ambus_MZU86040
Thamphil_berna_LSU45997	Thamphil_berna_L5136
Thamphil_caecen_LSU1684	Thamphil_caecen_LSU38284, Thamphil_caecen_LSU34687, Thamphil_caecen_LSU38384, Thamphil_caecen_LSU50102, Thamphil_caecen_MZU81155, Thamphil_caecen_MZU91197
Thamphil_caecen_LSU34687	Thamphil_caecen_LSU38284, Thamphil_caecen_LSU1684, Thamphil_caecen_LSU38384, Thamphil_caecen_LSU50102, Thamphil_caecen_MZU81155, Thamphil_caecen_MZU91197
Thamphil_caecen_LSU38284	Thamphil_caecen_LSU34687, Thamphil_caecen_LSU1684, Thamphil_caecen_LSU38384, Thamphil_caecen_LSU50102, Thamphil_caecen_MZU81155, Thamphil_caecen_MZU91197
Thamphil_caecen_LSU38384	Thamphil_caecen_LSU38284, Thamphil_caecen_LSU34687, Thamphil_caecen_LSU1684, Thamphil_caecen_LSU50102, Thamphil_caecen_MZU81155, Thamphil_caecen_MZU91197
Thamphil_caecen_LSU50102	Thamphil_caecen_LSU38284, Thamphil_caecen_LSU34687, Thamphil_caecen_LSU1684, Thamphil_caecen_LSU38384, Thamphil_caecen_MZU81155, Thamphil_caecen_MZU91197
Thamphil_caecen_MZU81155	Thamphil_caecen_LSU38284, Thamphil_caecen_LSU34687, Thamphil_caecen_LSU1684, Thamphil_caecen_LSU38384, Thamphil_caecen_LSU50102, Thamphil_caecen_MZU91197

Thamphil_caecen_MZU91197	Thamphil_caecen_LSU38284, Thamphil_caecen_LSU34687, Thamphil_caecen_LSU1684, Thamphil_caecen_LSU38384, Thamphil_caecen_LSU50102, Thamphil_caecen_MZU81155
Thamphil_dolia_L48534	Thamphil_dolia_LSU38980, Thamphil_dolia_LSU14854, Thamphil_dolia_LSU69823, Thamphil_dolia_LSU82201, Thamphil_dolia_MCP3129, Thamphil_dolia_LSU46527, Thamphil_dolia_LSU46645, Thamphil_dolia_LSU81964, Thamphil_dolia_LSU46193, Thamphil_dolia_MZU90071
Thamphil_dolia_LSU14854	Thamphil_dolia_L48534, Thamphil_dolia_LSU38980, Thamphil_dolia_LSU69823, Thamphil_dolia_LSU82201, Thamphil_dolia_MCP3129, Thamphil_dolia_LSU46527, Thamphil_dolia_LSU46645, Thamphil_dolia_LSU81964, Thamphil_dolia_LSU46193, Thamphil_dolia_MZU90071
Thamphil_dolia_LSU38980	Thamphil_dolia_L48534, Thamphil_dolia_LSU14854, Thamphil_dolia_LSU69823, Thamphil_dolia_LSU82201, Thamphil_dolia_MCP3129, Thamphil_dolia_LSU46527, Thamphil_dolia_LSU46645, Thamphil_dolia_LSU81964, Thamphil_dolia_LSU46193, Thamphil_dolia_MZU90071
Thamphil_dolia_LSU46193	Thamphil_dolia_L48534, Thamphil_dolia_LSU38980, Thamphil_dolia_LSU14854, Thamphil_dolia_LSU69823, Thamphil_dolia_LSU82201, Thamphil_dolia_MCP3129, Thamphil_dolia_LSU46527, Thamphil_dolia_LSU46645, Thamphil_dolia_LSU81964, Thamphil_dolia_MZU90071
Thamphil_dolia_LSU46527	Thamphil_dolia_L48534, Thamphil_dolia_LSU38980, Thamphil_dolia_LSU14854, Thamphil_dolia_LSU69823, Thamphil_dolia_LSU82201, Thamphil_dolia_MCP3129, Thamphil_dolia_LSU46645, Thamphil_dolia_LSU81964, Thamphil_dolia_LSU46193, Thamphil_dolia_MZU90071
Thamphil_dolia_LSU46645	Thamphil_dolia_L48534, Thamphil_dolia_LSU38980, Thamphil_dolia_LSU14854, Thamphil_dolia_LSU69823, Thamphil_dolia_LSU82201, Thamphil_dolia_MCP3129, Thamphil_dolia_LSU46527, Thamphil_dolia_LSU81964, Thamphil_dolia_LSU46193, Thamphil_dolia_MZU90071
Thamphil_dolia_LSU69823	Thamphil_dolia_L48534, Thamphil_dolia_LSU38980, Thamphil_dolia_LSU14854, Thamphil_dolia_LSU82201, Thamphil_dolia_MCP3129, Thamphil_dolia_LSU46527, Thamphil_dolia_LSU46645, Thamphil_dolia_LSU81964, Thamphil_dolia_LSU46193, Thamphil_dolia_MZU90071
Thamphil_dolia_LSU81964	Thamphil_dolia_L48534, Thamphil_dolia_LSU38980, Thamphil_dolia_LSU14854, Thamphil_dolia_LSU69823, Thamphil_dolia_LSU82201, Thamphil_dolia_MCP3129, Thamphil_dolia_LSU46527, Thamphil_dolia_LSU46645, Thamphil_dolia_LSU46193, Thamphil_dolia_MZU90071

Thamphil_dolia_LSU82201	Thamphil_dolia_L48534, Thamphil_dolia_LSU38980, Thamphil_dolia_LSU14854, Thamphil_dolia_LSU69823, Thamphil_dolia_MCP3129, Thamphil_dolia_LSU46527, Thamphil_dolia_LSU46645, Thamphil_dolia_LSU81964, Thamphil_dolia_LSU46193, Thamphil_dolia_MZU90071
Thamphil_dolia_MCP3129	Thamphil_dolia_L48534, Thamphil_dolia_LSU38980, Thamphil_dolia_LSU14854, Thamphil_dolia_LSU69823, Thamphil_dolia_LSU82201, Thamphil_dolia_LSU46527, Thamphil_dolia_LSU46645, Thamphil_dolia_LSU81964, Thamphil_dolia_LSU46193, Thamphil_dolia_MZU90071
Thamphil_dolia_MZU90071	Thamphil_dolia_L48534, Thamphil_dolia_LSU38980, Thamphil_dolia_LSU14854, Thamphil_dolia_LSU69823, Thamphil_dolia_LSU82201, Thamphil_dolia_MCP3129, Thamphil_dolia_LSU46527, Thamphil_dolia_LSU46645, Thamphil_dolia_LSU81964, Thamphil_dolia_LSU46193
Thamphil_murnus_MZU85950	Thamphil_murnus_MZU93756, Thamphil_murnus_MZUJ1050
Thamphil_murnus_MZU93756	Thamphil_murnus_MZU85950, Thamphil_murnus_MZUJ1050
Thamphil_murnus_MZUJ1050	Thamphil_murnus_MZU85950, Thamphil_murnus_MZU93756
Thamphil_nigroner_A295	Thamphil_nigroner_LSU20234, Thamphil_nigroner_MZU92841, Thamphil_nigroner_MZU93302, Thamphil_nigroner_OI001
Thamphil_nigroner_LSU20234	Thamphil_nigroner_MZU92841, Thamphil_nigroner_MZU93302, Thamphil_nigroner_A295, Thamphil_nigroner_OI001
Thamphil_nigroner_MZU92841	Thamphil_nigroner_LSU20234, Thamphil_nigroner_MZU93302, Thamphil_nigroner_A295, Thamphil_nigroner_OI001
Thamphil_nigroner_MZU93302	Thamphil_nigroner_LSU20234, Thamphil_nigroner_MZU92841, Thamphil_nigroner_A295, Thamphil_nigroner_OI001
Thamphil_nigroner_OI001	Thamphil_nigroner_LSU20234, Thamphil_nigroner_MZU92841, Thamphil_nigroner_MZU93302, Thamphil_nigroner_A295
Thamphil_paltus_H8245	Thamphil_paltus_LSU58400, Thamphil_paltus_MPEG55411, Thamphil_paltus_KU17412, Thamphil_paltus_MZU90917
Thamphil_paltus_KU17412	Thamphil_paltus_LSU58400, Thamphil_paltus_MPEG55411, Thamphil_paltus_H8245, Thamphil_paltus_MZU90917

Thamphil_paltus_LSU58400	Thamphil_paltus_MPEG55411, Thamphil_paltus_KU17412, Thamphil_paltus_H8245, Thamphil_paltus_MZU90917
Thamphil_paltus_MPEG55411	Thamphil_paltus_LSU58400, Thamphil_paltus_KU17412, Thamphil_paltus_H8245, Thamphil_paltus_MZU90917
Thamphil_paltus_MZU90917	Thamphil_paltus_LSU58400, Thamphil_paltus_MPEG55411, Thamphil_paltus_KU17412, Thamphil_paltus_H8245
Thamphil_pelzel_MPEGURC181	Thamphil_pelzel_MZUSP81730, Thamphil_pelzel_MZUSP81729, Thamphil_pelzel_MZU94631
Thamphil_pelzel_MZU94631	Thamphil_pelzel_MPEGURC181, Thamphil_pelzel_MZUSP81730, Thamphil_pelzel_MZUSP81729
Thamphil_pelzel_MZUSP81729	Thamphil_pelzel_MPEGURC181, Thamphil_pelzel_MZUSP81730, Thamphil_pelzel_MZU94631
Thamphil_pelzel_MZUSP81730	Thamphil_pelzel_MPEGURC181, Thamphil_pelzel_MZUSP81729, Thamphil_pelzel_MZU94631
Thamphil_puntat_L4172	Thamphil_puntat_LSU32837, Thamphil_puntat_LSU44235
Thamphil_puntat_LSU32837	Thamphil_puntat_L4172, Thamphil_puntat_LSU44235
Thamphil_puntat_LSU44235	Thamphil_puntat_L4172, Thamphil_puntat_LSU32837
Thamphil_rufcap_LSU32657	Thamphil_rufcap_MZUSP85427, Thamphil_rufcap_LSU58333, Thamphil_rufcap_LSU38230
Thamphil_rufcap_LSU38230	Thamphil_rufcap_MZUSP85427, Thamphil_rufcap_LSU58333, Thamphil_rufcap_LSU32657
Thamphil_rufcap_LSU58333	Thamphil_rufcap_MZUSP85427, Thamphil_rufcap_LSU38230, Thamphil_rufcap_LSU32657
Thamphil_rufcap_MZUSP85427	Thamphil_rufcap_LSU58333, Thamphil_rufcap_LSU38230, Thamphil_rufcap_LSU32657
Thamphil_scheus_LSU25407	Thamphil_scheus_LSU2724, Thamphil_scheus_MZU92834
Thamphil_scheus_LSU2724	Thamphil_scheus_MZU92834, Thamphil_scheus_LSU25407
Thamphil_scheus_MZU92834	Thamphil_scheus_LSU2724, Thamphil_scheus_LSU25407
Thamphil_stilus_LSU13850	Thamphil_stilus_MZUSP81267, Thamphil_stilus_MZUSP81266
Thamphil_stilus_MZUSP81266	Thamphil_stilus_MZUSP81267, Thamphil_stilus_LSU13850

Thamphil_stilus_MZUSP81267	Thamphil_stilus_MZUSP81266, Thamphil_stilus_LSU13850
Thamphil_stirus_KU2867	Thamphil_stirus_KU2916, Thamphil_stirus_LSU34608, Thamphil_stirus_MZU79317, Thamphil_stirus_MZU79318
Thamphil_stirus_KU2916	Thamphil_stirus_LSU34608, Thamphil_stirus_KU2867, Thamphil_stirus_MZU79317, Thamphil_stirus_MZU79318
Thamphil_stirus_LSU34608	Thamphil_stirus_KU2916, Thamphil_stirus_KU2867, Thamphil_stirus_MZU79317, Thamphil_stirus_MZU79318
Thamphil_stirus_MZU79317	Thamphil_stirus_KU2916, Thamphil_stirus_LSU34608, Thamphil_stirus_KU2867, Thamphil_stirus_MZU79318
Thamphil_stirus_MZU79318	Thamphil_stirus_KU2916, Thamphil_stirus_LSU34608, Thamphil_stirus_KU2867, Thamphil_stirus_MZU79317
Thamphil_unico_H2314	Thamphil_unico_LSU12144
Thamphil_unico_LSU12144	Thamphil_unico_H2314
Thamphil_zarum_LSU191	Thamphil_zarum_LSU67251
Thamphil_zarum_LSU67251	Thamphil_zarum_LSU191
Tityra_inquis_KU3625	Tityra_leucur_MZUSP32688
Todiro_chrcro_L5004	Todiro_cineum_L48285, Todiro_mactum_SB6939, Todiro_pictum_SB14508, Todiro_nigcep_L28763, Todiro_pollum_MPEGSC118, Todiro_virnum_AMNH388115
Todiro_cineum_L48285	Todiro_mactum_SB6939, Todiro_pictum_SB14508, Todiro_nigcep_L28763, Todiro_chrcro_L5004, Todiro_pollum_MPEGSC118, Todiro_virnum_AMNH388115, Todiro_virnum_AMNH388115
Todiro_mactum_SB6939	Todiro_cineum_L48285, Todiro_pictum_SB14508, Todiro_nigcep_L28763, Todiro_chrcro_L5004, Todiro_pollum_MPEGSC118, Todiro_virnum_AMNH388115
Todiro_nigcep_L28763	Todiro_cineum_L48285, Todiro_mactum_SB6939, Todiro_pictum_SB14508, Todiro_chrcro_L5004, Todiro_pollum_MPEGSC118, Todiro_virnum_AMNH388115
Todiro_pictum_SB14508	Todiro_cineum_L48285, Todiro_mactum_SB6939, Todiro_nigcep_L28763, Todiro_chrcro_L5004, Todiro_pollum_MPEGSC118, Todiro_virnum_AMNH388115
Todiro_pollum_MPEGSC118	Todiro_cineum_L48285, Todiro_mactum_SB6939, Todiro_pictum_SB14508, Todiro_nigcep_L28763, Todiro_chrcro_L5004, Todiro_virnum_AMNH388115
Willis_poetus_L55367	Willis_poetus_MCP2362

Willis_poetus_MCP2362	Willis_poetus_L55367
Xolmis_irupe_SB14801	Xolmis_pyrope_A12144
Xolmis_pyrope_A12144	Xolmis_irupe_SB14801
Zimmer_chrsop_L33819	Zimmer_vilmus_A5019
Zimmer_vilmus_A5019	Zimmer_chrsop_L33819

Table S9. List of fossils used for estimating the age of calibration nodes. Fossil ages (in Mega-annum) are indicated as the midpoint and the stratigraphic lower and upper bounds (within parenthesis). References list original descriptions and new information regarding phylogenetic placement and age

Taxon	Species	Fossil age (Ma)	Continent	References
Psittacopasserae				
Passeriformes	*Morsoravis sedilis* Bertelli et al 2010	54.3 (54 - 54.5)	Europe	*68-70*
Zygodactylidae	*Eozygodactylus americanus* Weidig 2010	52 (52 - 52)	N America	*70, 160, 161*
Psittaciformes	*Namapsitta praeruptorum* Mourer-Chauvire et al. 2015	38.8 (37.2 - 40.4)	Africa	*162*
Nestoridae	*Nelepsittacus minimus* Worthy et al 2011	17.5 (16 - 19)	Zealandia	*163*
Cacatuidae	*Cacatua* sp.	14.3 (12.5 - 16)	Australia	*164*
Psittaciformes	genus indet.	12.7 (11.6 - 13.7)	Asia	*165*
Psittacidae	*Nandayus vorohuensis* Toni & Noriega 1996	3.1 (2.6 - 3.6)	S America	*166*
eupasseres				
Tyranni	*Wieslochia weissi* Mayr & Manegold 2006	31.3 (30.5 - 32)	Europe	*71, 72*
Orthonychidae	*Orthonyx kaldowinyeri* Boles 1993	24 (23 - 25)	Australia	*167, 168*
Cracticiade	not named	17.5 (16 - 19)	Zealandia	*169*
Corvoidea	not named	16 (15.5 - 16.5)	Asia	*170*
Passeri	*Miocitta galbreathi* Brodkorb 1972	14.8 (13.6 - 16)	N America	*171, 172*
Muscicapidae	*Luscinia* cf. *megarhynchos*	13.8 (11.6 - 16)	Africa	*172, 173*
Tyranni	genus indet.		S America	*174*
Certhioidea				
Certhioidea	*Certhiops rummeli* Manegold 2008	19.3 (18 - 20.5)	Europe	*73*
Sittidae	*Sitta* sp.	2.9 (2.6 - 3.2)	Asia	*175*
Sittidae	*Sitta canadensis*	0.069 (0.012 - 0.13)	N America	*176*
Passeroidea-Emberizoidea				
Passeroidea	*Loxia* sp., *Passer* sp.	21.2 (20 - 22.4)	Europe	*74, 177*
Passerellidae	Palaeostruthus hatcheri Shufeldt 1913	8.5 (5.3 - 11.6)	N America	*178*
Fringillidae	*Pliocalcarius orkhonensis* Zelenkov & Kurochkin 2012	2.9 (2.6 - 3.2)	Asia	*175*
Passerellidae	*Zonotrichia robusta* Tonni 1970	0.8 (0.4 - 1.2)	S America	*179*
Emberizidae	*Emberiza alcoveri* Rando et al. 1999	0.06 (0.012 - 0.126)	Africa	*180*

Table S10. List of toe pads and samples with low-grade contamination removed for initial time calibration

Tip	Reason
Anaire_ferna_CM120730	Toepad
Nesotr_ridway_F299961	Toepad
Phaeo_murina_L90440	Toepad
Pyrrho_cinmeus_AMNH388114	Poor Quality
Pyrrho_cinmeus_FMNH262783	Toepad
Calytur_criata_A494721	Toepad
Pipreo_form_LSUMZ68564	Toepad
Pipreo_jucu_YPM40970	Toepad
Carpod_nitdus_A247754	Toepad
Carpod_antiae_YPM56780	Toepad
Cotin_macata_MZUSP25763	Toepad
Cotin_macata_LACM60338	Toepad
Cotin_ridway_LSUMZ161196	Toepad
Cotin_amabi_KU104762	Toepad
Procni_avera_MPEG33151	Toepad
Procni_avera_MPEG33152	Toepad
Neopel_aurons_MFV1262	Toepad
Corapi_leurho_ICN33757	Toepad
Lepthr_isirei_IC35523	Toepad
Machae_reglus_ICN37287	Toepad
Machae_reglus_FMNH344155	Toepad
Nestor_merlis_A11054	Poor Quality
Gallus_L36208	Poor Quality
Pseutom_graueri_F311050	Toepad
Pseutom_graueri_A764296	Toepad
Pitta_vensta_FMNH211861	Toepad
Pitta_arqu_WFVZ38387	Toepad
Pitta_elli_FMNH90286	Toepad
Pitta_gurn_FMNH373398	Toepad
Pitta_caelea_WFVZ38385	Toepad
Pitta_niplen_A463316	Toepad
Pitta_phayre_YPM68280	Toepad
Pitta_suprba_AMNH334850	Toepad
Pitta_maxima_USNM572244	Toepad
Pitta_molcen_USNM484025	Toepad
Pitta_bracura_A778678	Toepad
Pitta_reiowi_AMNH296892	Toepad

Gralria_gigant_ANS19619	Poor Quality
Gralria_haplo_COP79821	Toepad
Gralria_chth_COP62208	Toepad
Gralria_grinuc_FMNH288314	Toepad
Gralria_rufcin_USNM436486	Toepad
Gralria_flavtin_FMNH251116	Toepad
Gralria_dignis_ANS18198	Poor Quality
Cham_camson_ICN35539	Toepad
Cham_camson_USNM575267	Toepad
Cham_turdi_USNM595636	Toepad
Cham_turdi_ICN35838	Toepad
Berlep_rikeri_F391336	Toepad
Asthen_berle_AMNH348840	Toepad
Pseusei_criata_LSUMZ181472	Toepad
Crani_curta_USNM373226	Toepad
Aphras_masfue_AMNH156338	Toepad
Cincl_antcus_A817070	Toepad
Furnar_fig_F392829	Toepad
Psilor_gutus_A796861	Poor Quality
Eleosc_psypom_MZUSP33429	Toepad
Scyta_carcae_MLS13165	Toepad
Scyta_magel_MCZ85311	Toepad
Scyta_zimme_ANSP146343	Toepad
Scyta_zimme_ANSP146341	Toepad
Scyta_canu_USNM436508	Toepad
Myornis_senil_LSUMZ32297	Poor Quality
Myrmel_caure_FMNH319247	Toepad
Myrmel_caure_USNM444127	Toepad
Gymnop_leuca_FMNH248929	Toepad
Thamphil_puntat_ANSP168259	Toepad
Thamphil_dolia_USNM471360	Toepad
Thamphil_dolia_ANSP168260	Toepad
Dysith_mental_ANSP19107	Poor Quality
Herpsi_axill_ANSP158009	Toepad
Myrrul_sunsis_LSUMZ83142	Toepad
Myrrul_flum_MNRJ40786	Toepad
Euchre_humer_LSU40880	Poor Quality
Euchre_spoila_ANSP152407	Toepad
Iodop_pipra_SP50046	Toepad
Pachy_niger_MVZ149921	Toepad

Mionec_olieus_LSUMZ90443	Toepad
Mionec_olieus_FMNH43470	Toepad
Physca_krone_MZUSP67757	Toepad
Physca_krone_MZUSP67751	Toepad
Physca_krone_FMNH344612	Toepad
Physca_flavren_USNM525978	Toepad
Physca_pausta_MZUSP28600	Toepad
Physca_pausta_MZUSP24471	Toepad
Physca_vennus_LSUMZ68572	Toepad
Physca_lanoni_IC32557	Toepad
Physca_lanoni_IC31805	Toepad
Poeci_pullus_FMNH311517	Toepad
Hemit_miran_MZUSP41847	Toepad
Hemit_miran_MZUSP41848	Toepad
Rhynch_paccus_ANS17359	Poor Quality
Ochoec_diade_LSUMZ90427	Toepad
Myiopho_inotus_LSUMZ98534	Toepad
Cnemot_fustus_YPM137446	Toepad
Xenotr_mexic_LSUMZ24529	Toepad
Contop_cariba_USNM327749	Toepad
Contop_paldus_MVZ149935	Toepad
Musaxi_albfro_LSU22576	Poor Quality
Myiothe_pernix_USNM387496	Toepad
Agrior_livid_YPM83046	Toepad
Neoxol_ruftri_L70016	Toepad
Knipo_cyatri_S630514	Poor Quality
Phelps_inoata_IC38372	Toepad
Muspip_vetula_A315092	Poor Quality
Myiar_vensis_ICN36064	Toepad
Myiar_valdus_ROM109657	Toepad
Myiar_oberi_USNM572208	Toepad
Myiar_magni_MVZ151437	Toepad
Myiar_nugtor_ROM109720	Toepad
Myioze_lutei_LSU40646	Poor Quality
Tyranus_cube_YPM33527	Toepad
Tyranus_cube_YPM33528	Toepad
Ornith_semvum_MVZ161988	Toepad
Phymyi_urichi_FMNH92193	Poor Quality
Phymyi_reiser_MZUSP51944	Toepad
Phymyi_reiser_MZUSP51943	Toepad

Stigma_napen_FMNH392295	Toepad
Zimmer_chrsop_EBRG11267	Toepad
Myiopag_virata_LSU18455	Poor Quality
Elaen_ridyan_MZUSP80416	Toepad
Elaen_chisis_ICN34252	Toepad
Pseucol_dinel_A270377	Toepad
Serpop_grilla_MZU86172	Poor Quality

Table S11. Number of species in major geographic regions

Region	Species
Neotropics	1250
Nearctic	27
Old World	49

Table S12. Best-fit substitution models based on AICc for subset of 100 loci

Model	Number of Loci
GTRGAMMA	87
HKY85	7
JC69	0
K80	6

Table S13. Misidentified or heavily contaminated samples

Tip	Removed from:
Lepcol_alblin_LSUMZ7508	T400F and HGAPF datasets
Siptor_strcol_L6202	T400F and HGAPF datasets
Myiopag_cotta_LSUMZ143820	T400F and HGAPF datasets
Empinax_vircen_L64495	T400F and HGAPF datasets
Acropt_ortnyx_PhAMC1246	HGAPF dataset only

Table S14. Cases of paraphyly of suboscine genera

Genus
Chiroxiphia
Clytoctantes
Cranioleuca
Drymophila
Dysithamnus
Eurylaimus
Formicivora
Hemitriccus
Herpsilochmus
Hylopezus
Leptasthenura
Lipaugus
Lophotriccus
Mecocerculus
Muscisaxicola
Myiophobus
Myiornis
Myrmotherula
Neopelma
Ochthoeca
Phaeomyias
Philydor
Phyllomyias
Pitangus
Poecilotriccus
Polystictus
Ramphotrigon
Rhytipterna
Sakesphorus
Serpophaga
Suiriri
Synallaxis
Thripophaga
Tijuca
Xolmis

Table S15. Cases of paraphyly of suboscine species

Genus	Species
Asthenes	*dorbignyi*
Asthenes	*fuliginosa*
Camptostoma	*obsoletum*
Campylorhamphus	*procurvoides*
Campylorhamphus	*trochilirostris*
Chamaeza	*campanisona*
Clibanornis	*rubiginosus*
Contopus	*cinereus*
Cranioleuca	*curtata*
Dendrocincla	*fuliginosa*
Elaenia	*albiceps*
Elaenia	*obscura*
Elaenia	*pallatangae*
Euchrepomis	*callinota*
Euchrepomis	*humeralis*
Euchrepomis	*spodioptila*
Formicarius	*analis*
Furnarius	*leucopus*
Grallaria	*blakei*
Grallaria	*rufula*
Grallaricula	*ferrugineipectus*
Hylexetastes	*perrotii*
Knipolegus	*aterrimus*
Leptasthenura	*aegithaloides*
Manacus	*manacus*
Mionectes	*macconnelli*
Mionectes	*olivaceus*
Myiarchus	*swainsoni*
Myiarchus	*tuberculifer*
Myiarchus	*tyrannulus*
Myiopagis	*caniceps*
Myiophobus	*flavicans*
Myiornis	*auricularis*
Ochthoeca	*diadema*
Pachyramphus	*albogriseus*
Percnostola	*rufifrons*
Phaeomyias	*murina*
Pseudocolaptes	*lawrencii*

Rhytipterna	*simplex*
Sclerurus	*mexicanus*
Scytalopus	*altirostris*
Scytalopus	*atratus*
Scytalopus	*latrans*
Stigmatura	*budytoides*
Stigmatura	*napensis*
Synallaxis	*azarae*
Synallaxis	*gujanensis*
Synallaxis	*stictothorax*
Synallaxis	*unirufa*
Thamnomanes	*caesius*
Thamnophilus	*palliatus*
Thamnophilus	*ruficapillus*
Thamnophilus	*tenuepunctatus*
Tolmomyias	*assimilis*
Tolmomyias	*sulphurescens*
Xiphocolaptes	*promeropirhynchus*
Zimmerius	*chrysops*
Zimmerius	*vilissimus*

Table S16. Gamma (γ) test statistics without and with trimming of the most recent 2.5 Ma for all 6 taxonomies, the HGAPF tree for Howard and Moore classification, and the Astral tree with and without samples missing from >250 gene trees dropped for Howard and Moore classification

	Untrimmed γ	**Untrimmed P Value**	**Trimmed γ**	**Trimmed P Value**
T400F AOS H&M	-10.42	2.03×10^{-25}	3.99	6.61×10^{-5}
T400F AOS H&M with intraspecific sampling	-4.78	1.71×10^{-6}	6.98	2.87×10^{-12}
T400F AOS Clements	-10.35	4.23×10^{-25}	3.99	6.61×10^{-5}
T400F IUCN	-10.50	9.08×10^{-26}	4.44	8.79×10^{-6}
T400F 1 Ma cutoff	-7.52	5.28×10^{-14}	6.98	2.87×10^{-12}
T400F 2 Ma cutoff	-15.03	4.49×10^{-51}	6.98	2.87×10^{-12}
HGAPF H&M	-6.48	8.99×10^{-11}	3.56	3.69×10^{-4}
T400F Astral H&M	-10.70	1.01×10^{-26}	1.70	9.00×10^{-2}
T400F Astral H&M poor samples dropped	-7.96	1.75×10^{-15}	3.83	1.26×10^{-4}

Table S17. Likelihood ratio test results of TreePar models

Model	Chi-squared statistic*
addition of one shift	0.98
addition of a second shift	0.70
addition of a third shift	0.77
addition of a fourth shift	0.54
addition of a fifth shift	0.15
addition of a sixth shift	0.37
addition of a seventh shift	0.26
addition of an eigth shift	0.00
addition of a ninth shift	0.12

*values over 0.95 indicate improvement (alpha=0.05)

Table S18. FISSE results of difference in log ES between New World (λ_0) and Old World (λ_1) for 3 taxonomies, the HGAPF tree for Howard and Moore classification, and the Astral tree with and without samples missing from >250 gene trees dropped for Howard and Moore classification

	λ_0	λ_1	Null Mean Difference	P Value
AOS H&M	-1.6282	-2.3302	-0.0047	0.0889
AOS CLEMENTS	-1.6282	-2.2589	-0.0169	0.1049
IUCN	-1.6195	-2.2673	-0.0065	0.1019
HGAPF H&M	-1.5750	-2.4359	0.0063	0.0629
Astral T400F H&M	-1.6509	-2.3594	-0.0277	0.0809
Astral T400F H&M missing dropped	-1.5619	-2.3784	-0.0163	0.0649

Table S19. FISSE results of difference in log ES between Neotropics (λ_0) and Nearctic (λ_1) for 3 taxonomies, the HGAPF tree for Howard and Moore classification, and the Astral tree with and without samples missing from >250 gene trees dropped for Howard and Moore classification

	λ_0	λ_1	Null Mean Difference	P Value
AOS H&M	-1.6416	-1.0277	-0.0133	0.9980
AOS CLEMENTS	-1.6416	-1.0277	0.0043	0.9990
IUCN	-1.6324	-1.0277	-0.0031	0.9980
HGAPF H&M	-1.5925	-0.7900	0.0213	0.9990
Astral T400F H&M	-1.6639	-1.0694	-0.0128	0.9990
Astral T400F H&M missing dropped	-1.5758	-0.9673	0.0052	0.9990

Table S20. ESsim results of association between ES and absolute latitude for 3 taxonomies, the HGAPF tree for Howard and Moore classification, and the Astral tree with and without samples missing from >250 gene trees dropped for Howard and Moore classification

	ρ	P Value
AOS H&M	0.1587	0.1439
AOS CLEMENTS	0.1558	0.1359
IUCN	0.1528	0.1778
HGAPF H&M	0.1686	0.2098
Astral T400F H&M	0.0937	0.3556
Astral T400F H&M missing dropped	0.1576	0.1878

Table S21. FISSE results of differences in log ES among Neotropical regions (see Fig. S10) and between Neotropical regions and the Nearctic (NA) and Old World (OW) regions

Region1	Region2	P-Value	λ_0	λ_1	Null_Mean_Diff
WI	**AM**	**0.00**	**-0.80**	**-1.73**	**0.00**
WI	**AN**	**0.00**	**-0.80**	**-1.56**	**0.00**
WI	NA	0.16	-0.80	-1.08	0.00
WI	**OW**	**0.02**	**-0.80**	**-2.33**	**0.04**
WI	PA	0.08	-0.80	-1.51	0.00
WI	**DT**	**0.00**	**-0.80**	**-1.55**	**0.00**
WI	**AF**	**0.00**	**-0.80**	**-1.81**	**0.00**
WI	**CA**	**0.00**	**-0.80**	**-1.55**	**0.02**
AM	AN	0.96	-1.73	-1.56	0.00
AM	NA	0.98	-1.73	-1.08	-0.01
AM	OW	0.15	-1.73	-2.33	0.00
AM	PA	0.89	-1.73	-1.51	-0.01
AM	DT	0.97	-1.73	-1.55	0.00
AM	AF	NA	-1.73	-1.81	NA
AM	CA	0.98	-1.73	-1.55	0.00
AN	NA	0.96	-1.56	-1.08	-0.01
AN	OW	0.12	-1.56	-2.33	-0.01
AN	PA	0.64	-1.56	-1.51	-0.01
AN	DT	0.53	-1.56	-1.55	0.00
AN	**AF**	**0.00**	**-1.56**	**-1.81**	**0.00**
AN	CA	0.56	-1.56	-1.55	0.00
NA	**OW**	**0.03**	**-1.08**	**-2.33**	**0.03**
NA	PA	0.26	-1.08	-1.51	0.02
NA	DT	0.06	-1.08	-1.55	0.00
NA	**AF**	**0.01**	**-1.08**	**-1.81**	**0.00**
NA	**CA**	**0.02**	**-1.08**	**-1.55**	**0.00**
OW	PA	0.78	-2.33	-1.51	-0.01
OW	DT	0.84	-2.33	-1.55	-0.02
OW	AF	0.82	-2.33	-1.81	0.00
OW	CA	0.92	-2.33	-1.55	-0.02
PA	DT	0.40	-1.51	-1.55	0.00
PA	**AF**	**0.03**	**-1.51**	**-1.81**	**-0.01**
PA	CA	0.44	-1.51	-1.55	0.00
DT	**AF**	**0.00**	**-1.55**	**-1.81**	**0.00**
DT	CA	0.55	-1.55	-1.55	0.00
AF	CA	1.00	-1.81	-1.55	0.00

Table S22. FISSE results of difference in mean NH between Neotropics (nh0) and Nearctic (nh1) for 3 taxonomies, the HGAPF tree for Howard and Moore classification, and the Astral tree with and without samples missing from >250 gene trees dropped for Howard and Moore classification

	nh0	**nh1**	**Null Mean Difference**	**P Value**
AOS H&M	2.9794	2.7963	0.0002	**0.0050**
AOS CLEMENTS	2.9794	2.7963	0.0018	**0.0040**
IUCN	2.9785	2.7963	-0.0011	**0.0070**
HGAPF H&M	2.9846	2.7536	-0.0019	**0.0010**
Astral T400F H&M	2.8792	2.7050	0.0030	**0.0180**
Astral T400F H&M missing dropped	2.8964	2.6891	0.0000	**0.0030**

Table. S23. FISSE results between Nearctic and Neotropics using mean vs. median NH

	nh0	nh1	Null Mean Difference	P Value
Mean	2.9794	2.7963	0.0013	**0.0050**
Median	2.8223	2.6210	0.0003	0.0769

Table S24. FISSE results of difference in mean NH between Old World (nh0) and New World (nh1) for 3 taxonomies, the HGAPF tree for Howard and Moore classification, and the Astral tree with and without samples missing from >250 gene trees dropped for Howard and Moore classification

	nh0	**nh1**	**Null Mean Difference**	**P Value**
AOS H&M	2.9754	3.1935	0.0033	0.9151
AOS CLEMENTS	2.9754	3.1793	0.0022	0.9091
IUCN	2.9747	3.1802	-0.0062	0.9131
HGAPF H&M	2.9795	3.2357	0.0010	0.9311
Astral T400F H&M	2.8754	3.1899	-0.0009	0.9670
Astral T400F H&M missing dropped	2.8917	3.1902	0.0014	0.9500

Table. S25. FISSE results between Old World and New World using mean vs. median NH

	nh0	nh1	Null Mean Difference	P Value
Mean	2.9754	3.1935	-0.0050	0.9191
Median	2.8179	3.1485	-0.0074	0.9091

Table S26. NHsim results of association between mean NH and absolute latitude for 3 taxonomies, the HGAPF tree for Howard and Moore classification, and the Astral tree with and without samples missing from >250 gene trees dropped for Howard and Moore classification

	ρ	**P Value**
AOS H&M	-0.1223	0.3397
AOS CLEMENTS	-0.1203	0.3337
IUCN	-0.1145	0.4036
HGAPF H&M	-0.1389	0.4456
Astral T400F H&M	-0.0858	0.5315
Astral T400F H&M missing dropped	-0.1374	0.3337

Table. S27. NHsim versus latitude results using mean vs. median NH

	ρ	P Value
Mean	-0.1223	0.3397
Median	-0.0939	0.4575

Table S28. FISSE results of differences in mean NH among Neotropical regions (see Fig. S10) and between Neotropical regions and the Nearctic (NA) and Old World (OW) regions

Region1	Region2	P-Value	nh0	nh1	Null_Mean_Diff
WI	AM	1.00	2.76	3.00	0.01
WI	AN	0.99	2.76	2.96	0.00
WI	NA	0.70	2.76	2.80	0.00
WI	OW	0.95	2.76	3.19	0.00
WI	PA	0.89	2.76	2.98	0.00
WI	DT	0.99	2.76	2.95	0.00
WI	AF	1.00	2.76	3.01	0.00
WI	CA	0.99	2.76	2.96	0.00
AM	AN	0.07	3.00	2.96	0.00
AM	**NA**	**0.02**	**3.00**	**2.80**	**0.01**
AM	OW	0.84	3.00	3.19	0.00
AM	PA	0.38	3.00	2.98	0.00
AM	**DT**	**0.05**	**20.42**	**19.24**	**0.03**
AM	AF	NA	3.00	3.01	NA
AM	CA	0.07	3.00	2.96	0.00
AN	NA	0.05	2.96	2.80	0.00
AN	OW	0.89	2.96	3.19	0.00
AN	PA	0.72	19.51	20.09	-0.02
AN	DT	0.36	19.51	19.24	-0.01
AN	AF	0.99	2.96	3.01	0.00
AN	CA	0.49	2.96	2.96	0.00
NA	OW	0.95	2.80	3.19	0.01
NA	PA	0.81	2.80	2.98	0.00
NA	DT	0.94	2.80	2.95	0.00
NA	AF	0.97	2.80	3.01	0.01
NA	CA	0.99	2.80	2.96	0.00
OW	PA	0.23	3.19	2.98	0.01
OW	DT	0.15	3.19	2.95	0.00
OW	AF	0.16	3.19	3.01	0.00
OW	CA	0.09	3.19	2.96	0.00
PA	DT	0.23	20.09	19.24	-0.05
PA	AF	0.73	2.98	3.01	0.00
PA	CA	0.37	2.98	2.96	0.00
DT	AF	1.00	2.95	3.01	0.00
DT	CA	0.64	2.95	2.96	0.00
AF	**CA**	**0.01**	**3.01**	**2.96**	**0.00**

Table S29. FISSE results of difference in TB between Neotropics (tb0) and Nearctic (tb1) for 3 taxonomies, the HGAPF tree for Howard and Moore classification, and the Astral tree with and without samples missing from >250 gene trees dropped for Howard and Moore classification

	tb0	**tb1**	**Null Mean Difference**	**P Value**
AOS H&M	1.1702	0.6516	0.0155	**0.0040**
AOS Clements	1.1702	0.6516	0.0117	**0.0100**
IUCN	1.1558	0.6516	-0.0029	**0.0220**
HGAPF H&M	1.0706	0.3322	-0.0116	**0.0020**
Astral T400F H&M	1.2515	0.7357	0.0075	**0.0090**
Astral T400F H&M missing dropped	1.0940	0.6285	-0.0035	**0.0160**

Table S30. FISSE results of difference in TB between Old World (tb0) and New World (tb1) for 3 taxonomies, the HGAPF tree for Howard and Moore classification, and the Astral tree with and without samples missing from >250 gene trees dropped for Howard and Moore classification

	tb0	tb1	Null Mean Difference	P Value
AOS H&M	1.1589	1.7527	0.0237	0.8492
AOS Clements	1.1589	1.6044	0.0147	0.7682
IUCN	1.1451	1.6392	0.0138	0.8142
HGAPF H&M	1.0544	1.8302	-0.0009	0.8741
Astral T400F H&M	1.2403	1.8652	-0.0055	0.8881
Astral T400F H&M missing dropped	1.0834	1.7314	-0.0104	0.8861

Table S31. TBsim results of association between TB and absolute latitude for 3 taxonomies, the HGAPF tree for Howard and Moore classification, and the Astral tree with and without samples missing from >250 gene trees dropped for Howard and Moore classification

	ρ	P Value
AOS H&M	-0.1067	0.2857
AOS Clements	-0.1035	0.3157
IUCN	-0.1028	0.3197
HGAPF H&M	-0.1181	0.3037
Astral T400F H&M	-0.0615	0.3596
Astral T400F H&M missing dropped	-0.1089	0.2058

Table S32. FISSE results of difference in TB among Neotropical regions (see Fig. S10) and between Neotropical regions and the Nearctic (NA) and Old World (OW) regions

Region1	Region2	P-Value	λ_0	λ_1	Null_Mean_Diff
WI	AM	1.00	0.46	1.24	-0.01
WI	AN	0.99	0.46	1.12	-0.01
WI	NA	0.86	0.46	0.73	0.00
WI	OW	0.90	0.46	1.75	-0.04
WI	PA	0.90	0.46	1.04	-0.01
WI	DT	0.98	0.46	1.06	0.01
WI	AF	1.00	0.46	1.36	-0.01
WI	CA	0.97	0.46	1.01	-0.01
AM	AN	0.08	1.24	1.12	0.00
AM	NA	0.07	1.24	0.73	0.01
AM	OW	0.76	1.24	1.75	0.00
AM	PA	0.12	1.24	1.04	0.01
AM	DT	0.06	1.24	1.06	0.00
AM	AF	NA	1.24	1.36	NA
AM	**CA**	**0.01**	**1.24**	**1.01**	**0.00**
AN	NA	0.07	1.12	0.73	-0.01
AN	OW	0.83	1.12	1.75	0.01
AN	PA	0.29	1.12	1.04	0.01
AN	DT	0.31	1.12	1.06	0.00
AN	AF	1.00	1.12	1.36	0.00
AN	CA	0.12	1.12	1.01	0.00
NA	OW	0.88	0.73	1.75	0.02
NA	PA	0.71	0.73	1.04	0.03
NA	DT	0.87	0.73	1.06	-0.02
NA	AF	0.97	0.73	1.36	0.01
NA	CA	0.88	0.73	1.01	0.00
OW	PA	0.19	1.75	1.04	0.01
OW	DT	0.18	1.75	1.06	0.04
OW	AF	0.27	1.75	1.36	-0.02
OW	CA	0.09	1.75	1.01	0.00
PA	DT	0.54	1.04	1.06	0.00
PA	AF	0.96	1.04	1.36	0.00
PA	CA	0.48	1.04	1.01	-0.01
DT	AF	0.99	1.06	1.36	0.00
DT	CA	0.35	1.06	1.01	0.00
AF	**CA**	**0.00**	**1.36**	**1.01**	**0.00**

Table S33. FISSE results of difference in SR between Old World (sr0) and New World (sr1) for 3 taxonomies, the HGAPF tree for Howard and Moore classification, and the Astral tree with and without samples missing from >250 gene trees dropped for Howard and Moore classification

	sr0	sr1	Null Mean Difference	P Value
AOS H&M	0.0813	0.1012	-0.0002	0.9920
AOS Clements	0.0813	0.1012	0.0000	0.9910
IUCN	0.0811	0.1008	0.0002	0.9940
HGAPF H&M	0.0145	0.0214	0.0000	0.9920
Astral T400F H&M	0.0827	0.1009	-0.0001	0.9950
Astral T400F H&M missing dropped	0.0833	0.1027	0.0000	0.9880

Table S34. FISSE results of difference in SR between Neotropics (sr0) and Nearctic (sr1) for 3 taxonomies, the HGAPF tree for Howard and Moore classification, and the Astral tree with and without samples missing from >250 gene trees dropped for Howard and Moore classification

	sr0	sr1	Null Mean Difference	P Value
AOS H&M	0.0814	0.0803	-0.0001	0.3926
AOS Clements	0.0814	0.0803	0.0001	0.4026
IUCN	0.0812	0.0803	0.0000	0.3896
HGAPF H&M	0.0145	0.0135	0.0000	0.2308
Astral T400F H&M	0.0827	0.0820	0.0003	0.3926
Astral T400F H&M missing dropped	0.0834	0.0825	0.0002	0.3836

Table S35. SRsim results of association between SR and absolute latitude for 3 taxonomies, the HGAPF tree for Howard and Moore classification, and the Astral tree with and without samples missing from >250 gene trees dropped for Howard and Moore classification

	ρ	P Value
AOS H&M	-0.0804	0.7692
AOS Clements	-0.0785	0.8392
IUCN	-0.0676	0.8771
HGAPF H&M	-0.1875	0.5874
Astral T400F H&M	-0.0774	0.8312
Astral T400F H&M missing dropped	-0.0782	0.7972

Table S36. FISSE results of difference in SR among Neotropical regions (see Fig. S10) and between Neotropical regions and the Nearctic (NA) and Old World (OW) regions

Region1	Region2	P-Value	λ_0	λ_1	Null_Mean_Diff
WI	AM	1.00	0.05	0.07	0.00
WI	AN	0.99	0.05	0.07	0.00
WI	NA	1.00	0.05	0.08	0.00
WI	OW	0.84	0.05	0.08	0.00
WI	PA	0.91	0.05	0.06	0.00
WI	DT	0.99	0.05	0.07	0.00
WI	AF	0.99	0.05	0.07	0.00
WI	CA	1.00	0.05	0.07	0.00
AM	AN	0.28	0.07	0.07	0.00
AM	NA	0.75	0.07	0.08	0.00
AM	OW	0.69	0.07	0.08	0.00
AM	PA	0.13	0.07	0.06	0.00
AM	DT	0.68	0.07	0.07	0.00
AM	AF	NA	0.07	0.07	NA
AM	CA	0.66	0.07	0.07	0.00
AN	NA	0.88	0.07	0.08	0.00
AN	OW	0.74	0.07	0.08	0.00
AN	PA	0.14	0.07	0.06	0.00
AN	DT	0.75	0.07	0.07	0.00
AN	AF	0.60	0.07	0.07	0.00
AN	CA	0.80	0.07	0.07	0.00
NA	OW	0.48	0.08	0.08	0.00
NA	PA	0.10	0.08	0.06	0.00
NA	DT	0.32	0.08	0.07	0.00
NA	AF	0.22	0.08	0.07	0.00
NA	CA	0.22	0.08	0.07	0.00
OW	PA	0.28	0.08	0.06	0.00
OW	DT	0.33	0.08	0.07	0.00
OW	AF	0.28	0.08	0.07	0.00
OW	CA	0.35	0.08	0.07	0.00
PA	DT	0.84	0.06	0.07	0.00
PA	AF	0.78	0.06	0.07	0.00
PA	CA	0.78	0.06	0.07	0.00
DT	AF	0.27	0.07	0.07	0.00
DT	CA	0.51	0.07	0.07	0.00
AF	CA	0.73	0.07	0.07	0.00

Table S37. Relationships between speciation rates at tips inferred using ES, BAMM, Medusa, RevBayes with both FRCBDS and CBDS methods, MSBD, and ClaDS based on simple linear models

Comparison	R^2	P Value
ES vs. BAMM speciation rate	0.165	3.78×10^{-52}
ES vs. Medusa speciation rate	0.117	1.81×10^{-36}
ES vs. revBayes FRCBDS speciation rate	0.188	4.25×10^{-60}
ES vs. revBayes CBDS speciation rate	0.102	9.13×10^{-32}
ES vs. MSBD speciation rate	0.368	6.93×10^{-130}
ES vs. ClaDS speciation rate	0.366	3.70×10^{-129}
BAMM speciation rate vs. Medusa speciation rate	0.609	3.46×10^{-264}
BAMM speciation rate vs. revBayes FRCBDS speciation rate	0.695	0
BAMM speciation rate vs. revBayes CBDS speciation rate	0.193	6.94×10^{-62}
BAMM speciation rate vs. MSBD speciation rate	0.114	9.34×10^{-36}
BAMM speciation rate vs. ClaDS speciation rate	0.208	6.67×10^{-67}
Medusa speciation rate vs. revBayes FRCBDS speciation rate	0.555	1.01×10^{-227}
Medusa speciation rate vs. revBayes CBDS speciation rate	0.383	1.03×10^{-136}
Medusa speciation rate vs. MSBD speciation rate	0.089	1.01×10^{-27}
Medusa speciation rate vs. ClaDS speciation rate	0.162	3.35×10^{-51}
revBayes FRCBDS vs. revBayes CBDS speciation rate	0.249	5.09×10^{-82}
revBayes FRCBDS speciation rate vs. MSBD speciation rate	0.125	3.91×10^{-39}
revBayes FRCBDS speciation rate vs. ClaDS speciation rate	0.249	4.78×10^{-82}
revBayes CBDS speciation rate vs. MSBD speciation rate	0.061	3.49×10^{-19}
revBayes CBDS speciation rate vs. ClaDS speciation rate	0.143	5.09×10^{-45}
MSBD speciation rate vs. ClaDS speciation rate	0.100	2.75×10^{-31}

Table S38. The results of ESsim tests of speciation rate vs. species richness with different terminal branch length treatments.

Terminal branch length treatment	ρ	p-value
uniformly shortened	-0.249	0.007
uniformly lengthened	-0.229	0.005
poor-quality sampled retained	-0.221	0.017

Table S39. ESsim results for different taxonomic and geographic subsets of the data

Group	ρ	P value
Tyrannidae	-0.455	0.001
Amazonia	-0.224	0.007
Neotropics	-0.228	0.011
Dry Diagonal	-0.252	0.047
Thamnophilidae	-0.15	0.108
Andes	-0.191	0.121
Cotingidae	-0.263	0.135
Dendrocolaptidae	-0.25	0.155
Furnariidae	-0.13	0.176
Central America	-0.181	0.197
Atlantic Forest	-0.068	0.339
Rhynchocyclidae	-0.107	0.37
Old World	-0.097	0.401
Pipridae	-0.07	0.417
Nearctic	0.102	0.447
Grallariidae	-0.005	0.47
Rhinocryptidae	0.043	0.473
Patagonia	0.024	0.479
West Indies	0.006	0.48

Table S40. Associations between species richness and alternative tip-specific speciation rates

Speciation Rate	ρ	P value
BAMM	-0.115	0.337
MEDUSA	-0.128	0.301
RevBayes (FRCBDS)	-0.085	0.379
RevBayes (CBDS)	-0.147	0.370
MSBD	-0.141	0.078
ClaDS	-0.230	0.024

Table S41. Model comparison involving range size with PGLS

Model	AICc	Akaike weight
Species richness + Range size	733.445	0.444
Species richness	733.833	0.366
Range size	735.145	0.190

Table S42. Results of phylogenetic path analyses for four models

Model	P Value	CICc	ΔCICc
both	0	3722.71	0
indirect	0	3916.834	194.124
null	0	4161.993	439.284
direct	0	4162.766	440.056

Table S43. (online Excel file)
Sample information and classifications

Table S44. (online Excel file)
Locus sequence data summary table for the minimally filtered (T400F) dataset

Table S45. (online Excel file)
Locus sequence data summary table for the aggressively filtered (HGAPF) dataset

Table S46. (online Excel file)
Sample sequence data summary table for the minimally filtered (T400F) dataset

Table S47. (online Excel file)
Sample sequence data summary table for the aggressively filtered (HGAPF) dataset

References and Notes

1. D. Jablonski, K. Roy, J. W. Valentine, Out of the tropics: Evolutionary dynamics of the latitudinal diversity gradient. *Science* **314**, 102–106 (2006). doi:10.1126/science.1130880 Medline

2. J. Rolland, F. L. Condamine, F. Jiguet, H. Morlon, Faster speciation and reduced extinction in the tropics contribute to the Mammalian latitudinal diversity gradient. *PLOS Biol.* **12**, e1001775 (2014). doi:10.1371/journal.pbio.1001775 Medline

3. A. Antonelli, M. Ariza, J. Albert, T. Andermann, J. Azevedo, C. Bacon, S. Faurby, T. Guedes, C. Hoorn, L. G. Lohmann, P. Matos-Maraví, C. D. Ritter, I. Sanmartín, D. Silvestro, M. Tejedor, H. Ter Steege, H. Tuomisto, F. P. Werneck, A. Zizka, S. V. Edwards, Conceptual and empirical advances in Neotropical biodiversity research. *PeerJ* **6**, e5644 (2018). doi:10.7717/peerj.5644 Medline

4. G. L. Stebbins, *Flowering Plants: Evolution Above the Species Level* (Belknap, 1974).

5. J. Haffer, Speciation in Amazonian forest birds. *Science* **165**, 131–137 (1969). doi:10.1126/science.165.3889.131 Medline

6. D. H. Janzen, Why mountain passes are higher in the tropics. *Am. Nat.* **101**, 233–249 (1967). doi:10.1086/282487

7. J. T. Weir, Divergent timing and patterns of species accumulation in lowland and highland neotropical birds. *Evolution* **60**, 842–855 (2006). doi:10.1111/j.0014-3820.2006.tb01161.x Medline

8. I. Quintero, W. Jetz, Global elevational diversity and diversification of birds. *Nature* **555**, 246–250 (2018). doi:10.1038/nature25794 Medline

9. D. W. Schemske, "Biotic interactions and speciation in the tropics," in *Speciation and Pattterns of Diversity*, R. Butlin, J. Bridle, D. Schluter, Eds. (Cambridge Univ. Press, 2009), pp. 219–239.

10. J. H. Brown, Why are there so many species in the tropics? *J. Biogeogr*. **41**, 8–22 (2014). doi:10.1111/jbi.12228 Medline

11. D. Schluter, M. W. Pennell, Speciation gradients and the distribution of biodiversity. *Nature* **546**, 48–55 (2017). doi:10.1038/nature22897 Medline

12. M. C. Hansen, P. V. Potapov, R. Moore, M. Hancher, S. A. A. Turubanova, A. Tyukavina, D. Thau, S. V. Stehman, S. J. Goetz, T. R. Loveland, A. Kommareddy, A. Egorov, L. Chini, C. O. Justice, J. R. G. Townshend, High-resolution global maps of 21st-century forest cover change. *Science* **342**, 850–853 (2013). doi:10.1126/science.1244693 Medline

13. S. Claramunt, J. Cracraft, A new time tree reveals Earth history's imprint on the evolution of modern birds. *Sci. Adv.* **1**, e1501005 (2015). doi:10.1126/sciadv.1501005 Medline

14. R. O. Prum, J. S. Berv, A. Dornburg, D. J. Field, J. P. Townsend, E. M. Lemmon, A. R. Lemmon, A comprehensive phylogeny of birds (Aves) using targeted next-generation DNA sequencing. *Nature* **526**, 569–573 (2015). doi:10.1038/nature15697 Medline

15. C. H. Oliveros, D. J. Field, D. T. Ksepka, F. K. Barker, A. Aleixo, M. J. Andersen, P. Alström, B. W. Benz, E. L. Braun, M. J. Braun, G. A. Bravo, R. T. Brumfield, R. T.

Chesser, S. Claramunt, J. Cracraft, A. M. Cuervo, E. P. Derryberry, T. C. Glenn, M. G. Harvey, P. A. Hosner, L. Joseph, R. T. Kimball, A. L. Mack, C. M. Miskelly, A. T. Peterson, M. B. Robbins, F. H. Sheldon, L. F. Silveira, B. T. Smith, N. D. White, R. G. Moyle, B. C. Faircloth, Earth history and the passerine superradiation. *Proc. Natl. Acad. Sci. U.S.A.* **116**, 7916–7925 (2019). doi:10.1073/pnas.1813206116 Medline

16. D. F. Stotz, J. W. Fitzpatrick, T. A. Parker III, D. Moskovits, *Neotropical Birds: Ecology and Conservation* (Univ. of Chicago Press, 1996).

17. Materials and methods are available as supplementary materials.

18. S. Louca, M. W. Pennell, Extant timetrees are consistent with a myriad of diversification histories. *Nature* **580**, 502–505 (2020). doi:10.1038/s41586-020-2176-1 Medline

19. D. L. Rabosky, Diversity-dependence, ecological speciation, and the role of competition in macroevolution. *Annu. Rev. Ecol. Evol. Syst.* **44**, 481–502 (2013). doi:10.1146/annurev-ecolsys-110512-135800

20. J. J. Wiens, The causes of species richness patterns across space, time, and clades and the role of "ecological limits". *Q. Rev. Biol.* **86**, 75–96 (2011). doi:10.1086/659883 Medline

21. D. L. Rabosky, A. H. Hurlbert, Species richness at continental scales is dominated by ecological limits. *Am. Nat.* **185**, 572–583 (2015). doi:10.1086/680850 Medline

22. J. T. Weir, D. Schluter, The latitudinal gradient in recent speciation and extinction rates of birds and mammals. *Science* **315**, 1574–1576 (2007). doi:10.1126/science.1135590 Medline

23. D. L. Rabosky, J. Chang, P. O. Title, P. F. Cowman, L. Sallan, M. Friedman, K. Kaschner, C. Garilao, T. J. Near, M. Coll, M. E. Alfaro, An inverse latitudinal gradient in speciation rate for marine fishes. *Nature* **559**, 392–395 (2018). doi:10.1038/s41586-018-0273-1 Medline

24. J. D. Kennedy, Z. Wang, J. T. Weir, C. Rahbek, J. Fjeldså, T. D. Price, Into and out of the tropics: The generation of the latitudinal gradient among New World passerine birds. *J. Biogeogr.* **41**, 1746–1757 (2014). doi:10.1111/jbi.12346

25. J. C. Willis, *Age and Area: A Study in Geographical Distribution and Origin in Species* (Cambridge Univ. Press, 1922).

26. P. V. A. Fine, R. H. Ree, Evidence for a time-integrated species-area effect on the latitudinal gradient in tree diversity. *Am. Nat.* **168**, 796–804 (2006). doi:10.1086/508635 Medline

27. N. R. Polato, B. A. Gill, A. A. Shah, M. M. Gray, K. L. Casner, A. Barthelet, P. W. Messer, M. P. Simmons, J. M. Guayasamin, A. C. Encalada, B. C. Kondratieff, A. S. Flecker, S. A. Thomas, C. K. Ghalambor, N. L. Poff, W. C. Funk, K. R. Zamudio, Narrow thermal tolerance and low dispersal drive higher speciation in tropical mountains. *Proc. Natl. Acad. Sci. U.S.A.* **115**, 12471–12476 (2018). doi:10.1073/pnas.1809326115 Medline

28. J. T. Weir, T. D. Price, Limits to speciation inferred from times to secondary sympatry and ages of hybridizing species along a latitudinal gradient. *Am. Nat.* **177**, 462–469 (2011). doi:10.1086/658910 Medline

29. A. S. Meseguer, F. L. Condamine, Ancient tropical extinctions at high latitudes contribute to the latitudinal diversity gradient. *Evolution* (2020). 10.1111/evo.13967

30. T. F. Rangel, N. R. Edwards, P. B. Holden, J. A. F. Diniz-Filho, W. D. Gosling, M. T. P. Coelho, F. A. S. Cassemiro, C. Rahbek, R. K. Colwell, Modeling the ecology and evolution of biodiversity: Biogeographical cradles, museums, and graves. *Science* **361**, eaar5452 (2018). doi:10.1126/science.aar5452 Medline

31. M. G. Harvey, G. A. Bravo, S. Claramunt, A. M. Cuervo, G. E. Derryberry, J. Battilana, G. F. Seeholzer, J. Shearer McKay, B. C. O'Meara, B. C. Faircloth, S. V. Edwards, J. Pérez-Emán, R. G. Moyle, F. H. Sheldon, A. Aleixo, B. Tilston Smith, R. T. Chesser, L. Fábio Silveira, J. Cracraft, R. T. Brumfield, E. P. Derryberry, Protocols, code, trees, and alignments for: The evolution of a tropical biodiversity hotspot, Zenodo (2020); https://doi.org/10.5281/zenodo.3976115.

32. R. T. Chesser, K. J. Burns, C. Cicero, J. L. Dunn, A. W. Kratter, I. J. Lovette, P. C. Rasmussen, J. V. Remsen Jr., J. D. Rising, D. F. Stotz, K. Winker, Fifty-eighth supplement to the American Ornithologist Society's Check-list of North American birds. *Auk* **134**, 751–773 (2017). doi:10.1642/AUK-17-72.1

33. J. V. Remsen Jr., J. I. Areta, C. D. Cadena, S. Claramunt, A. Jaramillo, J. F. Pacheco, M. B. Robbins, F. G. Stiles, D. F. Stotz, K. J. Zimmer, A classification of the bird species of South America. South American Classification Committee, American Ornithological Society (2018).

34. E. C. Dickinson, J. V. Remsen Jr., *Non-Passerines*, vol. 2 of *The Howard and Moore Complete Checklist of the Birds of the World* (Aves Press, 2013).

35. E. C. Dickinson, L. Christidis, *Passerines*, vol. 1 of *The Howard and Moore Complete Checklist of the Birds of the World* (Aves Press, 2014).

36. B. C. Faircloth, J. E. McCormack, N. G. Crawford, M. G. Harvey, R. T. Brumfield, T. C. Glenn, Ultraconserved elements anchor thousands of genetic markers spanning multiple evolutionary timescales. *Syst. Biol.* **61**, 717–726 (2012). doi:10.1093/sysbio/sys004 Medline

37. M. G. Harvey, A. Aleixo, C. C. Ribas, R. T. Brumfield, Habitat association predicts genetic diversity and population divergence in Amazonian birds. *Am. Nat.* **190**, 631–648 (2017). doi:10.1086/693856 Medline

38. B. C. Faircloth, PHYLUCE is a software package for the analysis of conserved genomic loci. *Bioinformatics* **32**, 786–788 (2016). doi:10.1093/bioinformatics/btv646 Medline

39. D. R. Zerbino, E. Birney, Velvet: Algorithms for de novo short read assembly using de Bruijn graphs. *Genome Res.* **18**, 821–829 (2008). doi:10.1101/gr.074492.107 Medline

40. S. Gladman, VelvetOptimiser (2009); https://bioinformatics.net.au/software.velvetoptimiser.shtml .

41. H. Li, R. Durbin, Fast and accurate short read alignment with Burrows-Wheeler transform. *Bioinformatics* **25**, 1754–1760 (2009). doi:10.1093/bioinformatics/btp324 Medline

42. H. Li, B. Handsaker, A. Wysoker, T. Fennell, J. Ruan, N. Homer, G. Marth, G. Abecasis, R. Durbin; 1000 Genome Project Data Processing Subgroup, The Sequence Alignment/Map

format and SAMtools. *Bioinformatics* **25**, 2078–2079 (2009). doi:10.1093/bioinformatics/btp352 Medline

43. K. Katoh, K. Kuma, H. Toh, T. Miyata, MAFFT version 5: Improvement in accuracy of multiple sequence alignment. *Nucleic Acids Res.* **33**, 511–518 (2005). doi:10.1093/nar/gki198 Medline

44. P. A. Hosner, B. C. Faircloth, T. C. Glenn, E. L. Braun, R. T. Kimball, Avoiding missing data biases in phylogenomic inference: An empirical study in the landfowl (Aves: Galliformes). *Mol. Biol. Evol.* **33**, 1110–1125 (2016). doi:10.1093/molbev/msv347 Medline

45. Z. Xi, L. Liu, C. C. Davis, The impact of missing data on species tree estimation. *Mol. Biol. Evol.* **33**, 838–860 (2016). doi:10.1093/molbev/msv266 Medline

46. A. R. Lemmon, J. M. Brown, K. Stanger-Hall, E. M. Lemmon, The effect of ambiguous data on phylogenetic estimates obtained by maximum likelihood and Bayesian inference. *Syst. Biol.* **58**, 130–145 (2009). doi:10.1093/sysbio/syp017 Medline

47. W. Jiang, S. Y. Chen, H. Wang, D. Z. Li, J. J. Wiens, Should genes with missing data be excluded from phylogenetic analyses? *Mol. Phylogenet. Evol.* **80**, 308–318 (2014). doi:10.1016/j.ympev.2014.08.006 Medline

48. J. Castresana, Selection of conserved blocks from multiple alignments for their use in phylogenetic analysis. *Mol. Biol. Evol.* **17**, 540–552 (2000). doi:10.1093/oxfordjournals.molbev.a026334 Medline

49. W. C. Warren, D. F. Clayton, H. Ellegren, A. P. Arnold, L. W. Hillier, A. Künstner, S. Searle, S. White, A. J. Vilella, S. Fairley, A. Heger, L. Kong, C. P. Ponting, E. D. Jarvis, C. V. Mello, P. Minx, P. Lovell, T. A. F. Velho, M. Ferris, C. N. Balakrishnan, S. Sinha, C. Blatti, S. E. London, Y. Li, Y.-C. Lin, J. George, J. Sweedler, B. Southey, P. Gunaratne, M. Watson, K. Nam, N. Backström, L. Smeds, B. Nabholz, Y. Itoh, O. Whitney, A. R. Pfenning, J. Howard, M. Völker, B. M. Skinner, D. K. Griffin, L. Ye, W. M. McLaren, P. Flicek, V. Quesada, G. Velasco, C. Lopez-Otin, X. S. Puente, T. Olender, D. Lancet, A. F. A. Smit, R. Hubley, M. K. Konkel, J. A. Walker, M. A. Batzer, W. Gu, D. D. Pollock, L. Chen, Z. Cheng, E. E. Eichler, J. Stapley, J. Slate, R. Ekblom, T. Birkhead, T. Burke, D. Burt, C. Scharff, I. Adam, H. Richard, M. Sultan, A. Soldatov, H. Lehrach, S. V. Edwards, S.-P. Yang, X. Li, T. Graves, L. Fulton, J. Nelson, A. Chinwalla, S. Hou, E. R. Mardis, R. K. Wilson, The genome of a songbird. *Nature* **464**, 757–762 (2010). doi:10.1038/nature08819 Medline

50. E. D. Jarvis, S. Mirarab, A. J. Aberer, B. Li, P. Houde, C. Li, S. Y. W. Ho, B. C. Faircloth, B. Nabholz, J. T. Howard, A. Suh, C. C. Weber, R. R. da Fonseca, J. Li, F. Zhang, H. Li, L. Zhou, N. Narula, L. Liu, G. Ganapathy, B. Boussau, M. S. Bayzid, V. Zavidovych, S. Subramanian, T. Gabaldón, S. Capella-Gutiérrez, J. Huerta-Cepas, B. Rekepalli, K. Munch, M. Schierup, B. Lindow, W. C. Warren, D. Ray, R. E. Green, M. W. Bruford, X. Zhan, A. Dixon, S. Li, N. Li, Y. Huang, E. P. Derryberry, M. F. Bertelsen, F. H. Sheldon, R. T. Brumfield, C. V. Mello, P. V. Lovell, M. Wirthlin, M. P. C. Schneider, F. Prosdocimi, J. A. Samaniego, A. M. Vargas Velazquez, A. Alfaro-Núñez, P. F. Campos, B. Petersen, T. Sicheritz-Ponten, A. Pas, T. Bailey, P. Scofield, M. Bunce, D. M. Lambert, Q. Zhou, P. Perelman, A. C. Driskell, B. Shapiro, Z. Xiong, Y. Zeng, S. Liu, Z.

Li, B. Liu, K. Wu, J. Xiao, X. Yinqi, Q. Zheng, Y. Zhang, H. Yang, J. Wang, L. Smeds, F. E. Rheindt, M. Braun, J. Fjeldsa, L. Orlando, F. K. Barker, K. A. Jønsson, W. Johnson, K.-P. Koepfli, S. O'Brien, D. Haussler, O. A. Ryder, C. Rahbek, E. Willerslev, G. R. Graves, T. C. Glenn, J. McCormack, D. Burt, H. Ellegren, P. Alström, S. V. Edwards, A. Stamatakis, D. P. Mindell, J. Cracraft, E. L. Braun, T. Warnow, W. Jun, M. T. P. Gilbert, G. Zhang, Whole-genome analyses resolve early branches in the tree of life of modern birds. *Science* **346**, 1320–1331 (2014). doi:10.1126/science.1253451 Medline

51. D. T. Ksepka, M. J. Phillips, Avian diversification patterns across the K-Pg boundary: Influence of calibrations, datasets, and model misspecification. *Ann. Mo. Bot. Gard.* **100**, 300–328 (2015). doi:10.3417/2014032

52. S. F. Altschul, T. L. Madden, A. A. Schäffer, J. Zhang, Z. Zhang, W. Miller, D. J. Lipman, Gapped BLAST and PSI-BLAST: A new generation of protein database search programs. *Nucleic Acids Res.* **25**, 3389–3402 (1997). doi:10.1093/nar/25.17.3389 Medline

53. A. Stamatakis, RAxML version 8: A tool for phylogenetic analysis and post-analysis of large phylogenies. *Bioinformatics* **30**, 1312–1313 (2014). doi:10.1093/bioinformatics/btu033 Medline

54. S. Guindon, J. F. Dufayard, V. Lefort, M. Anisimova, W. Hordijk, O. Gascuel, New algorithms and methods to estimate maximum-likelihood phylogenies: Assessing the performance of PhyML 3.0. *Syst. Biol.* **59**, 307–321 (2010). doi:10.1093/sysbio/syq010 Medline

55. R Core Team, R: A language and environment for statistical computing (R Foundation for Statistical Computing, 2017); https://www.R-project.org/ .

56. K. P. Schliep, phangorn: Phylogenetic analysis in R. *Bioinformatics* **27**, 592–593 (2011). doi:10.1093/bioinformatics/btq706 Medline

57. A. M. Kozlov, A. J. Aberer, A. Stamatakis, ExaML version 3: A tool for phylogenomic analyses on supercomputers. *Bioinformatics* **31**, 2577–2579 (2015). doi:10.1093/bioinformatics/btv184 Medline

58. S. A. Smith, M. J. Moore, J. W. Brown, Y. Yang, Analysis of phylogenomic datasets reveals conflict, concordance, and gene duplications with examples from animals and plants. *BMC Evol. Biol.* **15**, 150 (2015). doi:10.1186/s12862-015-0423-0 Medline

59. J. F. Walker, Y. Yang, M. J. Moore, J. Mikenas, A. Timoneda, S. F. Brockington, S. A. Smith, Widespread paleopolyploidy, gene tree conflict, and recalcitrant relationships among the carnivorous Caryophyllales. *Am. J. Bot.* **104**, 858–867 (2017). doi:10.3732/ajb.1700083 Medline

60. C. Zhang, E. Sayyari, S. Mirarab, "ASTRAL-III: Increased scalability and impacts of contracting low support branches" in *Comparative Genomics. RECOMB-CG 2017. Lecture Notes in Computer Science.* J. Meidanis, L. Nakleh, Eds. (Springer, 2017), vol 10562, pp. 53–75.

61. S. Mirarab, T. Warnow, ASTRAL-II: Coalescent-based species tree estimation with many hundreds of taxa and thousands of genes. *Bioinformatics* **31**, i44–i52 (2015). doi:10.1093/bioinformatics/btv234 Medline

62. E. Sayyari, S. Mirarab, Fast coalescent-based computation of local branch support from quartet frequencies. *Mol. Biol. Evol.* **33**, 1654–1668 (2016). doi:10.1093/molbev/msw079 Medline

63. C. R. Marshall, The fossil record and estimating divergence times between lineages: Maximum divergence times and the importance of reliable phylogenies. *J. Mol. Evol.* **30**, 400–408 (1990). doi:10.1007/BF02101112 Medline

64. M. J. Sanderson, Estimating absolute rates of molecular evolution and divergence times: A penalized likelihood approach. *Mol. Biol. Evol.* **19**, 101–109 (2002). doi:10.1093/oxfordjournals.molbev.a003974 Medline

65. S. A. Smith, B. C. O'Meara, treePL: Divergence time estimation using penalized likelihood for large phylogenies. *Bioinformatics* **28**, 2689–2690 (2012). doi:10.1093/bioinformatics/bts492 Medline

66. D. Strauss, P. M. Sadler, Classical confidence intervals and Bayesian probability estimates for ends of local taxon ranges. *Math. Geol.* **21**, 411–427 (1989). doi:10.1007/BF00897326

67. A. R. Solow, Estimation of stratigraphic ranges when fossil finds are not randomly distributed. *Paleobiology* **29**, 181–185 (2003). doi:10.1666/0094-8373(2003)029<0181:EOSRWF>2.0.CO;2

68. G. Mayr, A reassessment of Eocene parrotlike fossils indicates a previously undetected radiation of zygodactyl stem group representatives of passerines (Passeriformes). *Zool. Scr.* **44**, 587–602 (2015). doi:10.1111/zsc.12128

69. S. Bertelli, B. E. Lindow, G. J. Dyke, L. M. Chiappe, A well-preserved 'charadriiform-like' fossil bird from the Early Eocene Fur Formation of Denmark. *Paleontology* **53**, 507–531 (2010). doi:10.1111/j.1475-4983.2010.00950.x

70. D. T. Ksepka, L. Grande, G. Mayr, Oldest finch-beaked birds reveal parallel ecological radiations in the earliest evolution of passerines. *Curr. Biol.* **29**, 657–663.e1 (2019). doi:10.1016/j.cub.2018.12.040 Medline

71. G. Mayr, A. Manegold, New specimens of the earliest European passeriform bird. *Acta Palaeontol. Pol.* **51**, 315–323 (2006).

72. E. E. Maxwell, S. Alexander, G. Bechly, K. Eck, E. Frey, K. Grimm, J. Kovar-Eder, G. Mayr, N. Micklich, M. Rasser, A. Roth-Nebelsick, R. B. Salvador, R. R. Schoch, G. Schweigert, W. Stinnesbeck, K. Wolf-Schwenninger, R. Ziegler, The Rauenberg fossil Lagerstätte (Baden-Württemberg, Germany): A window into early Oligocene marine and coastal ecosystems of Central Europe. *Palaeogeogr. Palaeoclimatol. Palaeoecol.* **463**, 238–260 (2016). doi:10.1016/j.palaeo.2016.10.002

73. A. Manegold, Earliest fossil record of the Certhioidea (treecreepers and allies) from the early Miocene of Germany. *J. Ornithol.* **149**, 223–228 (2008). doi:10.1007/s10336-007-0263-9

74. C. Mourer-Chauviré, Dynamics of the avifauna during the Paleogene and the early Neogene of France. Settling of the recent fauna. *Acta Zool. Cracov.* **38**, 325–342 (1995).

75. U. Mai, S. Mirarab, TreeShrink: Fast and accurate detection of outlier long branches in collections of phylogenetic trees. *BMC Genomics* **19** (Suppl 5), 272 (2018). doi:10.1186/s12864-018-4620-2 Medline

76. J. M. Eastman, L. J. Harmon, D. C. Tank, Congruificiation: Support for time scaling large phylogenetic trees. *Methods Ecol. Evol.* **4**, 688–691 (2013). doi:10.1111/2041-210X.12051

77. M. W. Pennell, J. M. Eastman, G. J. Slater, J. W. Brown, J. C. Uyeda, R. G. FitzJohn, M. E. Alfaro, L. J. Harmon, geiger v2.0: An expanded suite of methods for fitting macroevolutionary models to phylogenetic trees. *Bioinformatics* **30**, 2216–2218 (2014). doi:10.1093/bioinformatics/btu181 Medline

78. R. Bouckaert, J. Heled, D. Kühnert, T. Vaughan, C.-H. Wu, D. Xie, M. A. Suchard, A. Rambaut, A. J. Drummond, BEAST 2: A software platform for Bayesian evolutionary analysis. *PLOS Comput. Biol.* **10**, e1003537 (2014). doi:10.1371/journal.pcbi.1003537 Medline

79. A. J. Drummond, A. Rambaut, BEAST: Bayesian evolutionary analysis by sampling trees. *BMC Evol. Biol.* **7**, 214 (2007). doi:10.1186/1471-2148-7-214 Medline

80. T. Stadler, On incomplete sampling under birth-death models and connections to the sampling-based coalescent. *J. Theor. Biol.* **261**, 58–66 (2009). doi:10.1016/j.jtbi.2009.07.018 Medline

81. T. Stadler, D. Kühnert, S. Bonhoeffer, A. J. Drummond, Birth-death skyline plot reveals temporal changes of epidemic spread in HIV and hepatitis C virus (HCV). *Proc. Natl. Acad. Sci. U.S.A.* **110**, 228–233 (2013). doi:10.1073/pnas.1207965110 Medline

82. J. G. Tello, R. G. Moyle, D. J. Marchese, J. Cracraft, Phylogeny and phylogenetic classification of the tyrant flycatchers, cotingas, manakins, and their allies (Aves: Tyrannides). *Cladistics* **25**, 429–467 (2009). doi:10.1111/j.1096-0031.2009.00254.x

83. J. F. Clements, T. S. Schulenberg, M. J. Iliff, D. Roberson, T. A. Fredericks, B. L. Sullivan, C. L. Wood, "The eBird/Clements checklist of birds of the world: v2017" (2017); https://www.birds.cornell.edu/clementschecklist/download/ .

84. J. del Hoyo, N. J. Collar, D. A. Christie, A. Elliott, L. D. C. Fishpool, *Non-Passerines*, vol. 1 of *HBW and BirdLife International Illustrated Checklist of the Birds of the World* (Lynx Edicions and BirdLife International, Barcelona, 2014).

85. J. del Hoyo, N. J. Collar, D. A. Christie, A. Elliott, L. D. C. Fishpool, P. Boesman, G. M. Kirwan, *Passerines*, vol. 2 of *HBW and BirdLife International Illustrated Checklist of the Birds of the World* (Lynx Edicions and BirdLife International, 2016).

86. R. G. FitzJohn, Diversitree: Comparative phylogenetic analyses of diversification in R. *Methods Ecol. Evol.* **3**, 1084–1092 (2012). doi:10.1111/j.2041-210X.2012.00234.x

87. R. S. Etienne, A. L. Pigot, A. B. Phillimore, How reliably can we infer diversity-dependent diversification from phylogenies? *Methods Ecol. Evol.* **7**, 1092–1099 (2016). doi:10.1111/2041-210X.12565

88. T. Stadler, Mammalian phylogeny reveals recent diversification rate shifts. *Proc. Natl. Acad. Sci. U.S.A.* **108**, 6187–6192 (2011). doi:10.1073/pnas.1016876108 Medline

89. M. R. May, S. Höhna, B. R. Moore, A Bayesian approach for detecting the impact of mass-extinction events on molecular phylogenies when rates of lineage diversification may vary. *Methods Ecol. Evol.* **7**, 947–959 (2016). doi:10.1111/2041-210X.12563

90. S. Höhna, M. R. May, B. R. Moore, TESS: An R package for efficiently simulating phylogenetic trees and performing Bayesian inference of lineage diversification rates. *Bioinformatics* **32**, 789–791 (2016). doi:10.1093/bioinformatics/btv651 Medline

91. S. Louca, M. Doebeli, Efficient comparative phylogenetics on large trees. *Bioinformatics* **34**, 1053–1055 (2018). doi:10.1093/bioinformatics/btx701 Medline

92. T. G. Barraclough, A. P. Vogler, Detecting the geographical pattern of speciation from species-level phylogenies. *Am. Nat.* **155**, 419–434 (2000). doi:10.1086/303332 Medline

93. J. Belmaker, W. Jetz, Relative roles of ecological and energetic constraints, diversification rates and region history on global species richness gradients. *Ecol. Lett.* **18**, 563–571 (2015). doi:10.1111/ele.12438 Medline

94. M. G. Harvey, D. L. Rabosky, Continuous traits and speciation rates: Alternatives to state-dependent diversification models. *Methods Ecol. Evol.* **9**, 984–993 (2018). doi:10.1111/2041-210X.12949

95. D. W. Redding, A. Ø. Mooers, Incorporating evolutionary measures into conservation prioritization. *Conserv. Biol.* **20**, 1670–1678 (2006). doi:10.1111/j.1523-1739.2006.00555.x Medline

96. W. Jetz, G. H. Thomas, J. B. Joy, K. Hartmann, A. O. Mooers, The global diversity of birds in space and time. *Nature* **491**, 444–448 (2012). doi:10.1038/nature11631 Medline

97. A. C. R. Gomes, M. D. Sorenson, G. C. Cardoso, Speciation is associated with changing ornamentation rather than stronger sexual selection. *Evolution* **70**, 2823–2838 (2016). doi:10.1111/evo.13088 Medline

98. L.-M. Lu, L.-F. Mao, T. Yang, J.-F. Ye, B. Liu, H.-L. Li, M. Sun, J. T. Miller, S. Mathews, H.-H. Hu, Y.-T. Niu, D.-X. Peng, Y.-H. Chen, S. A. Smith, M. Chen, K.-L. Xiang, C.-T. Le, V.-C. Dang, A.-M. Lu, P. S. Soltis, D. E. Soltis, J.-H. Li, Z.-D. Chen, Evolutionary history of the angiosperm flora of China. *Nature* **554**, 234–238 (2018). doi:10.1038/nature25485 Medline

99. M. Pagel, Inferring evolutionary processes from phylogenies. *Zool. Scr.* **26**, 331–348 (1997). doi:10.1111/j.1463-6409.1997.tb00423.x

100. R. Bivand, T. Keitt, B. Rowlingson, "rgdal: Bindings for the geospatial data abstraction library," R package version 1.2-6 (2017); https://CRAN.R-project.org/package=rgdal.

101. R. J. Hijmans, "raster: Geographic data analysis and modeling," R package version 2.6-7 (2017); https://CRAN.R-project.org/package=raster.

102. R. Bivand, N. Lewin-Koh, "maptools: Tools for reading and handling spatial objects," R package version 0.9-2 (2017); https://CRAN.R-project.org/package=maptools.

103. R. A. Becker, A. R. Wilks, R. Brownrigg, T. P. Minka, A. Deckmyn, "maps: Draw geographical maps," R package version 3.2.0 (2017); https://CRAN.R-project.org/package=maps.

104. A. South, rworldmap: A new R package for mapping global data. *R J.* **3**, 35–43 (2011). doi:10.32614/RJ-2011-006

105. E. J. Pebesma, R. S. Bivand, Classes and methods for spatial data in R. *R News* **5**, 1–21 (2005).

106. R. S. Bivand, E. Pebesma, V. Gomez-Rubio, *Applied Spatial Data Analysis with R* (Springer, ed. 2, 2013).

107. W. Jetz, C. Rahbek, Geographic range size and determinants of avian species richness. *Science* **297**, 1548–1551 (2002). doi:10.1126/science.1072779 Medline

108. Birdlife International, *NatureServe: Bird Species Distribution Maps of the World* (BirdLife International and NatureServe, 2018).

109. B. R. Moore, S. Höhna, M. R. May, B. Rannala, J. P. Huelsenbeck, Critically evaluating the theory and performance of Bayesian analysis of macroevolutionary mixtures. *Proc. Natl. Acad. Sci. U.S.A.* **113**, 9569–9574 (2016). doi:10.1073/pnas.1518659113 Medline

110. M. R. May, B. R. Moore, How well can we detect lineage-specific diversification-rate shifts? A simulation study of sequential AIC methods. *Syst. Biol.* **65**, 1076–1084 (2016). doi:10.1093/sysbio/syw026 Medline

111. D. L. Rabosky, Automatic detection of key innovations, rate shifts, and diversity-dependence on phylogenetic trees. *PLOS ONE* **9**, e89543 (2014). doi:10.1371/journal.pone.0089543 Medline

112. D. L. Rabosky, S. C. Donnellan, M. Grundler, I. J. Lovette, Analysis and visualization of complex macroevolutionary dynamics: An example from Australian scincid lizards. *Syst. Biol.* **63**, 610–627 (2014). doi:10.1093/sysbio/syu025 Medline

113. J. S. Mitchell, D. L. Rabosky, Bayesian model selection with BAMM: Effects of the model prior on the inferred number of diversification shifts. *Methods Ecol. Evol.* **8**, 37–46 (2017). doi:10.1111/2041-210X.12626

114. D. L. Rabosky, J. S. Mitchell, J. Chang, Is BAMM flawed? Theoretical and practical concerns in the analysis of multi-rate diversification models. *Syst. Biol.* **66**, 477–498 (2017). doi:10.1093/sysbio/syx037 Medline

115. M. Plummer, N. Best, K. Cowles, K. Vines, CODA: Convergence diagnosis and output analysis for MCMC. *R News* **6**, 7–11 (2006).

116. D. L. Rabosky, M. Grundler, C. Anderson, P. Title, J. J. Shi, J. W. Brown, H. Huang, J. G. Larson, BAMMtools: An R package for the analysis of evolutionary dynamics on phylogenetic trees. *Methods Ecol. Evol.* **5**, 701–707 (2014). doi:10.1111/2041-210X.12199

117. M. E. Alfaro, F. Santini, C. Brock, H. Alamillo, A. Dornburg, D. L. Rabosky, G. Carnevale, L. J. Harmon, Nine exceptional radiations plus high turnover explain species diversity in jawed vertebrates. *Proc. Natl. Acad. Sci. U.S.A.* **106**, 13410–13414 (2009). doi:10.1073/pnas.0811087106 Medline

118. S. Höhna, M. J. Landis, T. A. Heath, B. Boussau, N. Lartillot, B. R. Moore, J. P. Huelsenbeck, F. Ronquist, RevBayes: Bayesian phylogenetic inference using graphical

models and an interactive model-specification language. *Syst. Biol.* **65**, 726–736 (2016). doi:10.1093/sysbio/syw021 Medline

119. A. Rambaut, M. Suchard, A. Drummond, "Tracer v.16" (2013); http://tree.bio.ed.ac.uk/software/tracer/.

120. J. Barido-Sottani *et al*., https://www.biorxiv.org/content/10.1101/440982v1 (2018).

121. O. Maliet, F. Hartig, H. Morlon, A model with many small shifts for estimating species-specific diversification rates. *Nat. Ecol. Evol.* **3**, 1086–1092 (2019). doi:10.1038/s41559-019-0908-0 Medline

122. H. Morlon, E. Lewitus, F. L. Condamine, M. Manceau, J. Clavel, J. Drury, RPANDA: An R package for macroevolutionary analyses on phylogenetic trees. *Methods Ecol. Evol.* **7**, 589–597 (2016). doi:10.1111/2041-210X.12526

123. D. M. Olson, E. Dinerstein, E. D. Wikramanayake, N. D. Burgess, G. V. N. Powell, E. C. Underwood, J. A. D'amico, I. Itoua, H. E. Strand, J. C. Morrison, C. J. Loucks, T. F. Allnutt, T. H. Ricketts, Y. Kura, J. F. Lamoreux, W. W. Wettengel, P. Hedao, K. R. Kassem, Terrestrial ecoregions of the world: a new map of life on earth: a new global map of terrestrial ecoregions provides an innovative tool for conserving biodiversity. *Bioscience* **51**, 933–938 (2001). doi:10.1641/0006-3568(2001)051[0933:TEOTWA]2.0.CO;2

124. J. L. Brown, D. J. Hill, A. M. Dolan, A. C. Carnaval, A. M. Haywood, PaleoClim, high spatial resolution paleoclimate surfaces for global land areas. *Sci. Data* **5**, 180254 (2018). doi:10.1038/sdata.2018.254 Medline

125. D. N. Karger, O. Conrad, J. Böhner, T. Kawohl, H. Kreft, R. W. Soria-Auza, N. E. Zimmermann, H. P. Linder, M. Kessler, Climatologies at high resolution for the earth's land surface areas. *Sci. Data* **4**, 170122 (2017). doi:10.1038/sdata.2017.122 Medline

126. D. J. Hill, The non-analogue nature of Pliocene temperature gradients. *Earth Planet. Sci. Lett.* **425**, 232–241 (2015). doi:10.1016/j.epsl.2015.05.044

127. A. M. Dolan, A. M. Haywood, S. J. Hunter, J. C. Tindall, H. J. Dowsett, D. J. Hill, S. J. Pickering, Modelling the enigmatic Late Pliocene Glacial Event – Marine Isotope Stage M2. *Global Planet. Change* **128**, 47–60 (2015). doi:10.1016/j.gloplacha.2015.02.001

128. P. Segurado, M. B. Araújo, W. E. Kunin, Consequences of spatial autocorrelation for niche-based models. *J. Appl. Ecol.* **43**, 433–444 (2006). doi:10.1111/j.1365-2664.2006.01162.x

129. R. H. Ree, B. R. Moore, C. O. Webb, M. J. Donoghue, A likelihood framework for inferring the evolution of geographic range on phylogenetic trees. *Evolution* **59**, 2299–2311 (2005). doi:10.1111/j.0014-3820.2005.tb00940.x Medline

130. N. J. Matzke, Probabilistic historical biogeography: New models for founder-event speciation, imperfect detection, and fossils allow improved accuracy and model-testing. *Front. Biogeogr.* **5**, 242–248 (2013). doi:10.21425/F55419694

131. J. Dupin, N. J. Matzke, T. Sarkinen, S. Knapp, R. Olmstead, L. Bohs, S. Smith, Bayesian estimation of the global biogeographic history of the Solanaceae. *J. Biogeogr.* **44**, 887–899 (2017). doi:10.1111/jbi.12898

132. J. J. Morrone, Biogeographical regionalisation of the Neotropical region. *Zootaxa* **3782**, 1–110 (2014). doi:10.11646/zootaxa.3782.1.1 Medline

133. D. L. Rabosky, E. E. Goldberg, FiSSE: A simple nonparametric test for the effects of a binary character on lineage diversification rates. *Evolution* **71**, 1432–1442 (2017). doi:10.1111/evo.13227 Medline

134. W. P. Maddison, P. E. Midford, S. P. Otto, Estimating a binary character's effect on speciation and extinction. *Syst. Biol.* **56**, 701–710 (2007). doi:10.1080/10635150701607033 Medline

135. R. G. FitzJohn, Quantitative traits and diversification. *Syst. Biol.* **59**, 619–633 (2010). doi:10.1093/sysbio/syq053 Medline

136. J. M. Beaulieu, B. C. O'Meara, Detecting hidden diversification shifts in models of trait-dependent speciation and extinction. *Syst. Biol.* **65**, 583–601 (2016). doi:10.1093/sysbio/syw022 Medline

137. D. S. Caetano, B. C. O'Meara, J. M. Beaulieu, Hidden state models improve state-dependent diversification approaches, including biogeographical models. *Evolution* **72**, 2308–2324 (2018). doi:10.1111/evo.13602 Medline

138. E. E. Goldberg, L. T. Lancaster, R. H. Ree, Phylogenetic inference of reciprocal effects between geographic range evolution and diversification. *Syst. Biol.* **60**, 451–465 (2011). doi:10.1093/sysbio/syr046 Medline

139. A. von Hardenberg, A. Gonzalez-Voyer, Disentangling evolutionary cause-effect relationships with phylogenetic confirmatory path analysis. *Evolution* **67**, 378–387 (2013). doi:10.1111/j.1558-5646.2012.01790.x Medline

140. B. Shipley, A new inferential test for path models based on directed acyclic graphs. *Struct. Equ. Modeling* **7**, 206–218 (2000). doi:10.1207/S15328007SEM0702_4

141. W. van der Bijl, *phylopath*: Easy phylogenetic path analysis in R. *PeerJ* **6**, e4718 (2018). doi:10.7717/peerj.4718 Medline

142. M. K. Kuhner, J. Felsenstein, A simulation comparison of phylogeny algorithms under equal and unequal evolutionary rates. *Mol. Biol. Evol.* **11**, 459–468 (1994). Medline

143. L. Liu, C. Anderson, D. Pearl, S. V. Edwards, "Modern phylogenomics: building phylogenetic trees using the multispecies coalescent model," in *Evolutionary Genomics* (Humana, 2019), pp. 211–239.

144. D. L. Rabosky, No substitute for real data: A cautionary note on the use of phylogenies from birth-death polytomy resolvers for downstream comparative analyses. *Evolution* **69**, 3207–3216 (2015). doi:10.1111/evo.12817 Medline

145. O. G. Pybus, P. H. Harvey, Testing macro-evolutionary models using incomplete molecular phylogenies. *Proc. Biol. Sci.* **267**, 2267–2272 (2000). doi:10.1098/rspb.2000.1278 Medline

146. J. A. Fordyce, Interpreting the γ statistic in phylogenetic diversification rate studies: A rate decrease does not necessarily indicate an early burst. *PLOS ONE* **5**, e11781 (2010). doi:10.1371/journal.pone.0011781 Medline

147. E. P. Derryberry, S. Claramunt, G. Derryberry, R. T. Chesser, J. Cracraft, A. Aleixo, J. Pérez-Emán, J. V. Remsen Jr., R. T. Brumfield, Lineage diversification and morphological evolution in a large-scale continental radiation: the neotropical ovenbirds and woodcreepers (aves: Furnariidae). *Evolution* **65**, 2973–2986 (2011). doi:10.1111/j.1558-5646.2011.01374.x Medline

148. P. A. Colinvaux, P. E. De Oliveira, J. E. Moreno, M. C. Miller, M. B. Bush, A long pollen record from lowland Amazonia: Forest and cooling in glacial times. *Science* **274**, 85–88 (1996). doi:10.1126/science.274.5284.85

149. M. B. Bush, Amazonian speciation: A necessarily complex model. *J. Biogeogr.* **21**, 5–17 (1994). doi:10.2307/2845600

150. P. G. P. Ericson, M. Irestedt, U. S. Johansson, Evolution, biogeography, and patterns of diversification in passerine birds. *J. Avian Biol.* **34**, 3–15 (2003). doi:10.1034/j.1600-048X.2003.03121.x

151. S. Faurby, W. L. Eiserhardt, J. C. Svenning, Strong effects of variation in taxonomic opinion on diversification analyses. *Methods Ecol. Evol.* **7**, 4–13 (2016). doi:10.1111/2041-210X.12449

152. C. F. Dormann, J. M. McPherson, M. B. Araújo, R. Bivand, J. Bolliger, G. Carl, R. G. Davies, A. Hirzel, W. Jetz, W. D. Kissling, I. Kühn, R. Ohlemüller, P. R. Peres-Neto, B. Reineking, B. Schröder, F. M. Schurr, R. Wilson, Method to account for spatial autocorrelation in the analysis of species distributional data: A review. *Ecography* **30**, 609–628 (2007). doi:10.1111/j.2007.0906-7590.05171.x

153. D. L. Rabosky, Extinction rates should not be estimated from molecular phylogenies. *Evolution* **64**, 1816–1824 (2010). doi:10.1111/j.1558-5646.2009.00926.x Medline

154. R. A. Pyron, J. J. Wiens, Large-scale phylogenetic analyses reveal the causes of high tropical amphibian diversity. *Proc. Biol. Sci.* **280**, 20131622 (2013). doi:10.1098/rspb.2013.1622 Medline

155. R. A. Pyron, Temperate extinction in squamate reptiles and the roots of latitudinal diversity gradients. *Glob. Ecol. Biogeogr.* **23**, 1126–1134 (2014). doi:10.1111/geb.12196

156. P. Pulido-Santacruz, J. T. Weir, Extinction as a driver of avian latitudinal diversity gradients. *Evolution* **70**, 860–872 (2016). doi:10.1111/evo.12899 Medline

157. S. A. Smith, J. W. Brown, Constructing a broadly inclusive seed plant phylogeny. *Am. J. Bot.* **105**, 302–314 (2018). doi:10.1002/ajb2.1019 Medline

158. I. Irisarri, D. Baurain, H. Brinkmann, F. Delsuc, J.-Y. Sire, A. Kupfer, J. Petersen, M. Jarek, A. Meyer, M. Vences, H. Philippe, Phylotranscriptomic consolidation of the jawed vertebrate timetree. *Nat. Ecol. Evol.* **1**, 1370–1378 (2017). doi:10.1038/s41559-017-0240-5 Medline

159. P. Simion, H. Philippe, D. Baurain, M. Jager, D. J. Richter, A. Di Franco, B. Roure, N. Satoh, É. Quéinnec, A. Ereskovsky, P. Lapébie, E. Corre, F. Delsuc, N. King, G. Wörheide, M. Manuel, A large and consistent phylogenomic dataset supports sponges as the sister group to all other animals. *Curr. Biol.* **27**, 958–967 (2017). doi:10.1016/j.cub.2017.02.031 Medline

160. I. Weidig, New birds from the Lower Eocene Green River Formation, North America. In Proceedings of the VII International Meeting of the Society of Avian Paleontology and Evolution, ed. W.E. Boles and T.H. Worthy. *Rec. Aust. Mus.* **62**, 29–44 (2010). doi:10.3853/j.0067-1975.62.2010.1544

161. N. A. Smith, A. M. DeBee, J. A. Clarke, Systematics and phylogeny of the Zygodactylidae (Aves, Neognathae) with description of a new species from the early Eocene of Wyoming, USA. *PeerJ* **6**, e4950 (2018). doi:10.7717/peerj.4950 Medline

162. C. Mourer-Chauviré, M. Pickford, B. Senut, Stem group galliform and stem group psittaciform birds (Aves, Galliformes, Paraortygidae, and Psittaciformes, family incertae sedis) from the Middle Eocene of Namibia. *J. Ornithol.* **156**, 275–286 (2015). doi:10.1007/s10336-014-1124-y

163. T. H. Worthy, A. J. Tennyson, R. P. Scofield, An early Miocene diversity of parrots (Aves, Strigopidae, Nestorinae) from New Zealand. *J. Vertebr. Paleontol.* **31**, 1102–1116 (2011). doi:10.1080/02724634.2011.595857

164. W. E. Boles, A new cockatoo (Psittaciformes: Cacatuidae) from the Tertiary of Riversleigh, northwestern Queensland, and an evaluation of rostral characters in the systematics of parrots. *Ibis* **135**, 8–18 (1993). doi:10.1111/j.1474-919X.1993.tb02804.x

165. N. V. Zelenkov, The first fossil parrot (Aves, Psittaciformes) from Siberia and its implications for the historical biogeography of Psittaciformes. *Biol. Lett.* **12**, 20160717 (2016). doi:10.1098/rsbl.2016.0717 Medline

166. E. P. Tonni, J. I. and Noriega, A new species of Nandayus Bonaparte, 1854 (Aves: Psittaciformes) from the Late Pliocene of Argentina. *Rev. Chil. Hist. Nat.* **69**, 97–104 (1996).

167. W. E. Boles, A logrunner Orthonyx (Passeriformes, Orthonychidae) from the Miocene of Riversleigh, north-western Queensland. *Emu* **93**, 44–49 (1993). doi:10.1071/MU9930044

168. J. M. Nguyen, W. E. Boles, T. H. Worthy, S. J. Hand, M. Archer, New specimens of the logrunner *Orthonyx kaldowinyeri* (Passeriformes: Orthonychidae) from the Oligo-Miocene of Australia. Alcheringa: An Australasian. *J. Paleontol.* **38**, 245–255 (2014).

169. T. H. Worthy, A. J. Tennyson, C. Jones, J. A. McNamara, B. J. Douglas, Miocene waterfowl and other birds from Central Otago, New Zealand. *J. Syst. Paleontol* **5**, 1–39 (2007). doi:10.1017/S1477201906001957

170. Y. Kakegawa, K. Hirao, A Miocene passeriform bird from the Iwami Formation, Tottori Group, Tottori, Japan. *Bull. Natl. Sci. Mus. Ser. D* **29**, 33–37 (2003).

171. P. Brodkorb, Neogene fossil jays from the Great Plains. *Condor* **74**, 347–349 (1972). doi:10.2307/1366596

172. A. Manegold, The early fossil record of perching birds (Passeriformes). *Palaeont. Afr* **44**, 103–107 (2009).

173. J. Brunet, Oiseaux. *Not. Mémoir. Serv. Géolog. Maroc* **155**, 105–108 (1961).

174. J. I. Noriega, L. M. Chiappe, An early Miocene passeriform from Argentina. *Auk* **110**, 936–938 (1993). doi:10.2307/4088653

175. N. V. Zelenkov, E. N. Kurochkin, The first representative Pliocene assemblages of passerine birds in Asia (Northern Mongolia and Russian Transbaikalia). *Geobios* **45**, 323–334 (2012). doi:10.1016/j.geobios.2011.10.001

176. A. Wetmore, Notes on fossil and subfossil birds. *Smithson. Misc. Collect.* **145**, 1–17 (1962).

177. C. Mourer-Chauviré, J.-B. Peyrouse, M. Hugueney, "A new roller (Aves: Coraciiformes s.s.: Coraciidae) from the Early Miocene of the Saint-Gérand-le-Puy area, Allier, France" in *Proc. 8th Int. Meet. Soc. Avian Paleontol. Evol* (Verlag Naturhistorisches Museum, 2013), pp. 81–92 (2013).

178. D. W. Steadman, M. C. McKitrick, A Pliocene bunting from Chihuahua, Mexico. *Condor* **84**, 240–241 (1982). doi:10.2307/1367680

179. E. P. Tonni, *Zonotrichia robusta* n. sp. (Aves, Passeriformes, Emberizidae) del Pleistoceno medio de la Provincia de Buenos Aires. *Ameghiniana* **7**, 161–165 (1970).

180. J. C. Rando, M. López, B. Seguó, A new species of extinct flightless passerine (Emberizidae: Emberiza) from the Canary Islands. *Condor* **101**, 1–13 (1999). doi:10.2307/1370440